3-26-2018 2:00 PM

Fabrication and Applications of Printed and Handwriting Electronics

Tengyuan Zhang
The University of Western Ontario

Supervisor
Yang, Jun
The University of Western Ontario

Graduate Program in Mechanical and Materials Engineering
A thesis submitted in partial fulfillment of the requirements for the degree in Doctor of Philosophy
© Tengyuan Zhang 2018

Recommended Citation

Abstract

The accelerating arrival of the Internet of Things (IoT) era creates a rapidly growing demand for printed electronic. As a low-cost and green substrate, cellulose paper has become the most attractive choice for the printing of sustainable and disposable electronics. However, manufacture of high quality circuits with high conductivity on cellulose paper remains a challenge due to the substrate's high porosity and roughness. In this thesis, a method for facile fabrication of hybrid copper-fiber highly conductive features on low-cost cellulose paper with strong adhesion and enhanced bending durability is introduced. With three-dimensional electroless deposition (ELD) of copper, the as-fabricated circuits show ultra-low sheet resistance down to 0.00544 Ω/sq. Taking advantages of the porous structure of paper, together with the precise control of the inkjet droplets, highly conductive vertical interconnected accesses (VIAs) are fabricated for multilayered devices without physically drilling holes or depositing additional dielectric material. To further utilize the unique porous structure of cellulose paper, a scalable fabrication method for flexible, binder-free and all-solid-state supercapacitors is proposed based on the low-cost chemical engraving technique, to construct Cu_xO nanostructure *in-situ* on the three-dimensional metallized cellulose fiber structures. Benefitting from both the "2D Materials on 3D Structures" design and the binder-free nature of the fabricated electrodes, substantial improvements to electrical conductivity, aerial capacitance, and electrochemical performance of the resulting supercapacitors (SCs) are achieved, fulfilling the increasing demand of highly customized power systems in the IoT and wearable electronics industries. The above-mentioned work all use inkjet printing for materials deposition. However, as a solvent-based printing technique, inkjet printer has strict requirement of ink properties and suffer from inevitable nozzle clogging. To address these challenges, a fabrication method based on solvent-free laser printing technique is proposed, pushing the manufacture of printed electronics towards an environmentally benign and more cost-efficient manor. Lastly, a one-step react-on-demand (RoD) method for fabricating flexible circuits with ultra-low sheet resistance, enhanced safety and durability is proposed. With the special functionalized substrate, a real-time synthesize of the 3D metal-polymer (3DMP) conductive structure is triggered on demand. The as-fabricated silver traces show an ultralow sheet resistance down to 4 mΩ/sq.

Keywords

Co-Authorship Statement

This thesis is based upon a combination of published work. Various chapters are adapted from the following list of published work.

Chapter 2 was drafted by T. Zhang based on the following publication:

T. Zhang, X. Cai, J. Liu, M. Hu, Q. Guo and J. Yang, Facile Fabrication of Hybrid Copper–Fiber Conductive Features with Enhanced Durability and Ultralow Sheet Resistance for Low-Cost High-Performance Paper-Based Electronics. *Advanced Sustainable Systems.* 2017, 1(9): 1700062

T. Zhang proposed the idea and did most of the experiment. X. Cai helped measuring the properties of the printed antenna. J. Liu and M. Hu helped revising the manuscript. Q. Guo and J. Yang provided many valuable ideas and suggestions.

Chapter 3 was drafted by T. Zhang based on the following publication:

T. Zhang, E. Asher and J. Yang, A New Printed Electronics Approach Eliminating Redundant Fabrication Process of Vertical Interconnect Accesses: Building Multilayered Circuits in Porous Materials, *Advanced Materials Technologies,* 2018, 1700346, DOI: 10.1002/admt.201700346

T. Zhang proposed the idea and did the experiment. E. Asher helped revising the manuscript. J. Yang provided many valuable ideas and suggestions.

Chapter 4 was drafted by T. Zhang. E. Asher helped revising the manuscript. J. Yang provided many valuable ideas and suggestions. The work of this chapter has not been published.

Chapter 5 was drafted by T. Zhang based on the following publication:

T. Zhang, M. Hu, Y. Liu, Q. Guo, X. Wang, W. Zhang, W. Lau, and J. Yang A Laser Printing Based Approach for Printed Electronics, *Applied Physics Letters,* 2016, 108(10): 103501

T. Zhang proposed the idea and did most of the experiment. M. Hu and Q. Guo helped on the preparation of modified toner composition. Y. Liu, W. Zhang, W. Lau and J. Yang provided many valuable ideas and suggestions about this project.

Chapter 6 was drafted by T. Zhang based on the following publication:

T. Zhang, J. Li, J. Liu and J. Yang, React-on-Demand (RoD) Fabrication of Highly Conductive Metal-Polymer Hybrid Structure for Flexible Electronics via One-Step Direct Writing or Printing, *Advanced Functional Materials*, 2018, 28(4): 1704671

T. Zhang proposed the idea and did most of the experiment. J. Li helped on the prepare of coating solution. J. Liu revised the manuscript. J. Yang provided many valuable ideas and suggestions about this project.

All other chapters are drafted and revised solely by T. Zhang.

Acknowledgement

First and foremost, I would like to thank my supervisor, Professor Jun Yang, and all of the outstanding colleagues I have had at the University of Western Ontario, for the brain storm discussions, for many sleepless nights we were working together, and for all the exciting moment we shared together. I have learned a lot from all of you and am very appreciative to have a team with people like you.

Also, I would like to thank my wife Mengmeng, all my families and my friends who are always standing by my side no matter what happened. Without any of you, I would never go this far.

Table of Contents

List of Tables

List of Figures

Chapter 1

1.   Introduction

1.1. Printed Electronics

1.1.1 Background

Traditionally, lithographic methods, such as e-beam, photolithography and ion-beam lithography, have been the primary technologies used for fabricating wearable and flexible devices.[1-3] Unfortunately, the attractive advantages of these techniques come at an extremely high financial cost. The requirement for expensive chemicals, clean-room facilities, harsh experimental condition and labor-intensive processes, make these lithographic techniques costly, so are the as-produced products. With the accelerating arrival of the Internet of Things era, trillions of low-cost/single-use disposable devices are being demanded each year, such as radio-frequency identification (RFID) tags,[4] smart labels,[5, 6] displays,[7, 8] solar cells[9] and portable sensors.[10-13] In these situations, inexpensive printing techniques can significantly lower the fabrication costs while producing devices at large scale with desired precision and accuracy.[14] Although printing technology was introduced centuries ago, it has only recently captured the imagination and attention of researchers in the development of printing devices.[2] Advances in materials science towards the development of novel ink formulations and the evolution of new printing technologies coupled with these new advances, have been the primary driving force for the growing recent interest in this field.

The concept of the contemporary printed electronics, including conductors, semiconductors, and insulators that use inks, was first proposed in the early 1990s. The goal back then was to use conductive ink to fabricate wires. By 1997, Bell Labs made a transistor using screen printing for the first time. [15] In 1998, University of California, Los Angeles (UCLA) showed an inkjet-printed logo with polymer light-emitting devices (PLEDs). [16] Over the last decade, there has been an increased interest generated in printed electronics. Printed electronics are more advantageous than conventional processes due to greater environmental benefit, reduction of material loss, higher productivity and large-scale customization [17]. Printed

electronics are currently moving from the laboratory towards the commercial market, with a predicted market size of over 30 billion US dollars in 2015 and 96 billion US dollars in 2020 [18]. The current state of the market suggests that techniques involving production and enhancement of printed electronics are becoming promising trends. With recent advances in printing techniques and materials science, various flexible and/or stretchable electronics devices have been printed with the pairing of various functional inks such as metal nanoparticle conductive inks, [19, 20] carbon-based inks,[21-23] liquid metals,[24] semi-conductive inks,[25-27] conductive polymer inks,[28] and insulated inks.[29, 30] However, delamination and/or peeling-off is always a concern because the functional materials are typically deposited on the top of substrates only. The possibility of failure under repeated mechanical loading limits its applications in areas where reliability and stability are demanded. In addition, unsatisfactory conductivity of the printed materials, that is far below that of the bulk material, is another major problem. Extensive research and development are required to overcome these technical hurdles to advance the material printing technology to the state of the art manufacturing process. Popular printing methods such as inkjet printing, screen printing, gravure printing, transfer printing and other newly developed printing technologies are now being applied to fabricate electronics. Each printing technology has its own advantages and disadvantages, and also requires different ink parameters for optimum printing quality. Therefore, it is of great important to get familiar with the features of these printing techniques to push the boundary of the fabrication of printed electronics. The printing techniques can be categorized into two types: digital and non-digital. Based on the comparison made by Fukuda et. al., the features of various printing methods is summarized in Table 1.[31] In this chapter, the most recent research progress about the fabrication of printed electronics based on digital printing process will be discussed in detail. The literature review will focus on the fabrication of the most fundamental element in electronics devices – conductive traces. The advantages and disadvantages of different fabrication strategies will be discussion in the following sections.

Table 1. Comparison of the features of different printing methods.

Type	Printing Method	Ink viscosity [mN/m]	Line width [μm]	Line thickness [μm]	Speed [m/min]
Digital Process	Inkjet	1–100	30–50	0.1–1	1–500
	E-jet	$1–10^4$	1	0.001–0.1	<1
	Direct Writing	$10^3–10^6$	10–1000	50–100	Slow
	Aerosol Jet	$1–10^4$	<1	0.001–0.1	Slow
	Laser Printing	-	30-50	8-20	500-1000
Non-Digital Process	Offset	$100–10^5$	10	1–10	1000
	Gravure	$100–10^3$	10–50	0.1–1	1000
	Flexo	50-500	45-100	<1	500
	Screen	500-100000	30-50	5-100	50-150
	Gravure-offset	5000-50000	5-20	5-100	50-150
	Reverse-offset	1-5	1-10	0.05-1	1-10
	Transfer Printing	-	0.1	1	Slow
	Nanoimprint	-	0.01	0.1	Slow

1.1.2 Fabrications of Printed Electronics based on Digital Printing Process

Digital printing refers to methods of printing from a digital-based image directly to a variety of media, without the need of preparing masks or templates. [1] Traditionally, digital printing has a higher cost per page than more traditional offset printing methods, but this price is usually offset by avoiding the cost of all the technical steps required to make printing plates. When it comes to printed electronics and the Internet of Things, where customized RFID tags, circuits, and devices are highly demanded, digital printing process shows its unique advantages such as on-demand production, short turnaround time, and even a modification to the device during production. [2] These features will also significantly benefit researchers in this area as well as the research & development (R&D) process for the industry. Currently, inkjet printing is the dominant printing techniques used for the fabrication of printed electronics, due to its low-cost, compact in size and ease of modification.

1.1.2.1   Inkjet Printing

1.1.2.1.1   Mechanism

Inkjet printing is a type of digital printing method that reproduces digital images by advancing ink droplets onto paper, plastic, etc. The concept of inkjet printing originated in the 20th century and was widely developed in the early 1950s. Ink-jet printers that can copy computer-generated digital images were developed in the late 1970s by three leading companies in this area: Epson, Hewlett-Packard (HP) and Canon. Currently, there are two main technologies for contemporary inkjet printers: continuous (CIJ) and drop-on-demand (DOD).[32] The original continuous jet printers used electrostatic plates to deflect drops to the paper or to a reservoir for recycling as shown in Figure 1(a). [33] The CIJ printers have largely been superseded by those printers with DOD systems which are more cost-efficient, reliable and easy to maintain than CIJ systems. There are two types of DOD systems popular on the market—thermal DOD and piezoelectric DOD. In a thermal DOD system, the print cartridge consists of a series of tiny chambers which are constructed by photolithography, each containing a heater, as shown in Figure 1(b). In order to eject droplets from each chamber, a current pulse passes through the heating element, causing rapid evaporation of the ink in the chamber and formation of air bubbles, which results in a large pressure increase to push the droplets onto the paper. The surface tension of the ink as well as the shrinkage of the steam bubbles will bring more ink into the chamber through the narrow channel connected to the ink reservoir to complete the refilling process. To make a thermal DOD system functional properly, the ink must have volatile components to form bubbles; otherwise, droplets cannot be jetted. Piezoelectric DOD systems use a piezoelectric material in an ink-filled chamber behind each nozzle instead of a heating element, as illustrated in Figure 1(c). When a voltage is applied, the piezoelectric material changes shape, creating a pressure pulse in the fluid chamber that forces the ink droplets out of the nozzle. Because no volatile components are required, piezoelectric inkjet printer allows a wider variety of inks. However, the manufacturing costs are higher due to the use of piezoelectric materials.[34]
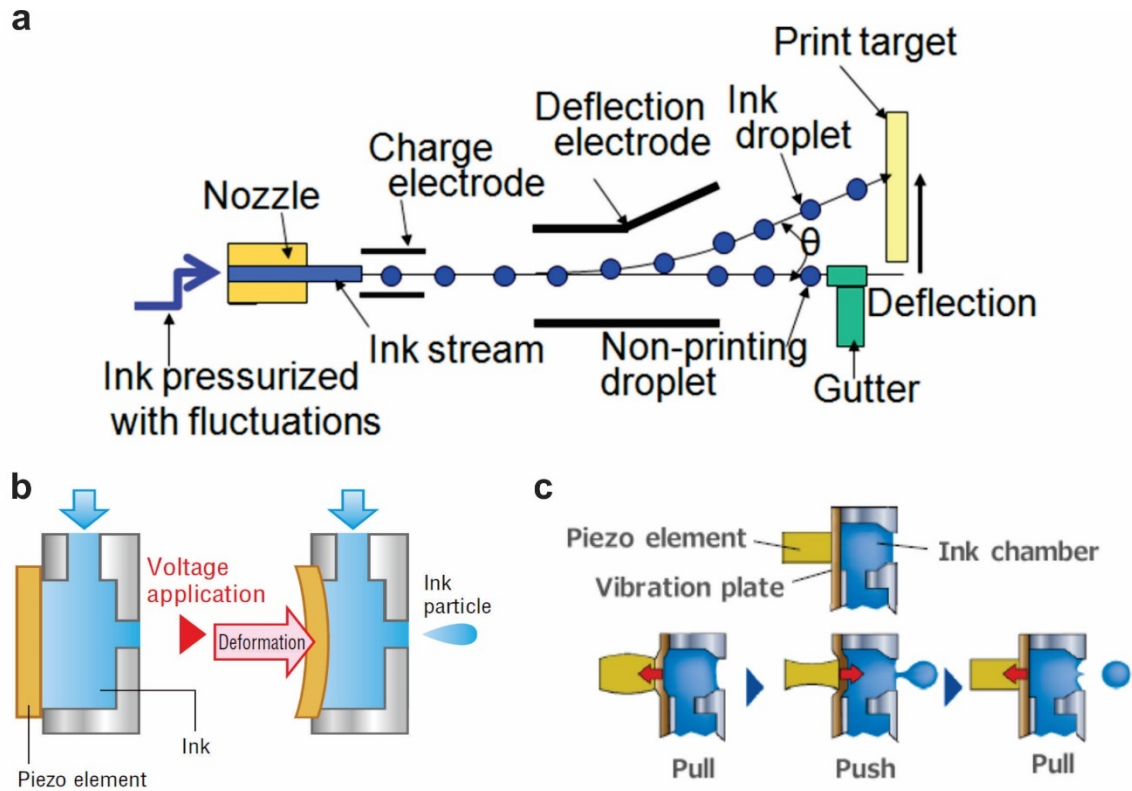
Figure 1-1. Printing mechanism of (a) continuous inkjet system, (b) thermal drop-on-demand inkjet systems and (c) piezo drop-on-demand systems. [33, 35, 36] [Copy with permission]

1.1.2.1.2   Fabrication Strategies

Inkjet printing can be presented as an advantageous and the most popular method of fabricating printed electronics because of low-capitalization of equipment, high materials efficiency, elimination of photolithography and non-contact processing [37]. Many inkjet-printed devices have been achieved by researchers in recent years, such as microfluidic analytical devices, [38, 39] heterostructures, [40] radio-frequency identification (RFID) tags,[41, 42] energy storage systems, [43-45] and thin film transistors. [46, 47] Among all these printed devices, the most fundamental and essential part is conductive traces. In most cased, the conductivity of the printed traces largely affects the overall performance of the printed devices. Thus, I focused on the fabrication of highly conductive circuits/traces in my PhD work. Based on different kinds of inks used in the inkjet printing systems, we can categorize the fabrication strategies into four types, as summarized by Chen et. al. which is shown in Figure 2.[48]
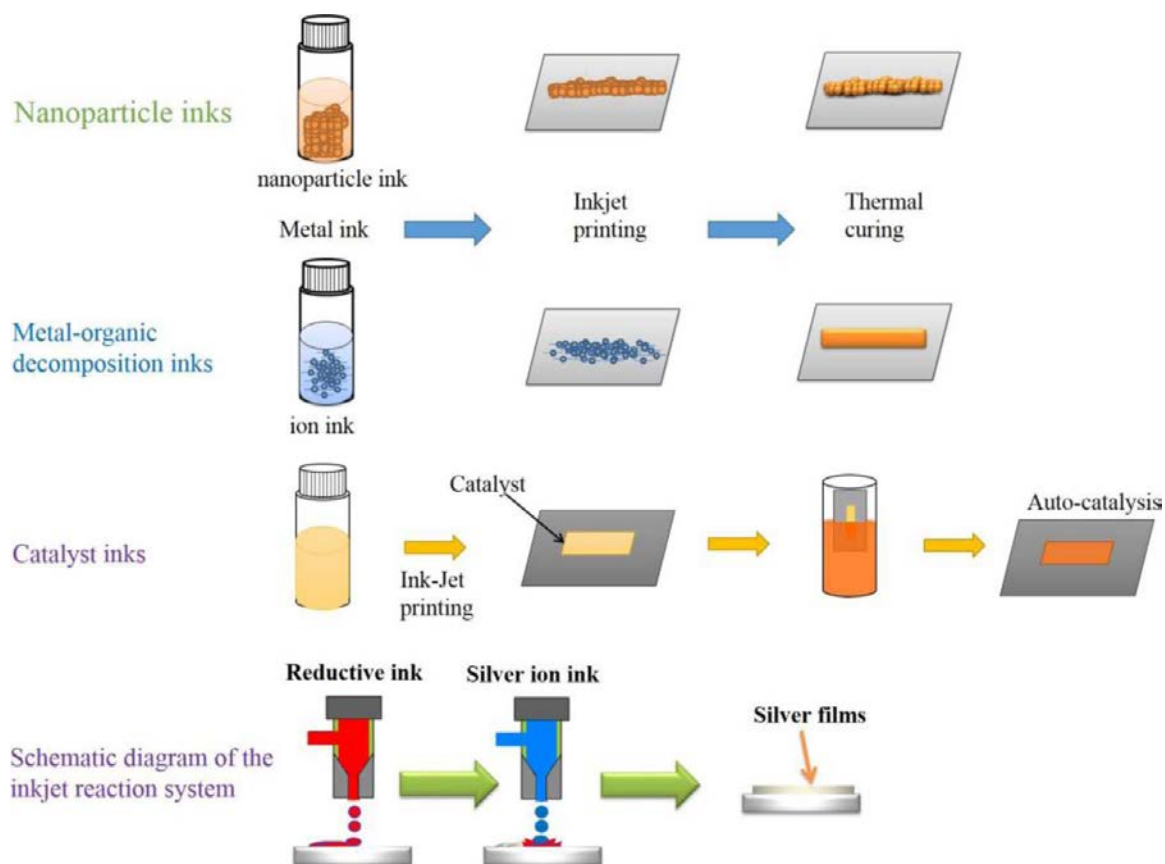
Figure 1-2. Various inkjet printing based fabrication strategies for conductive traces. [48] [Copy with permission]

Direct Printing of Conductive Materials

The most straightforward way is to directly print conductive inks onto the substrate. The inks can be metal nanoparticle inks, conductive polymer inks, carbon-based conductive inks and liquid metals. Currently, the most commonly used inks are metal nanoparticulate inks, which are metal nanoparticle suspensions with colloidal stabilizers to prevent particle aggregation or nozzle clogging. Currently, silver nanoparticles are the most commonly used inks for the manufacture of printed conductive tracks because of their high conductivity and low oxidation rate. Alternatively, copper has attracted widespread attention in recent years for the printing of conductive circuits due to its relatively low price and high electrical conductivity. [49] However, copper nanoparticles get oxidized easily, so they are often protected by noble metal anti-oxidant shells. Printed patterns from NP inks typically have higher resistivity and require sintering processes at elevated temperatures (usually ~30-60 mins, 100ºC – 200ºC) to remove some non-conductive organic components and stabilizers to enhance conductivity. Due to the

thermoplastic nature of plastic flexible substrates such as PET, the high sintering temperature limits the application of such fabrication methods. To reduce the ink sintering temperature, researchers have tried to exploit other sintering processes such as microwaves, laser curing, plasma processing and chemical sintering.[50-52] Although these alternative methods have yielded fruitful results, thermal post-treatment is still extensively used in printing commercial conductive inks because of its wide availability and easy accessibility. [48]

Printing Metal Precursor

Metal precursor inks are highly concentrated metal salts dissolved in organic solvents or aqueous solutions. After printing onto the substrate, the salt decomposes into conductive traces under heat, ultraviolet light or chemical treatment. The most commonly used salts are organic silver complexes that can be easily converted to silver thin films by thermal treatment with an electrical conductivity close to that of bulk silver.[53-57] In order to reduce the ink sintering temperature, various methods have been proposed to prepare a silver salt complex solution to achieve a low sintering temperature below 110°C. However, these metal-organic complexes take several synthetic steps to prepare, making it less attractive time. To solve this challenge, efforts have been taken to simply the synthesize process. For example, Chen et al. have simplified the preparation steps by mixing silver ammonia solution with diethanolamine to form a clear aqueous solution, which remains transparent for weeks under proper storage (Figure 1-3 (a)).[58] After heating at a moderate temperature (<100°C), the printed micropattern can easily be transformed into a highly conductive silver film with strong adhesion to the substrate. Another example is the work from J. A. Lewis's group. A transparent "reactive silver ink", which was stable at room temperature for months, was prepared by simplified process. Upon annealing at 90 °C, the printed electrodes using the reactive silver ink exhibited an electrical conductivity equivalent to that of bulk silver.[53] Besides thermal treatment, photo-curing processes have also been developed to fabricate conductive metal thin film patterns at room temperature. For example, Bromberg et al. adopted plasma process to convert inkjet-printed silver nitrate traces into highly conductive silver tracks.[59] Valeton et al. developed a UV curable metal precursor ink and demonstrated the rapid formation of highly conductive silver pattern at room temperature.[60] More recently, intensive pulsed light sintering (IPL) system have also been developed based on the high-power xenon pulsed light. Printed metal precursor inks were treated by the IPL system for only a few seconds to convert

the printed pattern to highly conductive traces, providing safer and faster solution for the sintering of metal precursor ink or other inks on thermal sensitive substrate.[61-63]
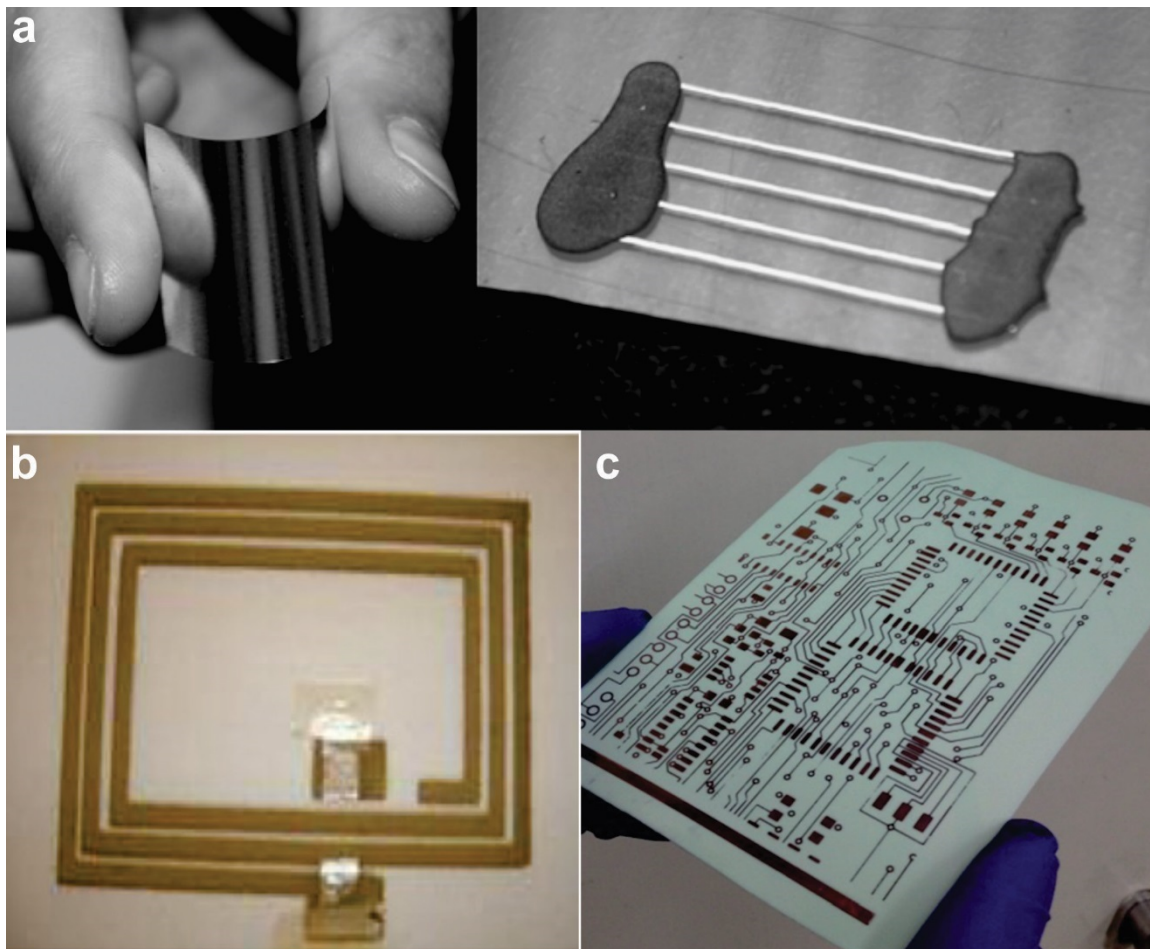
Figure 1-3. (a) A typical sample prepared by silver complex inks. (b) RFID antenna with metallic joints printed on paper using reactive ink printing method. (c) High resolution circuit board printed on paper by inkjet printing of catalyst and electroless copper deposition. [60, 64, 65] [Copy with permission]

Reactive Inkjet Printing

In order to prepare conductive circuits at room temperature, micro-reaction inkjet printing systems have recently been demonstrated. Based on the multi-cartridge design of an inkjet printer, metal ion inks and the corresponding reducing agent were filled into different cartridges and were jetted through two different channels. [55] When these two types of inks meet on the substrate, highly conductive metal traces will form after the redox reaction. This was first demonstrated by Bidoki et al. in 2007 through printing ascorbic acid and silver nitrate

solution sequentially on papers to produce several antenna and planer capacitor patterns, as shown in Figure 1-3(b).[65] Similarly, Kao et al. printed aqueous formaldehyde solutions and silver ammonium solution through two different nozzles to perform the silver mirror reaction to achieve highly conductive silver metal traces on plastic surfaces.[66] Although these reaction systems are feasible, however, accurate drop landing position and fast drop coalescence or mixing are required in the printing process.[48] Meanwhile, special maintenance must be taken to such systems due to the highly reactive inks.

Electroless Deposition Based Catalyst Printing

The above-mentioned fabrication strategies all rely on the content in the inks as a source of conductive materials. One of the critical issues is that the conductive materials in the inks are very limited, setting a cap for the conductivity of the printed patterns. To solve this problem, one promising solution is to use the electroless deposition (ELD) technique. ELD is an auto-catalytic technique used to deposit metals(copper, nickel, etc.) on various substrate such as paper, plastic, aluminum oxide, and even yarns (Figure 1-3(c)).[64, 67-69] The mechanism of ELD was thoroughly studied these years, making it a convincing technique for making metal coating and high resolution patterns.[70, 71] Abundant metal ions in the ELD bath can create patterns with dense surface, which in turn results in good conductivity close to that of the bulk materials. This absolute advantage drives researchers to involve this technique in the fabrication of flexible electronics. For example, ELD of Cu occurs by an autocatalytic redox reaction, where Cu is deposited onto a catalyst-activated surface, without the assistance of an external power source. Among all the activation catalysts, palladium (Pd) provides the best catalytic effect and thus is frequently used in electroless plating.[72] To fabricate metal conductive tracks, palladium (Pd) colloid or other Pd ion contacting inks are first inkjet printed on substrates following with a subsequent copper electroless plating. Due to the limited resources and high price of Pd, silver ion-based catalyst is found to be a good alternative for the catalyst of electroless copper plating. For example, a particle-free silver nitrate ink was printed on polyethylene terephthalate (PET) or polyimide (PI) films as an activating agent for copper plating.[73-75] Printed samples were electroless plated to produce a highly conductive copper pattern. Other catalyst inks, such as polydopamine, can also be used to make copper tracks or other metallization features.[76] By replacing the electroless plating solution, this approach can also be applied to form conductive patterns of nickel, silver, or even gold.[77-

79] Challenges of the ELD based fabrication strategy remain on how to modify/coat the surface of the substrate to capture the catalyst and deposited metal efficiently. If the substrate were not properly treated, the deposited metal would easily get peeled off from the substrate due to poor adhesion. In addition, during the ELD process, metal not only grow vertically, but also grow horizontally. The horizontal growth will significant lower the resolution of the printed patterns and cause short circuit in the device. Thus, it is of great importance to develop ELD formulas to limit the horizontal growth while enhance the vertical growth speed to shorten the deposition time.

1.1.2.2   Other Emerging Non-Contact Digital Printing Techniques

1.1.2.2.1   Laser Printing

Traditional laser printing is an electrostatic digital printing process. It produces high-quality text and graphics by repeatedly delivering laser beams on negatively charged cylinders called "drums" to define differentially charged images.[80] The drum then selectively collects the charged powdery ink (toner) and transfers the image to a sheet of paper, which is then heated to fuse the toner with substrate, as presented in Figure 1-4.
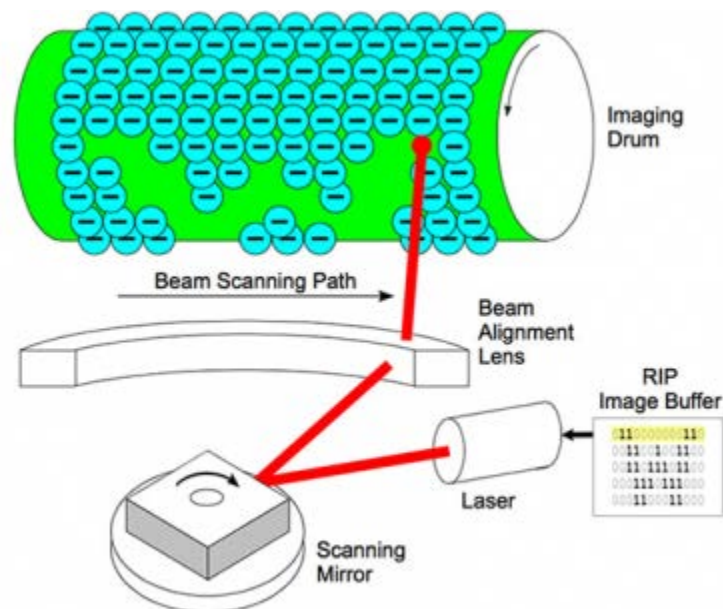
Figure 1-4. Working mechanism of electrostatic laser printing. [Copy with permission]

Laser printing is advantageous as there are no required solvents and so it unnecessary to worry about the solubility of the metal and toner powders. Unlike inkjet printing, laser-printing uses dry toner powder, so there is no constraint on viscosity and surface tension. Since the introduction of the laser printer, they have become more affordable, allowing them to become viable options in both printed electronics and personal use. In the area of printed electronics, few work has been reported based on the mechanism of office use laser printer, due to the strict requirement of toner composition. As one of the objectives "developing low-cost solvent-free printing method for the fabrication of printed electronics" of my PhD work, I have make efforts to develop laser printing-based fabrication strategies. Details of this work are presented in Chapter 6.

Another laser-based printing techniques called laser-induced forward transfer (LIFT) has been recently developed. [81-83] In a LIFT system, high energy laser is used to propels materials onto the substrate from the material tray as shown in Figure 1-5. LIFT can operate under atmospheric conditions, and is compatible with low laser fluences, allows the printing of organic and inorganic materials as well as biological elements and the printing can take place from liquid or solid phases. The resolution is defined by the size of laser spot; thus, a LIFT can achieve very high resolution down to a few microns.[83] However, such system is very expensive, and they are not commercially available on the market. In addition, it is almost impossible to use LIFT system for mass production.
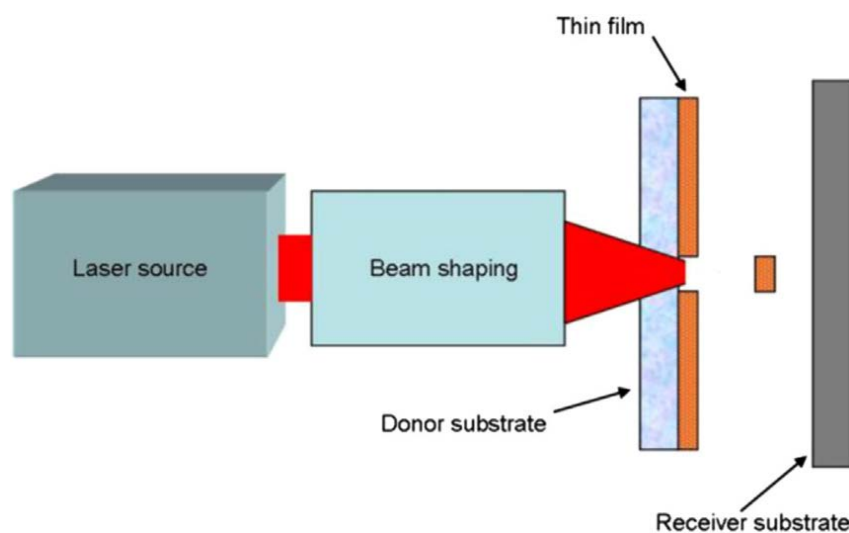
Figure 1-5. Scheme of LIFT process in solid phase. [82] [Copy with permission]

1.1.2.2.2 Electrohydrodynamic-Jet Printing

Electrohydrodynamic-jet printing, known as E-Jet printing, has emerged as a high-resolution alternative to other forms of non-contact digital solution-based fabrication approaches, such as ink-jet printing.[84, 85] Electrohydrodynamic jet (E-jet) printing uses an electric field to induce fluid flows from micro capillary nozzles to create devices in the micro/nano-scale range. It pulls the liquid inks out of the nozzle rather than pushing inks out, as illustrated in Figure 1-6.[86] The diameter of an E-Jet Printed droplet ranges from several hundreds of nanometers up to a few microns, which is ~1/10 in diameter or 1/1000 in volume smaller than that produced by conventional inkjet printers.[87] Depending on the application and the setting of the printer, E-Jet printer can either produce discrete droplets or continuous lines. Rogers et al. proposed and demonstrated such a system in 2007 and showed the ability of the system to produce conductive features down to sub-micrometer resolution.[84]. Based on the same mechanism, a further industrialized system called super inkjet (SIJ) technology was developed later by National Institute of Advanced Industrial Science and Technology (AIST) in Japan. The SIJ system can fabricate 2D and even 3D feature with high resolution (sub-micron size) on all kinds of substrates. Needless to say, such systems come at a price, a price that several orders higher than regular inkjet printer. Limited by its working mechanism, the printing speed of such systems is very slow, as shown in Table 1.
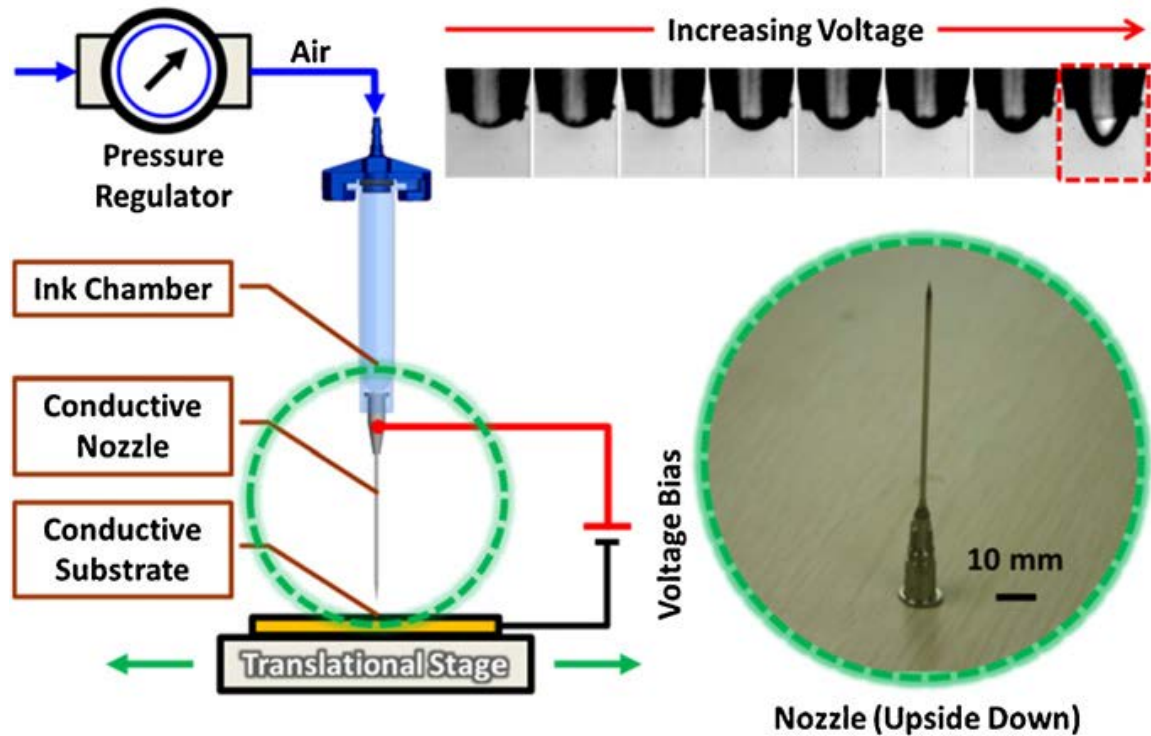
Figure 1-6. Schematic of a standard E-jet printer.[86] [Copy with permission]

1.1.2.2.3   Aerosol Jet

Metal aerosol jet printer is a mask-less non-contact printing system developed by the US company Optomec.[88] In contrast to inkjet systems, metal-containing inks are not printed directly. Instead, an aerosol is generated and delivered to the special designed print head, where the viscosity of the ink can be adjusted. In the deposition head, the aerosol flow is focused by the second sheath air flow and deposited onto the surface of the substrate by the nozzle, as shown in Figure 1-7.
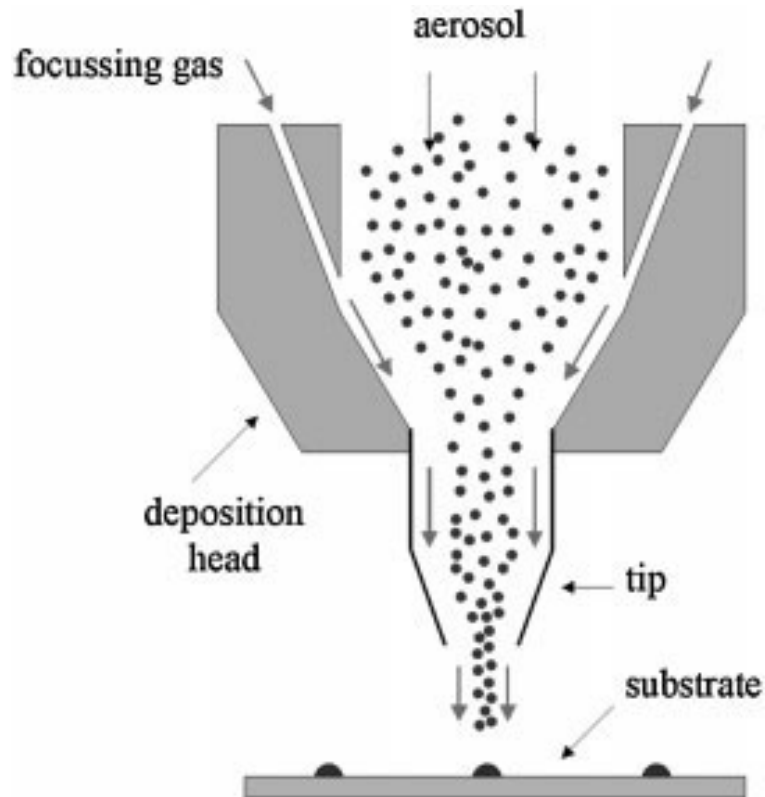
Figure 1-7. Working principle of the aerosol deposition head.[88] [Copy with permission]

Specially designed deposition head is a key part of the printer. In the printhead, the aerosol is surrounded by a stream of air, avoiding contact with nozzle. Since the aerosol flow is focused by laminar airflow, the width of the deposition line is only a fraction of the width of the nozzle diameter, resulting in much higher printing resolution. In addition, the distance between the tip and the surface can vary by 2 to 3 mm with no noticeable change in line width, so the technique is suitable for uneven surfaces.[89, 90] Aerosol jet system has been reported as a printing method for layers for flexible electronics such as flexible displays,[91] thin-film transistors,[92] energy storage systems,[93]23 and biological sensors.[94, 95] However, in comparison to regular inkjet printing system, the number of scientific publications is much less. Compared with regular inkjet printing systems, aerosol jet allows the deposition of thinner layers with much higher resolution. In addition, the aerosol jet printer allows much broader range of ink viscosity and larger particle sizes and loadings in the ink. However, such system is also very expensive, and due to the single nozzle design, the printing speed is much slower than that of an inkjet printer.

1.1.3 Conclusion

Fruitful achievements have been achieved using non-contact digital printing process, especially the inkjet printing. However, there are still many limitations when working with inkjet printing, such as the requirement of control over ink viscosity and surface tension parameters in the printer design [96-98]. Droplet viscosity must be low enough so that channels can be refilled quickly while surface tension must be high enough, but pressure must stay low, so that ink stays within the nozzle without dripping [99]. In order to minimize clogging, heavy dilution, high solubility, low volatility and acceptable surface-interaction must be optimized, allowing for proper drop formation, accuracy and continuous film formation [100]. When working with nanoparticles in a laboratory, nozzle clogging is a common issue as nanoparticles will accumulate at the opening of the nozzle [101]. Liquid printing is negatively impacted by the "coffee-stain" effect due to differential evaporation of a solvent resulting in dual-peaked height profiles of the droplet. This effect is influenced by a joint effect evaporation rate difference and contact line with solvent composition also making an impact [102]. Other emerging non-contact digital fabrication techniques, such as e-jet, aerojet and LIFT, show promising results for the enhancement of printing resolution, however, none of them is capable of doing mass production of printed electronics. In addition, such techniques are in the development stage, the equipment is extremely expensive, making them still far away from industrial applications.

1.2. Handwriting Electronics

1.2.1. Background

Printed electronics is transforming the electronics industry by replacing expensive electronic components, devices and even systems fabricated with traditional manufacturing methods. Various printing techniques have been demonstrated to fabricate flexible electronics, such as screen printing, [103-105] inkjet printing, [25, 106-108] gravure offset printing, [109-111] flexo printing, [112, 113] and even laser printing. [114-116] More recently, the emerging 3D printing technology just added one more dimension to printed electronics, thus facilitating achievement of functional printed 3D electronics. [117-119] However, these techniques are usually inaccessible to general users, due to the inevitable enrollment of special expensive

equipment, intractable troubleshooting process, harsh requirement of the ink and need for professional skills.

As an alternative technique, targeted at point-of-care applications and end-users with no professional skills, direct pen writing of flexible electronics is gaining popularity for its low-cost, simplicity, ultrahigh portability and ease of use. Various types of writing tools, such as ball pen, [120-122] pencil,[123-125] marker pen, [126, 127] brush pen, [128-130] and fountain pen, [131, 132] have been recently adopted to directly write electronics on various substrates. Direct writing is a simple, cost-effective, and fast way to deposition functional materials onto various substrate to form all kinds of flexible/stretchable devices for emerging applications such as electric circuits, [120, 126] flexible sensors, [133-135] energy storage devices and radio frequency (RF) devices. [121, 136, 137] Moreover, hybrid fabrication methods, which take the simplicity and cost efficiency of handwriting electronics and high resolution and scalability from printing techniques, were demonstrated by researchers, including the electrohydrodynamic direct writing and micro-plasma-based direct writing. [87, 138]

In this chapter, the most recent research progress about handwriting electronics and their applications will be discussed. I will first introduce all kinds of popular writing techniques that has been used for the fabrication of handwriting electronics in section 1.2.2 and ended with a conclusion to summarize the challenges we are facing and the future perspectives of this area in section 1.2.3.

1.2.2.Fabrication Method for Handwriting Electronics

Since the invention of the first writing tool, writing has become one of the most essential things in people's daily life and has greatly boosted the development of human civilization. Now in the 21st century, with the rapid development of materials science and nanotechnology, writing tools not only can be used to write down the culture, but also can be used to fabricate electronics. The writing techniques can be categorized into four types: brush/marker pen, pencil, fountain pen and ball pen. Each pen-based writing method has its own advantages and disadvantages. The performance of handwriting electronics devices is greatly affected by the conductivity, microstructure, mechanical properties of the written traces; while the properties of written traces are dominated by the writing methods (ink flow rate, width, uniformity, etc.). Therefore, a proper writing method should be chosen based on the required properties of electronics and

their applications. In this section, the writing techniques are classified into four types: brush/marker pen, pencil, ball pen and fountain pen. The advantages and disadvantages of each methods are reviewed and summarized in detail in the following sections.

1.2.2.1.   Brush/Marker Pen

Brush pen is a writing instrument geared toward East-Asian calligraphy. [139] It was invented before Christ in China and has been used as the main writing device in eastern countries for over thousands of years since then. It usually consists of a pen nib that mimics the brush-like quality of the ink brush with either brush strands as in a normal ink brush or a soft or hard felt/foam tip which is popular in modern societies and is called "marker pen". For a traditional brush pen, before each writing, the brush pen is immersed in an ink container to draw ink into the tip by capillary force, and then the ink is delivered onto a substrate to form continuous pattern by hand writing. In modern societies, such tradition brush pens are seldom used in daily life, but still keep their popularity in calligraphy and artwork painting. Alternatively, based on the principle of ancient brush pen, new types of cartridges-based brush pen equipped with a soft or hard felt/form tip remain popular in our daily life, and they are usually called "marker". In terms of the fabrication of electronics, brush pen has the capability of writing functional materials on both rigid (wood, plastic, glass, etc.) substrates and soft (paper, polyethylene terephthalate (PET), polyimide (PI), etc.) substrate. Prior to writing, non-porous substrates are often treated with plasma or ultraviolet (UV)/ozone to improve the wettability or coated with an ink absorption layer to make the surface become writable. [140-142] During writing, there is a shear stress applied on the solution existing between the two boundaries, the solution– substrate and the solution– brush interfaces (Figure 1-8(a)). [129] The electrical properties of the written traces are related to repeated writing cycles, ink properties, writing speed, and substrate temperature, among which, the writing speed is a dominate parameter to control the uniformity of the traces and ink volume per specific area. A high writing speed will induce a discontinuous trace while a low writing speed will result in a non-uniform trace (Figure 1-8 (a2)). Furthermore, the number of writing cycles needs to be optimized since it determines the amount of conductive materials on specific area and thus has a significant impact on the electrical performance.[143] In addition, it is also necessary to control and adjust the solution viscosity and evaporation rate to precisely control the width and thickness of the writing pattern. (Figure 1-8 (a3)).[144-146]
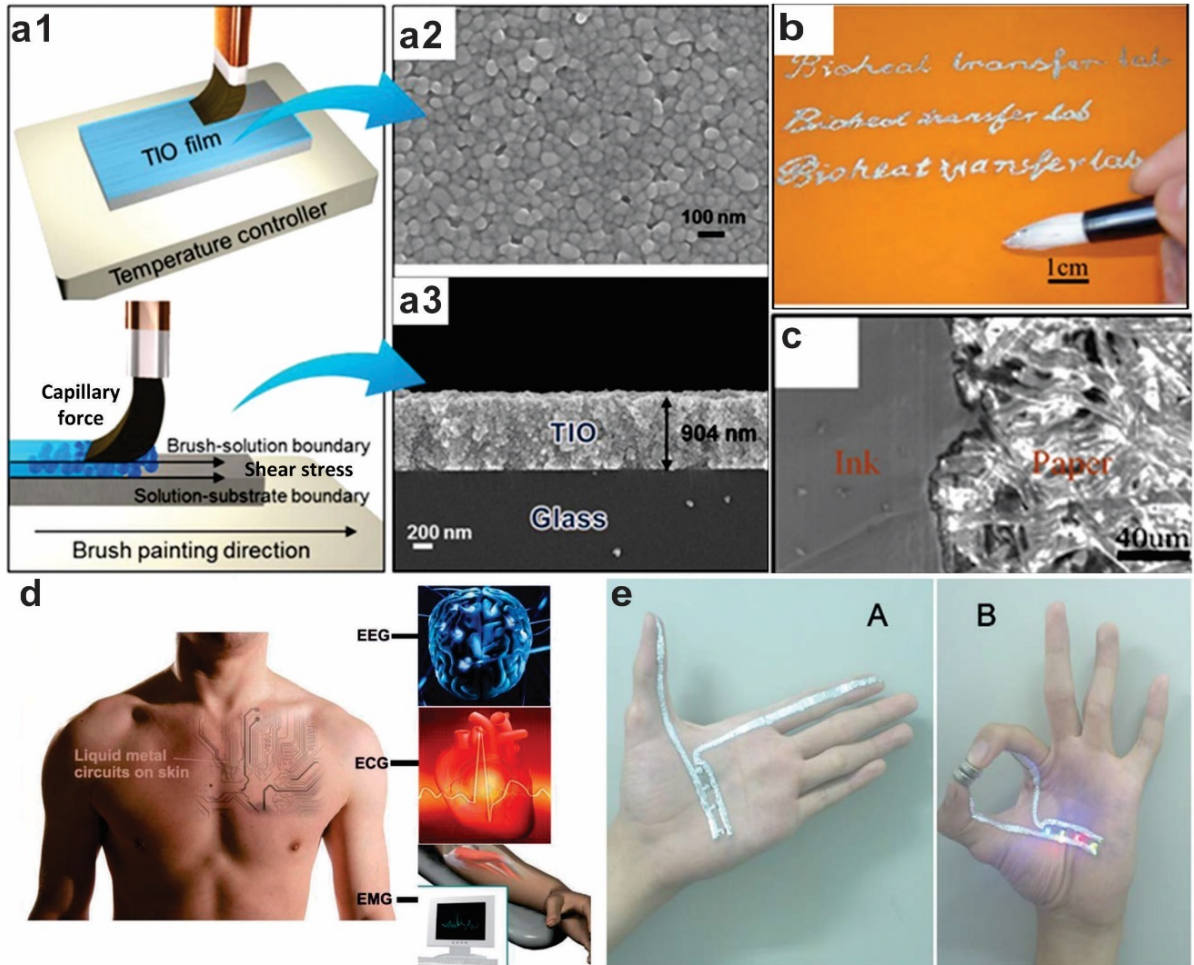
Figure 1-8. (a) Typical fabraction process (a1) using a brush pen and the SEM images of (a2)surface and (a3) cross-section of the as-fabricated device. (b) Handwriting of gallium-based liquid metal ink with brush pen and (c) its surface morphology under SEM. (d)(e) Handwritten functional circuits on human skin with busheh pen using liquid metal.[129, 135, 147] [Copy with permission]

Brush pen is compactable with various inks. For example, Liu's team wrote a gallium-based liquid metal ink on a variety of substrates using a brush at room temperature (Figures 1-8 (b),(c)). [130] When exposed to the atmosphere, the geometry of the liquid metal pattern can be well maintained by the passivation contribution of the oxide scale that forms instantaneously on the liquid metal surface, even on human skin (Figures 1-8 (d)(e)). [135, 147] In addition, the width of the conductive traces is also affected by the tip size of the brush and the writing pressure applied. The bristles have a negligible effect on the roughness of the writing pattern. For example, smooth brushes made of nylon fibrils have been used to make smooth films with

relatively low roughness (2.26 nm).[144] The amount of ink on the brush and how the ink is delivered may affect the performance of the electronic device. However, the effect can be minimized by repeating the writing. Brush writing has proven to be a promising method of making electronics with the cost-effective, simple, fast, features and the benefits of high-volume production compatible with roll-to-roll systems. However, in brush writing, it is often necessary to customize the mask to precisely control the geometry of the design on the substrate and improve the resolution. Moreover, the precise control of the pattern thickness and width remains a challenge.

1.2.2.2.   Ball Pen

A ball pen is a pen that jets ink on a metal pen at its point, as shown in Figure 1-9 (a). Commonly used metal is steel, brass or tungsten carbide. It was conceived and evolved into a cleaner and more reliable alternative to brush pens and fountain pens, and it is now the most-used writing instrument in the world. Therefore, it affects the art and graphic design, resulting in an art type. During writing process, the ballpoint on the tip is rotated to make the ink to flow out of the ink filling cartridge so that traces are formed on the substrate, as illustrated in Figure 1-9 (b). [148] Ball pen uses a quick-drying ink from the newspaper printing industry to meet the need to eliminate spatter and smear that often occur with pencils and pens. In addition, ball pens are disposable, reusable and durable, giving consumers superior user experience in writing, and are therefore simple, practical and suitable for everyday use. Thanks to these excellent properties, portable writing electronic devices fabricated using ubiquitous ball pens have become increasingly attractive. [120, 149, 150]
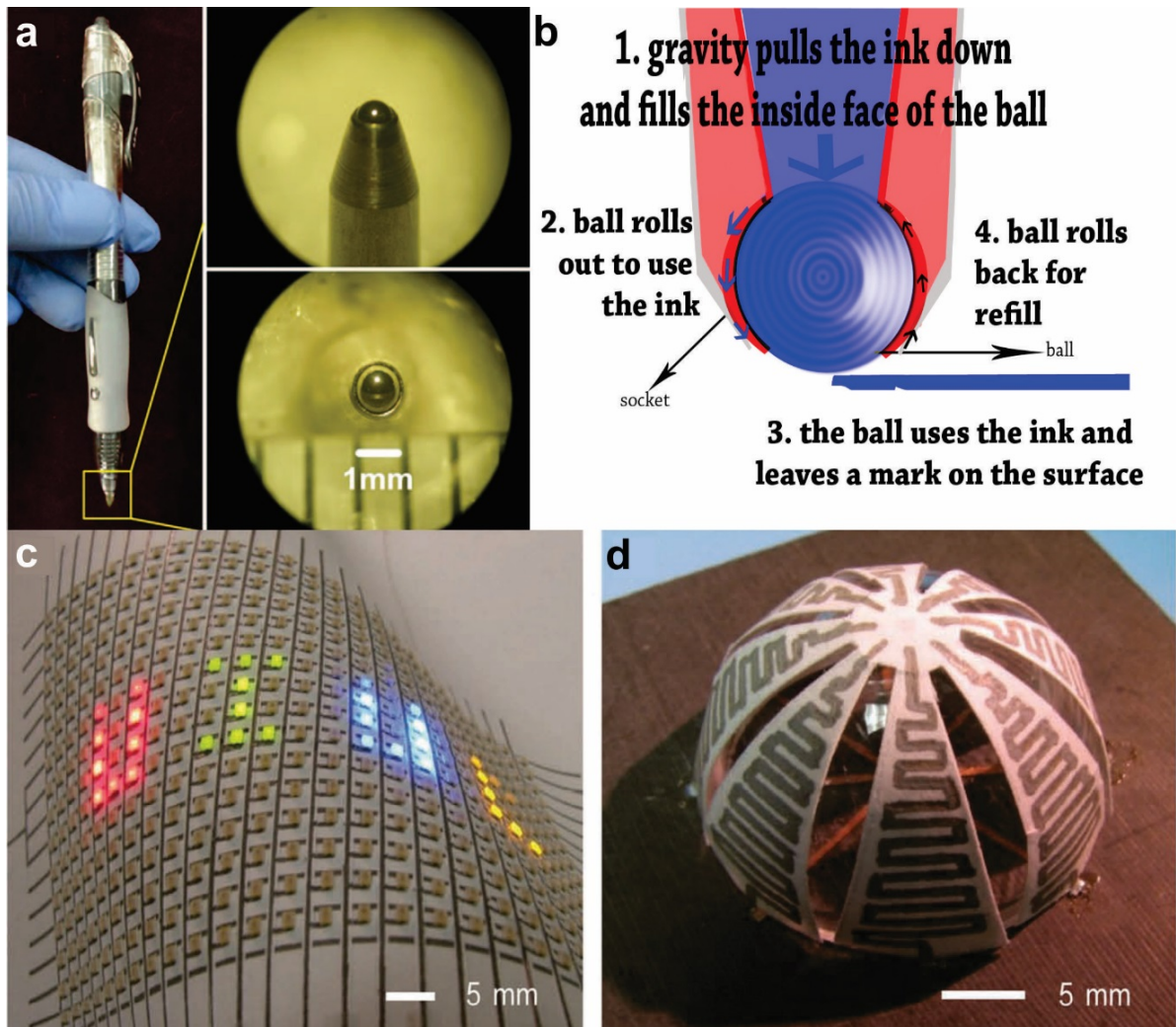
Figure 1-9. (a) Optical image of a regular ball pen and zoomed-in pictures showing the details of the tip. (b) Typical strucutrue of a ball pen's tip and its working mechanism. (c)(d) Functional circuits fabricated by handwriting silver conductive inks on paper using a modified ball pen.[120, 148] [Copy with permission]

Lewis Group demonstrated the idea of making electronic components with ball pens for the first time in 2011, in which a ubiquitous roller ball pen was remodeled and filled with conductive silver ink and used to write patterns directly on Xerox paper. [120] Their writing approach, which was named as "pen-on-paper", was proved to be simple and high efficient, allowing the fabrication of electronic devices with 3D structures in a low-cost, fast and user-configurable manner (Figure 1-9 (c) (d)). Following their work, the academic interest in pen-written electronics has greatly increased as more and more research groups report the expanded application and the improved performance of handwriting electronic. [151-153] Different from

the pencil, which is only capable of writing carbon-related materials with fixed compositions and relatively low electrical conductivity, ball pens are compatible with a wide range of functional inks, including conductive silver/copper inks, [120, 132, 154] liquid metals, [128, 149] enzyme inks and organic semiconductor crystals. [134, 155] However, directly writing of electronics using ball pen is also facing some challenges. For example, for writing nanoparticle-based inks (silver/copper nanoparticles) an extra time-consuming sintering step is necessary to make the written trace conductive or to enhance its conductivity. The demand for high temperatures (120°C to 160°C) in this process further complicates the whole fabrication process, making it inaccessible to end users and restricting their wide application and compatibility with temperature sensitive substrates such as polyethylene terephthalate (PET) and poly(methyl methacrylate) (PMMA) substrates. In addition, the nanomaterials evolved in these conductive inks make the cost of the ink significant higher than that of the regular ink and impose safety concerns as nanoparticles are capable of penetrating human skin. Even though various conductive traces working as electrodes or interconnects have been successfully written on different substrates using ball pen, more complicated electronic components have not been achieved yet.

1.2.2.3.　　Fountain Pen

A fountain pen is a nib pen that contains an internal reservoir of liquid ink. A typical fountain pen normally consists of four sections, including the nib as the contact point with the substrate, a round barrel on the writing end to hold the nib and feed, the feed under the nib to control the ink flow from the reservoir to the nib, and a self-filling soft rubber sac to reserve ink internally, as shown in Figure 1-10 (a). In writing, the pen draws ink from the inkwell through the ink fed to the pen tip and deposits the ink on the paper by gravity and capillary action.
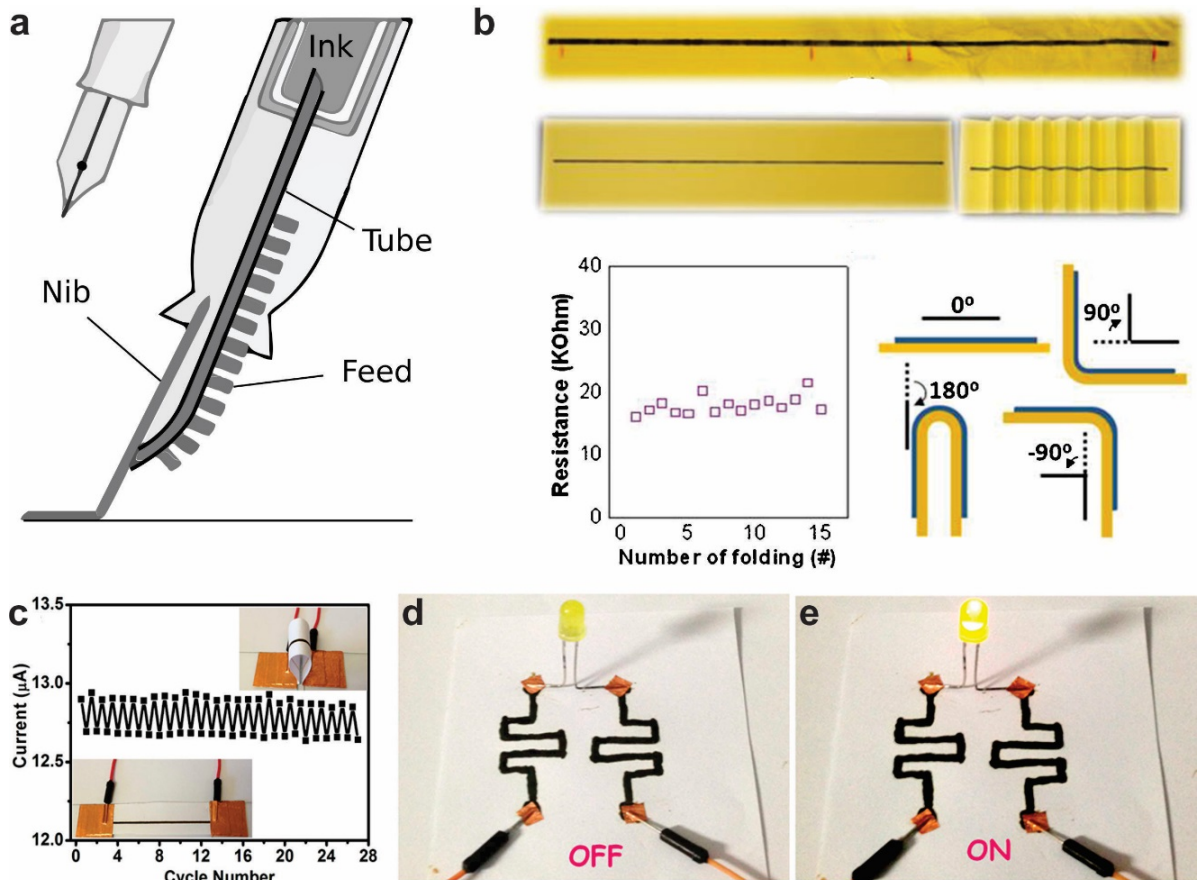
Figure 1-10. (a) Typical structure and working mechanism of a regular fountain pen. (b) Functional carbon-based circuits written using fountain pen and its resistance change under different numbers of folding cycles. (c)(d)(e) Conductive polyprrole arrays written on paper using foutain pens by reactive handwriting method.[156, 157] [Copy with permission]

Similar to the pen-based writing electronics approach, the fountain pen-based writing process is also based on the nature of solution processing technology, involving all kinds of functional materials. [156, 157] For example, light emitting diode (LED) circuits and chemical sensors that use carbon nanotubes as inks are successfully written on different surfaces. They retain their electrical function even after several prunes and indentations under water (Figure 1-11 (b)). [156] In another example, by writing electronic components with a fountain pen, a series of general purpose real-time gas sensors were fabricated for the detection of ammonia, heat and near-infrared radiation. Moreover, the electronics types can be further expanded by the so-called "reactive handwriting" electronics fabrication process. For example, conductive polypyrrole arrays were written on paper using $FeCl_3$ as polymerization agent, creating

conductive traces with enhanced durability and robust conductivity when bent (Figures 1-11 (c)-(e)). [157] Surface enhanced Raman scatterings (SERS) arrays on paper substrates were also achieved with a fountain pen loaded with noble metal nanoparticles by Polavarapu's group. [132] The as fabricated sensor arrays were capable of detecting toxic parasiticide molecules on sample substrate with concentration of 20 ppb in a 10 μL sample volume, demonstrating a promising future for handwritten sensors. The choice of conductive ink for direct writing of electronic devices using fountain pen is wider because of the limited evaporation rate of the ink and does not have a significant impact on the inks coming out of the nib tip. Therefore, a broad range of functional inks, such as metal nanoparticle inks, metal precursor inks, and carbon-based inks have been used to fabrication electronics using fountain pen.

Fountain pen with self-supplied conductive inks provides a simple, portable and inexpensive technique for direct writing of electronics. However, this kind of pen also has many drawbacks such as discontinuity, unexpected instability and spattering during writing caused by writing mechanism, resulting in great loss of resolution and the uniformity of the written pattern. Meanwhile, similar to the electronics written with ball pen, the written traces usually need time-consuming post treatment process for a better conductivity. The above-mentioned disadvantages greatly reduce the popularity of fountain pen in the area of handwriting electronics and cloud the future perspective of such tool as a fabricating tool for flexible electronics.

1.2.2.4.   Pencil

Pencil is a type of writing instrument made up of a narrow, solid core of paint in the center with a protective shell to prevent it from being damaged or leaving dirt on the user's hand, as shown in Figure 1-11 (a). [158]Different from the above-mentioned writing tools which rely on liquid or gel inks, pencil creates marks on substrates by physical abrasion (Figures 1-11 (b), (c)). [158] The first pencil was invented in England in the 16th century after the graphite was widely used to mark. Most pencil cores are made of graphite mixed with clay binder, leaving gray or black marks that can be easily erased. Graphite pencils are used for writing and drawing and produce durable markings which are highly resistant to moisture, most chemicals, UV radiation and natural aging. Attribute to the excellent electrical conductivity of graphite, commercially available pencils and home-made pencils have recently been used to fabricate flexible electronics. [159, 160] There are many different types of pencils on the market,

categorized by its hardness (H) and blackness (B). Pencils with greater "H" value (like 2H, 3H) have higher percentage of clay and binder in the core, making it more brittle and harder; while pencils with great "B" value (like 3B, 4B) have higher percentage of graphite (>70%) in the core, causing a darker written trace. Normally, traces written with higher "B" value show better conductivity due to the higher percentage of graphite and good conductivity of graphite. In addition, traces written by harder (larger H value) pencils are more electrically sensitive to substrate deformation. Therefore, based on these properties, different types of pencils are chosen for different applications.

For example, trace written with an HB pencil has been used as the anode and cathode of a paper-based fuel cell, and as the resistor element in fabricating resistor-capacitor filters. [161, 162] Pencils with higher H value have been employed to write sensors based on the resistance change, such as piezo-resistive sensors, [163] strain gauges and chemi-resistors. [164] Pencil with higher B value have been employed to write electronics with good conductivity, such as UV sensors and photodetectors written by 4B pencil (Figure 1-11 (d)),[165, 166] and carbon electrodes for paper-based electrochemical devices fabricated using 3B pencils.[167, 168] Pure graphite rods with higher electrical conductivity have also been utilized to write electronics on paper for better performance of the devices.[169]

Due to the fixed hardness and graphite content ratio of the commercially available pencil, the types and performance of sensors and written devices are greatly limited. Thus, home-made pencils with customized core composition have been developed and used to write electronics. [133, 170] For instance, Swage 's group developed a rapid strategy to fabricate carbon-based chemi-resistive sensors through writing with a home-made "pencil" which was produced by loading carbon-based nanomaterials, such as graphite, single-wall carbon nanotubes (SWNTs) or multiwall carbon nanotubes (MWNTs)), and special active agents for chemical detection into a die and subsequently compressing the mixed powder into the shape of conventional pencil, as shown in Figure 1-11 (e),(f). [171] As another example, Dossi et al. created customized pencils doped with electrode modifiers and with electrochemical deposition of Ag and AgCl for the production of stable and durable real-time biochemical sensors. [172, 173] Compared to commercial pencils, the customized pencils have more flexibility in the composition of the core, allowing the integration of other functional materials for written devices with tunable properties.
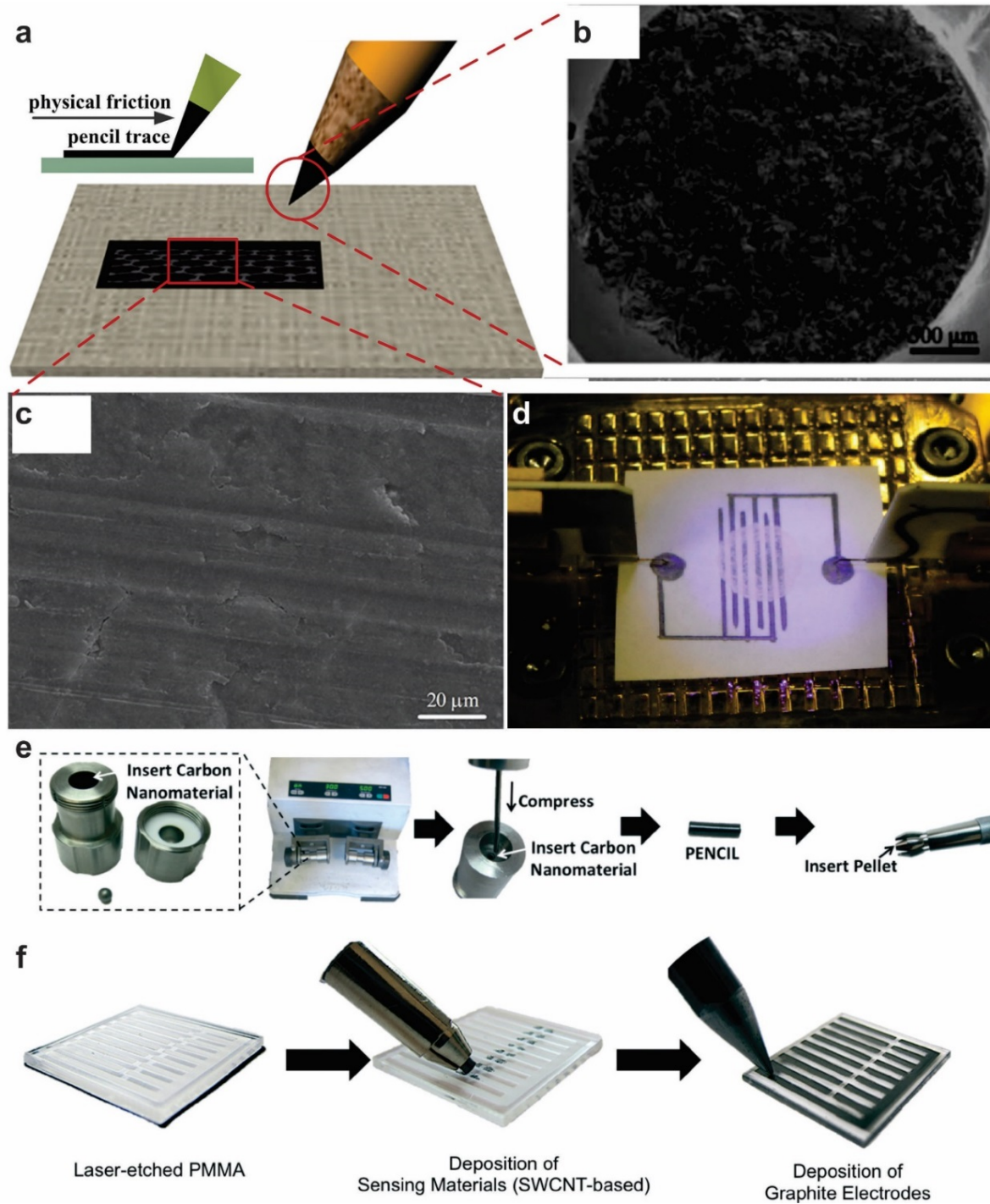
Figure 1-11. (a) Typical structure and working principle of a pencile. SEM images of (b) the core of pencile and (c) the surface morphology of the trace written with pencil. (d) Functional UV snesor written by 4B pencil. (e) Fabrcations process of a pencil with customized core compostion. (f) Handwritten sensors using pencil with different core composition. [160, 165, 171] [Copy with permission]

Writing electronics using pencils has been proved to be a low-cost and solvent-free technique for the fabrication of carbon-based electronics via repeated rubbing pencil lead onto substrates to form thin conductive graphite films. However, enough friction force is needed in the writing process in order to rub off the materials from the pencil core. This makes a rough surface of substrates is necessary for sufficient writing with a pencil and it is very difficult for a pencil to write on smooth surface, such as glass and plastic. Meanwhile, the harsh experimental environment needed for the fabrication of customized pencil core also makes this technique less attractive for both researcher and end-users.

1.2.3. Conclusion

Direct writing of flexible electronics is gaining popularity due to its low cost, simplicity, high portability and ease of use. Despite the reduced resolution and accuracy, pen writes are less demanding on the properties of inks and can be easily manipulated without professional skills. This combination of basic hand-held tools and modern electronic devices represents a significant step forward that enables DIY and desktop manufacturing of wearable electronics, biomedical sensing/diagnostic systems, and new generation of power storage systems. Circuit prototypes can be quickly made on site without the need for advanced equipment, providing great convenience for end-users and resource-limited areas. Traditional writing instruments, such as ball-point pens, pencils, pens, brush pens and marker pens, have been ingeniously modified as practical apparatus for achieving writing electronics. Most of the work focused on the direct writing of conductive inks, including metal nanoparticles inks, carbon-based inks, conductive polymer inks and liquid metals, among which, metal nanoparticle inks hold the advantage of relative high conductivity but are subjected to high cost (compared to metal salt) due to the professional equipment and strict synthesis process needed during the production. Such metallic inks are associated with a critical limitation of demand for post-treatment such as heating, laser annealing, hot pressing and plasma to form patterns with good conductivity.

It is worth of notice that although the direct pen writing process proves to be rapid, simple and portable, it is still a bit far away from an ideally easy, safe and cost-effective method for fabricating electronics. The required conditions like high temperature, long time, and vacuum atmosphere are essentially required for many specific applications. The other evident challenge for handwriting electronics refers to the present shortage of accessibility with complicated electronic components and devices, and even integrated circuits, which are of crucial

importance to electronics industry. Targeted at end-users with no professional skills and point-of-care applications, safety becomes one of the most important concern for hand writing electronics. The written circuits are expected to be handled and touched randomly by our fingers. If not properly treated, those exposed, unsealed nanoparticles will stick on the skin no matter of what. Metallic inks usually contain large numbers of nanoparticles smaller than 50 nm, at this scale, these nanoparticles get great chances to go through skins and finally circulate in the body. Many reports have recently addressed the protential toxicity of metal nanoparticle to human body, thus it is urgent to develop new techniques to enhance the safety of this emerging technology. In addition, it is suggested that more fundamental work is urgently needed to focus on developing new ink materials and new fabrication strategies to reduce time and energy consumption in post-treatment processes, and enhance the safety, to further perfect the direct writing paradigm. Meanwhile, the combination with printing technology with enhanced productivity, namely the pen-analogue writing technique, is worthy of investments and efforts to further transform the pen-based writing electronics into wide-spread manufacturing.

1.3. Challenges

Printed electronics has experienced enormous breakthrough during last decade, however, most of the existing printing techniques are based on wet methods. Usually, solution processable and electrically active materials, such as metal nanoparticles or conductive polymers, are formulated into different inks for printed electronics. Metal nanoparticles like Ag nanoparticles have been widely studied as promising functional materials for conductive inks, enabling the printing of conductive patterns on flexible substrates. However, for conductive inks composed of small metal nanoparticles, large amounts of stabling, capping and modified agent are required to prevent the nanoparticles from aggregation, precipitation and oxidization, resulting in a low solid loading and high impurity content, and consequently, causing a high resistance of the printed patterns. Though many efficient sintering methods such as selective laser sintering, pulsed light sintering, plasma and microwave flash sintering have been well developed recently to anneal the pattern and yield an improved conductivity up to 60% of bulk materials, the resistance of these printed conductive traces are still high due to the thin (<1 μm) conductive layer, making the printed electrodes hard to fulfill the requirements of the electronics industry. In addition, the preparation of high-quality ink is usually complicated and

costly. In terms of ink formulation, it often has strict requirements of viscosity and surface tension. The printing quality can be easily affected by the intrinsic limitation, like pinhole formation, and the adhesion of the ink to the substrate is also a common challenge for all wet processing techniques.

As an alternative to those printing techniques, direct pen writing of flexible electronics is gaining popularity for its low-cost, simplicity, ultrahigh portability and ease of use. Handwriting electronics face similar challenges with printed electronics, since they both use similar ideas to fabrication electronics. The difference is that handwriting electronics target at end-users who have no access to those professional sintering equipment, adding new barrier for the applications of such emerging technology. Thought self-sintering of silver nanoparticles was demonstrated recently by triggering the self-assemble and/or coalescence of nanoparticles at room temperature. [174-176] However, the conductivity of such self-sintered traces is still in the low-end range with sheet resistance in the level of several hundreds of mΩ/sq and resistivity 2-3 times higher than bulk materials. In addition, the use of nanomaterials-based inks imposes safety concerns. The written circuits are expected to be handled and touched by users during normal use, providing good chances for those exposed and unsealed nanoparticles to adhere to the skin. Metallic inks usually contain large numbers of nanoparticles smaller than 50 nm; at this scale, these nanoparticles can permeate skin and enter the bloodstream, which may have unknown damage to human's body. [177-181] In brief, though direct pen writing process has proven to be rapid, simple and portable, there are still ways to go before it is an ideal easy, safe and cost-effective method for fabricating electronics, considering all the aforementioned challenges and limitations.

1.4. Objectives

Conductive traces are the most fundamental element in all kinds of electronics devices, and in most cases, will largely affect the overall performance of final products. Therefore, the ultimate objective of this thesis is to develop new technologies for the fabrication of conductive traces that are capable of improving the performance, while at the same time lowering the manufacturing cost of the printed/handwriting electronics. To accomplish this, new fabrication strategies will be proposed and investigated to address some of the challenges in this area. The specific objectives include:

- Development of low-cost fabrication strategies for printed electronics on paper.

- Development of special engineered coating for adhesion enhancement and substrate protection.

- Fabrication of single and multilayer circuits on paper.

- Fabrication of electronics devices on paper.

- Development of solvent-free printing method to fabricate printed electronics.

- Development of a low-cost fabrication strategy for handwriting electronics with enhanced performance and safety.

1.5. Thesis Outline

As already seen, Chapter 1 consists of background information relevant to the thesis work and the overall project objectives. In Chapter 2, a strategy to easily fabricate hybrid copper-fiber highly conductive features on low-cost cellulose paper with strong adhesion and enhanced bending durability will be introduced, including the development of functional coating for fast surface modification of cellulose paper via an in-situ cross-linking mechanism between pyridine and epoxy groups. Chapter 3 will introduce the fabrication of high performance, multilayered paper-based circuits which contain highly conductive vertical interconnected accesses (VIAs) without physically drilling holes or depositing additional dielectric material. Chapter 4 will introduce the development of a scalable fabrication strategy for high-performance, binder-free, all-solid-state supercapacitors using conventional cellulose paper and an inkjet printer. The idea of "engraving 2D materials on 3D structures" will be proposed and discussed in detail in this chapter. Chapter 5 will highlight the development of a solvent-free digital printing method for the fabrication of highly conductive circuits, which eliminates those critical disadvantages faced in solvent-based printing techniques. In Chapter 6, a one-step react-on-demand (RoD) method for fabricating flexible circuits with ultra-low sheet resistance, enhanced safety and durability using a regular marker pen will be discussed in detail. In addition, a special functionalized coating and a three-dimensional metal-polymer conductive structure will be introduced in this chapter. Finally, Chapter 7 provides conclusions and summary of all the results reported within the thesis, along with recommendations for future work.

Chapter 2

2. Fabrication Strategy of Hybrid Copper–Fiber Conductive Features for Low-Cost High-Performance Paper-Based Electronics

2.1 Introduction

Printed electronics (PE) technology, which harnesses the existing manufacturing capabilities of the graphic industry to produce circuitries cheaply and quickly, has garnered remarkable attention in the last decade.[50, 182, 183] This vibrant new technology is transforming the electronics industry by replacing traditional costly methods of fabricating electronic components, devices or even systems. Increasingly, printed thin-film transistors,[184-186] conductors,[187, 188] inductors and capacitors are being integrating with electronics devices to develop novel systems,[189-191] such as thin-film energy harvesting/storage system, smart labels, radio frequency identification (RFID) tags and memory devices.[192-195] A world full of flexible, wearable, even stretchable devices developed by printing technology is foreseeable in the near future. Many demonstrations of paper electronics have been made recently; however, many examples involve the use of plastic-covered paper substrates, photopaper lamination of a plastic film (electronics paper tickets), gluing of electronics components, or silicon chips onto a paper substrate.[196, 197] These substrates have better chemical and physical properties than regular cellulose paper, but are generally more than 10 times as expensive. Fabricating highly conductive circuit on cellulose paper is challenging; cellulose paper typically has high roughness, and cellulose fiber forms a highly porous structure that tends to absorb functional materials (e.g. metal nanomaterials, carbon nanotubes) instead of leaving them on the surface. This prevents conductive materials inside the ink from contacting each other, making it impossible to form a highly conductive layer even after sintering, which leads to relative low performance in paper-based electronics.[120, 198] Meanwhile, the capillary effect of the paper also causes a significant loss of resolution when printing with solvent-based ink. Furthermore, the thickness of the conductor is crucial to many electronics applications. For the same conductor, a thicker layer means a smaller sheet resistance, and thus the thickness usually determines the maximum current the circuits can handle. In the electronics industry, a standard

printed circuit board with a 35 μm thick copper layer is adopted for most devices. IoT requires a large number of RF devices to communicate with each other and harvest wireless energy for power. Typically, if the working frequency is higher than 1 MHz, then we need to consider the skin effect, i.e. the antenna conductor has to reach a certain thickness for optimum performance.[199] For example, a copper antenna operating at 13.56 MHz has a skin effect depth of 17.7 μm which means the thickness of the printed antenna has to be at least ~17.7 μm for best performance.[200] However, direct printing of conductive materials via a roll-to-roll compatible digital printing process cannot reach this level,[182] which greatly limits its application in both RF devices and regular printed circuits. All these obstacles cause traditional paper-based electronics to suffer in performance and resolution. Thus, it is important to find a solution to these issues to fully utilize the low-cost, environmental-friendly properties of cellulose paper.

Electroless metal deposition (ELD), which relies on an autocatalytic redox reaction to deposit various metals on a catalyst-preloaded substrate,[72] offers a low-cost yet convincing solution to the thickness issue. Printed circuits fabricated using ELD have been demonstrated on various substrates such as PET, PI, photopaper, and even yarns.[64, 201-203] The thickness of the deposited metal layer can be finely tuned by the deposition time, but new challenges concerning adhesion and diffusion appear when thickness is increased. Untreated flexible substrates struggle with capturing catalyst moieties due to lack of binding sites, and simple physical absorption cannot prevent peeling of the deposited metal, especially if the thickness of the deposited metal exceeds 5 μm. For cellulose paper, the loosely deposited metal particles tend to migrate out of the printed edge, resulting in a severe loss of resolution. As deposition time increases to achieve a thicker metal layer, more and more traces in the circuit will form connections with one another and become short circuited. Surface modification techniques such as UV-oxygen plasma,[204] surface silanization,[205, 206] polyelectrolyte multilayer (PEM),[207, 208] and polymer grafting have been reported to enhance the adhesion between the electroless deposited metal layer and substrate.[209] However, most of them are still far away from scalable cost-effective application, due to their complex and/or environmentally unfriendly process, harsh experimental conditions, and/or the difficulty of scaling up. Thus, there is a need to develop a simple, low-cost, and effective surface modification method for

cellulose paper to achieve fabrication of high resolution thick copper (>20 um) paper-based electronics with strong metal-paper bonding.

In this paper, a simple, cost-effective one-step dip-coating method is developed based on the thermal-initiated crosslinking of epoxy and pyridine rings for surface modification of cellulose paper. Inkjet printing and silver-ion-catalyzed ELD were employed to metalize the surface selectively. Due to abundant pyridine ligands on the surface, the modified paper shows a strong and reliable ability to bond with deposited copper during ELD. Despite the strong bonding between the deposited metal and coated polymer, the unique porous structure of paper allows its cellulose fibers to act as physical anchors, producing a copper-fiber conductive structure. Such reinforced structure not only prevents the delamination of copper film, but also enhance its bending durability. Through this method, highly conductive copper layers with sheet resistances as low as 0.00544 Ω/sq can be achieved on cellulose paper without visible loss of resolution. Thanks to its unique copper-fiber structure, the change in resistance after 10000 bending cycles is kept within 13% of the original value. To demonstrate the promising applications of the proposed method, a battery-free functional lightening circuit and a RFID antenna were fabricated and tested. The as-fabricated narrow band paper antenna exhibits a return loss of -30db at its working frequency, demonstrating its potential use in low energy consumption RF devices.

2.2 Experiment Details

Materials

Polyvinylpyrrolidone (PVP, Mw ~40,000), Poly(4-vinyl pyridine) (P4VP, Mw ~60,000), anhydrous glycerol ($C_3H_5(OH)_3$,99%), 1,4-dioxane (99.8%), 2-propanol, silver nitrate (99%), ethanol (anhydrous, denatured), copper sulfate pentahydrate ($CuSO4\cdot5H2O$, 98%), formaldehyde (36.5-38% in water), sodium hydroxide (97%), potassium sodium tartrate tetrahydrate($C4O6H4KNa\cdot4H2O$, 99%), ethylenediaminetetraacetic acid disodium salt dihydrate (EDTA·2Na, 98%), 2,2'-dipyridyl (98%), and potassium ferrocyanide (II) trihydrate ($K4Fe(CN)6\cdot3H2O$, 98.5-102.0%) were purchased from Sigma-Aldrich. SU-8 was provided by Kayaku Micro Chem. All chemicals were used as received without further purification. Cellulose paper substrate was provided by Xerox.

Preparation of Coating Solution

2.5 g of Poly (4-vinyl pyridine) and 100 mg of polyvinylpyrrolidone were dissolved in 50 mL ethanol, and 2 grams of SU-8 was dissolved in 1,4-dioxane to obtain 40 mg/ml solution. The two solutions were then mixed at 1:1 volume ratio to obtain a transparent solution. The final solution contains 25 mg/mL P4VP, 1 mg/Ml PVP and 25 mg/mL SU-8.

Surface Modification of Cellulose Paper

Untreated cellulose paper was directly immersed into the coating solution for 5 seconds. The paper was then slowly drawn out of the solution and dried in air at room temperature for 5 minutes. Lastly, the coated paper was placed into an oven at 135°C for 20 minutes for in-situ cross-linking of SU-8 and P4VP molecules.

Preparation of Catalyst Ink for Inkjet Printing

A glycerol–water solution was prepared by mixing anhydrous glycerol and distilled water at a volume ratio of 3:2. Silver nitrate was then added, followed by mixing in a VWR mixer for 4 minutes to form a 60mg/mL silver slat solution. The prepared ink was degassed in a vacuum chamber at 2 psi for 1 hour to remove dissolved gases and bubbles. The viscosity and surface tension of the final ink were 11.5 cp and 53.5 mN/m, respectively. These values fall within the optimum operating range for the Dimatix DMP-2800 printer. A 0.2 μm nylon syringe filter was used to remove undesired particles from the ink.

Inkjet Printing

The ink was filled into a cartridge mounted on a 10 pL piezo-electric drop-on-demand (DOD) inkjet printhead. Printing parameters were set as following: drop space, 30 μm; meniscus vacuum, 3.5 inch of H$_2$O; print head temperature, 25 ^{o}C; print head angle: 4.2^o; jetting voltage 25.1 V. Printing was conducted at room temperature.

Electroless Deposition of Copper

An electroless copper plating bath consisting of CuSO4·5H2O (14 g/L), NaOH (12 g/L), potassium sodium tartrate (16 g/L), EDTA·2Na (20 g/L), HCHO (26 mL/L), 2,2'-dipyridyl (20 mg/L), and potassium ferrocyanide (10 mg/L) was prepared according to literature. Modified

cellulose papers with printed silver nitrate patterns were immersed into the bath for different periods of time.

Characterization

FT-IR analysis was performed using a FT-IR NICOLET 6700 (Thermo Scientific Co.). FE-SEM images were taken by a LEO (Zeiss) 1530 field-emission scanning electron microscope (FE-SEM). The viscosity of the ink was measured with a Gilmont GV-2100 Falling Ball Viscometer using a 316-stainless steel measuring ball. Sheet resistances were measured by a four-point probe station Lucas Labs S-302-4 (probe SP4) connected to a Keithley 2750 multimeter. Height information was generated using a Dimension V atomic force microscope (AFM). X-ray diffraction analysis was done using a Rigaku Ultima-IV XRD goniometer.

2.3 Results and Discussion

Poly (4-vinylpyridine) (P4VP) has been used for surface modification purposes to uptake silver ions due to its strong chelating ability with transitional metal ions.[210, 211] As a reactive monomer, 4-vinylpyridine was used to modify substrate via in-situ polymerization triggered by UV and/or plasma. Such cross-linked molecules form covalent bonds with the pretreated substrate, achieving good adhesion. However, a low film production rate and high equipment demands make this method not cost-effective and unsuitable for coating cellulose paper. P4VP molecules can be directly coated onto the substrate by physical absorption, but the poor adhesion will result in serious delamination of the electroless deposited metal.[212] The reaction mechanism between epoxy and pyridine groups has been well studied in recent years, and P4VP molecules have been shown to be also capable of crosslinking with epoxy.[213, 214] Meanwhile, the highly reactive epoxy groups can form strong bonds with cellulose fiber due to the many hydroxyl groups along its surface. Thus, in this work, SU-8 and Poly (4-vinylpyridine) (P4VP) were adopted as the main components of the coating compound. Figure 2-1 shows the fabrication process of making high performance circuits on cellulose paper.
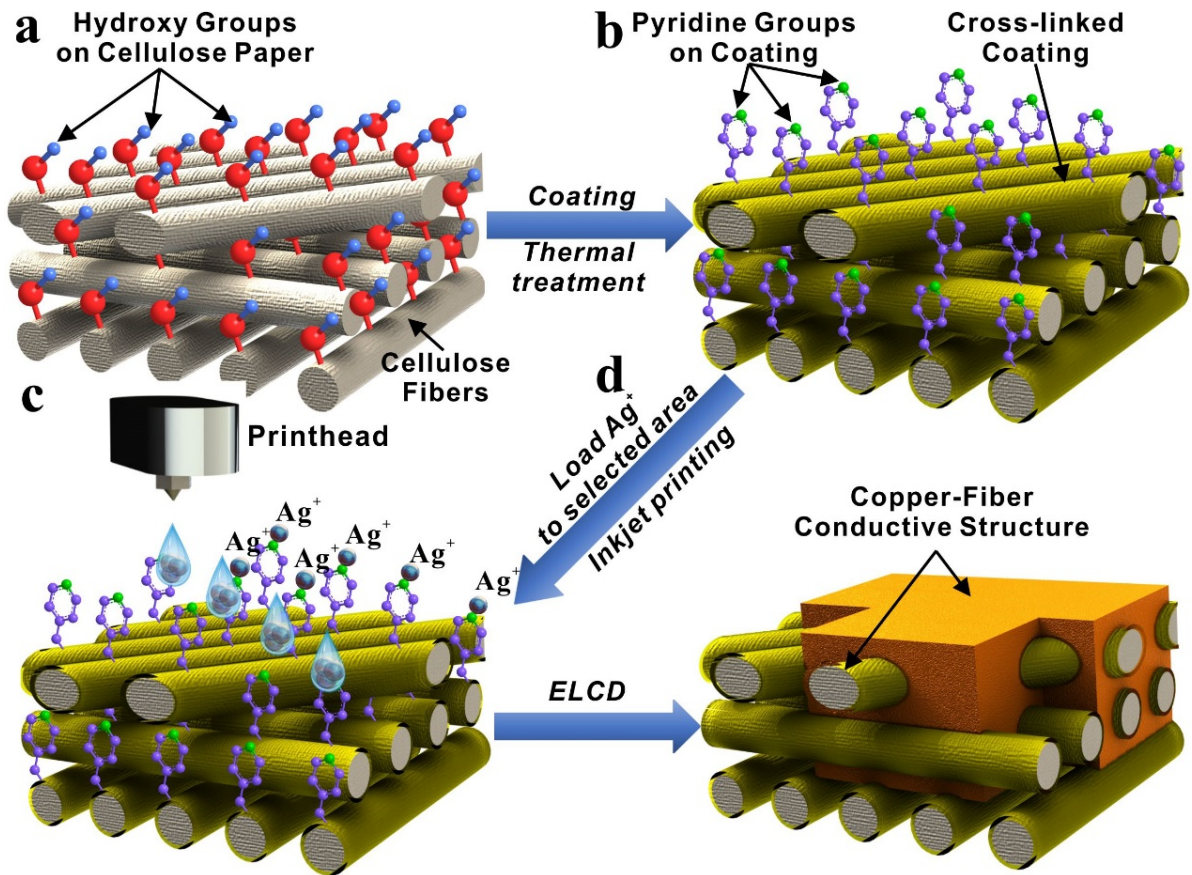
Figure 2-1. Fabrication process of a copper-fiber conductive structure on cellulose paper. (a) Cellulose paper with hydroxy groups on the surface. (b) Coated cellulose fibers with abundant pyridine groups. (c) Inkjet printing of silver ion loaded inks. Silver ions are captured by pyridine groups along fibers. (d) Copper-fiber structure forms after ELCD process.

The coating solution was prepared by dissolving P4VP and SU-8 in a mixture of 1,4-doxane and 2-propanol. A small amount of polyvinylpyrrolidone (PVP) was also added to the coating solution to enhance its ability to capture silver nanoparticle in the initial step of the electroless copper deposition (ELCD) process. The coating was then applied to cellulose paper via the dip-coating method and cured in air at 130°C, inducing covalent bonding between cellulose paper and SU-8 and forming a thin layer of functional coating. Meanwhile, SU-8 forms covalent bonds with the pyridine groups of P4VP, leaving abundant pyridine ligands along the fiber to capture catalyst metal ions during the subsequent step (Figure 2-1(b)). Aside from serving as a bridging agent between P4VP and the fiber surface, SU-8 also helps to protect the paper during an extended ELCD process. Due to the ring-opening reaction of epoxide groups,

the dominant bonding type will be carbon-oxygen bonds. Such bonds are highly resistant to alkali solutions, allowing the proposed coating to withstand the highly alkaline ELCD solution (12 pH). In the following step, silver ions were loaded to selected areas of the coated paper by inkjet printing of silver nitrate ink (Figure 2-1(c)). When the ink hits the substrate, the lone electron pair in the nitrogen atom of the pyridine ligands will attach to the silver ions to form strong coordination bonds. Such chemical bonding is much stronger than simple physical absorption and helps keep the absorbed silver ions adhered to the surface. The sample was then put into an ELCD bath to induce copper growth. Due to the porous structure of cellulose paper, the ink will penetrate to a certain depth, forming a 3D catalyst-loaded area. This special feature allows the copper to grow in a three-dimensional manner, generating copper at a much faster rate than traditional surface-only reactions. Lastly, a highly conductive copper-fiber structure is generated (Figure 2-1(d)). The fibers not only enhance the flexibility of the circuits, but also act as anchors to firmly hold onto the deposited copper, preventing any delamination and/or peeling of the metal.
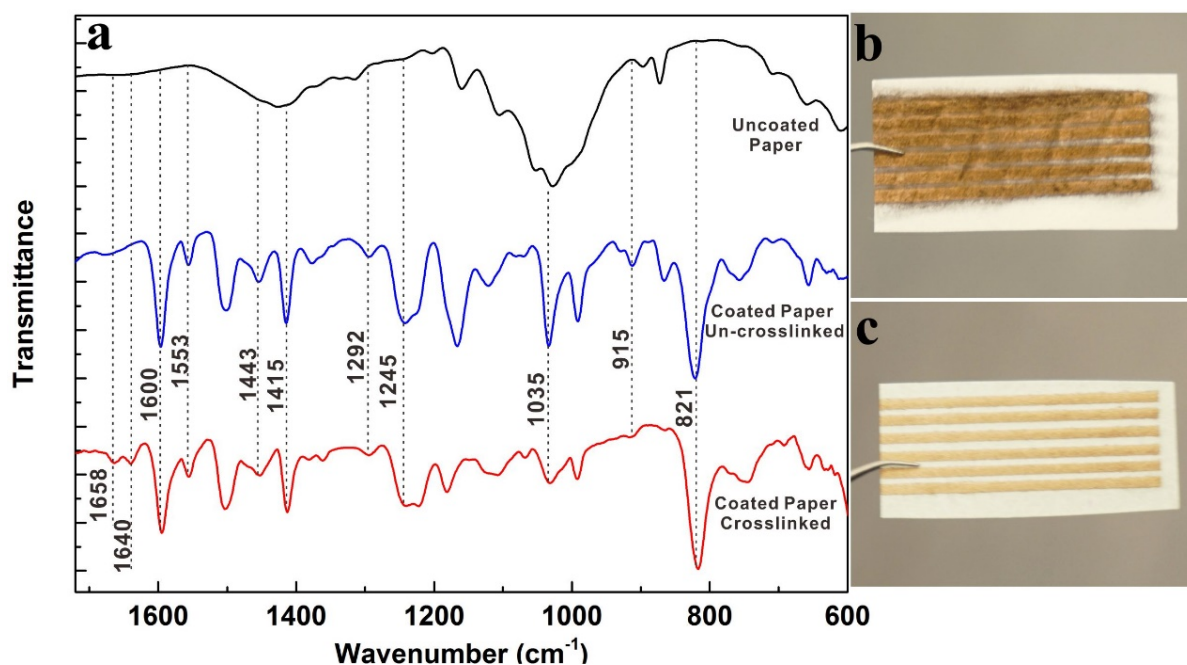
Figure 2-2. (a) FT-IR spectra of uncoated cellulose paper, coated paper and coated paper after thermal treatment from top to bottom with marked characteristic peaks; (b) Optical image of 3-hour electroless copper plating on uncoated cellulose paper; (c) Optical image of 3-hour electroless copper plating on coated and cross-linked cellulose paper. Both samples share the exact same fabrication process.

Figure 2-2(a) shows the FT-IR spectra of uncoated cellulose paper, coated paper before thermal treatment, and coated paper after thermal treatment. By comparing these spectra with the standard infrared transmittance spectra, we can determine the interaction between different functional groups on the substrate and coating. Bands at 821, 1415, 1553, 1600 cm^{-1} corresponding to pyridine groups are present only on the spectra of coated papers, implying the successfully introduction of P4VP in the composite coating layer.[213] The peaks at 915 and 1245 cm^{-1} correspond to the stretching vibration bands of epoxide groups in SU-8, and the peaks at 1443 and 1292 cm^{-1} match the stretching frequency of C-N-C and N-C, respectively, which belong to the pyrrolidone groups in PVP.[215, 216] These peaks prove the presence of PVP and SU-8 on the coated paper. After thermal treatment, the stretching vibration band of epoxide groups at 1245 and 915 cm^{-1} are weakened greatly, which suggests the occurrence of the crosslinking reaction. Meanwhile, two new peaks appear at 1640 and 1658 cm^{-1}, which can be ascribed to the newly-formed carbonyls of pyridone and the unconjugated carbon double bonds.[213] In addition, the peaks for pyridine groups at 1415 and 1600 cm^{-1} show a slight decrease in strength while the other two pyridine peaks at 821 and 1553 cm^{-1} remain the same. This indicates that only a small amount of pyridine ligands reacts with epoxide groups during the thermal treatment process, and so many available pyridine groups remain along the fibers to uptake silver ions in the following fabrication step. Figure 2-2 also shows a comparison of 3-hour ELCD results on uncoated (Figure 2-2(b)) and coated (Figure 2-2(c)) cellulose paper. Both samples were prepared in the exact same way except for the coating. The uncoated paper (Figure 2-2(b)) suffers serious loss of resolution during the ELCD process due to the lack of strong bonding between silver ions/nanoparticles and the substrate. Highly water-soluble silver nitrate will migrate around when the sample is submerged in the ELCD bath. Although silver nanoparticles will form at the very early stage of ELCD and the unique porous structure of paper will help trap them to some extent, physical absorption is not sufficient to fully prevent diffusion. In cases where extended ELCD is required to lower resistances, the severely diffused copper will cover the whole area of the substrate, leaving no printed feature on it. Conversely, Figure 2-2(c) shows the results of coated paper after 3 hours of ELCD, from which we can see negligible diffusion and clear conductive copper traces with clean edges.
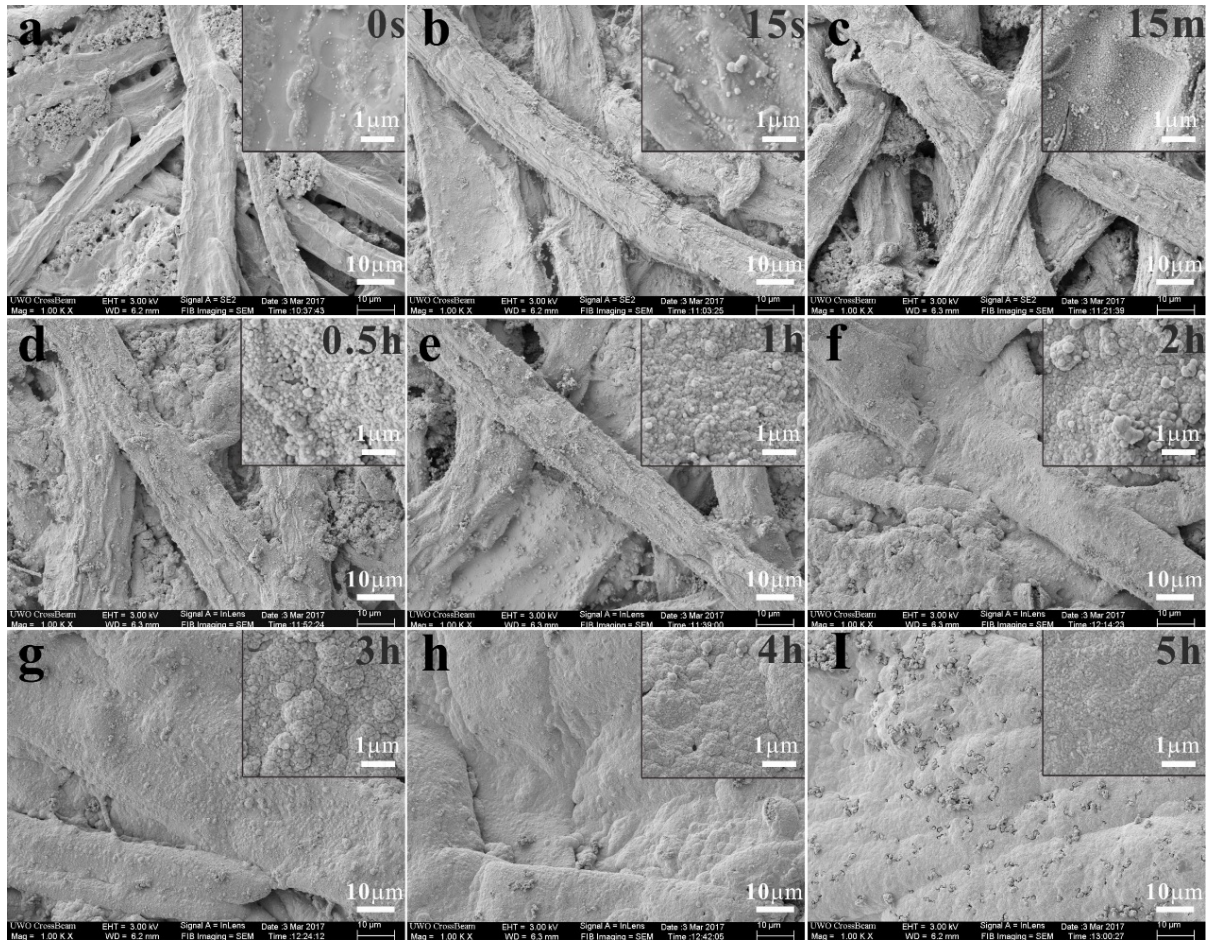
Figure 2-3. SEM images of surface morphologies of electroless deposited copper samples with different plating times of (a) 0 second; (b) 15 seconds; (c) 15 minutes; (d) 0.5 hour; (e) 1h; (f) 2h; (g) 3h; (h) 4h; (I) 5h. At the top right corner of each image is a zoomed-in picture of each sample.

The surface morphology during the ELCD process was investigated with field emission scanning electron microscopy (FE-SEM). FE-SEM images of samples with ELCD time ranging from 0 to 5 hours are shown in Figure 2-3, illustrating the formation of the copper-fiber structure. At the top-right corner of each picture is a zoomed-in area of the same sample. Figure 2-3(a) shows the surface of the coated cellulose paper after loading of silver ions via inkjet printing, revealing a porous structure formed by irregularly arranged cellulose fibers. In the zoomed-in picture, some nanoparticles several nanometers in diameter can be observed along each fiber; these nanoparticles are silver nanoparticles generated from a small fraction of the printed silver nitrate undergoing self-decomposition in light. 15 seconds after ELCD, many particles with diameters ranging from several to several hundreds of nanometers have

formed on the surface of each fiber (Figure 2-3(b)). Figure 2-3(c) shows the surface after 15 minutes ELCD; most parts of the cellulose fiber have been uniformly covered by nanoparticles, but the porosity of the substrate remains mostly unchanged. Figure 2-3(d)-(f) are FE-SEM images of the samples after 0.5h, 1h and 2h ELCD, respectively. During this period, copper grains of larger sizes are generated at higher density, while gaps between the fibers are gradually filled in by the newly grown copper. After 2 hours (Figure 2-3(f)), the coated cellulose fibers have been covered by a significant amount of copper and the porosity of the substrate has greatly decreased, but all fibers remain visible. After 3 hours (Figure 2-3(g)), cellulose fibers with clear edges are barely seen, since most gaps have been filled in by deposited copper, indicating formation of the copper-fiber structure. Most of the copper growth will occur on the surface from this point on. Figure 2-3(g)-(i), corresponding to surface morphologies of 3h, 4h and 5h ELCD samples, respectively, show how the surface becomes increasingly smooth as more copper is deposited. By the end of 5h (Figure 2-3(i)), there are no cellulose fibers that can be clearly seen on the surface, as all gaps have been completely filled in by deposited metal. The surface exhibits a slightly rippled morphology due to the underlying fiber structure. Some tiny pits are observed on the surface of the 5h sample, which may be attributed to hydrogen bubbles rising from the inner layer to the surface during electroless copper plating.
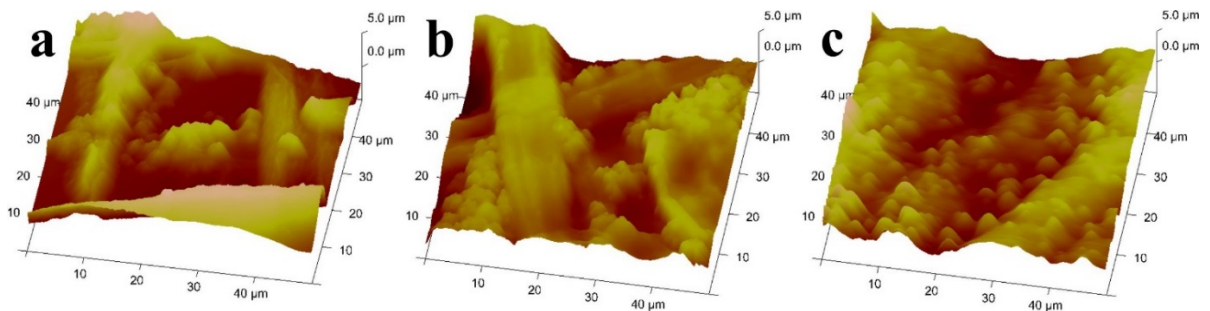
Figure 2-4. AFM three-dimentional images of surface morphologies of samples with different copper deposition time of (a) 0s; (b) 2 hours; and (c) 5 hours.
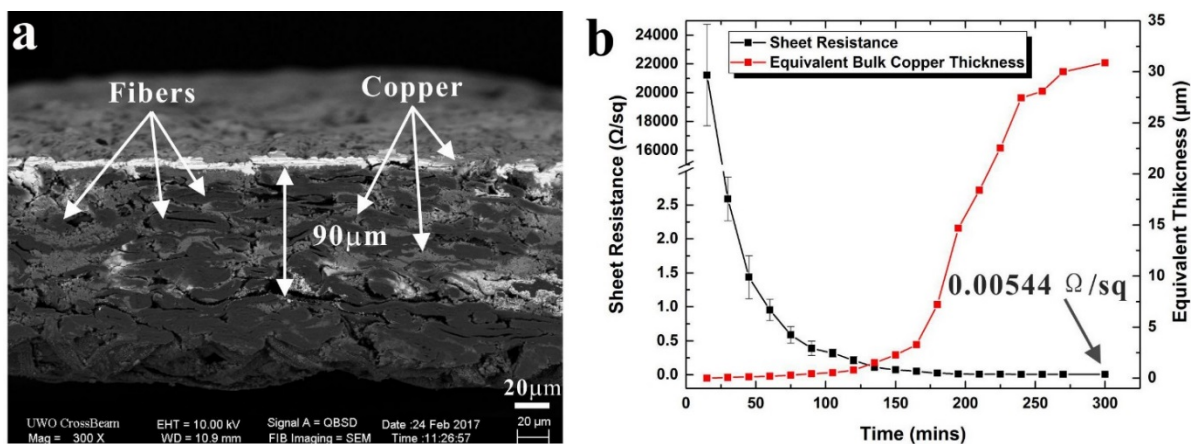
Figure 2-5. (a) FE-SEM cross-sectional image of sample with 300 minutes plating time, showing a copper-fiber hybrid structure with thickness of around 90 μm. The darker area represents cellulose fibers and areas with grey color represent deposited. (b) Graph showing the change of sheet resistance and its equivalent thickness in samples with different plating times ranging from 0 to 300 minutes. The lowest sheet resistance of 0.00544 Ω/sq was achieved after 300 minutes copper plating. copper.

To achieve a better visualization of the surface morphology, an atomic force microscope (AFM) was used to characterize the aforementioned samples. Figure 2-4 shows 3D images generated based on height information acquired from the AFM in tapping mode. Figure 2-4(a) presents the 3D surface of a sample prior to ELCD, in a 50 μm × 50 μm window. Cellulose fibers can be clearly seen in the image, with many gaps in between. Figure 2-4(b) and (c) show samples after 2h and 5h of plating, respectively. The gaps are gradually filled in with copper as plating progresses, and after 5 hours, the average surface roughness is reduced from 14.5 μm Ra (2h sample) to 3.3 μm Ra (5h sample). A rippled surface morphology consistent with the FE-SEM images is observed. The surface roughness of the sample prior to ELCD was not calculated because many gaps had a depth greater than 8 μm, which exceeds the maximum vertical displacement of the AFM tip. Figure 2-5(a) shows a cross-sectional image of the sample after 5h of plating, showing presence of copper growth underneath the surface, to a depth of around 90 μm. This indicates that with our current printing parameters, ink droplets can penetrate about 90 μm below the surface and activate a three-dimensional catalyst-loaded volume for ELCD. In theory, the penetration depth can also be fine-tuned by adjusting the printing parameters. For example, a jetting waveform can be used to control the volume and velocity

of a single droplet, factors which have a dramatic influence on the depth of ink penetration. From the cross-sectional image, we can also see that most of the gaps have been filled in with copper at the catalyst-loaded area. On top of the surface, a thin layer of copper with a thickness of around 2 μm can be observed, covering all of the deposited area. The cross-sectional image further confirms the formation of a copper-fiber structure.

The change of sheet resistance with plating time was investigated using a four-probe method. The measurement was conducted every 15 minutes during a 5-hour copper plating experiment. Due to the unique porous structure of the cellulose paper, the thickness of the deposited copper is impossible to measure directly, as all samples have the same ink penetration depth. Thus, in order to quantify the amount of copper per unit area, we matched the measured sheet resistance with the equivalent amount of bulk copper of a specific thickness (Figure 2-5(b)). After 15 minutes of plating, the sample becomes conductive with a very high sheet resistance of ~2.15 $\times 10^4$ Ω/sq, corresponding to the thin and loose copper layer shown in Figure 2-3(c). The sheet resistance quickly decreases during the first hour of ELCD, which is attributed to the growth and connection of copper grains. As the copper grains grows larger during the first hour, they progressively form more contacts with other grains and increase sheet conductivity, until finally, a dense and uniform copper layer is formed along each fiber (Figure 2-3(e)). The sample exhibits the fastest growing rate in equivalent thickness from 2.5 h to 3.5 h, which may be attributed to the rapid formation of copper-fiber conductive structure and the three-dimensional copper plating mechanism shown in Figure 2-3(f)-(h). In the following 1.5 h, the equivalent thickness growth rate decreases as most gaps have been already filled with copper and thus copper growth mainly occurs on the surface. After 5 h of electroless plating, samples present a fairly low sheet resistance of ~0.00544 Ω/sq, which is the same as bulk copper with a thickness of ~30 μm. This value is difficult to achieve with any other printing method and fulfills most thickness requirements of the printed circuit board industry. Thanks to the novel three-dimensional catalyst-loaded structure, we can also achieve a much higher average deposition rate (~6 μm/h) than in our previous ELCD papers.[73, 116, 217]

Traditionally, if a piece of electroless plated copper is thicker than 10 μm, then the coated copper tends to delaminate or bubble up from the substrate due to the lack of interlock between the top copper layer and the substrate. In this work, the functional coating and the cellulose fiber itself act as chemical and physical anchors for the deposited copper to achieve strong

adhesion, preventing any delamination or peeling of the copper. An ASTM standard tape test was conducted to evaluate copper adhesion in the previously prepared samples.[218] During the test, deposited copper conformally adhered to the surface during all iterations except the first, when an extremely small amount of surface particles was removed. The sheet resistance also remained unchanged throughout several iterations, demonstrating excellent adhesion according to the ASTM D3359 standard.
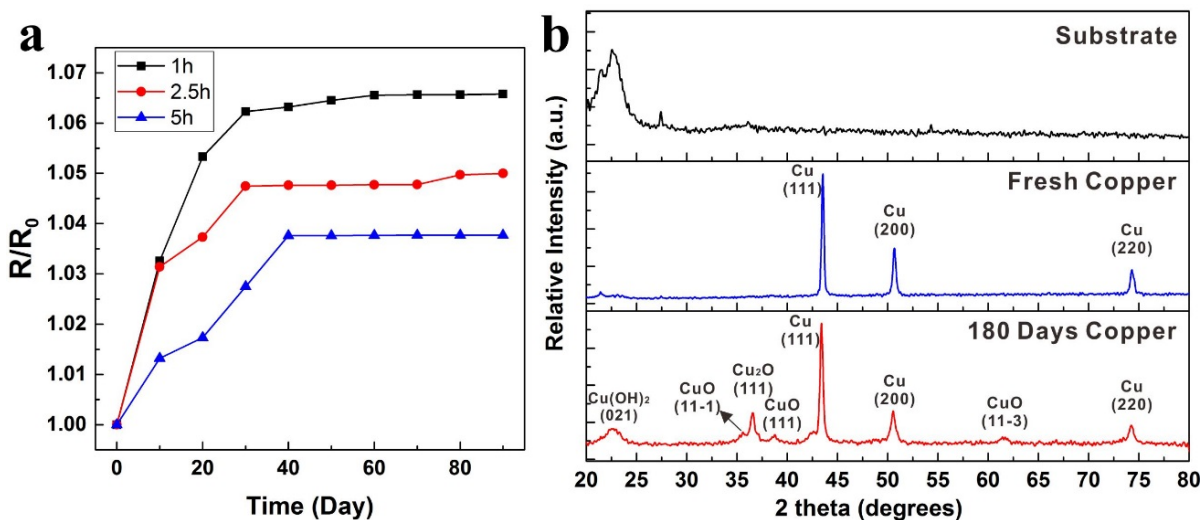
Figure 2-6 (a) The resistance changes of copper-fiber conductive traces with different copper plating time of 1 hour, 2.5 hours and 5 hours as a function of time. (b) X-ray diffraction spectra of substrate before copper plating, freshly deposited copper traces and copper traces stored in air for 180 days.

The porous structure of cellulose paper greatly enhances its deposition rate, adhesion and flexibility; however, the drawback of such a structure is that it could be more easily oxidized in air. Hence, the relationship between resistance and storing time was investigated. Figure 2-6(a) shows the resistance change of samples with 1h, 2.5h and 5h electroless plating time over a period of 90 days. All samples were left out in open air in a room without any temperature or humidity control. The resistance of all samples increases at a nearly constant rate (about ~0.15% per day) for the first 30 days before plateauing afterwards. The sample with the longest deposition time (5h) exhibits the smallest increase in resistance after 90 days (3.5%), which may be attributed to its lower porosity and the generation of a thin copper top layer due to the extended ELCD. The other two samples show slightly higher increases, with the maximum resistance increase of ~6.5% seen in the 1h ELCD sample. X-ray diffraction (XRD) was

conducted to study the crystalline structure of the resultant copper layer, as well as the surface metal composition of fresh samples compared to samples stored for 90 days. Figure 2-6(b) presents the XRD patterns of the coated paper substrate, freshly made copper, and copper stored in air for 90 days. Both freshly prepared samples showed peaks at 43.46°, 50.43° and 74.25 ° that could be assigned to Cu crystal plane (111), (200) and (220), respectively (JCPDS Data 04-836). For the sample stored in air for 90 days, several new weak peaks appeared in the spectrum. Peaks at 23.8° and 36.4° correspond to the (021) plane of $Cu(OH)_2$ crystal (JCPDS Data 80-0656) and (111) plane of Cu_2O (JCPDS Data 05-0667) crystal, respectively. The other three very weak peaks at 35.5°, 38.7° and 61.5° can be assigned to the (11-1), (111) and (11-3) planes of CuO (JCPDS Data 48-1548), respectively, indicating a very small amount of CuO present on the surface. From the XRD results, we can conclude that oxidation from extended storage in open air generates mostly Cu_2O and $Cu(OH)_2$. Furthermore, most oxidation takes place in the first 30 days and has limited influence on the resistance of the samples (<10%). It is also worth mentioning that the circuits could be easily protected from oxidization using either conformal coatings or electroless nickel plating for longer shelf life.
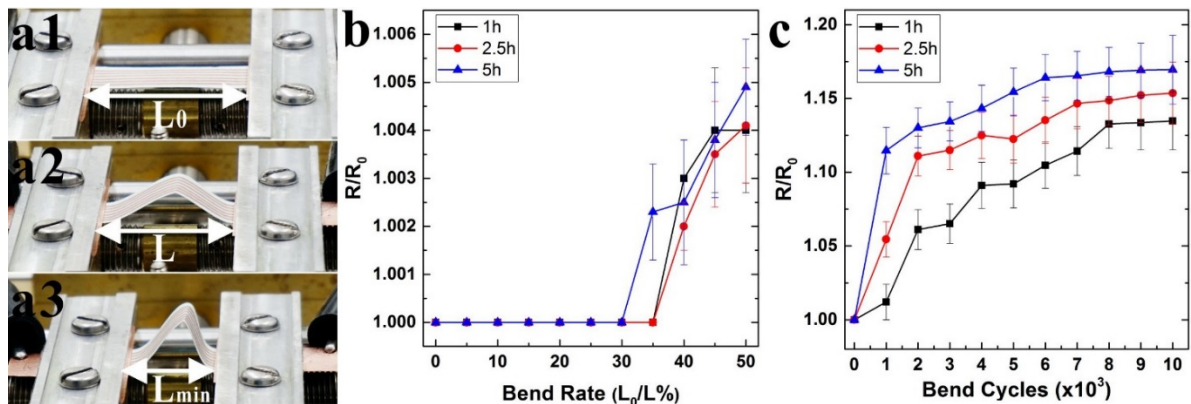
Figure 2-7(a) Optical images of a copper electrode array in flat state with initial length of L0 (a1) and bent states with length of L (a2) and maximum bend radii with Lmin (a3). The change of electrical resistance in electrodes with 1 hour, 2.5 hours and 5 hours copper plating time as a function of (b) bend rate (L0/L) and (c) bend cycles.

To investigate the mechanical flexibility of the fabricated features, a linear array of five copper traces (length = 5 cm, width = 2 mm) spaced 1.5 mm apart was fabricated on cellulose paper using the proposed method. The electrode-patterned cellulose paper was actuated between flat

and bent states at a bending rate of 3 cm/s using a custom-made stretching stage coupled to a computer-controlled step motor. A Kethley multimeter was connected to the two terminals of the stretching stage in a four-probe sensing mode to measure the resistance of the sample. Figure 2-7(a) shows the tested sample at different bending states. L_0 is the initial distance of the two terminals; we divide this value by the actual terminal distance L to calculate the "bend rate" of the sample, i.e. Figure 2-7(a3) shows a specimen with a bend rate of 50% ($L_{min} = 2.5$ cm, $L_0 = 5$ cm). Figure 2-7(b) shows the average change in resistance under different bending ratios, ranging from 0% to 50%. When the bending ratio is less than 30%, the resistance is unaffected, and even when the bending ratio exceeds 30%, there is just a slight increase in resistance (maximum increase of <0.5%). These results demonstrate the excellent flexibility of the sample. We also measured the resistance change of samples with different electroless plating times as a function of bend cycles (Figure 2-7(c)), where for each cycle, the sample was actuated from a bending ratio of 0% to 50% at a rate of 3 cm/s. All samples exhibit a slight but rapid increase in their electrical resistances during the first 2000 cycles, which thereafter continues to increase but at a slower rate. The crack on the surface copper could explain the initial rapid increase in the resistance, and thus samples with a thinner copper top layer (shorter ELCD time) exhibit smaller increases in resistance. Overall, however, all samples exhibit good bending durability after 10000 cycles, with a total resistance increase of 13%, 14% and 17% over original values for the 1h, 2.5h and 5h samples, respectively. Compared to traditional surface-only conductive features, the bending durability is greatly enhanced by the copper-fiber conductive structure. Figure 2-8(a1),(a2) shows how an LED light powered by our copper-cellulose conductive traces remains operational under both normal and bent states.

To demonstrate the versatility of the proposed technique in real world applications, we produced a battery-free flexible LED lighting array and a RFID antenna on cellulose paper. For the first example, a circuit with a receiving coil operating at 150 kHz was designed and fabricated using the proposed method to harvest energy from RF. Nine LEDs with different colors (red, orange, yellow) were then mounted onto the circuit by 3M z-axis conductive tape (Figure 2-8(b)). As a battery-free device, these LEDs will light up using energy harvested from the receiving coil. The fabricated device is flexible and lightweight and can be attached to various surfaces. For example, the device was attached to a glass bottle and placed into a 150-kHz 3D electromagnetic field (EMF) generated by a custom-made device. All LEDs lit up and

remained fully lit when the device was moved or bent, as shown in Figure 2-8(c). It is worth mentioning that the LEDs shown could be interchanged with other electronic components, such as sensors, displays or actuators, to form a variety of low-cost battery-free devices and open up new possible applications.
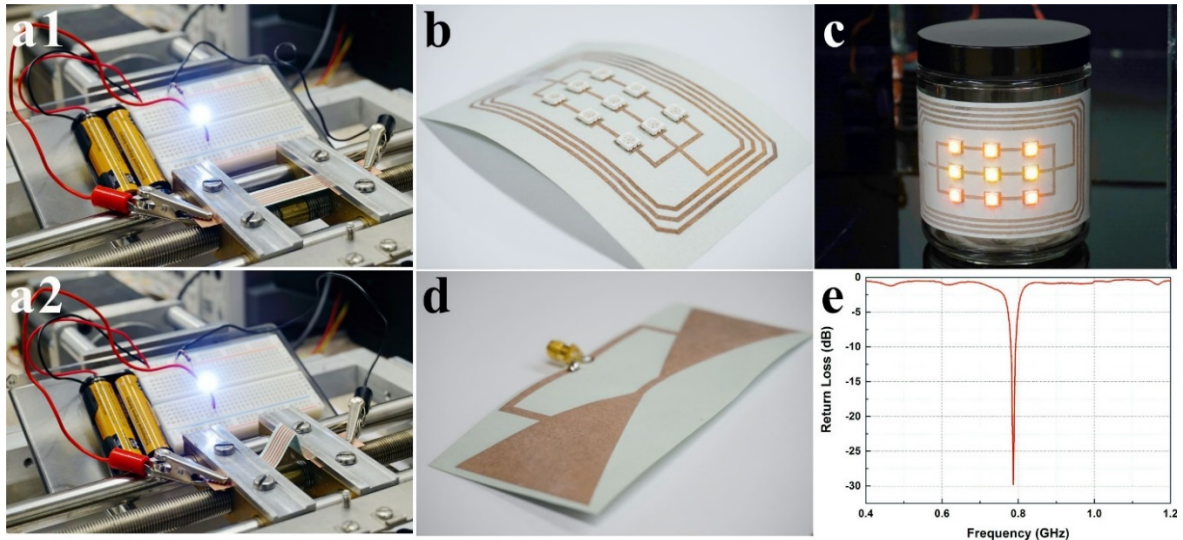
Figure 2-8. (a) Optical images of an LED powered by the copper-fiber electrode array operating as intended in (a1) normal flat state and (a2) bend state. (b) Optical image of the battery-free lighting device containing a 3 × 3 LED array on cellulose paper and (c) havesting RF energy in a bend state to light up all LEDs. (d) Optical image of a bow-tie type RFID antenna with an SMA adaptor attached to its terminal for testing. (e) Return Loss of the RFID antenna as a function of frequency.

The era of Internet of Things (IoT) is just around the corner, and soon, millions of passive RF devices will be fabricated yearly. With such a large number of interconnected RF devices, the possible interference between devices and its implications on personal privacy have become a grave concern. One promising solution is to use ultra-narrow band antennas with low return loss to better utilize the limited bandwidth and keep information secure.[219, 220] To achieve this goal, conductors with low resistance and relatively large thickness are desired; however, it is difficult to fulfill all these requirements with current printed electronics techniques. Thus, in the second example, we designed and fabricated a paper-based RFID antenna based on the popular bow-tie design, to demonstrate the advantages of the proposed method. Figure 2-8(d) shows an image of the antenna with an SMA adaptor. The reflection coefficient of this antenna

was measured using an Agilent Network Analyzer and the result is presented in Figure 2-8(e). Return loss quantifies how well energy of a selected frequency can be coupled from the transceiver to the antenna; the lower the value, the better the antenna.[221] The measured center frequency is 780 MHz with a return loss of ~-30 db, which is significant lower than any result achieved by an additive printing process. The antenna also exhibits an ultra-narrow working bandwidth of ~15 MHz (775 MHz – 790 MHz, <-15 db), making it very suitable for low-cost, energy-saving and interference-sensitive applications.

2.4 Conclusion

In summary, the proposed method offers a low-cost, simple and scalable fabrication route to produce high-quality, flexible printed electronics. The proposed coating formula is composed of reactive adhesive and desired polymer ligands, which can not only form cross-linked functional polymer networks but also strong bonds with cellulose fiber. This produces a highly adhesive, alkaline-resistant layer for effective uptake of catalyst moieties and bonding with deposited copper. Benefiting from the porous structure of cellulose paper, the electroless deposition of copper occurs in a three-dimensional manner, forming a unique copper-fiber conductive structure with enhanced conductivity, bending durability and adhesion. Copper layers with an equivalent bulk thickness of up to 30 μm can be easily achieved with the proposed method, removing many barriers for the additive manufacturing of flexible printed circuits. The fabrication strategy described above is quite general and can be extended to other substrates with little effort. We therefore envision that the proposed technique can be implemented for large-scale production of high-quality, low-cost, paper-based electronics, and can be adapted to meet new requirements as set by the emerging industry.

Chapter 3

3. Building Multilayered Circuits with Drill-less VIA on Paper

3.1 Introduction

Emerging applications for electronics have created an unprecedented demand for systems which are flexible, lightweight, environmental friendly, and even stretchable. Due to their ability to exploit existing manufacturing equipment, printed electronics (PE) have garnered remarkable attention in recent years. [50, 183, 222-225] Recent breakthroughs in material sciences have transformed the electronics industry by allowing simple and complex electronics to be fabricated in a much more cost-efficient manner using existing equipment from the graphics and printing industries. In addition, many new applications have become possible, including flexible/stretchable circuits, [64, 116, 188, 226, 227] thin-film transistors, [228] smart labels, [229, 230] thin-film energy harvesting/storage systems, [74, 231] flexible printed memory devices, [193, 232] wearable sensors, [233] conformal coils and antenna arrays. [234, 235] With the rapidly growing market of PE technology, we can foresee a world that is full of flexible, wearable, lightweight and stretchable devices in the near future. Modern consumer printed devices are striving for smaller size, increased functionality and lower energy consumption, which impose critical demand for double and/or multilayer printed circuits. Multilayered printed circuits allow electrically conductive wires to pass over and under the others wires and allow for more functionality, more compact design and more freedom in the placement of electronics components. In many cases, a double-sided structure is a must. For example, in devices which require coils/antennas to harvest and transmit energy or signals (E.g. smart labels with NFC, RFID, etc.), there must be wires to go across the coils/antennas to connect coils or antennas to the main circuits of the device. One of the most challenging jobs in making these multilayered circuits lies in the fabrication of highly conductive through holes. These vertical interconnect access (VIA) connections perform the task of transmitting electrical current from one side of the circuit board to the other. In the traditional PCB industry, VIAs are fabricated by laser or mechanical drilling in the buildup of dielectric layers, followed by a metallization process to bridge this gap using electro or electroless plating. Due to the importance of these connections, VIAs have been the focus of intense study with manufacturers

competing to maximise adhesion and conductivity of the wires whilst minimising the void depth. These techniques have seen great advancement over the past few decades, resulting in the ability to fabricate PCBs with high quality VIAs. [236, 237] However, this maturely developed technology involves complicated processing steps, many chemicals, specialized equipment and workers, and is not compatible with the current printed electronics technology, which is based on the existing graphic printing industry and features low-cost production of highly customized devices. Multilayered printed electronics have been attempted by many researchers as well as the printing industry, either by manually drilling/punching holes on the substrate followed by the printing of conductive materials around the holes; or by printing/laminating dielectric materials or substrates to cover the conductive traces but leaving small uncovered area which are then then followed by printing another conductive layer around it.[107, 238-242] The most critical issue with these additive approaches of VIA fabrication is the presence of slanted walls on the edges of drilled holes or printed dielectric structures. This non-uniform distribution of ink results in poor and inconsistent conductivity at the top of the VIAs. [243, 244] Meanwhile, the dielectric-conductive additive printing approach is not applicable for the low-cost cellulose paper, mainly because such substrate contains a porous structure which will draw printed materials inside. This wicking of dielectric material makes it nigh impossible to form quality, well-defined VIAs on similar nature-fiber based substrates. Though some of the above mentioned additive approaches are currently adopted by the printing industry, the extra cutting, drilling, laminating, gluing, and printing add significant processing cost to multilayered devices, making the multilayered area several times more expensive to produce than the rest of the device. Thus, developing a new solution for the low-cost fabrication of multilayered PE is badly needed.

Paper is ubiquitous in modern society and is compatible perfectly with all types and ages of printing technology. This positioning provides a unique opportunity to make paper-based electronics seamlessly integrated into any paper-containing product, book, package, label, disposable medical device, biodegradable sensor, and microfluidic device and more with little-to-no change in infrastructure.[197, 245, 246] As a fiber-based substrate, cellulose paper offers many properties that are totally different from those of polymer based plastic substrates used in the conventional PCB industry. As mentioned above, these properties make the fabrication of reliably conductive circuits on cellulose paper rather challenging. The rough and porous

nature of the substrate allows the ink to penetrate into it, instead of leaving them on the surface, and thus prevent the printed conductive materials (e.g. carbon nanotube, metal nanomaterials, conductive polymers) inside the ink from contacting with each other, making it impossible to form a highly conductive layer even after sintering, which greatly limits the performance and application of paper-based electronics. Meanwhile, the capillary effect of cellulose paper also results in loss of resolution when printing with solvent-based low viscosity inks. However, if properly utilized, these drawbacks of cellulose paper can be turned into advantages for making high performance flexible multilayered circuits.

To address the caveats of traditional manufacturing methods, we present a simple and cost-effective method in this paper the means to fabricate high performance, high resolution, and multilayered paper-based circuits which contain highly conductive VIAs without the need of physically drilling holes or depositing additional dielectric materials. A facile, one-step dip-coating method based on the thermal-initiated crosslinking of epoxy and pyridine rings was developed to convert the porous surface of cellulose paper to a functional substrate. Silver-ion-catalyzed electroless deposition (ELD) and inkjet printing were employed for selective metallization of the substrate. Due to the now-abundant pyridine groups on the modified surface, the substrate is capable of forming strong, reliable bonds with the electroless deposited copper. Meanwhile, the unique porous structure of paper allows its cellulose fibers to act as strong physical anchors, producing a highly conductive reinforced copper-fiber hybrid structure. This unique structure not only enhances its durability when bending, but also eliminates the delamination of copper. In addition, different metallization depths can be controlled easily by taking advantage of the precise drop-spacing control of the average inkjet printing system.[247] By exploiting this controllability, printing on both sides of the substrate allows the formation of highly conductive, copper fiber-reinforced interconnects (VIAs), without the need for drilling/punching holes in the substrate.

Through the proposed method, a flexible, high performance, double layer circuit with drill-less VIAs was successfully fabricated for the first time. The as-fabricated circuits on cellulose paper show ultra-low sheet resistance of 4.8 mΩ/sq (single layer) and 2.6 mΩ/sq (drill-less VIA), which is more than 10 times better than current commercialized product (~50 mΩ/sq). To prove the usefulness of this concept, we fabricated a functional, double-layer and battery-free lighting device on regular cellulose paper capable of harvesting radio frequency (RF) energy to power

a 3 by 3 LED array. This proof of concept demonstrates the promising potential of this technology for application in all sorts of paper-based electronics.

3.2 Experiment Details

Materials

Polyvinylpyrrolidone (PVP, Mw ~40,000), ethanol (anhydrous, denatured), 1,4-dioxane (99.8%), Poly(4-vinyl pyridine) (P4VP, Mw ~60,000), formaldehyde (36.5-38% in water), anhydrous glycerol ($C_3H_5(OH)_3$,99%), 2-propanol, silver nitrate (99%), copper sulfate pentahydrate ($CuSO4·5H2O$, 98%), 2,2'-dipyridyl (98%), sodium hydroxide (97%), potassium sodium tartrate tetrahydrate($C4O6H4KNa·4H2O$, 99%), ethylenediaminetetraacetic acid disodium salt dihydrate (EDTA·2Na, 98%), and potassium ferrocyanide (II) trihydrate ($K4Fe(CN)6·3H2O$, 98.5-102.0%) were purchased from Sigma-Aldrich. SU-8 was provided by Kayaku Micro Chem. All chemicals were used as received without further purification. Cellulose paper substrate was provided by Xerox.

Preparation of Coating Solution

polyvinylpyrrolidone (100mg) and Poly (4-vinyl pyridine) (2.5g) were dissolved in ethanol (50mL), and SU-8 (2.5g) was dissolved in 1,4-dioxane to obtain 50 mg/ml transparent solution. The two solutions were then mixed at 1:1 volume ratio to obtain a transparent solution. The final solution contains 25 mg/mL P4VP, 1 mg/mL PVP and 25 mg/mL SU-8.

Surface Modification of Cellulose Paper

Untreated cellulose paper was directly immersed into the coating solution for 10 seconds. The paper was then slowly drawn out of the solution in a constant speed and dried in air at room temperature for 8 minutes. Lastly, the coated paper was placed into an oven at 135°C for 20 minutes for in-situ cross-linking of P4VP and SU-8molecules. After the cross-linking process, the modified substrates were collected and stored in a dry and dark environment.

Preparation of Catalyst Ink for Inkjet Printing

A glycerol–water solution was prepared by mixing anhydrous glycerol and distilled water at a volume ratio of 3:2. Silver nitrate was then added, followed by mixing in a VWR mixer for 3

minutes to form a 60mg/mL silver slat solution. The prepared ink was degassed in a vacuum chamber at 2 psi for 1 hour to remove dissolved gases and bubbles. The viscosity and surface tension of the final ink were 11.5 cp and 51.2 mN/m, respectively. These values fall within the optimum operating range for the Dimatix DMP-2800 printer. A 0.2 μm nylon syringe filter was used to remove undesired particles from the ink before the ink was fed into the cartridge.

Inkjet Printing

The ink was filled into a cartridge mounted on a 10 pL piezo-electric drop-on-demand (DOD) inkjet printhead with 16 nozzles operating at the same time. The drop spacing was set to 5 μm to 45 μm for different groups and a specific print head angle was assigned for each different drop spacing for uniform droplets overlapping in both directions. The other printing parameters were kept the same for all groups and were set as following: meniscus vacuum, 3.5 inch of H_2O; print head temperature, 25 ^{o}C;; jetting voltage 25.1 V. Printing was conducted at room temperature.

Electroless Deposition of Copper

An electroless copper plating bath consisting of $CuSO4·5H2O$ (14 g/L), NaOH (12 g/L), potassium sodium tartrate (16 g/L), EDTA·2Na (20 g/L), HCHO (26 mL/L), 2,2'-dipyridyl (20 mg/L), and potassium ferrocyanide (10 mg/L) was prepared according to literature. Modified cellulose papers with printed silver nitrate patterns were immersed into the bath for different periods of time. The temperature was kept at 35 ^{o}C for high speed deposition of copper.

Characterization

FT-IR analysis was performed using a FT-IR NICOLET 6700 (Thermo Scientific Co.). FE-SEM images were taken by a LEO (Zeiss) 1540 field-emission scanning electron microscope (FE-SEM). The viscosity of the ink was measured with a fully automatic HAAKE Viscotester 262. Surface tension of the ink was measured by VETUS BZY-3B fully automatic tensiometer. Sheet resistances were measured by a four-point probe station Lucas Labs S-302-4 (probe SP4) connected to a Keithley 2750 multimeter. X-ray diffraction analysis was done using a Rigaku Ultima-IV XRD goniometer. Bending test was conducted using a customized bending stage controlled by Anheim Automation DPD75601 motor controller.

3.3   Results and Discussion

4-vinylpyridine, a reactive monomer, was used to modify substrate via *in-situ* polymerization, triggered by plasma or UV to uptake silver ions thanks to its strong chelating ability with transitional metal ions.[211, 248] The monomer cross-links with the pretreated substrate and other monomers via covalent bonds, achieving a strong bond between the two. Due to the low film production rate and intense demands on equipment, this approach was deemed not cost-effective and unsuitable for coating high-porosity cellulose paper. Another straight forward method is directly coating poly(4-vinylpyridine) (P4VP) molecules onto the substrate by physical absorption, but the poor adhesion will result in significant loss of resolution during the electroless deposition of metal.[249] The reaction mechanism between pyridine and epoxy groups has been well studied in recent years, showing P4VP molecules to be able to crosslink with epoxy groups.[250, 251] In addition, the highly reactive epoxy groups can form strong covalent bonds with cellulose fibers due to the abundant hydroxyl groups present on its surface. According to the above-mentioned mechanisms, for the purpose of this work, Poly (4-vinylpyridine) (P4VP) and SU-8 were adopted as the main components of the coating compound.

Figure 3-1 shows the fabrication process of making high performance double-layer circuits with drill-less VIAs on cellulose paper. The zoomed-in areas under each fabrication step show the micro-structure of the sample at different stages. The coating solution was prepared by dissolving SU-8 and P4VP in a 1:1 mixture of 1,4-dioxiane and 2-propanol. A small amount of polyvinylpyrrolidone (PVP) was added to the solution to enhance its wettability and ability to capture silver nanoparticles in the initial electroless deposition (ELD) step. The untreated cellulose paper has many hydroxyl groups on the surface, which was expected to react with the coated polymer in the following step. After dip coating, the substrate was then baked in an oven for 15 minutes at 130 $^\circ$C. This was done to initiate the covalent bonding between SU-8, P4VP and the cellulose paper, forming a thin layer of functional coating alongside each cellulose fiber, as illustrated in Figure 3-1. A small number of pyridine ligands crosslinked with epoxy groups in SU-8, leaving the rest of them along the fiber available to capture silver ions in the following inkjet printing step. When the ink hits the treated substrate, the lone electron pair in the nitrogen atom of the unoccupied pyridine ligands will attach to the silver ions to form strong coordination bonds, which are much stronger than that formed by simple

physical absorption. Such chemical bonding keeps the absorbed silver ions adhere to the surface and promotes the adhesion of deposited copper generated in the following ELD step.
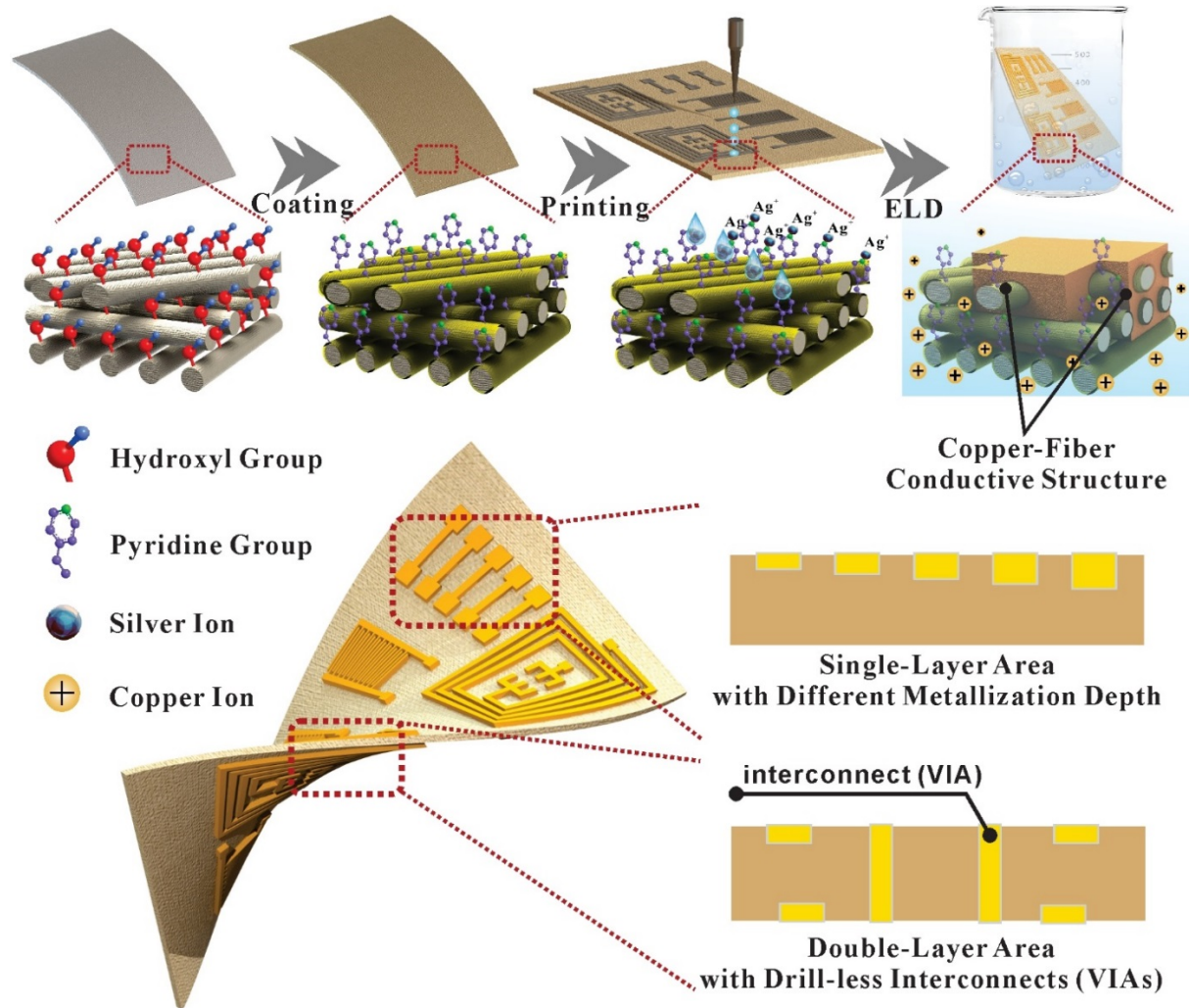
Figure 3-1. Schematic diagram of the low-cost fabrication process of the single/double layer flexible circuits on cellulose paper.

Thanks to the fiber-based porous structure of the cellulose paper, the ink will penetrate to a certain depth, forming a 3D catalyst-loaded area. This unique feature allows the copper to grow in a three-dimensional manner, generating copper at a much faster rate than traditional surface-only reactions. The result of this reaction is the formation of a highly conductive copper-fiber structure, as illustrated in Figure 3-1. The fibers not only enhance the flexibility of the circuits, but also serve as anchors to which the copper can hold, preventing any unwanted delamination

and/or peeling of the metal. In addition to this increased flexibility, the penetration depth of the ink can be simply controlled by adjusting the ink volume per unit area. By printing on both sides of the substrate with specific settings, double-layered circuits with highly conductive drill-less interconnects can be fabricated with ease.
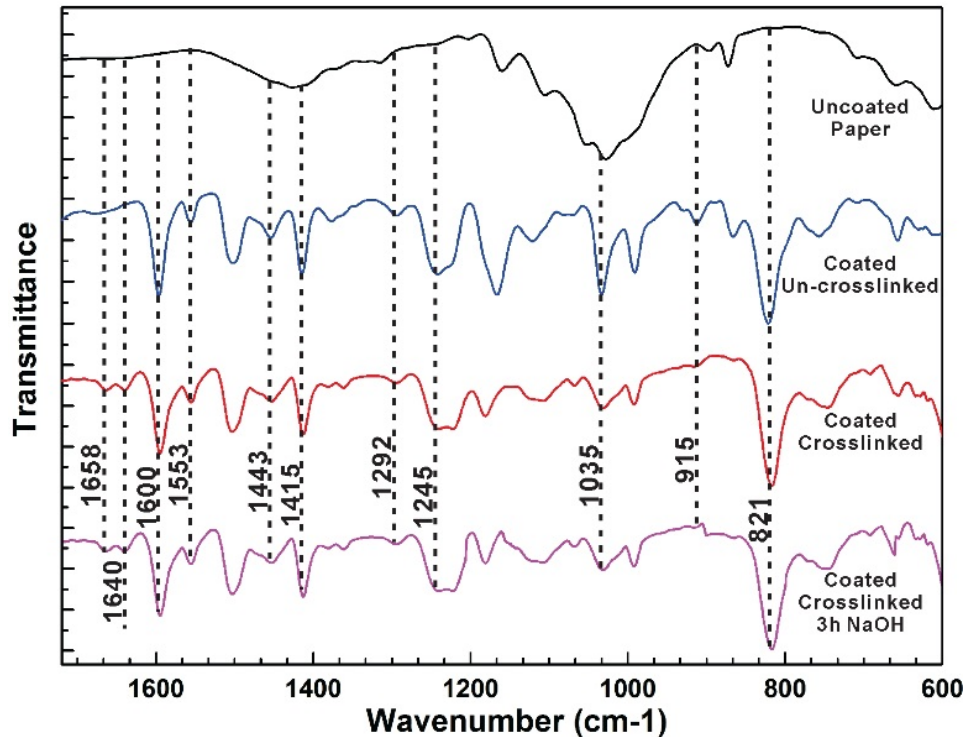
Figure 3-2. FT-IR spectra of uncoated cellulose paper, paper with un-crosslinked coating, paper with crosslinked coating before and after 3 hours alkaline solution treatment.

Cellulose paper is not alkali-resistant, as long-term immersion in alkaline solution will weaken the paper making it fragile and prone to tearing. Thus, aside from serving as a catalyst ion trapping layer, another important function of the coating is to protect the paper in the ELD bath, which is a highly alkaline solution with a pH of ~12.[72, 217] Attributed to the ring-opening reaction of the epoxide groups, the dominant bonding type will be carbon-oxygen bonds. Such bonds are highly resistant to alkali solutions, which conveniently allow the proposed coating to withstand the long ELD process. Figure 3-2 shows the FT-IR spectra at various stages of production beginning with uncoated cellulose paper at the top and finishing with the crosslinked paper immersed in pH ~12 NaOH for 3 hours at the bottom. By comparing these spectra with the standard infrared transmittance spectra, we can gain some insight as to what

happens on the surface at each stage. The peaks at 821, 1415, 1553, 1600 cm^{-1}, which correspond to pyridine groups, and the peaks seen at 443 and 1292 cm^{-1}, which match the stretching frequency characteristic of pyrrolidone groups (C-N-C and N-C) in PVP, are present only on the spectra of coated papers, implying the successful introduction of the composite coating layer.[215, 249, 252] The observed peaks at 1245, 915 cm^{-1} and 1415, 1600 cm^{-1}, corresponding to the stretching vibration of epoxide groups in SU-8 and pyridine groups in P4VP respectively, appear weakened post-thermal treatment, which suggests that cross-linking between epoxide and pyridine groups have occurred. After the thermal treatment, two new peaks appear at 1640 and 1658 cm^{-1}. These can be ascribed to the newly-formed carbonyls of pyridone and the unconjugated carbon double bonds.[250, 251] Despite these changes, the FT-IR spectrum shows strong pyridine peaks at 1415, 1600, 821 and 1553 cm^{-1}, proving that only a small number of pyridine ligands actually reacted with the epoxide groups during the crosslinking, implying that there are still many pyridine groups exposed along each fiber. The elimination of copper diffusion during the ELD process supports the notion that a sufficient number of functional pyridine groups were available on the surface. Figure 3-2 also presents the FT-IR spectrum (bottom) of the cured composite layers treated by NaOH (pH=~12) solution for 3 hours. The spectrum of the treated paper is very similar to that of the sample tested prior to alkaline exposure, suggesting that the initial coating layer is intact and well maintained. This, along with the paper's normal physical appearance, demonstrates the alkaline-resistant property expected of the coating.
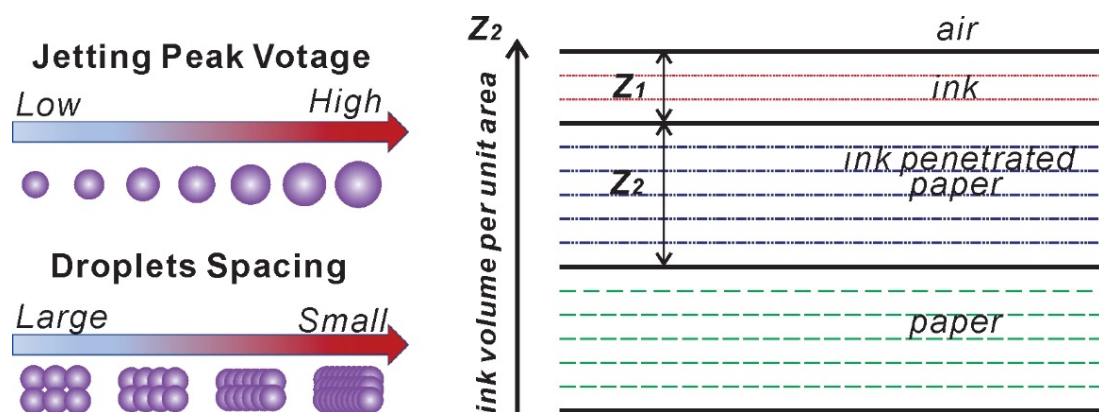
Figure 3-3. The relationship between ink volume per unit area and the jetting peak voltage/droplets spacing (left); The microscopic sketch of the printed area of the coated cellulose paper.

For fiber-based substrate, the porous surface promotes printing ink penetration. The ink penetration in cellulose paper has been well-studied by the conventional graphic printing industry, and there are several theoretical models which describe this phenomenon very well.[236] These models usually consist of four discrete layers of media, corresponding to the extent of interaction between ink and substrate: air, ink, ink penetrated paper and virgin paper (see Figure 3-3). The penetration depth is highly dependent on the properties of both the chosen paper and the ink. For example, inks which contain no particle (pigments, conductive metal nanoparticles, etc.), can be considered to have a thickness of zero, meaning that the "ink" layer (Z_1 in Figure 3-3) is negligible. The penetration depth (Z_2; Figure 3-3) of the ink, in the same porous substrate, is mainly determined by i) the physical properties of the ink (e.g. surface tension, density, viscosity) and ii) the volume of ink per unit area. In this work, the ink properties are fixed for optimum performance with the printer with a viscosity of 11.5 cp and surface tension of 51.2 mN/m. The penetration depth in our experiment was therefore predominantly controlled by the ink volume per unit area.

There are two common methods by which one can control the ink volume per unit area for a piezo inkjet system. The first, is to control the peak voltage of the jetting waveform. A higher peak jetting voltage will create a larger droplet, as shown in Figure 3-3. However, according to our investigation, this increment is limited to an increase in single droplet volume less than 20%. Beyond this volume, the boosted jetting voltages can result in satellite droplets, lowering the print quality and compromising circuit quality. The second way, is to control the distance between each droplet (drop spacing, DS). The smaller the DS, the greater the ink volume per unit area will be (see Figure 3-3 for illustration). Adjusting the DS between each droplet allows for the efficient and precise control of ink volume. For example, with two different DS setting of 5 µm and 50 µm, we can extract an ink volume per unit area difference of 1000%. For these reasons, we chose to adopt the DS control method for ink volume management.

With the ink and experiment settings used in this work, a single droplet will form a round wetting area on the coated substrate with a diameter of ~ 55 µm. To form a continuous and uniform wetted area, the maximum DS needs to be smaller than the diameter of the droplet. Based on this, we used five different DS settings (5 µm, 15 µm, 25 µm, 35 µm, 45 µm) to investigate the metallization depth after ELD process. The metallization depth, the variable which will allow the formation of VIA connections, was characterized by imaging cross-

sections of samples using a SEM in back-scattered mode. Each sample was cut with a one-time sharp knife with the metalized layer facing down (one-layer circuit). The results are shown in Figure 3-4.
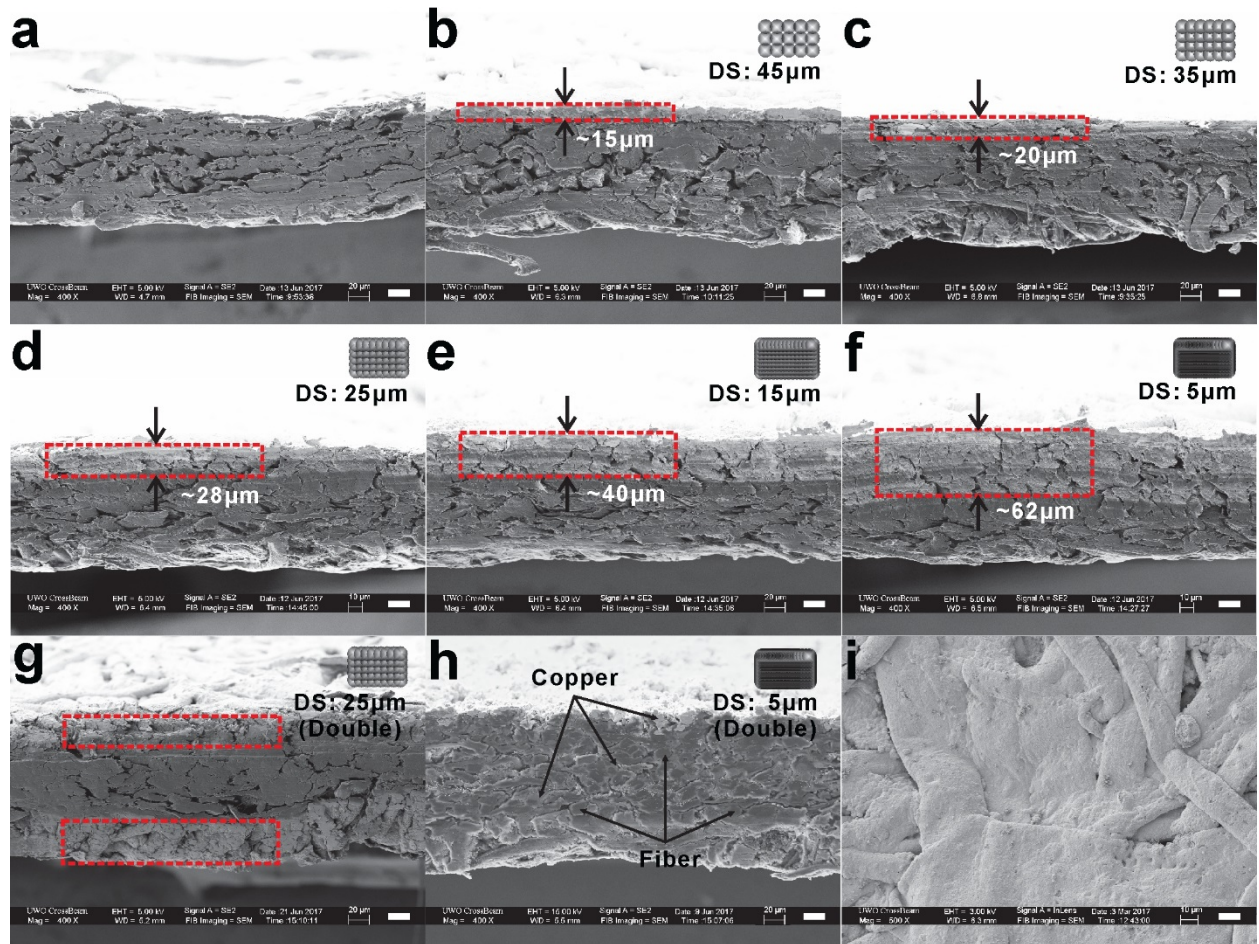
Figure 3-4. (a) SEM image of the coated substrate without copper deposition; SEM images of cross-section of electroless deposited copper samples with different drop spacing of (b) 45 µm; (c) 35 µm; (d) 25 µm; (e) 15 µm; (f) 5 µm; (g) 25 µm double side printed and (h) 5 µm double side printed. (i) Surface morphology of (f).

Figure 3-4(a) shows the cross-section of the coated cellulose paper, revealing a porous structure formed by irregularly arranged cellulose fibers. Randomly orientated cellulose fibers of varying diameters can be seen in this image. The paper substrate used in this work came with a standard thickness of ~ 150 µm, however, the picture shows an average substrate thickness of ~ 135 µm. This change was consistent between samples and was thus likely caused by the cutting process used to prepare samples. Upon further investigation, it was determined that as

the knife was run across the paper, the porous substrate was compressed, resulting the observed thinner cross-section. Samples shown in Figures 3-4(b-f) were printed on a single side with varying DS setting ranging from 5 µm to 45 µm; the setting used is indicated at the top-right corner of each image. All other experimental settings and conditions, including jetting waveform and appropriate variables of the ELD process, were kept constant between trials. The metallized portion of each sample is highlighted with red dashed box. For the DS-45 (drop spacing = 45 µm) group as shown in Figure 3-4(b), a metallized layer depth of ~ 15 µm is observed. Interestingly, a clear boundary between copper and paper can be seen. One possible explanation for this is that due to the relatively large drop spacing, the ink volume per unit area is similarly low, penetrating the surface only slightly prior to drying. It is therefore logical to conclude that in the following ELD processes, copper growth primarily takes place on the topmost surface-or to be more precise the topmost part of the first layer-of cellulose fibers. When the drop spacing is reduced to 35 µm, as shown in Figure 3-4(c), the DS-35 group distinctly penetrates the copper-fiber layer to a depth of ~ 20 µm. Unlike the DS-45 group, there is no clear boundary between the deposited metal and the substrate. We suspect that increased ink volume per unit area created a deeper penetration depth, allowing the deposition of copper to take place not only on the surface, but also inside the substrate. This three-dimensional ELD of copper resulted in the first observed copper-fiber hybrid structure. As the drop spacing was reduced, deeper ink penetration was achieved. Figures 3-4(d-f) shows the cross-sections of DS-25, DS-15 and DS-5 groups, respectively, wherein metallized copper-fiber layers of thickness ~28 µm, ~40 µm and ~62 µm can be observed. Interestingly, despite a 900% increase in ink volume per unit area from DS-45 to DS-5, we did not observe a consecutive nine-fold increase in penetration depth. On the contrary, the smallest drop spacing setting only yielded a deeper penetration of four times that of the largest drop spacing. This peculiarity is attributed to the fast rate of evaporation of the ink's solvent. Due to the large area on the surface, the solvent which carries the ink likely evaporated completely before the ink could travel any deeper.

The main purpose behind investigating which factors best influence the depth of ink penetration, was to determine if it is possible to reliably fabricate quality VIA connections linking two sides of a substrate without the need of drilling or punching holes. Through manipulation of the drop space setting on a conventional inkjet printer, we were able to

consistently reproduce several depths of metallization. Combined with double-sided printing, control of this single variable allowed us to fabricate double-layered circuits and fully metallized copper-fiber VIAs without any short-circuits. The cross-section of a double-side printed sample with drop spacing of 25 µm is presented in Figure 3-4(g). The sample shows double-sided metallized layers on the top and the bottom with an insulated un-metallized substrate of ~85 µm in between. Similar to the single-sided DS-25 group (Figure 3-4(d)), the double-sided DS-25 group (Figure 3-4(g)) produced a metallized copper-fiber layer with a thickness of ~28 µm on the top; this contrasts with the much thicker layer observed on the bottom (~41 µm). Through careful examination, the variance was determined to be caused by the cutting process used. Every double-printed sample imaged under SEM had the same irregularity: the metallized layer on the surface facing up during the cutting process was always thicker than that on the surface facing down. Figure 3-4(h) presents a fully metallized VIA, printed using a DS-5 (drop spacing = 5 µm) setting on both sides, showing a clear copper-fiber hybrid structure and the presence of copper growth underneath the surface. After 2 hours of ELD, all samples showed very similar surface morphology (see Figure 3-4(i)). The metallized cellulose fibers and copper-filled gaps between each fiber can clearly be seen, revealing the expected copper-fiber hybrid structure from another perspective. Typically, if electroless plated copper is deposited in thicknesses greater than 10 µm, the copper tends to bubble up or delaminate from the substrate due to the lack of interlock between the top copper layer and the substrate. In this work, the coated cellulose fibers act as a chemical as well as physical anchors for the deposited copper to achieve strong adhesion, preventing any this delamination or peeling of the copper. The ASTM standard tape test was utilised to evaluate copper adhesion of the as-fabricated samples.[218] During the tape test, deposited copper of all samples, printed using different drop spacing settings, conformally adhered to the substrate during all but the first iteration, wherein a small number of surface particles were removed. The sheet resistance also remained undetectable throughout several iterations, demonstrating excellent adhesion according to the ASTM D3359 standard.

The change in sheet resistance (mΩ/sq) versus ELD plating duration was investigated using the four-probe method for various increments of ink drop-spacing. A measurement of each samples' resistance was collected at 15-minute intervals during the 3-hour ELD process. The results are shown in Figure 3-5(a).
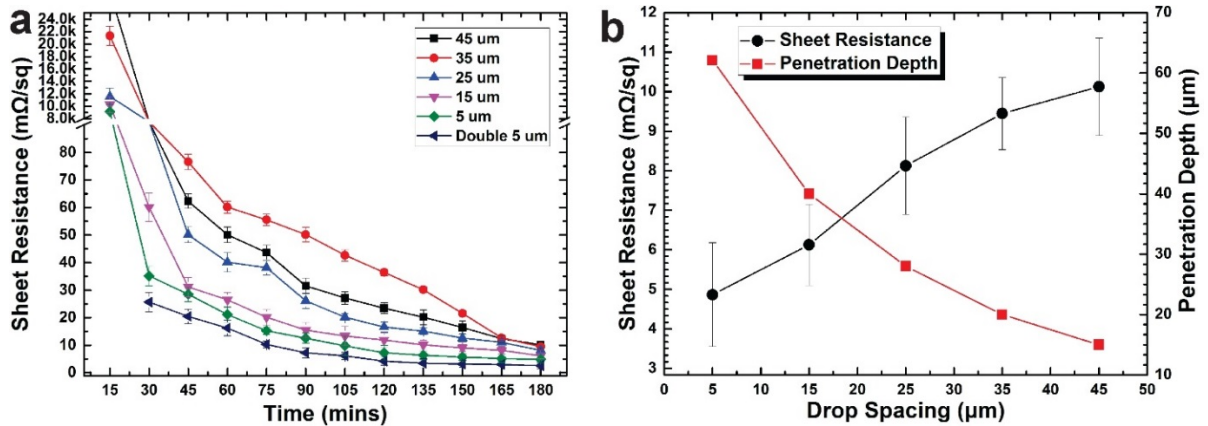
Figure 3-5. Graph showing (a) the change of sheet resistance versus time of samples printed with different drop spacing ranging from 5 μm to 45 μm; (b) the change of sheet resistance/penetration depth as a function of drop spacing.

According to these results, it can be generalised that decreased spacing between subsequent ink drops result in corresponding decreases in sheet resistance, following a full three-hour ELD process. Smaller drop spacing allows deeper penetration of the ink into the paper. This increase in catalyst-loaded volume increases the amount of deposited copper per unit area, in turn yielding better conductivity. After just 15 minutes of plating, all samples become conductive with a relatively high sheet resistance ranging from 0.9×10^2 Ω/sq to 3×10^2 Ω/sq – corresponding to the thin and loose copper layer on top of each fiber. The sheet resistance dramatically drops to the range of 10^{-2} Ω/sq (minimum: 2×10^{-2} Ω/sq, Double DS-5; maximum: 6.2×10^{-2} Ω/sq, DS-45) during the first 45 minutes of ELD, which can be attributed to the growth and connection of newly generated copper seeds. Once initiated, these seeds quickly grow larger and progressively form contacts with other copper seeds. As these gaps between copper deposits bridge, the sheet resistance steadily declines until a dense and uniform copper layer is formed along each fiber (see Figure 3-4 (i)). By the end of the three-hour ELD process, the three-dimensional copper-fiber conductive structure is generated, exhibiting an ultra-low sheet resistance of 2.5×10^{-3} Ω/sq for the Double DS-5 group (VIAs) and 9.8×10^{-3} Ω/sq for the DS-5 group. It is worth noting that these resistance values are 20 times less than even those of commercially printed electronics currently available on the market. To illustrate how drop spacing affects sheet resistance and penetration depth, we plotted the final sheet resistance and penetration depth of samples, after undergoing 3 hours of ELD (see Figure 3-5(b)). This graph

reveals the robust linear relationship between drop spacing and penetration depth/sheet resistance, providing a strong theoretical reference for future circuit design.
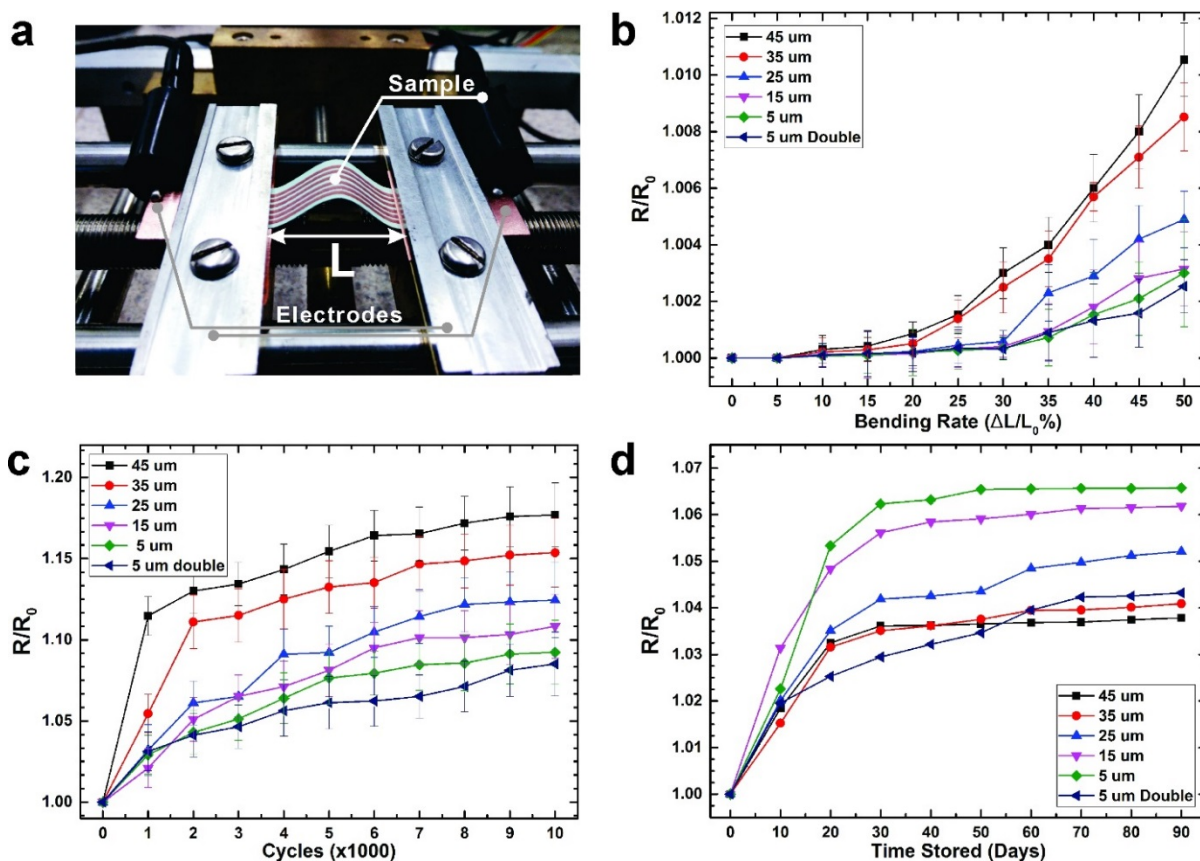
Figure 3-6. (a) Photograph of the as-prepared copper electrode array setup on a custom-made bend testing stage. The change in electrical resistance of electrodes, printed with drop spacing 5 μm to 45 μm, as a function of (b) bend rate; (c) bend cycles and (d) storing time. The "5 μm double" refers to a sample, having been printed on both sides, using drop spacing of 5 μm.

To investigate the bending durability of the fabricated features, a linear array of six copper traces (length = 7.5 cm, width = 2 mm) spaced 1.5 mm apart was fabricated on cellulose paper using different drop spacing settings ranging from 5 μm to 45 μm, including a double printed VIA array with 5 μm drop spacing. Each sample was electroless copper plated for 3 hours, washed and then dried using the same procedure. The electrode-patterned sample was then attached to a customized stretching stage, coupled to a computer-controlled step motor. This was then actuated between flat and bent states at a rate of 3 cm/s, as shown in Figure 3-6(a). To measure resistance, a Keithley multimeter was connected to the two terminals of the

stretching stage in a four-probe sensing setup to measure the resistance of the sample. To calculate the "bend rate" of the sample, the actual distance changing between terminals (ΔL), which varied as they moved closer to each other, was divided by the original distance separating the two terminals (L_0). For instance, if the minimum distance between the two terminals is $L_{min} = 3$ cm, and the initial distance (flat state) is $L_0 = 6$ cm, then we have a maximum bend rate of $\Delta L/L_0 \% = 50\%$. Figure 3-6(b) shows the average change in resistance under different bend rates, ranging from 0% to a maximum of 50%. When the bend rate is less than 15%, the resistance is almost unaffected for all six groups of samples. For bend rates up to 30%, DS-25, DS-15, DS-5 and Double-DS-5 groups experience a negligible increase in resistance (<0.5%). Beyond a 30% bend rate, these four groups show near-linear increases to resistance. In comparison, the groups with DS-45 and DS-35 show similar linear changes in resistance when the bend rate surpasses 15%.

In summary, the larger the space between ink drops, the greater the observed increase in resistance when bent. The greatest increase in resistance can be observed at the maximum bend rate (50%) of the group printed with the largest spacing between drops (~1.1%; DS-45). The double-sided DS-5 group presents the smallest increase in resistance, reaching a mere ~ 0.2% at maximum bend rate. At maximum bending rate, small cracks appeared on the surface of the deposited copper, which suggests that they are the primary cause of conductivity loss. This notion is supported by the fact that samples printed with smaller drop spacing have a thicker copper-fiber metallization layer, which compensates the for the loss in conductivity from the surface. It is thus reasonable to generalise that decreases in drop spacing results in smaller losses to conductivity when bent.

To test the longevity of these electrodes, we investigated how the resistance of various DS groups change as a function of bend cycles (Figure 3-6(c)). For each cycle, samples were actuated from a bend rate of 0% to 50%, at a speed of 4 cm/s. DS-45 and DS-35 groups exhibited a rapid increase to their electrical resistances during the first 2000 cycles, but then adopted the linear increases characteristic of the other four groups. These four groups showed steady increases to their electrical resistances during the 10000-bend cycle test. As postulated prior, cracking on the copper surface could explain the initial rapid increase in resistance, explaining why samples with a thicker metallization layer (smaller drop spacing) exhibit smaller increases in resistance over the duration of bend cycles. Despite these occurrence, all

samples exhibit good bending durability after 10000 cycles, with total resistance increasing 8.5%, 9.2%, 10.8%, 12.4%, 15.3% and 17.6% over original values for the Double-DS-5, DS-5, DS-15, DS-25, DS-35 and DS-45 samples respectively. Compared to traditional surface-only conductive features, we can see that the bending durability is greatly enhanced by the copper-fiber conductive structure.

The unique, fiber-based, porous structure of cellulose paper greatly enhances the electroless deposition rate of copper, which contributes to the added adhesion and bending durability. It was anticipated that such a structure would have drawbacks, particularly to that of oxidation. Paper has the ability to hold moisture and this, coupled with the increased surface area of the copper bound to the fibers, makes for prime oxidation conditions. To understand the extent to which this affected the copper's ability to conduct, the relationship between the resistance and storing time was investigated. Figure 3-6(d) shows the resistance change of DS-45, DS-35, DS-25, DS-15, DS-5 and Double-DS-5 groups over a period of 90 days. All groups of samples were left out in open air in the lab without any temperature or humidity control to simulate common conditions. The temperature and humidity of the room are set to 23 ^{o}C and 45% respectively. The resistance of all groups increased quickly during the first 30 days, after which they levelled off significantly. Contrary to the results obtained during the bending test, the samples printed with larger drop spacing showed smaller resistance increases after 90 days than did those with smaller drop spaces (DS-45, ~3.7%; DS-35, 4.1%; DS-25, 5.2%; DS-15, 6.6%;). This is thought to be caused by the surface area variations, of which the samples bearing larger drop spaces have less due to their decreased penetration into the fibrous substrate. As would be predicted by this explanation, the double-sided DS-5 group does not fall into this regular patter. The increase in resistance of this group after 90 days is 4.3%, which falls somewhere between that of DS-35 and DS-25. Although we were unable to determine the exact cause of this phenomenon, a possible explanation is that the double-layered fully metallized structure was able to offer some protection against the elements, preventing it from getting completely oxidized.
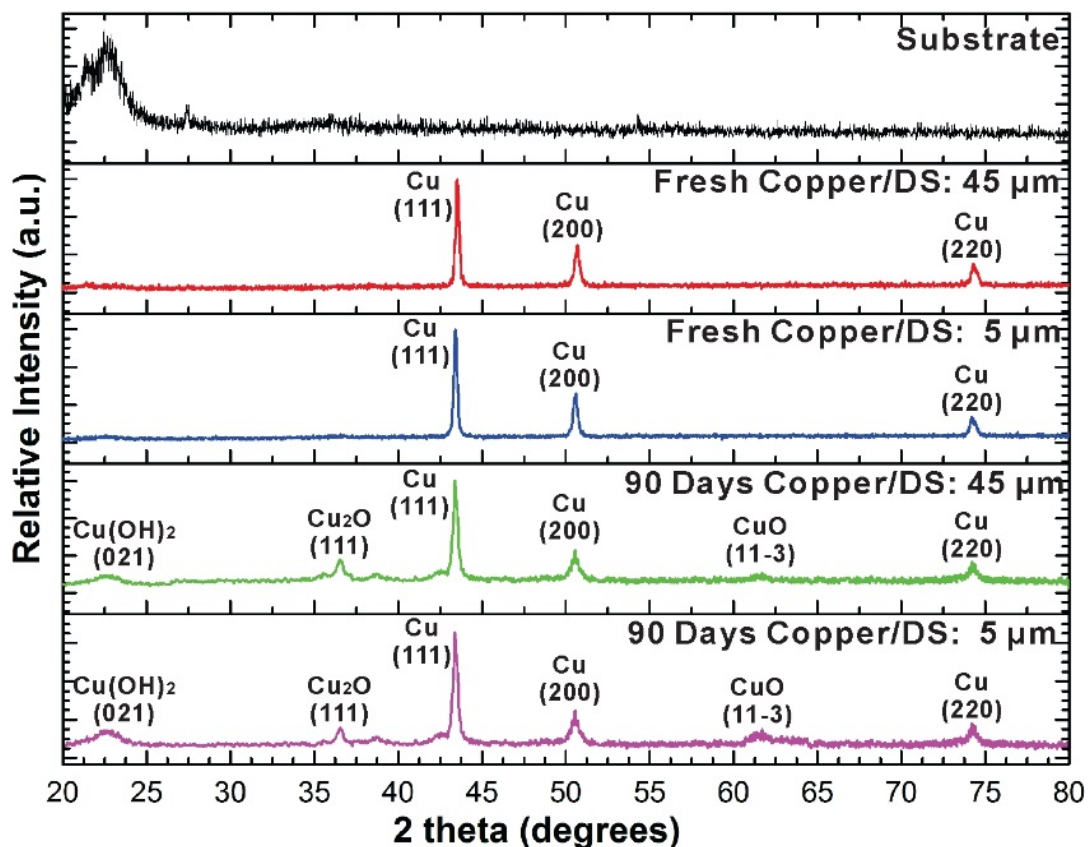
Figure 3-7. X-ray diffraction spectra of coated substrate before and after copper plating. Comparison of DS-45 and DS-15 between freshly deposited copper traces and those stored in open air for 90 days.

X-ray diffraction (XRD) was conducted to study the crystalline structure of the resultant copper layer, as well as to investigate the changes in composition which take place over the 90 days of storage. Interestingly, the obtained XRD spectrums showed relatively little variation between the two tested groups (see Figure 3-7). Each group maintained close similarity to each other both prior to exposure and after. The similarity between peaks suggest that both groups-regardless of drop spacing-react to the environment in the same manner. We selected results from either end of the drop settings tested, DS-45 and DS-5, to be displayed in Figure 3-7. This image represents the XRD patterns of the plain, coated paper substrate, two freshly made copper electrodes (DS-45 and DS-5), and copper electrodes exposed to air for 90 days (DS-45 and DS-5). As mentioned previously, both freshly prepared samples showed peaks at $43.46°$, $50.43°$ and $74.25°$, which can be attributed to Cu crystal plane (111), (200) and (220), respectively (JCPDS Data 04-836). For the samples which had been exposed to air for 90 days,

a number of new, weaker peaks appeared in the spectrum; peaks at 23.8º and 36.4º correspond to the (021) plane of Cu(OH)2 crystal (JCPDS Data 80-0656) and the (111) plane of Cu2O (JCPDS Data 05-0667) crystal, respectively. The other, very weak peaks at 61.5º, can be attributed to the (11-3) plane of CuO (JCPDS Data 48-1548), indicating a very small amount of CuO present on the surface. From these XRD results, we conclude that oxidation from extended storage in open air leads, for the most part, to the formation of Cu_2O and $Cu(OH)_2$. Furthermore, it was observed that most oxidation took place in the first 30 days of air exposure, with limited influence on the overall resistance of the samples ($<7\%$). For future applications, the loss of conductivity during time could be greatly reduced by protecting the samples with either conformal coating or electroless nickel plating.

To prove this concept and to test its viability as an alternative to traditional circuit manufacturing, we fabricated several prototypes which would demonstrate the various features of this technology. The features of particular interest included double-layer electrodes, which demonstrate the good conductivity of the drill-less interconnects, and the insulation of the circuit on both sides, proving there is little chance of unintentional short-circuiting. Figures 3-8(a) and (b) show a circuit structure working whilst being bent; this circuit element has two separates conductive traces-on both sides of the substrate-with no overlapping areas and is connected by a drill-less interconnect (VIA) in the middle (white dashed circle; Figure 3-8(b)). During this test, the resistance of the drill-less VIA was nearly undetectable using a regular multimeter. This result demonstrates the exceptional level of conductivity that can be achieved using this new type of interconnect. Another circuit structure we fabricated comprised a few sets of electrodes on either side of the paper, each with several overlapping areas (see Figures 3-8(c & d)). Under light, the over-lapping area can be clearly identified (Figure 3-8(c)). When tested using a multimeter the over-lapping area, between which is absent of copper wiring (see Figure 3-4(g)), demonstrated sufficient insulation showing no conductivity across circuits on opposing sides of the paper (Figure 3-8(d)).
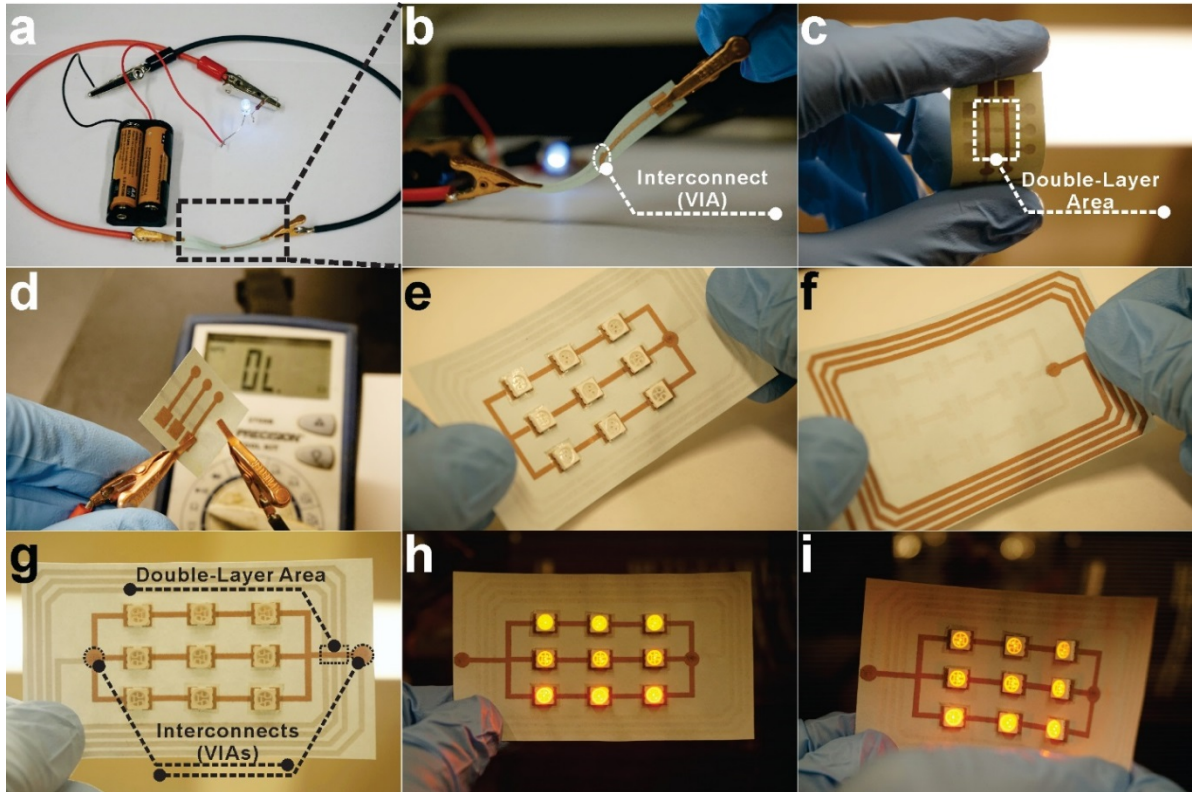
Figure 3-8. (a) Optical images of a double layer electrode with drill-less interconnect (via) operating in bent state. (b) A close-up image of the electrode showing the drill-less interconnect in the marked area. (c) Optical image of double layer arrays with overlapping area. (d) Electrodes along each side of the paper show no contact and good insulation. (e) The front and (f) back side of the double-layer battery-free device. (g) The battery-free device under light showing both of its front and back side with interconnect and overlapped area marked out. The device harvests energy and lights up nine LEDs in both (h) normal flat state and (i) bent state.

To demonstrate the versatility of the proposed technique in real world applications, we designed and fabricated a double-layer, battery-free LED lighting array on cellulose paper. The front and the back sides of the device are shown in Figures 3-8(e) and (f) respectively. On the front side, nine LEDs with different colours (yellow, orange and red) were mounted on to the circuit using 3M conductive tape. On the reverse side, a receiving coil operating at 150 kHz was fabricated, using the method proposed in this paper, to harvest RF energy to power the LEDs array. The two terminals of the coil were then connected to the front side of the device via two drill-less VIAs. The double-layered structure can be seen when the circuit is put under

light, as shown in Figure 3-8(g) (overlapping areas and drill-less interconnects are marked for clear illustration). As a battery-free device, these LEDs will light up using only the energy harvested from the receiving coil. The fabricated device is flexible, lightweight, and can be attached to many surfaces. When the device was placed into a 150-kHz 3D electromagnetic field (EMF,) generated by a custom field-generator, all nine LEDs lit up (Figure 3-8(h)), and remained fully lit even when the device was bent (see Figure 3-8(i)). It is worth mentioning that the LEDs shown in these images could be interchanged with other electronic components-such as sensors, displays or actuators-to form a variety of low-cost, battery-free devices, opening up many new applications.

3.4   Conclusion

Unnecessary complexity and inevitable performance trade-offs have dogged the electronics industry for many years, preventing it from forming successful partnerships with the graphics and printing industries. By utilising recent developments in material sciences, we not only circumvented limitations thought to be insurmountable, but demonstrated a means of transforming them into strengths. In this research, we present a simple, cost-effective, and scalable method of building circuits, capable of fabricating high performance, high resolution, and multilayered paper-based circuits containing highly conductive VIAs, all without the need to physically drill holes or deposit extra dielectric materials. A facile one-step dip-coating method was developed, to functionalise the surface of common cellulose paper, exploiting the thermal-initiated crosslinking of epoxy and pyridine rings. Silver ion-catalyzed electroless deposition (ELD) and inkjet printing were employed for the selective metallization of the substrate. Benefiting from the porous structure of cellulose paper, the electroless deposition of copper forms in a three-dimensional manner, resulting in a unique, highly conductive copper-fiber structure exhibiting enhanced adhesion to the paper, conductivity and bending durability. To control the metallization depth of the copper structures, the spacing between drops of ink was controlled by utilising the inkjet printer's easy-to-control settings. Furthermore, printing on both sides of the paper substrate, using appropriate drop space settings, enabled the creation of highly conductive interconnects (VIAs) with ultra-low sheet resistance down to 2.6 mΩ/sq without the need for drilling or punching holes of in the substrate. Based on the proposed method, high performance double layer flexible circuits with drill-less VIAs were successfully fabricated for the first time. With minimal additional development, the described fabrication

strategy can be extended to other fiber-based and porous substrates, expanding its usefulness to countless applications. We envision that the proposed technique can be adapted for the large-scale production of low-cost, high-quality, and ecologically sustainable multi-layered flexible electronics.

Chapter 4

4. Paper with Power: Engraving 2D Materials on 3D Structures for High-Performance, Binder-Free, All-Solid-State Supercapacitors

4.1 Introduction

The rapid development of technology has conceded a corresponding expansion of what "things" may now constitute as candidates for network connectedness. As seen in its application to wearable electronics—a market which has grown over 1100% in 6 years—the Internet of Things (IoT) has accelerated the insatiable demand for low-cost energy storage systems capable of seamlessly integrating with their intended applications.[253-255] Electrochemical capacitors, also known as supercapacitors (SCs), have been the subject of intense study due to their superior power density, longer cycle life, and unparalleled charge-discharge speed when compared to conventional batteries and traditional capacitors.[256-259] There are two types of supercapacitors, which are divided by the mechanism by which they store energy: electrochemical double-layer capacitors, and pseudocapacitors. The former is based on charge separation at the electrolyte/electrode interfaces, whereas the latter is based on electrochemical Faradaic redox reactions which take place within the active material of the electrodes.

To achieve the high energy density desired of pseudocapacitors, several challenges must be surmounted. Specifically, these capacitors must maximise surface area of the electrodes, exhibit high electrical conductivity, and allow for rapid ion diffusion. Research has shown ruthenium oxides/hydroxides to exhibit the desired high pseudo-charge capacitance as an active electrode material, however, the high cost for such materials greatly hinders its wide applications.[260, 261] Other transition metal oxides, such as MnO_2, Cu_xO, NiO, Co_3O_4 and VO_x, have each been meticulously studied in hopes of providing a cheaper, equally efficient alternative.[262-272] Of the above-mentioned metal oxides, Cu_xO was considered to be particularly promising due to its low-cost, relatively high theoretical capacity, proven safety, and abundance as a natural resource. Long-term scalability of any solutions to electrochemical energy storage is imperative if the technology is to be implemented in industry; the use of

exotic and expensive materials simply cannot meet demand.[273, 274] Generally speaking, a supercapacitor will contain sheet-type electrodes, liquid electrolytes, and separator membranes as its core components. These elements are most commonly fabricated through a stacking or winding process. Although they are the industry standard, such traditional assembly of components greatly limits the capacitor's flexibility, as well as variety of form factors. Recent advances in material sciences and printed electronics technology have started to overcome these challenges, offering a variety power sources, such as thin-film battery and all-printed supercapacitors. These next-generation power sources boast performance comparable to existing techniques, yet are foldable, bendable, and some even stretchable.[275-277] In the conventional fabrication process of a printed supercapacitor, the electrochemical active materials are directly printed onto the substrate, adhering to the current collectors by simple physical absorption. [278-280] Though this may simplify the fabrication process, the electrode materials will quickly flake off from the current collector due to the weak adhesion and great volume changes during charging/discharging processes. This resulting structural failure significantly decreases charge capacity and reduces cycle life. One solution to this issue of poor adhesion between electroactive and supporting particles, is to incorporate the binding agent; in a more traditional electrode, a polymer binder usually plays the role of integrating electroactive particles onto the supporting materials and/or current collectors. A caveat to adding these insulating and electrochemically inactive polymer binders is, it will increase the inner resistance of the assembly which will inevitably offset the any gained improvements to the supercapacitor's performance. Furthermore, the addition of a step to the manufacturing process greatly increases the cost of the device, a feature that is unacceptable to many manufacturers; trillions of these energy storage components are demanded each year and, with the current growth trend seen in wearable technology and the IoT, trillions more will be needed at lower-than-ever prices.[253] In light of electrodes both with and without binders showing significant disadvantages-those with being cost-prohibitive, and those without suffering from morphological collapse with cycling-researchers have hunted for a third solution to this problem.

By taking advantage of the immense surface area found in three-dimensional, nano-scale structures, researchers have been able to create supercapacitors which promise increased performance and decreased susceptibility to morphological changes. The added space between

current conductors, which is provided by the three-dimensional structure, provides accommodation for the added strain associated with volumes changes during the electrochemical reactions. This promotes diffusion of the electrolyte into the inner areas of the electrodes, increasing the performance of the supercapacitor.[281] One promising strategy to create a binder-free, nano-structured electrode has been to grow the electrochemically active materials directly on to the current collectors. In recent years, nano-structured copper oxide/hydroxide for energy storage applications has been deposited onto current collectors in a variety of methods including electrodeposition, hydrothermal synthesis, chemical vapor deposition, chemical bath deposition, as well as dry and wet oxidization.[282-286] Among these methods, wet oxidization is considered to be the simplest and the least expensive way to fabricate nano-structured copper oxide/hydroxide on current collectors-on a large scale-without the use of harsh chemicals. However, to the best of our knowledge, this method has only been successfully demonstrated on bulk copper products such as copper foil, copper tape, and copper wire.[273, 274, 287-289] Traditionally printed copper circuits, which utilise copper nanomaterials, cannot survive the wet chemical oxidation (engraving) process because the deposited nano-sized copper particles become oxidized and lose a majority of their conductivity. This happens very quickly, before any nano-structured copper oxide and/or hydroxide can form to protect the conductive, inner contents. Furthermore, even if one was to successfully engrave nano-structured copper onto the current collectors, the oxidized layer would only exist on the surface of the copper foil or wire, which would result in very little electrochemically active material available to contribute to the performance of the electrodes. It is therefore urgent to develop a facile and effective strategy to take full advantages of both the emerging printed electronics technology, and low-cost wet chemical oxidation method for the large-scale fabrication of high-performance, binder-free nano-structured electrode with various form factors and flexibility.

To address the above-mentioned challenges, we present a strategy for the scalable production of low-cost, high-performance, binder-free, all-solid-state flexible supercapacitors using inkjet printers and regular paper. Herein, we demonstrate the possibility of using low-cost, low-temperature techniques to manufacture high-performance electrodes in a scalable manner. Through electroless deposition, we have created flexible circuits easily surpassing an electrical conductance of 0.005 Ω/sq, without the use of any exotic materials or sensitive manufacturing

steps. Our binder-free alternative to traditional electrodes takes advantage of the porous nature of cellulose fibers, engraving CuxO nanosheets in-situ to produce a complex three-dimensional electrode without the hassle of creating a complex, three-dimensional electrode. Due to the papers' randomly orientated cellulose fibers, the engraved Cu_xO nanosheets bind to every metallised fiber creating a thick electrode, each with its own hierarchical micro-nano-structure, averaging roughly 90 µm in depth. Again, due to the binder-free design, the paper-based electrodes show very low inner resistance values (~0.3 Ω) and remarkably high area-specific capacitance (384.2 mF/cm^2 at a scanning speed of 10 mV/s). What is perhaps most exciting, is that this simple low-cost method repeatedly produced supercapacitors with good cycling stability, achieving ~80% capacity retention after 10000 cycles with no post-production alterations. With the adoption of this technology, printed supercapacitors can be monolithically integrated into printed circuits using little more than paper for substrate. This technology adds a dimension of functionality that lends itself nicely to applications in wearable electronics and the ever-expanding IoT. As a proof-of-concept, we present in the following section an all-solid-state, flexible array of SCs capable of powering LED lights.

4.2 Experiment Details

Materials

Ethanol (anhydrous, denatured), 1,4-dioxane ($C_4H_8O_2$, 99.8%), Poly(4-vinyl pyridine) (P4VP, Mw ~60,000), formaldehyde (HCHO, 36.5-38% in water), anhydrous glycerol (C3H5(OH)3,99%), 2-propanol, silver nitrate ($AgNO_3$, 99%), copper sulfate pentahydrate ($CuSO_4·5H_2O$, 98%), 2,2'-dipyridyl ($C_{10}H_8N_2O_2$, 98%), sodium hydroxide (NaOH, 97%), potassium sodium tartrate tetrahydrate ($C_4O_6H_4KNa·4H_2O$, 99%), ethylenediaminetetraacetic acid disodium salt dihydrate (EDTA·2Na, 98%), glycerol ($C_3H_8O_3$, 99%), hydrochloric acid (HCl, 37%), Poly(vinyl alcohol) (PVA, Mw ~9,000), potassium hydroxide (KOH, 90%) and potassium ferrocyanide (II) trihydrate ($K_4Fe(CN)_6·3H_2O$, 98.5-102.0%) were purchased from Sigma-Aldrich (now Millipore-Sigma). SU-8 was provided by Kayaku Micro Chem. All chemicals were used as-received without any further purification or processing. Cellulose paper substrate was provided by Xerox.

Preparation of Coating Solution

Poly (4-vinyl pyridine) (2.5g), and SU-8 (2.5g), were dissolved into ethanol (50mL), and 1,4-dioxane (50mL) respectively, to obtain 50 mg/ml transparent solution. The two solutions were then mixed at 1:1 volume ratio to obtain a transparent solution. The final solution contains 25 mg/mL P4VP and 25 mg/mL SU-8.

Surface Modification of Cellulose Paper

Untreated cellulose paper was immersed into the coating solution for 10 seconds. The paper was then drawn out of the solution in a constant, slow, manner and allowed to dry in ambient room conditions for 5 minutes. Lastly, the coated paper was placed into an oven at 135°C for 20 minutes for in-situ cross-linking of P4VP and SU-8 molecules. Once cross-linked, the modified substrates were collected and stored in a cool, dry, and dark environment.

Preparation of Catalyst Ink for Inkjet Printing

A glycerol–water solution was prepared by mixing anhydrous glycerol and distilled water at a V/V ratio of 3:2. Silver nitrate was then added, followed by mixing in a VWR mixer for 3 minutes, to form a 40 mg/mL silver slat solution. The prepared ink was degassed in a vacuum chamber at 2 psi for 1 hour to remove dissolved gases and bubbles. The viscosity and surface tension of the final ink were 11.5 cp and 51.8 mN/m, respectively. These values fall within the optimum operating range for the Dimatix DMP-2800 Inkjet printer. A 0.2 μm nylon syringe filter was used to remove undesired particles from the ink prior to it being fed into the cartridge.

Inkjet Printing

The ink was filled into a cartridge mounted on a 10 pL piezo-electric drop-on-demand (DOD) inkjet printhead with 16 nozzles operating at the same time. The printer was set as following: drop spacing: 35 μm; meniscus vacuum: 3.5 inch of H2O; print head temperature: 25°C; jetting voltage 25.3 V. Printing was conducted at room temperature.

Electroless Deposition of Copper

An electroless copper plating bath consisting of $CuSO_4 \cdot 5H_2O$ (14 g/L), NaOH (12 g/L), potassium sodium tartrate (16 g/L), EDTA·2Na (20 g/L), HCHO (26 mL/L), 2,2'-dipyridyl (20 mg/L), and potassium ferrocyanide (10 mg/L) was prepared. Modified cellulose-fiber paper

with printed silver nitrate patterns were immersed into the bath for 3 hours. The temperature was kept at 35°C to ensure high speed deposition of the copper.

Chemical Engraving

Samples from the prior electroless deposition process were rinsed thoroughly under deionized water for 5 minutes. After rinsing, samples were immersed in 1M HCl solution for 3 minutes, followed by another rinsing under deionized water for another 5 minutes. Sodium hydroxide was dissolved in deionized water to form a 40 mg/mL NaOH solution, which was preheated to 60 °C in a thermostatic water bath. Next, the pre-washed samples were put into the sodium hydroxide solution and were kept in a sealed contained with the temperature holding at 60 °C for 48 hours. After that the samples were gently washed using deionized water and dried in a vacuum chamber for 3 hours.

Preparation of the electrolyte and device assembly

Five grams of PVA was dissolved in 100 mL deionized water at 80 °C and was stirred for 8 hours until a clear, transparent solution was formed. 3.5 g KOH was dissolved into a separate container containing 10 mL of deionized water, which was then added to the PVA solution dropwise under gentle stirring. The final solution was kept stirring for another two hours until a homogeneous electrolyte was produced. After cooling down to room temperature, the electrolyte was deposited onto previously prepared planar electrodes using a pipette gun and was spread gently ensuring no contact was made with the surface of the electrodes. The samples were dried in air at room temperature for 8 hours for further testing.

Characterization

FE-SEM images were taken using a LEO (Zeiss) 1540 field-emission scanning electron microscope (FE-SEM). The viscosity of the ink was measured with a fully automatic HAAKE Viscotester 262. Surface tension of the ink was measured by VETUS BZY-3B fully automatic tensiometer. Sheet resistances were measured by a four-point probe station Lucas Labs S-302-4 (probe SP4), connected to a Keithley 2750 multimeter. Cyclic voltammetry (CV) and electrochemical impedance spectroscopy (EIS) tests were performed on a Bio-Logic multichannel potentiostat 3/Z (VMP3), with various scanning rates in a potential range of 0–0.6 V at room temperature. Galvanostatic charge/discharge and cyclic stability tests were

carried out using an Arbin BT 2000 testing station with a current density of 20 mA/cm2 and a voltage window of 0-0.6 V. All electrochemical tests were configured as a two-electrode system. X-ray diffraction analysis (XRD) was done using a Rigaku Ultima-IV XRD goniometer, and X-ray photoelectron spectroscopy (XPS) was performed using a Kratos AXIS Ultra spectrometer.

4.3   Results and Discussion

Fabricating highly conductive current collectors on cellulose paper is challenging. It may look smooth and orderly to the naked eye, but it is in fact made of a highly complex network of randomly orientated cellulose fibers. The porous property of these fibers enables them to absorb conductive inks (e.g. silver nanoparticles, copper nanoparticles) into them, instead of leaving them on the surface, preventing the nanomaterials inside the ink from touching with each other, resulting in low conductivity. Furthermore, conductive copper traces printed with nanomaterials are incompatible with the simple and low-cost chemical engraving method for synthesize of nano-structured copper oxide due to the significant conductivity loss during the engraving process. Other *in-situ* synthesis methods, mentioned previously, each suffer from one or more prohibitive drawbacks. Whether it is the requirement of special equipment, harsh chemicals, excessive energy consumption, or complicated fabrication processes, each new 'solution' to this problem faces its own self-defeating limitation which makes commercial low-cost scalable production impractical.

To overcome these challenges, we adopt the electroless metal deposition (ELD) technique as a bridge to combine the printed electronics and chemical engraving together for low-cost large-scale fabrication of 3D nano-structured electrode. The ELD technique relies on an autocatalytic redox reaction to deposit metals on a catalyst-preloaded substrate, offers a low-cost way to fabricate metallized substrate with properties closed to bulk metal. However, untreated cellulose paper substrate struggle with capturing catalyst ions due to lack of binding sites, resulting in sever resolution loss and poor adhesion between deposited metal and substrate during the ELD process.[64, 74] Untreated cellulose paper does not readily accept catalyst ions during the ELD process due to a lack of binding sites. Attempting to do so results in very poor ELCD resolution and subsequently leads to a failure of adhesion between the deposited metal and substrate.[74] Thus, one of the key step in the proposed approach is to modify the cellulose

paper with a special developed coating. Poly (4-vinylpyridine) (P4VP) has been used in the past to modify substrates, allowing them to uptake silver ions. It achieves this through its strong ability to chelate with transitional metal ions.[211, 290] P4VP polymers can be directly coated onto substrate by physical absorption, however, these coating will eventually come off during the long-time emersion in acrylic solution for chemical engraving. Epoxy groups have been observed to form strong covalent bonds with the hydroxyl groups found on cellulose paper. This, combined with the fact that it also cross-links with the pyridine groups found in P4VP molecules, makes SU-8 a great candidate for use as an intermediary between P4VP and the cellulose substrate. Meanwhile, the highly reactive epoxy groups can also form strong covalent bonds with the abundant hydroxyl groups presenting on each cellulose fiber. Thanks to these properties, epoxy can be used as a bridge to graft P4VP molecules onto cellulose fibers, achieving a strong chemical bonding with the substrate which can withstand the long time chemical engraving process. Thus, in this work, P4VP and SU-8 were employed as the main coating components for the surface modification of cellulose paper. Figure 4-1 shows the proposed fabrication method of making high-performance 3D Cu_xO nanostructured electrodes on regular paper.

The coating solution was prepared by dissolving SU-8, P4VP, and a small amount of polyvinylpyrolidone (PVP) into a mixture of 2-propanol and 1,4-dioxane. The solution was then applied to the substrate by immersing the pre-cut cellulose paper in the solution for 5 seconds. The sample was then baked in an oven at 130oC for 15 minutes to introduce covalent bonding between SU-8, P4VP, and the paper's cellulose fibres. The resulting substrate will have abundant pyridine ligands along each fiber (Figure 4-1(b)), which are necessary to capture catalyst silver ions in the subsequent step. Attributed to the ring-opening reaction of epoxide groups, the dominant bonding type of the coating will be carbon-oxygen bonds, which are highly resistant to alkali solutions and allow the treated substrate to withstand the following ELD and chemical engraving process – both of which involve alkali solutions. Next, silver ions were deposited onto selected areas-planar SCs pattern in this case-through the use of inkjet printing (Figure 4-1(c)). When the silver nitrate contacts the primed paper substrate an electron pair, from the nitrogen atom in the unoccupied pyridine group, will capture the silver ions to form strong coordination bonds. These chemical bonds ensure a much more resistant link between the substrate and P4VP than that achieved through simple absorption. As mentioned

prior, this physical resilience is important for the deposition of copper. Such chemical bonds keep the printed silver ions firmly attached to the surface of each cellulose fiber, enhancing the adhesion between substrate and copper generated in the following ELCD process (Figure 4-1(f)).
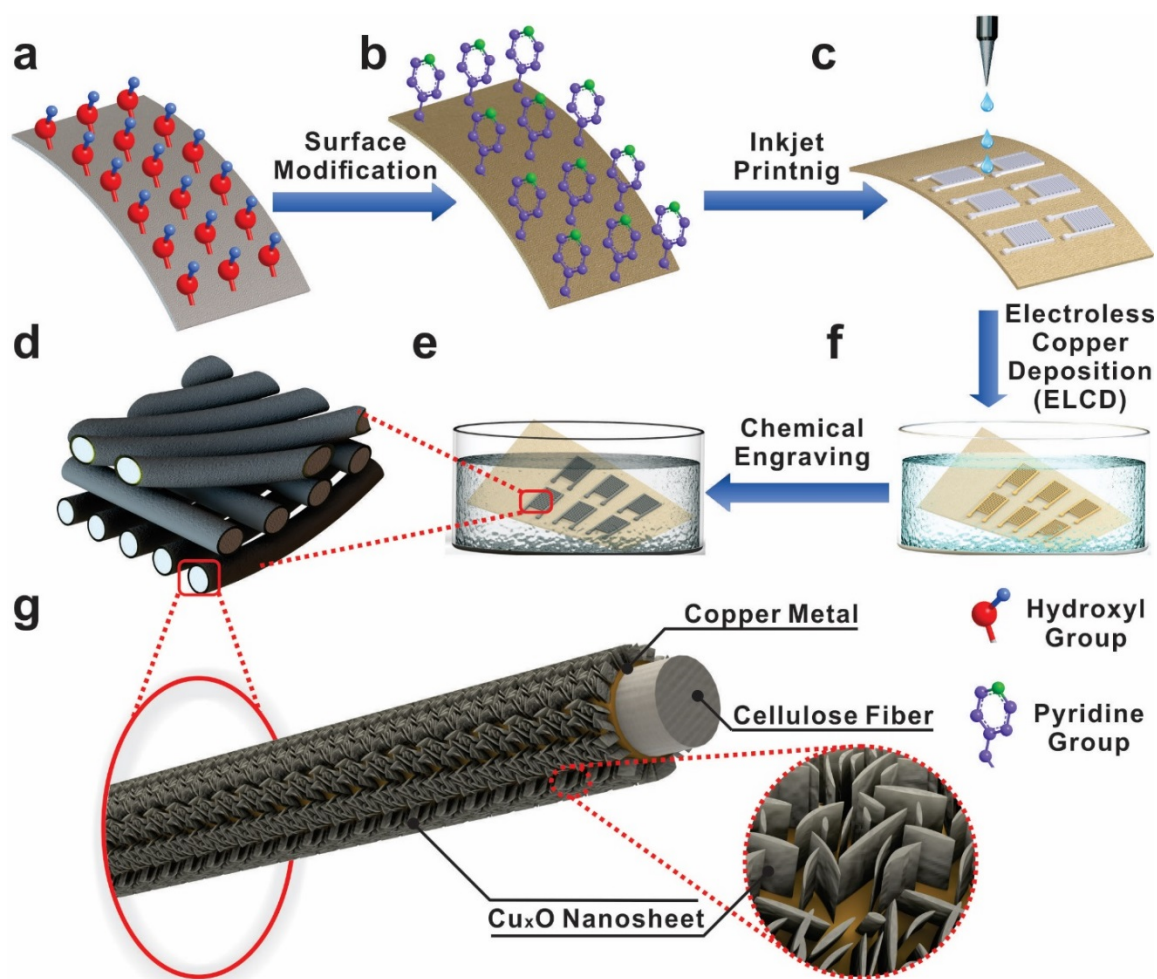
Figure 4-1. Fabrication process of binder-free 3D CuxO nanostructure on cellulose paper. (a) Surface of cellulose paper with large amount of hydroxyl groups. (b) The substrate present abundant pyridine groups after surface modification. (c) Inkjet printing of planar supercapacitor. (d) Microstructure of the sample after chemical engraving. (e) Chemical engraving of the selectively metallized substrate. (f) Electroless copper deposition for the metallization of catalyst-activated area. (g) A single cellulose fiber after chemical engraving with binder-free nanostructured active materials.

The unique fiber-based porous structure of the cellulose paper allows the ink to penetrate through to a certain depth, creating a 3D catalyst-loaded area which significantly increases the number of available targets for copper deposition. Thanks to this phenomenon, cellulose fibers not only get metallized on the very top surface, but also inside the substrate, creating a 3D porous metallized area with a thickness of ~90 µm. Details of this process can be found in the experimental section. In the following chemical engraving process, the selectively metallized paper was immersed in NaOH solution for 48 hours, as depicted in Figure 4-1(e). Under basic solution conditions in the presence of oxygen, the copper metal was gradually oxidized, giving rise to $Cu_XO/Cu(OH)_2$ arrays along the surface of each metallized cellulose fiber. After annealing at 130 ^{o}C, most of the copper hydroxide was converted to copper oxide, revealing the Cu_XO nanosheets produced *in-situ* along each metallized fiber. Figure 4-1(d) shows the microstructure of the sample after chemical engraving. Each fiber is covered by a layer of Cu_XO nanosheet arrays, which are shown to be black in the picture. The chemically-engraved fibers orientate randomly to form a porous 3D structure, greatly increasing the concentration of electrochemically active materials per unit area. Figure 4-1(g) gives a more detailed look of a single cellulose fiber after chemical engraving, with binder-free nanostructure of active materials. As depicted a layer of copper metal, shown in the colour orange, tightly wraps around the cellulose fiber (gray in colour). Vast amounts of vertically oriented Cu_XO nanosheets are present on the surface, providing a high flux of ions and fast conducting pathways for electrons throughout the electrodes. This also provides ample space for Cu_XO nanosheets to accommodate the strain of volume change during the charge/discharge process, allowing the device to remain high performance and good flexibility with longer cycling life. Furthermore, thanks to the facile process and the absence of special equipment, high quality Cu_XO nanosheet arrays of this kind can be fabricated at a large scale at low cost. Moreover, as the Cu_xO nanosheet arrays are grown *in-situ* by the direct engraving of metallized cellulose fibers, the printed patterns can be used immediately-without further modifications-as flexible electrodes for supercapacitors. The absence of polymer binder improves the conductivity and eliminates the concern of polymer swelling, as has been observed in some cases. This will enhance the structural and cycling stability as well as the electrochemical performance of the assembled supercapacitors.
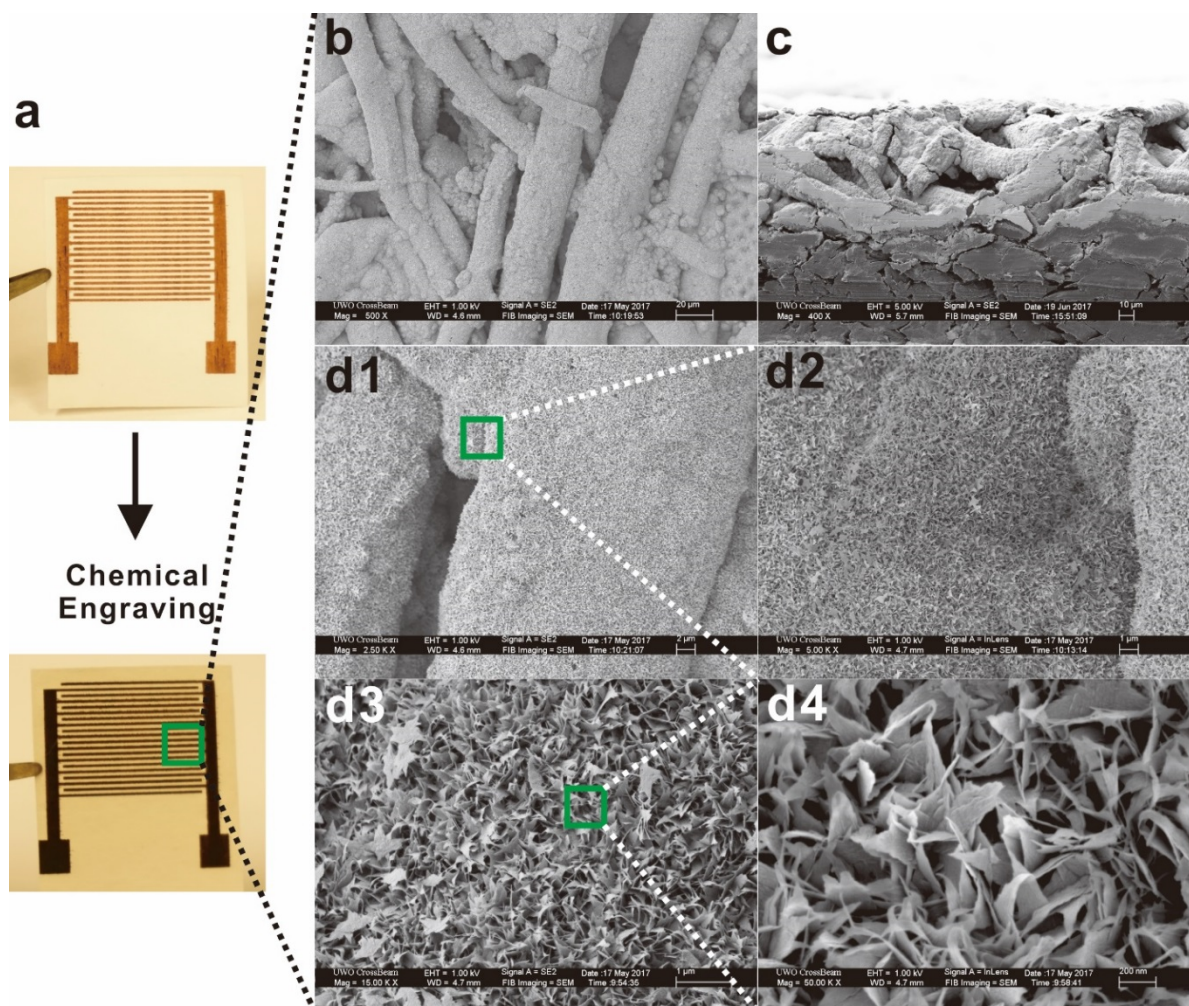
Figure 4-2. (a) Optical images of samples after electroless copper deposition (up) and after chemical engraving (down). SEM images of (b) surface morphology (c) cross-section of the chemical engraved sample. (d) SEM images taken using magnifications of 2.5 K (d1), 5 K (d2), 10 K(d3) and 50 K(d4) respectively to reveal the hierarchical micro-nano structures of the post-engraved samples.

Figure 4-2(a) shows the picture of the same sample after ELCD (up) and after chemical engraving (down). The colour of the electrodes changes from dark-yellow to black after the chemical engraving process, indicating the formation of copper oxide layer. Though the chemical engraving process introduces $Cu(OH)_2$ on the surface, which typically presents itself as blue in colour, the sample appears pure black. An interesting consequence of chemical engraving, we hypothesise this to be caused by the nano-structured $Cu(OH)_2$ nanosheets, which absorb most of the incident light making the surface appear to be black. The microstructure of

the engraved sample was investigated using field emission scanning electron microscopy (FESEM), the result of which is presented in Figure 4-2(b-d). Figure 4-2(b) shows the surface morphology of the sample, depicting the randomly oriented metallized cellulose fibers, with different diameters, forming a porous 3D microstructure. Figure 4-2(c) shows a cross-sectional image of the sample post-chemical engraving. The presence of copper/copper oxide underneath the surface can be seen to a depth of around 90 µm, indicating that the ink had penetrated 90 µm below the surface and generate a 3D metallized volume after ELCD. FE-SEM images with increasing magnification were taken to further reveal the nano-structure on the surface of each fibers (Figure 2d1-d4). Figures 4-2(d1)-(d4) were taken using magnifications of 2.5 K, 5 K, 10 K and 50 K respectively. Both the microstructure, formed by cellulose fibers, and nanostructure, formed by Cu_xO nanosheets, can be clearly seen in Figure 4-2(d1). Figure 4-2(d2) shows the magnified area of Figure 4-2(d1), wherein dense, uniform, homogeneous arrays of these nanosheet arrays can be clearly identified. The nanosheet layer conforms to the surface of the cellulose fibers with predominantly vertical orientation. Under greater magnification (Figures 4-2(d3) and (d4)), we can see that the nanosheets are several nanometers thick and cross with each other in a variety of different angles. This has left a highly porous nanostructure with adequate space between each other to accommodate the volume change during the charge/discharge process. It is worth mentioning that the concentration of NaOH in the chemical engraving solution had a significant effect on the surface morphology of the nanostructures. We observed that lower NaOH concentrations (<30 mg/mL) resulted in a flower-like nanostructure, while higher NaOH concentrations (>50 mg/mL) resulted in a coral-like nanostructure. The chemical-electrical performance of all three of these nanostructures were investigated, and it was found that samples displaying the currently presented morphology of nanosheet arrays showed far superior performance to the others. The required concentration of NaOH in the solution need to be controlled at ~ 40 mg/mL for the generation nanosheet arrays shown in Figures 4-2(b-d).
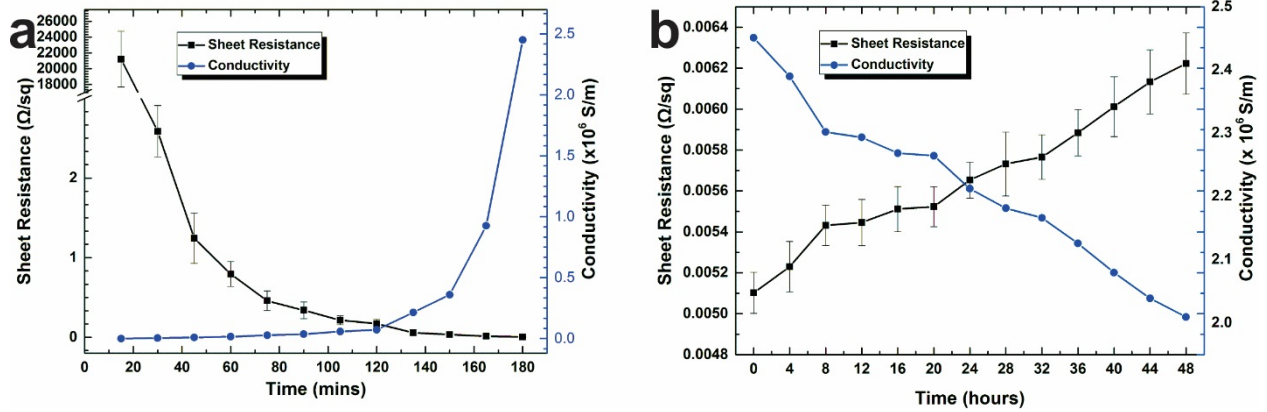
Figure 4-3. **(a) Graph showing the change of sheet resistance and its equivalent conductivity with different electroless copper plating time ranging from 0 to 180 minutes. (b) Graph showing the sheet resistance and equivalent conductivity change of samples with 3h electroless copper plating time over a 48h period of chemical engraving.**

Conductivity of the electrode is critical to the performance of the final assembled device; lower levels of resistance greatly reduces the power lost to inefficiency, and also minimises the drop in available voltage during the charging/discharging process. Maximising the conductivity of electrodes, where possible, will result in greater the performance of the SCs. In a regular printed electronics fabrication process, the electrode is produced by the direct inkjet printing of conductive inks. As the conductive properties are-in this case-entirely dependent on the ink's scarcely applied particles, this process results in a relatively high level of resistance within the circuit and thus not ideal for most applications. In comparison, during the ELCD process adopted in this work, the source of conductive material (copper) is from the electroless plating bath. When the auto-catalytic reaction is triggered by the printed silver ion, copper begins growing on the catalyst-activated (i.e. printed) areas and will continue to do so until it is removed from the solution. The thickness of the deposited copper layer can be precisely controlled by manipulating the time in which the substrate resides in the solution. Because this layer thickness in turn determines the conductivity of the substrate, it is reasonable to predict that the conductivity of the printed electrodes can be precisely controlled by altering the time of their residence in the ELCD solution. The change in each sheet's resistance as a function of ELCD processing time was investigated using the conventional four-probe method. The resistance was measured at 15-minute intervals, and the conductivity of the sample was

calculated according to the value of measured sheet resistance and metallization depth. This was used to further reveal the intrinsic electrical properties of the materials. These results are summarised in Figure 4-3(a).

According to these results, the sheet resistance of the printed electrodes steadily decreases during the ELCD process, which corresponds to the progressive formation of connection between copper grains and the increased thickness of the copper layer. After 180 minutes (3 hours) of electroless copper plating, samples displayed a sheet resistance of ~5.2 mΩ/sq – which is much better than that of the electrodes fabricated by direct printing of conductive inks (~50 mΩ/sq). The conductivity of these samples at this point is roughly 2.45×10^6 S/m, which is only about 24 times lower than that of bulk copper (59.6×10^6 S/m). These results are reasonable due to the existence of cellulose fiber inside the deposited copper and high porosity of the copper-fiber conductive structure. ELCD process shows promise to provide ultra-low sheet resistance in electrodes that has been difficult to achieve with other printing methods. It is worth mentioning that the conductivity of these electrodes can be further enhanced by increasing the ELCD residence time. Although this is an attractive quality for circuits, it was not utilised for the present study because of its inherent trade-offs: any increases to the density of the generated copper will result in corresponding decreases to the space between cellulose fibers, which an important factor to consider when fabricating SCs. Through trial-and-error, we determined that an ELCD duration of approximately 3 hours led to a nice balance between electrode conductivity and supercapacitor performance, motivating us to use this as the standard ELCD residence time for all electrodes utilised in this work. Recognising that the chemical engraving process is in fact a kind of oxidization process, we were concerned that there may be undesired losses in conductivity due to copper oxidisation. Hence, the relationship between sheet resistance/conductivity and chemical engraving time was investigated. Figure 4-3(b) shows the sheet resistance/conductivity change of samples with 3h electroless plating time over a 48h period of chemical engraving. Data was collected every four hours using the same four-probe measurement station. The resistance of samples increases at a near-constant rate of about 0.46% per hour from the beginning (~5.1 mΩ/sq), to its final value (~6.2 mΩ/sq) attained after 48h. This increase in sheet resistance, totalling 22% throughout the entire process, can be attributed to the oxidization of the metallized cellulose fibers. In summary, the chemical engraving process does in fact introduce a conductivity loss

of ~22%, but when that is held in context to its exceptionally low initial sheet resistance, the loss in conductivity is minimal and has little appreciable impact on its ability to be used in high performance devices.
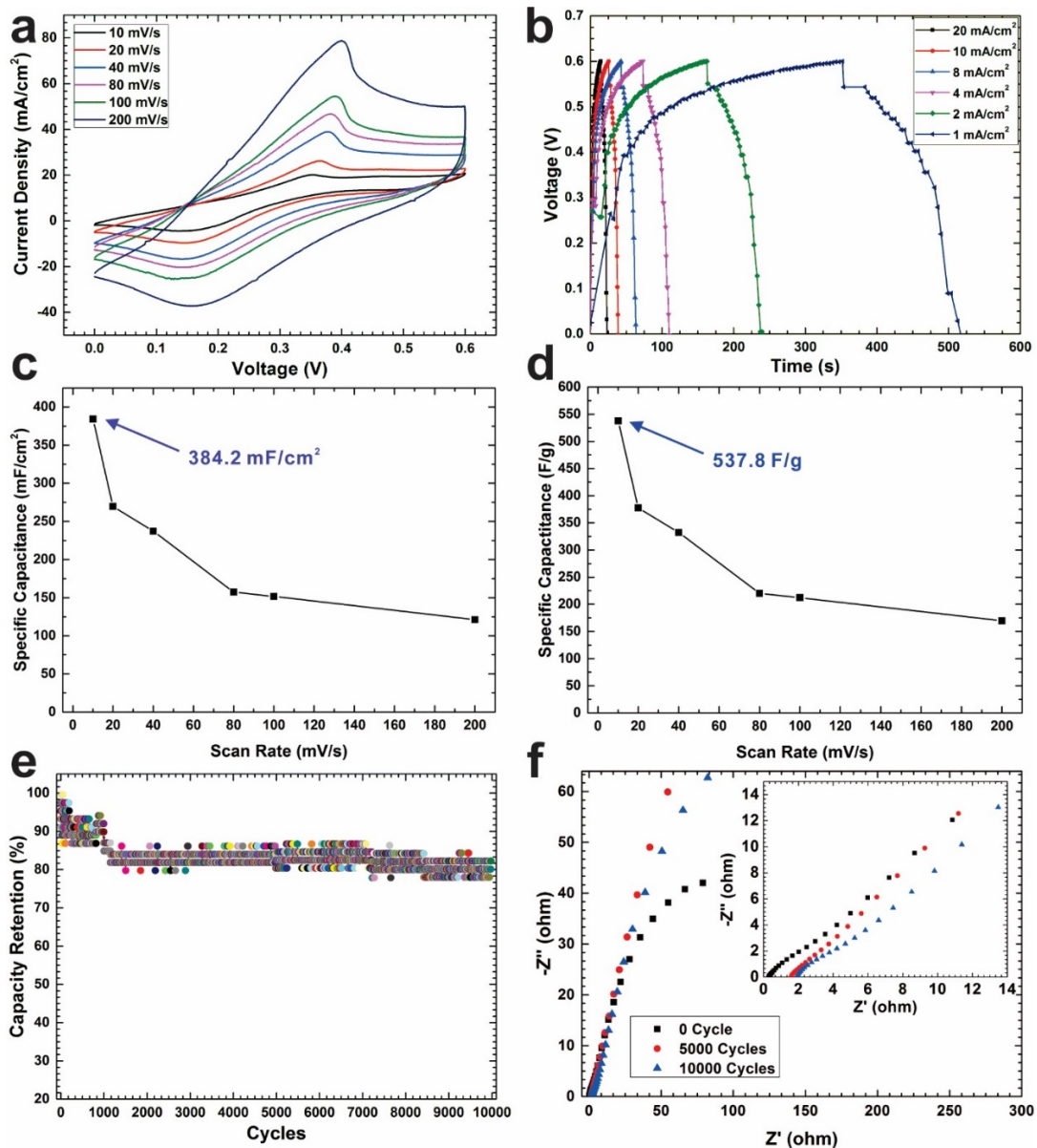
Figure 4-4. Graphs showing (a) cyclic voltammetry (CV) curves at different scan rate of 10, 20, 40, 80, 100, 200 mV/s respectively, (b) galvanostatic charge/discharge profiles with different current density of 1, 2, 4, 8, 10, 20 mA/cm2, specific capacitance versus area (c) and mass (d), (e) capacity retention as a function of cycle number with current density of 20 mA/cm2 and (f) Nyquist plots collected at open circuit potential of the as-prepared SCs.

Symmetric planar SCs-with as-prepared, binder-free electrodes-were assembled using KOH-PVA gel as the solid-state electrolyte. The cyclic voltammetry (CV) studies were performed to analyze the electrochemical behaviour of the assembled device using a two-electrode setup with potential ranging from 0 to 0.6 V at different scan rate of 10, 20, 40, 80, 100, 200 mV/s respectively. The results are shown in Figure 4-4(a). Each CV curve consists of a pair of strong redox peaks which are attributed to the Cu^{2+}/Cu^+ and Cu^+/Cu^{2+} transition, revealing the pseudo-capacitance behaviour of the electrodes.[272, 273] It is further noted that when the scan rate increases, the shape of the CV curve changes. The cathodic peaks show right-shift to high voltages, while the anodic peaks shift to lower values at higher scan rate. To reveal more about the electrochemical capacitive performance of the electrode, galvanostatic charge-discharge was measured at various current densities (Figure 4-4(b)). None of the resulting six curves exhibit the ideal triangular shape, whose deviance suggests contribution from the faradaic redox reaction. The initial drop in voltage whilst discharging the SCs can be attributed to the internal resistance of the assembled device. Both the capacitance per unit area and the capacitance per gram at different scanning rate were calculated according to the CV curves, area of the electrodes and the total mass of the active materials on the electrodes. The total mass of the active materials was determined by measuring the difference in weight before and after washing the sample in 1M HCl solution. The results are shown in Figure 4-4(c) and Figure 4-4(d) respectively. The specific capacitance of these samples was found to decrease as scan rate was increased. This is to be expected, as ions passed at lower current densities can penetrate deeper in to the three-dimensional structure of the electrode material, providing them access to a greater number of pores; at higher current densities, utilisation of electrode material was limited to only the outer surface of electrodes. At a scan rate of 5 mV/s, the material exhibited its highest specific capacitance of 384.2 mF/cm^2 (Figure 4-4(c)) and 537.8 F/g (Figure 4-4(d)). It is worth mentioning that, other researchers have investigated the super-capacitive properties of nano-structured, binder-free Cu_xO electrodes.[273, 274, 287-289] Unlike the presented work however, these electrodes were produced on non-porous copper tape or foil where electrochemical active Cu_xO grew only on the top surface, limiting its aerial capacitance in a great extent. In this work, taking advantages of the micro-porous structure of paper, the loading of Cu_xO expand from a 2-D surface to a three-dimensional architecture of cellulose fibers, resulting in boosted specific capacitance. Moreover, the 3D nanostructured architecture provides a fast, ionic transportation path, contributing to the improved

performance as well. To the best knowledge of the authors, the aerial capacitance of the presented samples exceeds those of all other Cu_xO electrodes produced by any means of printing.

To determine if the proposed technology is robust enough to withstand the endless number of charge-recharge cycles demanded by industry, the printed capacitors' cycling performance was investigated. Capacitance retention as a function of cycle number was explored using the charge-discharge curves at the highest current-density (20 mA/cm^2; Figure 4-4(e)). As illustrated, a sharp decrease in specific capacity can be observed during the first few hundred cycles, levelling out to roughly 85% of its initial capacity by cycle 1000. At this point the slope evens out, losing only 3% capacitance over the subsequent 9000 cycles (Figure 4-4(e)). The observed loss of capacitance is believed to have resulted from a combination of collapsed Cu_xO nanosheets, ineffective electrode-electrolyte contacts, and deteriorated ionic transfer pathways. Electrochemical impedance test was conducted at open circuit potential in the frequency range from 0.01 Hz to 100 kHz, to further show the properties of the as-prepared devices. The Nyquist plots were created for samples having underwent 0, 5000, and 10000 charge/discharge cycles (see Figure 4-4(f)). It can be seen that all three samples displayed similar shapes in both high frequency (semi-circle) and low frequency (linear) circuit potentials. The shifted intercept of impedance, down the real axis at high frequencies, reflects the equivalent series resistance (ESR) of the device. This is closely related to the electrolytic resistance, the intrinsic electrical resistance of the Cu_xO nanostructured layers, as well as the contact resistance between electrolyte, electrodes, and current collectors. The ESR values of the three tested samples were 0.27, 1.56, and 1.90 Ω, corresponding to samples having undergone 0, 5000, and 10000 charging/discharging cycles respectively. The resistance to charge-transfer (RCT) can be estimated from the Nyquist plot using the diameters of the semicircles plotted along the real (x) axis, confirming the findings in the cycling tests. The devices' RCT increases as a function of cycle number, reflecting the large initial drop in specific capacitance followed by the levelling out after the first few hundred cycles.
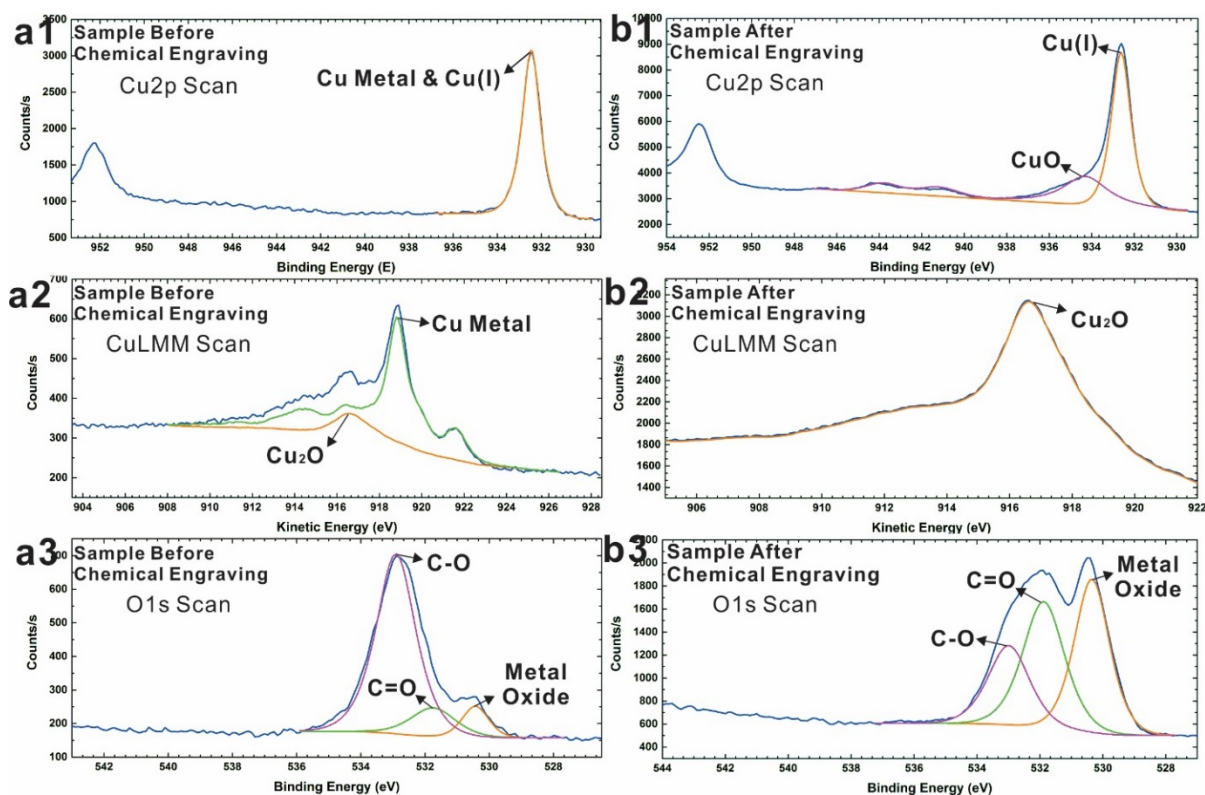
Figure 4-5. High resolution XPS survey spectra of Cu 2p, Cu LMM and O 1s of samples (a)before and (b) after chemical engraving process.

X-ray photoelectron spectroscopy (XPS) was used initially to determine out the precise species of copper present on the surface of the samples. XPS survey spectra of samples both before and after chemical engraving process are shown in Figures 4-5 (a) and (b), respectively. In the sample analysed prior to chemical engraving (left), the high resolution XPS captured a strong peak of 932.6 eV, suggesting the presence of Cu $2p_{3/2}$ (Figure 4-5(a1)). This peak may reflect the presence of Cu metal, Cu(I) oxide, or more likely, a mixture of both. It is difficult to confidently ascertain which copper species is present here due to the close proximity between characteristic peaks of Cu metal (932.6eV) and Cu(I) oxide (932.7eV). Cu LMM was scanned to further identify the copper species on the surface. The Cu LMM spectrum, shown in Figure 4-5(a2), reveals two distinct peaks, 916.8 eV and 918.6 eV, which can be ascribed to Cu(I) oxide and Cu metal, respectively, implying the presence of both Cu_2O and Cu metal on the surface. By calculating the integral area of the two peaks, the relative proportions of the two identified copper species were determined to be 23% Cu_2O and 77% Cu metal. This result indicates that the majority metal found on the surface of the electrode-prior to engraving-was

Cu metal. The O 1s high resolution spectrum is shown in Figure 4-5(a3)). As expected, a weak O1s metal oxide peak was found at 529.5 eV, further confirming the existence of Cu_2O on the surface. When characterising the sample which had been chemically engraved, a similar process involving XPS was employed. As illustrated in Figure 4-5(b1), the Cu $2p_{3/2}$ spectrum presents two peaks, one at 934.8 eV and the other at 932.7 eV. The peak at 934.8 eV can be ascribed to $Cu(OH)_2$, whilst the peak at 932.7 eV requires further analysis. The Cu LMM spectrum (Figure 4-5(b2)) of the engraved sample shows only one peak which well fits the Auger peak of Cu_2O at 916.8 eV. According to this, the peak at 932.7 eV from Cu $2p_{3/2}$ spectrum can be identified as peak from Cu_2O species and there is no Cu metal on the surface. By calculating the integral area of the two peaks from Cu $2p_{3/2}$, we found that the proportion of Cu $(OH)_2$ and Cu_2O was 39% and 61% respectively. In the O1s spectrum presented in Figure 4-5(b3), a strong peak at 529.4 eV was observed. This peak belongs to the metal oxide found on the surface of the sample and corresponds to the chemically engraved $Cu(OH)_2$ and Cu_2O. In brief, the XPS survey provides direct evidence that Cu(II) and Cu(I) species are both successfully introduced onto the surface through chemical engraving. It is acknowledged however, that XPS study can only reveal the insights into the surface layer (<5 nm thickness) and not further. To fully characterise the constituents of these samples, X-ray diffraction (XRD) was employed to better understand the composition and crystalline structure of the electrodes.

Figure 4-6 shows the XRD spectra of three different paper substrates. The first was taken just before metallization (top), the second was shortly after metallization by ELCD (middle), and the third sample was analyses after chemical engraving (bottom). The freshly metallized sample (middle) shows three clean and sharp peaks at 43.46º, 50.43º and 74.25º, which coincide with the Cu metal crystal planes (111), (200) and (220), respectively (JCPDS Data 04-836). Interestingly, the XRD spectra is absent of any peaks pertaining to the presence of $Cu(OH)_2$, which contrasts that of the previous XPS survey (Figure 4-5(a)). This finding implies that $Cu(OH)_2$ only exists on the very top surface of the sample, as there are no detectable quantities for the XRD machine. In the samples which had been chemically engraved for 48 hours, the same three peaks observed in the freshly prepared sample are present but are accompanied by five others as well. The three familiar peaks appear to be of similar shape to those of the freshly metallized sample, but the peaks at 50.43º for Cu (200) and 74.25º for Cu (220) are considerably weaker, indicating that copper metal with such crystal structures may

tend to get oxidized more easily during the chemical engraving process. A number of new but weaker peaks appear in the XRD spectrum; the peak at 23.8º corresponds to the (021) plane of $Cu(OH)_2$ crystal (JCPDS Data 80-0656), while the peak at 36.4º corresponds to the (111) plane of Cu_2O (JCPDS Data 05-0667) crystal. The three peaks clustered together at 35.7º, 38.7º, and 61.5º can be ascribed to the (11-1), (111), and (11-3) planes of the CuO crystal respectively (JCPDS Data 48-1548). As observed in the fresh sample, different results were obtained in the XRD survey when compared to those of the XPS, which is again likely due to the much deeper detection depth of the XRD equipment. Based on the results obtained using XRD and XPS, we conclude that the electrochemically active materials generated by the engraving process are mainly Cu_xO, with small amounts of $Cu(OH)_2$ below the surface.
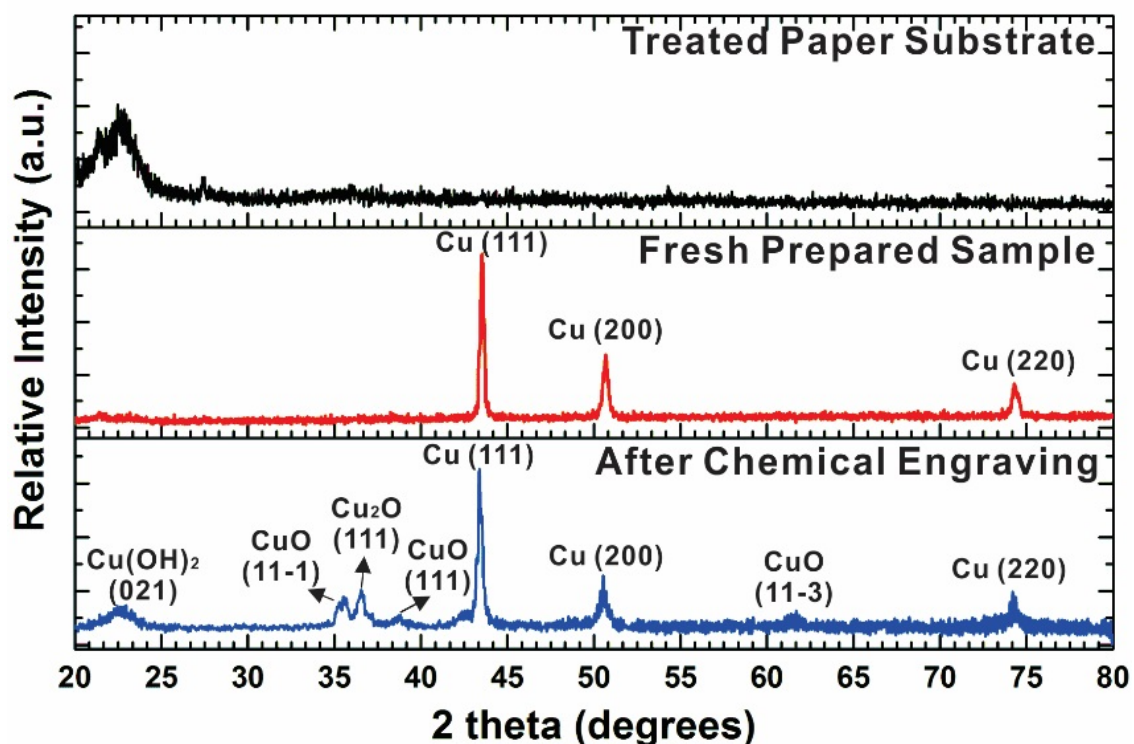
Figure 4-6. X-ray diffraction spectra of treated paper substrate before metallization (top), sample after electroless copper deposition (middle) and sample after chemical engraving (bottom).
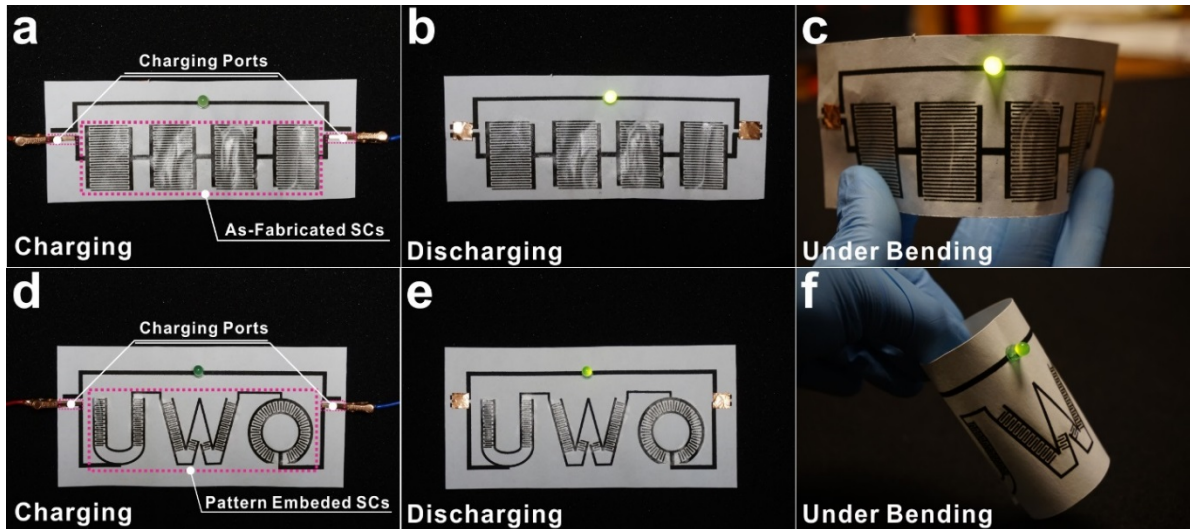
Figure 4-7. As-fabricated SCs with various form factors as object-tailored and monolithically integrated power sources. (a) Charging and (b) discharging of four SC cells connected in series. (c) The as-fabricated device operating as intended in bend state. (d) Charging and (e) discharging of electronic art with four monolithically integrated SCs (one in letter "U", two in letter "W" and one in letter "O") connected in series. (f) The device working properly when rolled into a cylinder.

One of the most attractive advantages of inkjet-printed SC is the strong ability of monolithically integration with other devices and its provision of aesthetic versatility. Using the fabrication method proposed in this work, the printed SCs can be readily connected in series or parallels without the use of extra metallic interconnects. To demonstrate the versatility of the proposed technique in real world applications, a flexible SCs array with four cells connected in series is fabricated on regular cellulose paper, which is able to provide a total voltage of ~1.9 V (Figure 4-7(a)). The printed SCs adopted a planar design with 26 fingers crossing with each other. Each finger was 2 cm long, 400 µm wide, and was separated by a 400 µm gap in between. Charging ports (positive, negative) were printed on each side of the SCs array to accommodate the attachment of alligator clips, as shown in Figure 4-7(a). Once charged, the two charging ports were each patched over by a piece of copper tape, closing the circuit with the single mounted light-emitting diode (LED). Note that the charging ports used in this example are arbitrary and could easily be replaced by a switch or a diode for the simple control of charging/discharging in real-world applications. The LED remained fully lit even when the device was bent and creased (see Figure 4-7(c)), reflecting excellent device flexibility.

To demonstrate its capability of integrating with its intended application, a second pattern was created using the well-known abbreviation of the authors' institute, "UWO" (see Figure 4-7(d)). The electronic art utilised four SCs (one in letter "U", two in letter "W" and one in letter "O") connected in series, which when combined were enough to power the LED lamp with ease (Figure 4-7(e)). To demonstrate the devices flexibility yet again, the device was rolled into a cylinder and showed changes to its performance as an LED-powering supercapacitor (Figure 4-7(f)). The above demonstration is evidence that the inkjet-printing-based technique proposed herein allows for the easy control of electrical properties (i.e. voltage, current) of the produced power sources through simple designing of the printing patterns. In addition to the facile control of the power source properties, the printed SCs can be seamlessly integrated into any printed circuits or even art work.

4.4 Conclusion

The demand for cheaper, more efficient, more reliable, safer, and environmentally sustainable alternatives to current energy storage systems is unquenchable. By exploiting the perfectly imperfect, overlooked properties of regular cellulose paper, we present a scalable method of fabricating low-cost, high-performance, all-solid-state supercapacitors which are more flexible than any other comparable solution. The binder-free SCs capitalize on the randomly oriented cellulose fibers to house porous Cu_xO nanosheets, all using little more than a common inkjet printer. For the first time, we bridged the emerging printed electronics technology with a low-temperature chemical engraving method to construct nanostructured Cu_xO-*in-situ*-on highly conductive current collectors. The new SCs can be seamlessly integrated to any printed circuit-artwork or otherwise-demonstrating their exceptional versatility and promise for applicability as a new generation of object-tailored power sources. The utilization of low-cost cellulose paper in tandem with electroless copper deposition and chemical engraving, has led to substantial improvements to the printed supercapacitors all whilst significantly lowering their production cost. Moreover, with the involvement of inkjet printing, the printed SCs can be easily connected in series or parallel, allowing the user-customized control of the properties of the power sources. Thus, we believe that the facile, low-cost and large-scale method proposed here provides a promising way to produce a new class of monolithically-integrated high-performance power sources, which are badly needed by the booming flexible/wearable electronics and IoT industries.

Chapter 5

5.   A Solvent-Free Laser Printing Approach for Printed Electronics

5.1   Introduction

Printed electronics, flexible electronics and wearable electronics, with the potential of reforming the electronics industry and changing our daily life, constitute a rapidly growing area of research.[291-294] Various printing techniques, such as inkjet printing,[295, 296] gravure printing,[297] screen printing,[298, 299] aerosol-jet printing and laser-induced forward transfer printing (LIFT),[300-303] have been adopted to fabricate electrical and electronic devices for a broad variety of applications. High-efficiency and scalable printing techniques are always appealing to printed electronics community. In this study, a high-speed and solvent-free laser printing technique has been developed for printed electronics. In this technique, special toners that are synthesized with desirable function(s), can be loaded into office laser printers to print electronics on either flexible or rigid substrates. This new laser printing based printed electronics approach is robust, reliable and scalable, which opens a new avenue for printed electronics.

R&D of printed electronics have been significantly advanced these years. Most of the existing printed electronics techniques are solution-based methods, involving solvent(s). Usually, solution processable and electrically active materials, such as metal nanoparticles or conductive polymers, are formulated into different inks for printing. Metal nanoparticles like Ag nanoparticles have been widely explored as conductive inks, playing a major role in printed electronics. However, for the existing conductive inks composed of small metal nanoparticles, large amounts of stabilizing, capping and/or modified agent(s) are required in order to prevent the nanoparticles from aggregation, precipitation and oxidization,[304-306] resulting in a low solid loading and high impurity content, and consequently, causing a high electrical resistance of the printed patterns. Though many efficient sintering methods such as selective laser sintering,[307] pulsed light sintering,[308, 309] plasma and microwave flash sintering have been employed to anneal the printed patterns and yield an improved conductivity up to 60% of the bulk materials,[295, 310] the resistance of these printed conductive traces are still high due

to the thin (<1 µm) conductive layer, making the printed electrodes hard to fulfill the requirements of the electronics industry. In addition, the preparation of high-quality ink is usually complicated and costly.[307, 311, 312] In terms of ink formulation, it often has strict requirements for viscosity and surface tension. The printing quality can be easily affected by the intrinsic limitation, like pinhole formation, and the adhesion of the ink to the substrate is also a common challenge for all wet processing techniques.

Here we report a high-speed and solvent-free printed electronics approach based on the laser printing mechanism. In this method, catalyst(s)-containing toners are synthesized and printed on the substrate followed by electroless deposition (ELD) to achieve a thick and high-resolution metal pattern, and thus to achieve good electrical performance. This approach, printing catalysts followed by ELD, can significantly improve the printing speed (few times faster than traditional inkjet printing), as a result, productivity and efficiency, while lower the manufacturing costs.[67, 217, 313-315] In our previous work, we demonstrated a strategy of printing catalyst followed by a low cost ELD-based method for fabricating flexible electronics on regular photopaper via inkjet printing which offers a low-cost additive technique for rapid prototyping of circuits.[316] In this work, the toner particles were functionalized with catalyst additive(s) and printed using laser printers. Here we demonstrate high-performance copper-based flexible electronics (e.g. an LED array display as a demo) can be fabricated.

Laser printing is a solvent-free, high-speed, and electrostatic digital printing process that rapidly produces high quality patterns by passing a laser beam over a charged drum in order to define a differentially charged image and has been widely used in our daily life. Although laser printing has been widely utilized in graphic printings, using laser printing for device fabrication is rarely reported except few cases such as laser-induced forward transfer printing, [301, 302, 317] laser printed pattern for controlling the growth of carbon nanotube and fabricating microfluidic devices[318-320] . Here we report a study of laser printing of electronics using an office use laser printer, the first demonstration of using laser printing technology for printed electronics. In this approach, toners containing catalyst(s) are synthesized first, and then loaded into a office laser printer to print desired patterns. Taking the advantages of ELD, a thick metal layer is deposited on the patterns of the substrate. Thus high-resolution and high-conductivity electronic circuits are fabricated. Importantly, the toner acts as an adhesion-promoting buffer layer, forming as a strong adhesive between the deposited metal and the substrate. In addition,

the easy metallization of printed patterns makes it an especially effective method for massive production of flexible printed circuits. The high-speed, solvent-free laser printing process is a high throughput, low cost, efficient and environmentally benign method for flexible electronics manufacturing.

5.2 Experiment Details

Materials

The transparent PET substrate used for laser printing was bought from 3M Canada. Ammonium tetrachloropalladate (II) ($(NH_4)_2PdCl_4$, 97%) and [2-(Methacryloyloxy)ethyl] trimethylammonium chloride used for synthesizing toner additive were bought from SIGMA-ALDRICH. Chemicals used for ELD process were copper (II) sulfate pentahydrate ($CuSO_4 \cdot 5H_2O$, 98%, SIGMA-ALDRICH), potassium sodium tartrate tetrahydrate ($C_4H_4KNaO_6.4H_2O$, 99%, SIGMA-ALDRICH), formaldehyde solution (HCHO, 36.5-38% in H_2O, SIGMA-ALDRICH) and Sodium Hydroxide (NaOH, 97%, CALEDON).

Synthesize of toner additive

Poly (2-(methacryloyloxy)ethyl-trimethylammonium chloride) (PMETAC) was synthesized by solution polymerization of 2-(methacryloyloxy)ethyl-trimethylammonium chloride in water at 50 wt % concentration, the prepared solution was then catalyzed by 1 wt % potassium persulfate at 75 °C for 1h. Excessive acetone, a poor solvent for PMETAC, was added to the solution after cooling down to precipitate the produced PMETAC. The supernatant liquid was removed and the precipitate was washed by acetone for 3 times. The outcome was dried in vacuum at 60 °C for 12 hours yielding white crystal powder. 3.32g synthesized PMETAC was then dissolved in 10mL DI water yielding a PMETAC aqueous solution with a concentration of 1.6 M. 4.55g $(NH_4)_2PdCl_4$ was added into the solution, making the molar mass ratio of these two chemicals 1:1. Brown precipitation was formed right after the adding of $(NH_4)_2PdCl_4$. The solution was stirred for 24 hours to make the immobilization thoroughly. The generated brown precipitation was washed by acetone for 3 times to eliminate the water inside it and was then put into vacuum chamber for drying for 12 hours at 40 °C. The $PdCl_4^{2-}$ loaded PMETAC showing in a light brown color was generated after 12 hours drying and was ready to use.

Preparation of the modified toner

2g PdCl$_4{}^{2-}$ loaded PMETAC toner additive was ball milled for 3 hours and then 20g regular laser printing toner was added. The regular toner was standard capacity toner for a Xerox Phaser 3300mpf laser printer. The ball milling continued for another 2 hours to generate a uniformly mixed modified toner. The prepared modified toner was then filled in a cleaned toner cartridge for Xerox Phaser 3300mpf laser printer.

ELD of copper

ELD process was conducted to apply copper pattern onto the printed feature. The detailed process of ELD can be found in former literatures.[12] Briefly, patterns printed with modified toner were put into a plating bath containing 1:1 mixture of freshly prepared solutions I and II. Solution I consists of 13 g/L CuSO$_4$•5H$_2$O, 12 g/L NaOH and 29 g/L KNaC$_4$H$_4$O$_6$•4H$_2$O which were added into distilled water in sequence. Solution II is 9.5 mL/L HCHO in distilled water. Deposition time was controlled to 10 minutes to 110 minutes with an interval of 10 minutes. Deposited copper lines were air dried and were ready for characterization.

Characterization

A Hitachi S-4500 field emission scanning electron microscopy (SEM) was used to observe the surface morphologies of the plated patterns. Atomic force microscope (AFM, Dimension V equipped with a Nanoscope controller V and Nanoscope software 7.30, Veeco) was used to obtain height and roughness information. Adhesion was determined by the use of a cross scotch tape test, following ASTM D-3359 using 3M # 600 tape. A four-probe station (Lucas Labs s-302-4 with SP4 four point probe head) together with the M2400 Keithley Multimeter was used to carry out the measurement of the sheet resistance, from which conductivity was calculated. X-ray diffraction analysis was done using Rigaku Ultima-IV XRD goniometer.

5.3 Results and Discussion

Figure 5-1 schematically illustrates the fabrication procedure. The toner cartridge was filled with modified functional toner. During printing, the photosensitive drum was uniformly negatively charged. Then a laser beam was raster scanning to expose a designed pattern on the photosensitive drum, which will neutralize the exposed part, leaving the negative charge on the unexposed surface to repel the negatively charged toner particles. Then the patterned functional toner particles were absorbed and transferred onto the substrate by electrostatic

attraction. Finally, the toner particles were melted and fixed tightly on the substrate by fuser roller and pressure roller.
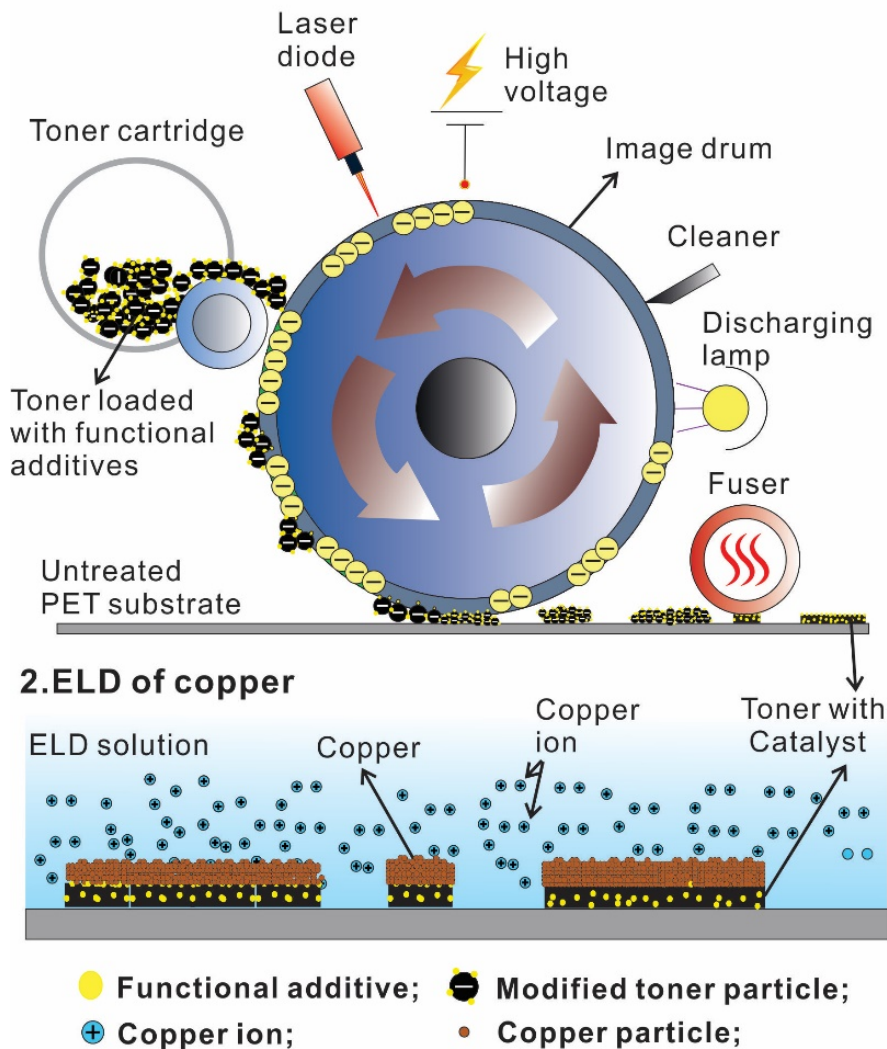
Figure 5-1. Schematic diagram of laser printing of catalyst-based toner for copper patterning.

The printed catalyst-containing patterns were then put into a fresh prepared ELD bath to induce copper deposition on the toner pattern, yielding high-resolution metal patterns with good conductivity. The central strategy of this solvent-free laser printing method is the preparation of a functional toner additive that is compatible with the regular laser printer. The catalyst additive was introduced without affecting the electric charge properties of the original toner. In addition, the additive was uniformly mixed to allow a strong adhesion with the printed toner.

To achieve all these attributes, a polyelectrolyte molecule was employed as a linker between the functional catalyst additive, tetrachloropalladate ($PdCl_4^{2-}$), and the toner. Briefly, the ammonium tetrachloropalladate (II) ((NH_4)2$PdCl_4$) was mixed with the polymerized 2-(methacryloyloxy) ethyl-trimethylammonium chloride (PMETAC) in the solution, forming a new water-insoluble polyelectrolyte with tetrachloropalladate (II) groups taking place of chloride ion of PMETAC. The new palladium-containing polyelectrolyte contained a lot of functional groups and was well compatible with toner particles mainly composed of polyester. Once mixed, they can interact with toner particles to form strong bonding and thus does not impair printability of the toner. Figure 5-2(a) shows the scanning electron microscope (SEM) images of the resulted polyelectrolyte additive after drying. The as-prepared polyelectrolyte particles have an average size of ~600 nm, which is not fine enough for optimized mixing with the toner. Therefore, finer polyelectrolyte powder was obtained by ball milling using a high energy ball mill machine for 10 minutes before mixing with regular toner powders. Another 2 hours' low-speed ball milling of toner particles and palladium-containing polyelectrolyte was conducted to get a uniform and well-mixed functional toner. Finally, the synthesized polyelectrolyte particles were well dispersed and mixed with the regular toner particles, and the size of modified functional toner powders ranges from ~3 µm to ~12 µm (Figure 5-2(b)). It can be observed clearly that the small polyelectrolyte particles adhere onto the surface of the original toner particles (Figure 5-2(c)).
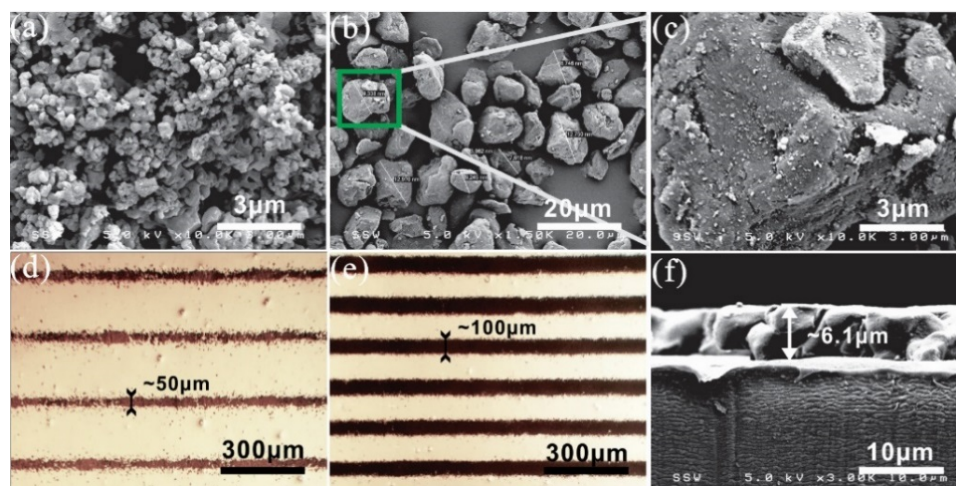
Figure 5-2. SEM images of (a) polyelectrolyte particles; (b) the mixed toner particles; (c) single toner particle; (d), (e) optical images of laser printed toner pattern with different line width; (f) SEM image of cross-section of laser printed toner.

Figures 5-2(d) and (e) show a microscope image of a line array printed on a pristine PET substrate with a width of ~50 µm and ~100 µm, illustrating that the modified toner particles are uniformly aligned on the substrate creating high quality patterns. In addition, the cross-section image of printed toner on PET (Figure 5-2(f)) indicates that the toner layer presents uniform thickness of ~6 µm on the whole pattern. More importantly, the catalyst-containing toner pattern adhered to the substrate tightly, which will function as adhesion promotion layer for the metal layer. Subsequently the metal pattern was deposited by ELD of copper. The printed patterns were immersed in a fresh made ELD solution, prepared according to the recipe used in our previous study.[40] Under the help of catalyst, copper was deposited along the printed pattern to keep high controllability. Immersion time and temperature are two important factors for controlling copper deposition thickness and rate, [41,42] which will directly influence the performance of printed pattern, like the roughness of the pattern and especially the resistivity of the deposited copper. Figure 5-3(c) shows the copper layer thickness with respect to the deposition time under room temperature. For the first 30 min, copper grew slowly, and the resistivity was high (more than 5 times bulk copper). But after the copper grew continuously with a higher speed of ~22 nm/min, the resistivity gradually went down. After 110 min of deposition, the copper layer achieved a thickness of ~2 µm and a resistivity of ~2.55×10^{-8} $\Omega \cdot m$ which is only 1.5× of bulk copper (1.68×10^{-8} $\Omega \cdot m$). AFM analysis was conducted to investigate the surface profile of copper layer and the results were shown in Figure 5-3(c). The relative height value curves of a selected scanning area of 10 µm × 10 µm (Figure 5-3) and the average roughness value were given in Figure 5-4, indicating that the surface roughness decreased with increasing of copper deposition time.
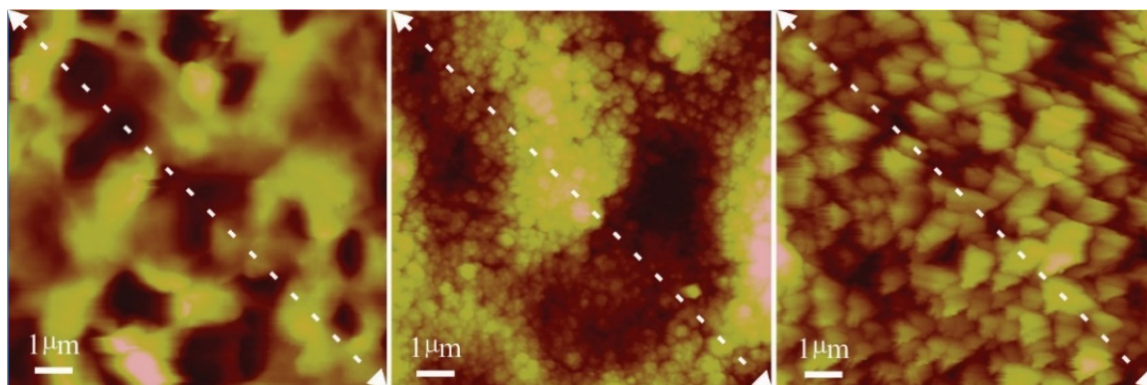
Figure 5-3. Height information of printed toner, 30min after ELD of copper, 60min after ELD of copper (from left to right).
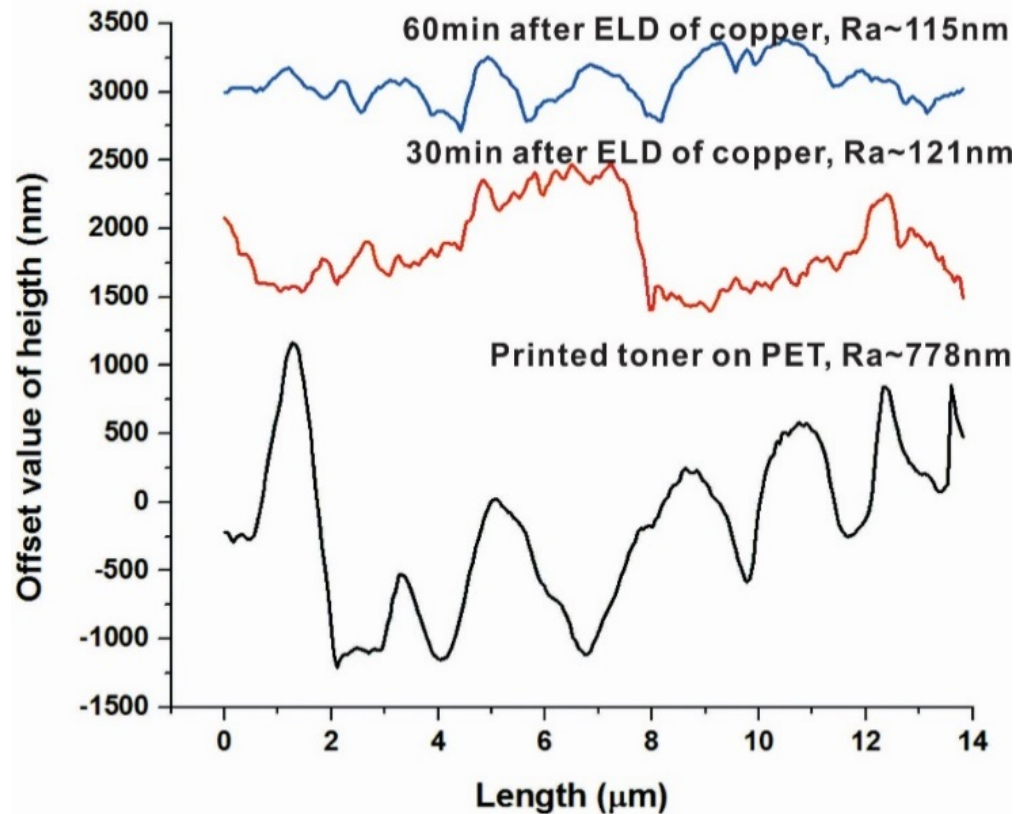
Figure 5-4. AFM section profile and area roughness information of selected parts shown in Figure 8with white dashed lines corresponding to the printed toner on PET, 30min after ELD of copper, 60min after ELD of copper (from bottom to top).

The original printed toner has a high roughness value of ~778 nm, resulting in the initial deposition of discontinuous copper particles, giving an explanation to the low conductivity of the copper layer in the first 10 minutes. High roughness also makes the growth rate of copper uneven in the first few minutes since the newly deposited copper particles tend to fill the sunken area, deducting the copper growing speed. After 30 minutes, surface roughness was reduced to ~110 nm and a faster copper growth rate was observed in the following 60 minutes (Figure 5-5).

Copper clusters grew larger and larger as the immersion time increased, creating a copper layer with lower roughness and better conductivity. Figures 5-6 (a), (b), (d) show the surface of the deposited copper layer after 110 minutes of ELD, which is dense and uniform and also shows

a crystalline structure, leading to a high-quality copper pattern with the conductivity close to that of the bulk material.
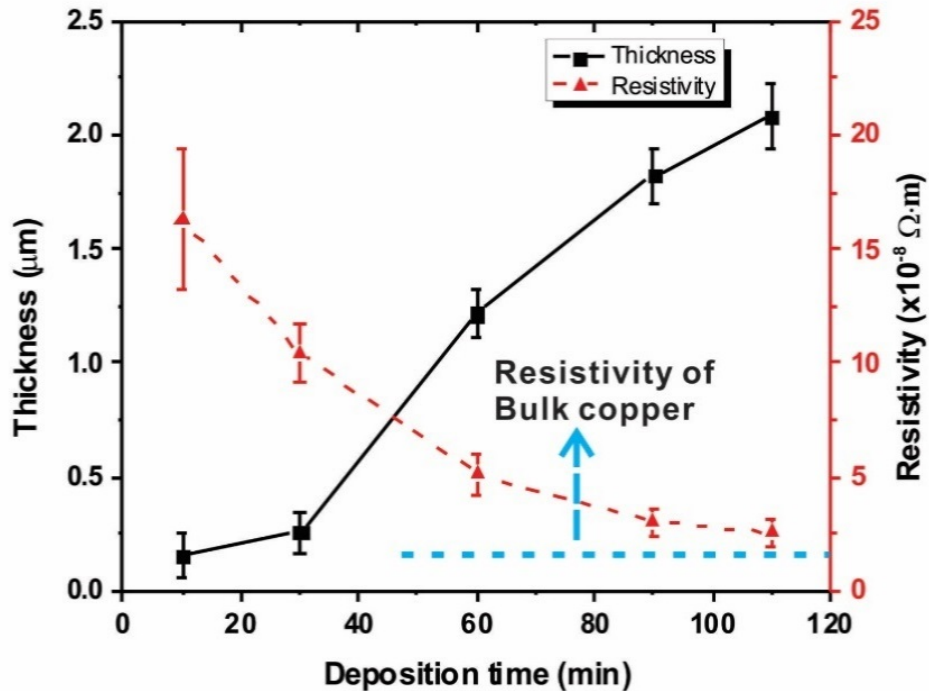
Figure 5-5. The curves of deposited copper thickness and resistance versus deposition time (the blue dash line shows the resistance of bulk copper).

The cross section of the printed pattern was shown in Figure 5-6(e), and a layer of copper with a thickness of ~2 µm was observed on the surface, bonding tightly with the printed toner. In this method, the printed toner layer also acts as an adhesion-promoting layer, which can significantly enhance adhesion of the copper layer to the substrate and thus facilitate the formation of thick copper layer that is necessary to improve electrical performance of the metal pattern to meet the quality requirements of the current electronics industry. This is essential for printed electronics technology to become industrially viable. Both adhesion and electrical performance were common challenges in the existing printed electronics techniques. X-ray diffraction (XRD) was conducted to further study the crystalline structure of the resultant copper layer. For reference, XRD measurement of the original PET substrate and substrate with printed toner were also conducted, the results are shown in Figure 5-7.
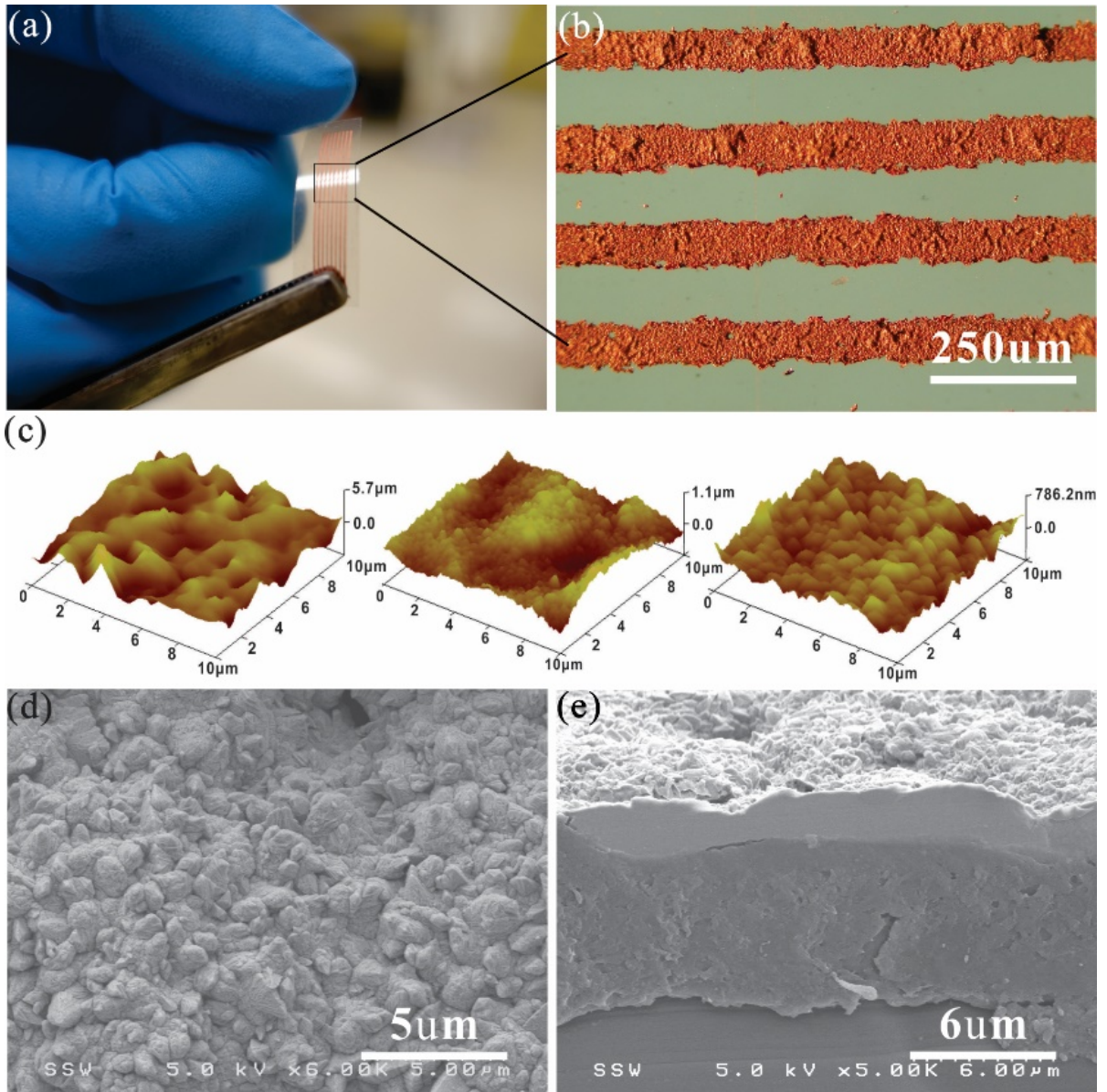
Figure 5-6. (a) copper pattern on PET film; (b) copper pattern with the line width of 100 μm; (c) AFM 3D images of surface morphology of copper layer with different deposition time; (d) SEM images of copper surface after ELD of 110 min; (e) SEM images of cross section of copper layer after ELD of 110 min.
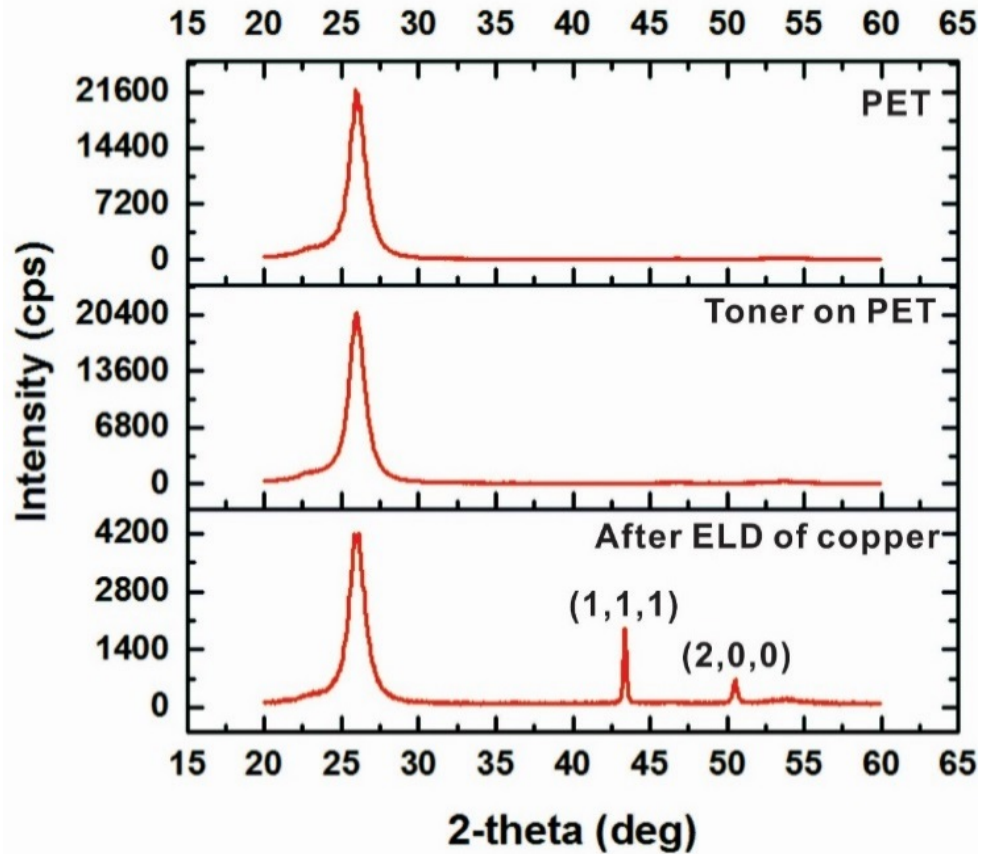
Figure 5-7. XRD Results of PET film, printed toner on PET and copper layer after ELD.

XRD pattern shows two narrow characteristic peaks at 43o and 51o corresponding to the (1,1,1) and (2,0,0) planes of the FCC structure of copper, indicating the high crystallinity of the deposited copper. Oxidizing test and bending test were also conducted to evaluate the stability and flexibility of the as-prepared samples, the results are presented in Figure 5-8. Four groups of line arrays were produced and the copper deposition time of 110 min was applied, and each of them had 5 lines with width of 500 µm, length of 2 cm, and spacing of 500 µm. Group 1 was stored in open air under room temperature for more than 120 days, and group 2 was heated up to 120°C in open air for 3 hours to study the oxidation resistance of the deposited copper. Resistivity was measured using a four-point-probe station. Inward bending and outward bending tests were conducted on Group 3 and Group 4, where samples were connected to a high accuracy M2400 Keithley Multimeter by the four-probe station to record the resistivity under different bending curvature. Samples stored under room temperature with ~30% humidity in open air experienced a continuous increment in resistivity but leveled off to a stable

resistivity (~3.7× bulk) after 60 days due to oxidization (Figure 5-8(a)). The resistivity of the oxidized samples under heating in the open air with the same humidity condition continuously increased in the first 2.5 hours with a decreasing rate and reached a stable value in 2.5 hours and remained nearly constant (~ 4.1× bulk) (Figure 5-8(b)). Therefore, the resistivity of copper patterns fabricated by this technique will reach a plateau of resistivity of ~4× of bulk copper and then remain unchanged thereafter. Though a rapid increment in the resistivity was observed, the fabricated copper patterns still shows a very low bulk resistance because of the large copper thickness and therefore perform better than patterns fabricated by directly ink-jetting metal nanoparticles which has a thickness of only ~500 nm. For the flexibility of the fabricated copper pattern, as is shown in Figure 5-8(c) and (d), the increment of resistivity was barely observed when bending inward. It is intuitive because that the copper crystal and cluster get closer with each other, and even when counteracting slight damage due to internal stress, the conductive path is still active. However, when bending outward, the resistivity increased as the bending curvature increased, which might be caused by the tiny cracks occurred on the surface during bending. Most of the decrements in conductivity are reversible. When patterns are restored to their original shapes, the resistivity will then go down to ~1.6× bulk copper, almost the same as the initial value before bending (~1.5× bulk copper).

Thanks to the adhesion promotion layer, the copper pattern showed great adhesion on the substrate. The adhesion strength was examined by the use of a cross scotch tape test, following ASTM D-3359 using 3M #600 tape.[43] Only a few tiny copper particles were observed on the tape after the first time tearing and no peeling off was observed in the next two tape tests, indicating a strong adhesion between the copper and the toner as well as the toner and the PET substrate. The copper particles left on the tape in the first type test are seen as residue copper particles during ELD process, since the resistivity was not changed after the tape test.
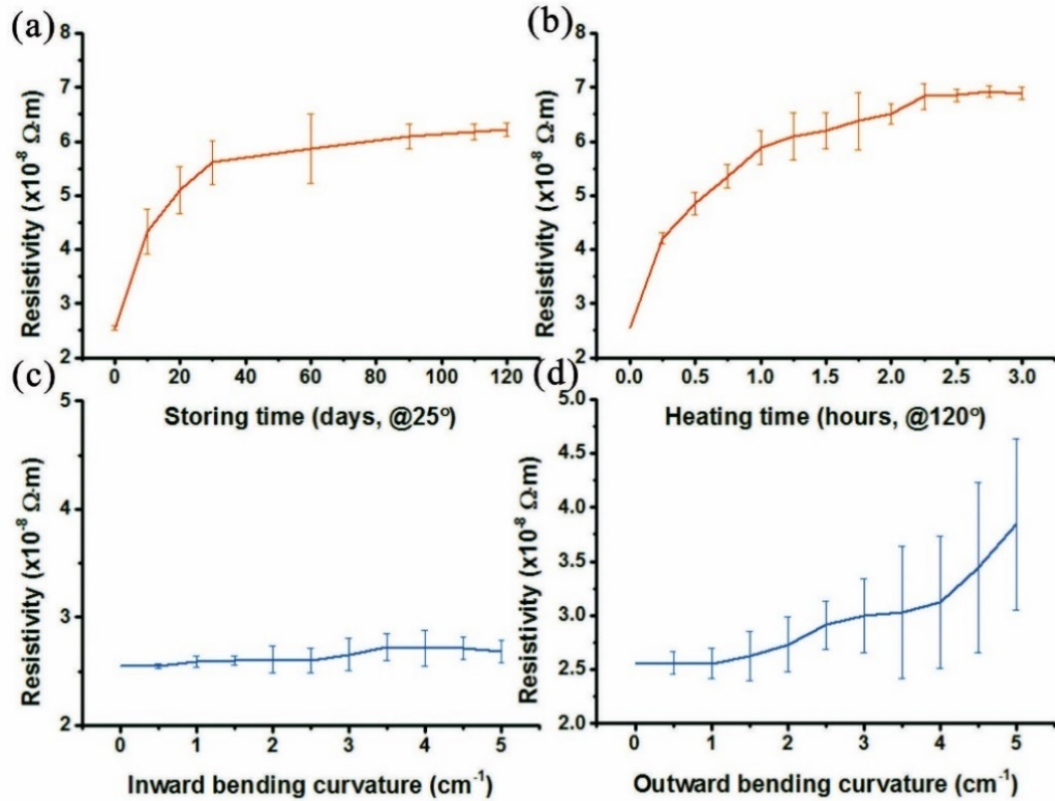
Figure 5-8. Chemical and mechanical stability of deposited copper pattern. The resistivity with the relation to (a) storing time; (b) heating time; (c) inward bending curvature and (d) outward bending curvature.
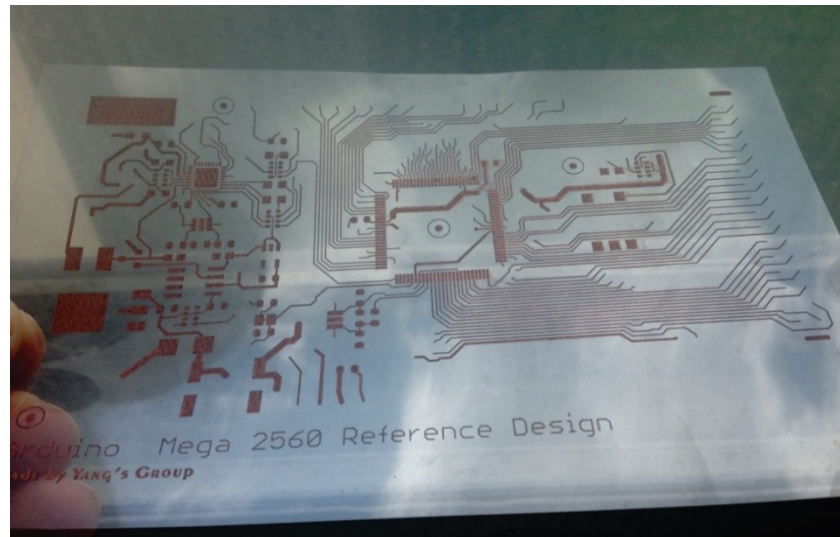
Figure 5-9. A typical copper-based circuit printed on PET produced by as-proposed laser printing method.

A single layer of high resolution flexible printed circuit board on PET substrate was produced using the proposed method, the picture is given in Figure 5-9. Double layer flexible LED displays were prepared on pristine PET films to demonstrate the fabrication ability of this new developed technique. The flexible LED array display was able to display different moving patterns and letters. The double layer circuits were printed separated and bonded together using commercial instant glue. Through holes were cut using a high resolution mechanical plotter and silver glue was used to connect both layers and all mounted components. Figure 5-10 shows the working display illuminating a total of 25 LEDs, forming a flashing pattern of "UWO". Even under bending, the display can still work well (Figure 5-10(b)), which indicated that as-produced flexible circuit by this method is applicable completely in flexible electronics. Another LED array display with 32 LEDs fabricated the same way was controlled by a programmed single chip microcomputer.
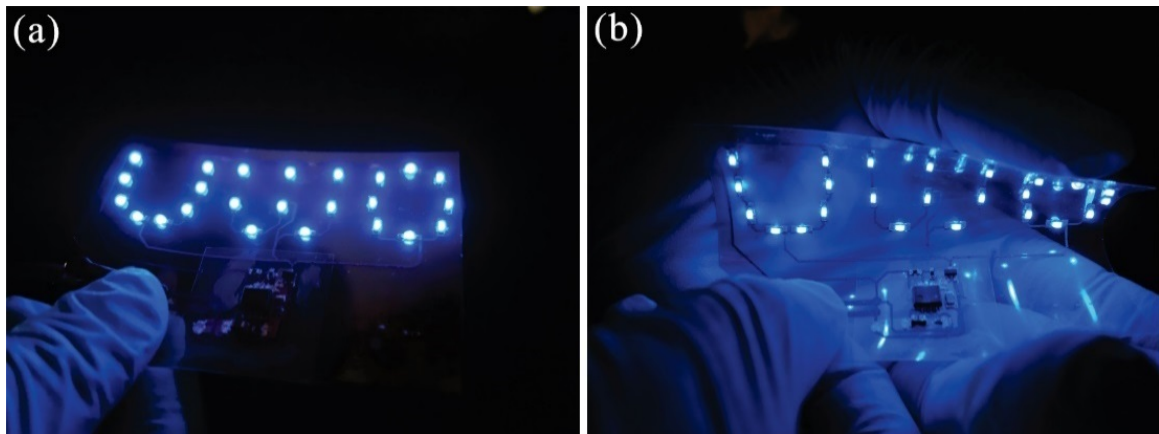
Figure 5-10. As-produced flexible LED display under working, a) without bending; b) under bending.

In summary, this new printed electronics technique based on laser printing mechanism offers a high-speed, low-cost and high-resolution fabrication route for printed electronics. Compared to the solvent-based printing methods, this solvent-free approach shows a great promise for the printed electronics industry. With the utility of ELD technique, high-quality and highly conductive flexible metal patterns can be easily fabricated. In addition, with the help of toner as adhesion promotion layer, the durability of printed patterns was greatly improved. It's worth mentioning that this method is suitable for a wide variety of substrates such as glass, textile,

paper, etc. We can envision that our approach could advance current technique of printed electronics and pave a new way for the large-scale production of printed electronics.

5.4 Conclusion

In summary, this new printed electronics technique based on laser printing mechanism offers a high-speed, low-cost, solvent-free and high-resolution fabrication route for printed electronics. Compared to the solvent-based printing methods, this solvent-free approach shows a great promise for the printed electronics industry. With the utility of ELD technique, high-quality and highly conductive flexible metal patterns can be easily fabricated. In addition, with the help of toner as adhesion promotion layer, the durability of printed patterns was greatly improved. It's worth mentioning that this method is suitable for a wide variety of substrates. With proper surface modification, the developed method can also be extended to fabricate conductive patterns on many other substrates such as glass, textile, paper, etc. This solvent-free, high-speed laser printing technique opens a new avenue for printed electronics. This technique is reliable and scalable. We can envision that our approach could advance current technique of printed electronics and pave a new way for the large-scale production of printed electronics.

Chapter 6

6. React-on-Demand (RoD) Fabrication of Highly Conductive Metal-Polymer Hybrid Structure for Flexible Electronics

6.1 Introduction

Printed flexible electronics technology, which takes advantage of the existing manufacturing capabilities of the graphics industry to produce circuitries at significantly lower cost and with high speed, has gained remarkable attention in the last decade.[224, 225, 321, 322] This vibrant new technology is transforming the electronics industry by replacing expensive electronic components, devices and even systems fabricated with traditional manufacturing methods. Much research has been carried out on flexible substrates and many new applications have been explored, such as thin-film transistors,[228, 323, 324] flexible displays,[325] flexible energy-storage devices,[326-328] radio frequency identification (RFID) tags,[329] medical and cosmetic devices.[330, 331] One can foresee a world full of flexible, wearable, and stretchable devices developed by this emerging technology.

Recently, various printing techniques have been demonstrated to fabricate flexible electronics, such as inkjet printing, [64, 332] gravure printing, [333] screen printing, [334, 335] transfer printing,[336] extrusion printing, [226] laser printing and aerosol jet printing. [116, 337-339] In addition, based on the newly developed integrated 3D printing system, printed electronics can be fabricated in a three-dimensional manner, exhibiting huge potential for the manufacturing of devices that require arbitrary constructs and unique functions.[239, 340] However, these techniques are usually inaccessible to general users, due to the inevitable enrollment of special expensive equipment, high energy consumption, intractable troubleshooting process, harsh requirement of the ink and extensive need for professional skills.

As an alternative technique, direct pen writing of flexible electronics is gaining popularity for its low-cost, simplicity, ultrahigh portability and ease of use.[341] Despite lower resolution and accuracy, pen-writing has no harsh requirement for the ink and can be easily operated without professional skills. Circuit prototypes can be rapidly fabricated on-site without use of sophisticated equipment, affording great convenience for practical use by end-users and in

areas with limited resources. Various writing instruments have been recently adopted to write electronics directly, such as with ball pen,[155, 342-344] pencil,[163, 345] fountain pen, [346, 347] brush pen and marker pen.[135, 348] Most of the work has been focused on the direct writing of conductive inks, including metal nanoparticles inks, carbon-based inks, conductive polymer inks and liquid metals. Among these, metal nanoparticle inks hold the advantage of relatively high conductivity but are subjected to high cost (compared to metal salt) due to the professional equipment and strict synthesis process needed during production. Such metallic inks require extensive post-treatment, such as heating, laser annealing, hot pressing and plasma, to form patterns with good conductivity. For instance, after the writing of silver nanoparticle inks, an extra time-consuming sintering step of ~ 2 hour is needed to further enhance its conductivity, where the need for high temperatures ($120^{o}C$ ~ $160^{o}C$) further complicate the whole fabrication process. [341, 343, 349] Though the sheet resistance of the written trace can be greatly reduced by post-treatment to 50 mΩ/sq, it is still much higher than that generated by a wet chemistry process due to the limited metal loading in the ink.[350] Self-sintering of silver nanoparticles was demonstrated recently by triggering the self-assemble and/or coalescence of nanoparticles at room temperature. [174-176] Using similar mechanism, start-up companies like AgIC (Japan), Nectro Inc. (Canada) were making efforts to commercialize conductive ink pen which did not require sintering. However, the conductivity of such self-sintered traces is still in the low-end range with sheet resistance in the level of several hundreds of mΩ/sq and resistivity 2-3 times higher than bulk materials. Meanwhile, the use of nanomaterials in the ink greatly increases the cost of the pen and imposes potential safety issues. Targeted at end-users with no professional skills and point-of-care applications, safety becomes one of the most important concerns for handwritten electronics. The written circuits are expected to be handled and touched by users during normal use. Thus, if the circuits are not properly treated, the exposed and unsealed nanoparticles will adhere to the skin. Metallic inks usually contain large numbers of nanoparticles smaller than 50 nm; at this scale, these nanoparticles can permeate skin and enter the bloodstream. [177, 178] Many reports have recently addressed the protentional toxicity of metal nanoparticles in the human body,[179-181] thus it is crucial to develop new techniques to enhance the safety of this emerging technology.

It is worth noting that although the direct pen writing process has proven to be rapid, simple and portable, there are still ways to go before it is an ideal easy, safe and cost-effective method for fabricating electronics, considering all the aforementioned challenges and limitations. In this paper, we propose a one-step react-on-demand method for fabricating flexible circuits with ultra-low sheet resistance, enhanced safety and durability to accomplish this goal. Instead of using nanomaterial-based ink, a none-toxic vitamin C functionalized polyvinyl alcohol (PVA) coating was introduced as the media for real-time in-situ three-dimensional reduction of silver salt ink at room temperature. Utilizing the water-swellable property of PVA, the reduction of silver takes place immediately on the surface as well as in between the polymer chains, when the ink is written onto the substrate at room temperature. A highly conductive three-dimensional metal-polymer (3DMP) hybrid structure of about 7 µm thickness can be generated in a few seconds after the evaporation of the solvent. The PVA not only serves as the reaction media for the in-situ reduction of silver, but also serves to bind and protect the materials to seal all small particles inside the film, enhancing its safety and durability. Thanks to the high solubility of silver nitrate in water and the unique 3DMP structure, the as-fabricated silver traces show an ultralow sheet resistance of down to 4 mΩ/sq without post-treatment, which is far better than any other method described in the literature thus far. Since no nanomaterials, post-treatment or harsh experimental conditions were required, the proposed method proves to be a truly cost-effective, simple and safe alternative to current methods. We believed that this work could bring the emerging handwritten electronics technology one step closer to those end-users who require performance, safety, ease-of-use and cost-efficiency at the same time.

6.2 Experiment Details

Materials

Poly (vinyl alcohol) (PVA) (Mw ≈ 40 000, 98-99% hydrolyzed), ascorbic acid (99%), anhydrous glycerol ($C_3H_5(OH)_3$, 99%), silver nitrate ($AgNO_3$, 99%), xanthan gum (($C_{35}H_{49}O_{29}$)$_n$, 98%) were purchased from Sigma-Aldrich. Ink absorption coating (clear) was provided by inkAID. All chemicals were used as received without further purification. Polyethylene terephthalate (PET) substrate was provided by 3M.

Preparation of Coating Solution

Poly (vinyl alcohol) (PVA) (5 g) was dissolved in DI water (90 mL) with continuous stirring for 72 hours at 85 ºC, yielding a clear, transparent solution. Xanthan gum (0.1 g) was dissolved in DI water (100 mL) at 70 ºC with continuous stirring for 3 hours. After the solution cooling down to room temperature, excessive amount of ascorbic acid was added into the solution followed by gentle stirring for 1 hours. The solution was then filtered with filter paper to remove undissolved ascorbic acid, and after the filtration, we got a transparent, clear solution.

Preparation of the Functionalized PET

Transparent PET film was cleaned by the mixed solution of 1:1 ethanol and acetone in ultrasonic bath for 10 mins, and was air dried at room temperature. InkAID ink absorption coating was applied onto the substrate by a foam brush. After the sample was completely dried in air (about 3 hours), PVA coating was applied onto the substrate as the second layer using foam brush and dried in air. Saturated ascorbic acid solution was then spin coating onto the sample using a Laurell WS-650-23B spin coating at 900 rpm. As the final step, the coated PET was dried in vacuum overnight.

Preparation of Ink for Direct Writing

Silver nitrate solutions with different silver nitrate concentration were prepared by dissolving specific amount of silver nitrate in DI water. The as-prepared silver nitrate solutions were directly filled into a liquid-ink based marker pen for the following experiment.

Preparation of ink for Inkjet Printing

A glycerol–water solution was prepared by mixing anhydrous glycerol and distilled water at a volume ratio of 3:2. Silver nitrate was then added, followed by mixing in a VWR mixer for 4 min to form a 1.2 g/mL silver slat solution. The prepared ink was degassed in a vacuum chamber at 2 psi for 2 h to remove dissolved gases and bubbles. The viscosity and surface tension of the final ink were 12.3 cp and 50.1 mN m−1, respectively. These values fall within the optimum operating range for the Dimatix DMP-2800 printer. A 0.2 µm nylon syringe filter was used to remove undesired particles from the ink.

Inkjet Printing

The ink was filled into a cartridge mounted on a 10 pL piezoelectric drop-on-demand inkjet print head. Printing parameters were set as following: drop space, 15 µm; meniscus vacuum, 3.5 in. of H_2O; print head temperature, 25 °C; print head angle: 2.1°; jetting voltage ~25.1 V. Printing was conducted at room temperature.

Characterization

FE-SEM images were taken by a LEO (Zeiss) 1540 FE-SEM. The viscosity of the ink was measured with a fully automatic HAAKE Viscotester 262. Surface tension was measured using a BZY -3B automatic surface tension meter. Sheet resistances were measured by a four-point probe station Lucas Labs S-302-4 (probe SP4) connected to a Keithley 2750 multimeter. X-ray Photoelectron Spectroscopy (XPS) was conducted using Kratos AXIS Ultra. X-ray diffraction analysis was done using a Rigaku Ultima-IV XRD goniometer. Bending test was conducted using a customized bending stage controlled by Anheim Automation DPD75601 motor controller.

6.3   Results and Discussion

Extensive work has been carried out to synthesize silver nanoparticles with controllable shape, size and properties in recent years. The development of a biocompatible and environmental friendly synthesis process brings popularity to many eco-friendly reducing agents such as ascorbic acid, sodium citrate and tannic acid.[351, 352] As a biologically originated compound, ascorbic acid (Vitamin C) was chosen as the reductant in this work for its powerful reducing property and good stability in cool and dry air. The fabrication of traditional metal nanoparticles inks involves large amounts of capping agents, stabilizers and/or dispersing agents to control the size, shape of the particles and prevent agglomeration. To achieve a good dispersibility as well as a relatively high loading (~ 50%) of silver in the solvent, the size distribution peak of the silver nanoparticles needs to be smaller than 100 nm for low-viscosity inkjet ink. However, smaller particle size typically means worse conductivity, since a higher ratio of additives will wrap and/or bond to the surface of the nanoparticles, preventing the nanoparticles from contacting with one another when the ink dries. A post-sintering process can help to remove these additives using a high energy method, but the equipment needed for post-treatment is inaccessible to end-users, which consequently limits its application to handwritten electronics. Thus, we proposed a react-on-demand (RoD) method, which offers a

unique approach to fabricate high performance flexible devices by on-site synthesis of highly conductive silver plates without any additives. Figure 6-1 shows the general idea and fabrication process of the RoD method.
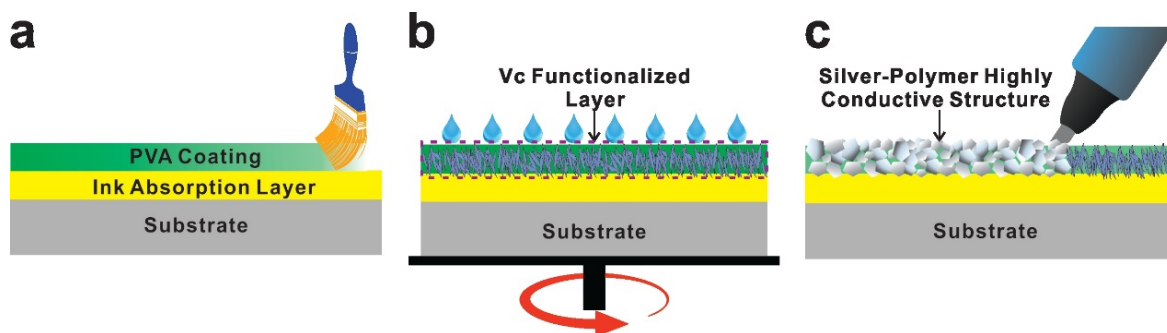
Figure 6-1. Fabrication process of the react-on-demand method. a) The ink absorption layer and a thin layer of PVA polymer are brush coated onto PET substrate one by one. b) Spin coating saturated ascorbic acid (Vitamin C) solution to functionalize the PVA coating. c) Direct writing or printing of silver nitrate solution onto the coated layer, generating a metal-polymer highly conductive structure.

Pristine polyethylene terephthalate (PET) substrate was washed and brush-coated with multiple materials (Figure 6-1(a)). The first layer of coating is a commercially available water-proof ink absorption material. This kind of coating can absorb excessive solvent, which in turn reduces the drying time and helps with the ink bleeding issue.[353] A second layer of polyvinyl alcohol (PVA) coating was then introduced as the reaction media for the RoD method. As a water-soluble synthetic polymer, PVA is widely used in textiles, paper making and a variety of coatings due to its cheap price, non-toxicity and good flexibility. PVA is only soluble in hot water (>80 ^{o}C), and will swell if the water is at room temperature (~20 ^{o}C). The mechanism of the swelling of PVA has been well studied and has been widely used in drug delivery applications in the past decades.[354, 355] Briefly, small solvent molecules, like water, will diffuse into the partially cross-linked polymers in a short period of time and reside in between polymer chains. Utilizing the water-swelling property of PVA, we embedded the reducing agent into the PVA film by spin coating the saturated ascorbic acid solution, as shown in Figure 6-1(b). As the solvent evaporates, the ascorbic acid will crystallize and precipitate, forming small reducing crystals in between the PVA polymer chains as well as on the surface. The PVA film seals the Vc crystals when the solvent dries and protect them from being oxidized in air.

The functionalized film retains good reducing ability and function after three months of storage in a dark and dry environment.
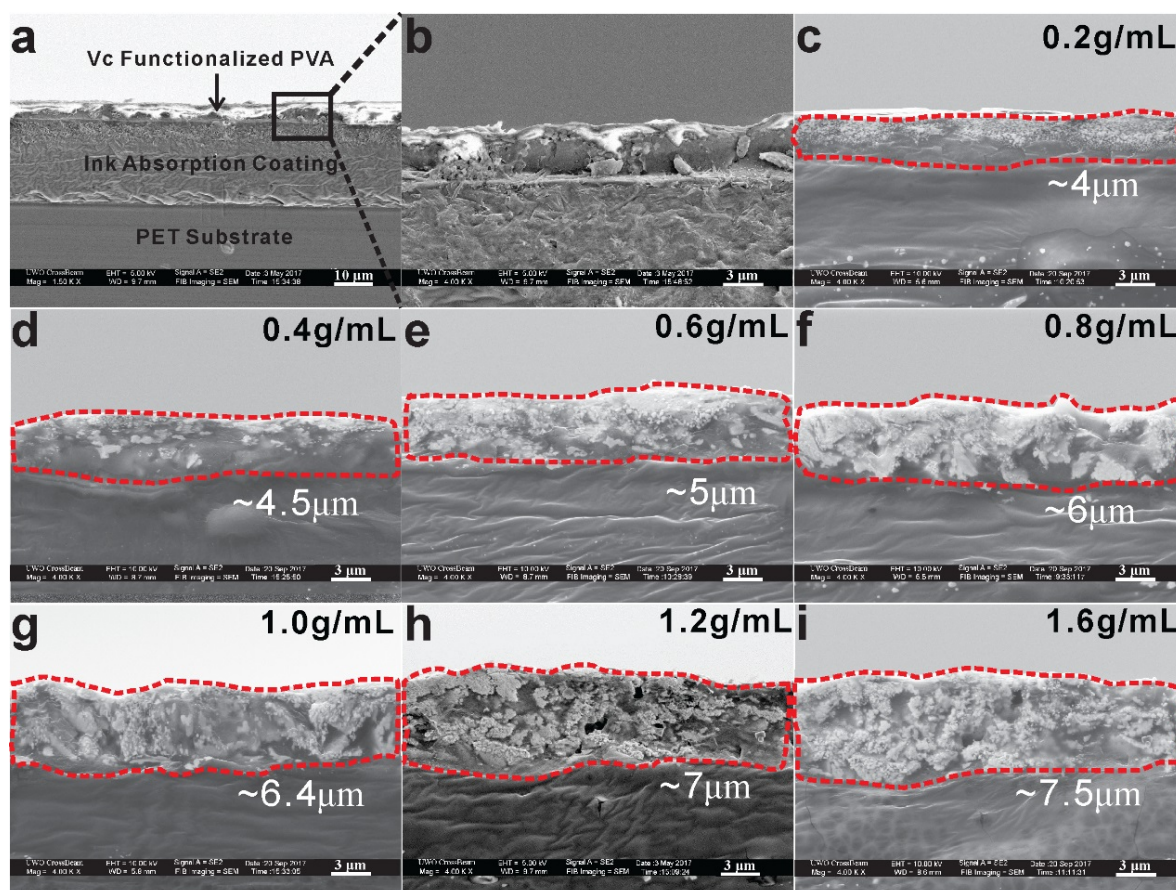
Figure 6-2. SEM images of the cross-section of a) the multi-coated PET substrate before writing or printing silver nitrate ink; b) zoomed-in part of the squared area in a); after react-on-demand generation of silver-polymer highly conductive layer using different silver nitrate concentration of c) 0.2 g/mL, d) 0.4 g/mL, e) 0.6 g/mL, f) 0.8 g/mL, g) 1.0 g/mL, h) 1.2 g/mL and 1.6 g/mL. The average measured thickness of the silver-polymer layer is shown in the middle right of each image.

The cross-section of the finalized coating is shown in Figure 6-2(a), and Figure 6-2(b) is a zoom-in of the area marked with a box in Figure 6-2(a). From the SEM images, we see that the first layer of coating has a thickness of about 20 µm for efficient absorption of the solvent. Right above it, the PVA forms a thinner layer (~3 µm) of coating with embedded Vc crystal. In Figure 6-2(b), some large Vc crystals are observable at the interface of the two layers, illustrating a successful functionalization of the coating. Silver nitrate was chosen as the metal

precursor for its ultra-high solubility in water. The solubility of silver nitrate in water can reach 256g/100mL at room temperature (25 ^{o}C). This gives a maximum silver content loading of more than 120% (w/v), which is much higher than any commercial available silver ink. High solubility facilitates high loading of metal slat without increasing the amount of ink, and further contributes to the high metal content in written traces after the on-site RoD reduction. Aqueous silver nitrate solution was filled into a liquid ink marker with a chisel tip. This type of marker is compatible with low-viscosity ink, and the chisel tip allows users to write traces of different widths with ease, offering excellent user experience. When the ink flows out of the tip onto the functionalized coating, the three-dimensional reduction of silver takes place in a few seconds as the PVA layer swells under the action of water. Silver ions diffuse with water molecules into the PVA film, where the ascorbic acid is dissolved at the same time, forming a sectional solution system to trigger the RoD of silver reduction. Thanks to the water-swelling property of PVA, this reaction takes place both on the surface and inside the film between polymer chains. As the solvent evaporates, a three-dimensional metal-polymer highly conductive structure will form in a few seconds. The cross-section of the generated 3DMP structure using different silver nitrate concentrations with one stroke are shown in Figures 6-2(c)-(i) through SEM. The silver-polymer hybrid structures are highlighted with red dotted box with their thickness shown right below the structure. As expected, the thickness of the 3DMP structure increases slowly with the concentration of silver nitrate. When the concentration is below 0.6 g/mL, most of the reduced silver particles/flakes present in the upper layer of the PVA film which can be explained by the relative low silver ion concentration in the ink (Figures 6-2(c) and (d)). Starting from 0.6 g/mL, the reduced silver is able to fill the entire PVA film. The increasing silver nitrate concentration brings thicker 3DMP structure and denser silver content in the structure, which are clearly presented in Figures 6-2(e)-(i). When the concentration reaches 1.6 g/mL, the 3DMP structure is much thicker (~7.5 µm) than that of the functionalized PVA coating itself (~3 µm), which can be explained by the newly generated silver metal between the polymer chains. It is worth mentioning that when the concentration is higher than 1.6 g/mL, the thickness of the 3DMP structure barely changes, and the cross-section looks the same as Figure 6-2(i). One possible reason for this is that almost all the ascorbic acid in the PVA film get consumed when the concentration reaches 1.6 g/mL and thus no more silver metal can be generated. The relationship between silver nitrate concentration and 3DMP thickness is summarized in a graph, which is shown in Figure 6-3.
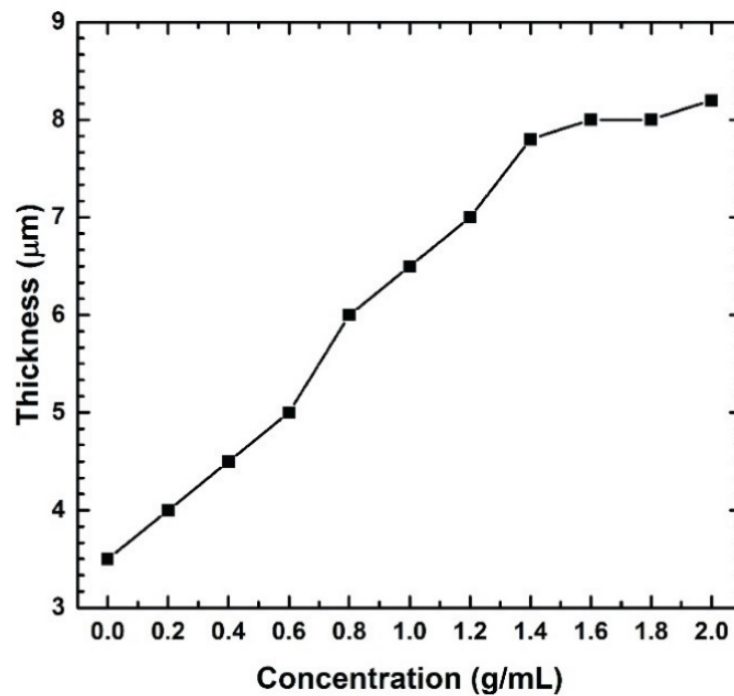
Figure 6-3. Graph showing the change of the silver-polymer hybrid structure with different silver nitrate concentration.
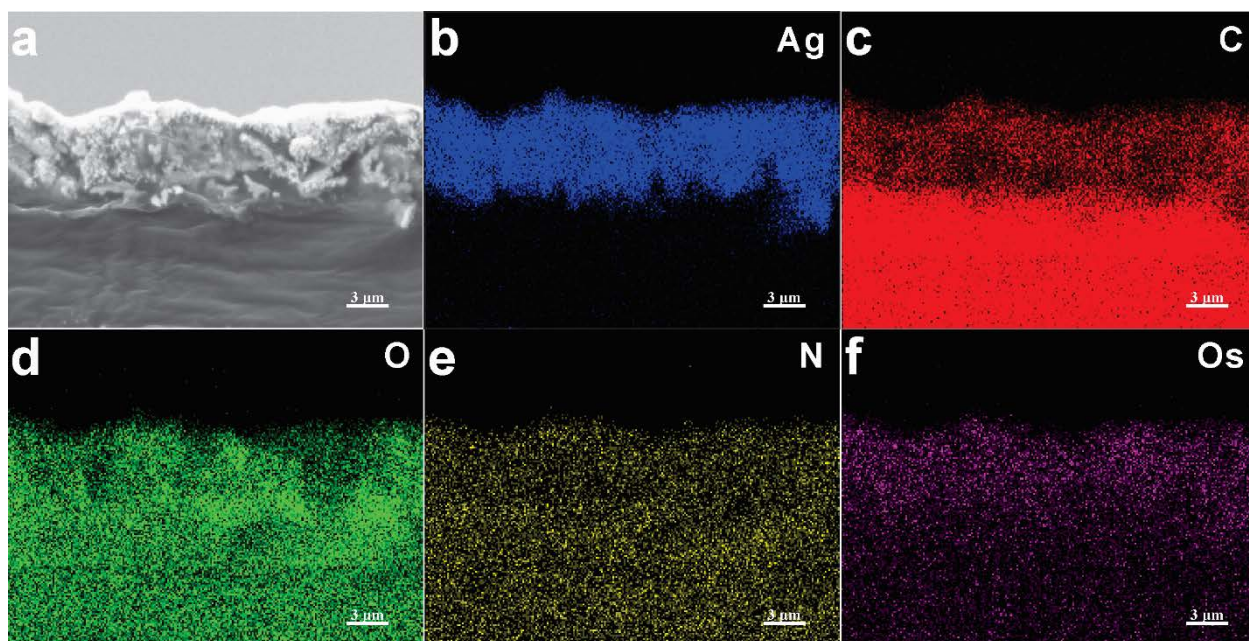
Figure 6-4. (a) SEM image of the site of interest in the EDX analyze. The element map of the site of interest for (b) Ag; (c) C; (d) O; (e) N and (f) Os.

EDS analyze was conducted to further investigate the 3DMP structure. Single-stroke sample written with 1.0 g/mL silver nitrate ink was chosen for EDS survey due to its good performance in both conductivity and bending durability, which will be addressed in this paper later. The sample was coated by osmium for better conductivity. The site of interest is shown in Figure 6-4(a) and the maps of different elements are shown in Figures 6-4(b)-(f) followed by the full spectrum of EDS as shown in Figure 6-5. There are five elements in total presenting on the sample --- silver, carbon, oxygen, nitrogen and osmium. The map of silver and carbon (Figures 6-4(b) and (c)) well match the shape of the observed 3DMP structure, further confirms the existence of the hybrid structure.
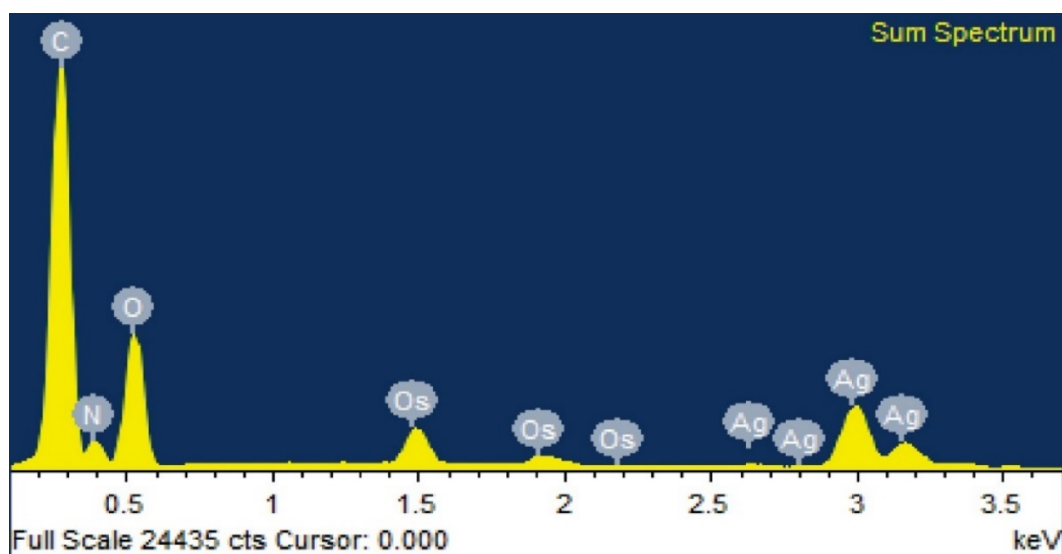
Figure 6-5. EDX full spectrum of cross-section of the sample written with 1.0 g/mL silver nitrate ink.

Figure 6-6(a) shows the silver reduction process using the proposed RoD method from 0 to 30 seconds after reaction at room temperature. The trace was written with 1.2 g/mL silver nitrate ink and the photos were taken under the same lighting conditions. For the first 5 seconds, the silver trace is barely seen. During this period, the water molecules and silver ions are absorbed by the PVA film, while at the same time, the ascorbic acid molecules embedded in the film are dissolved, forming a sectional reducing solution which reduces the silver ions immediately. The above process continues, and more and more silver ions are reduced; the generated silver plates/particles tend to grow larger since no capping agent is used. After 10 seconds, the trace shows a silver metallic color with a clear edge. After 30 seconds, a solid silver trace with ultra-

low sheet resistance is formed. The silver generated by the RoD method is well bonded and sealed by the PVA film, and resists erosion when rubbed by fingers.
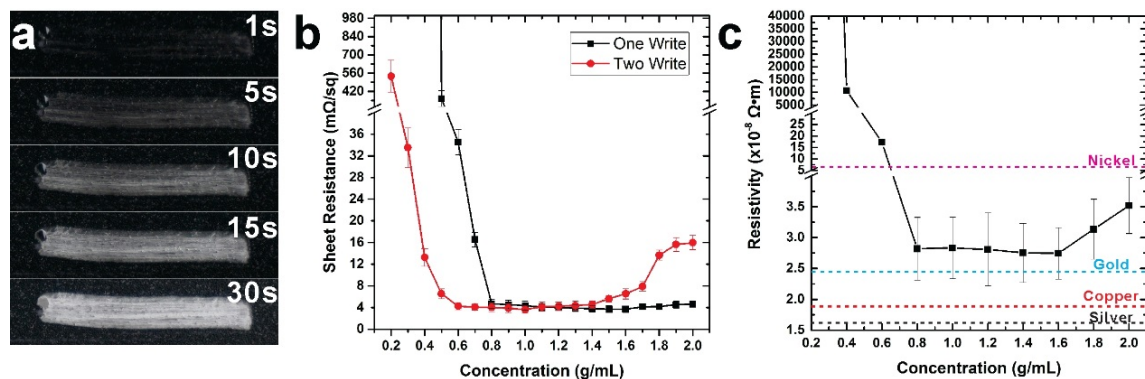
Figure 6-6. a) Optical images showing the surface of the substrate after direct-writing with 1.2 g/mL silver nitrate ink at 1s, 5s, 10s, 15s and 30s. b) Graph showing the change of sheet resistance with different silver nitrate concentration. The black line with square symbol corresponds to traces written with single stroke; the red line with circle symbol corresponds to traces written with double strokes. c) Graph showing the change of resistivity with different silver nitrate concentration. As a comparison, the resistivity of bulk silver, copper, gold and nickel are shown in the graph using dashed lines with different color.

For the silver nanoparticle-based ink, the silver content loading plays a critical role in the conductivity of the final product. This is also true in the RoD method. To investigate the relationship between the silver nitrate concentration and sheet resistance of the written traces, we prepared inks with different concentrations ranging from 0.2 g/mL to 2.0 g/mL. The final resistance of the written traces is also affected by the amount of ink, which can be determined by the number of repeats. Thus, two groups of experiments were conducted; one without repeat writing (single-stroke) and the other with one repeat (double-stroke). The results are shown in Figure 6-6(b). For the one-write group, the sheet resistance initially drops drastically with increase in concentration and starts showing good conductivity when the silver slat load reaches 0.6 g/mL. At this point, it has a sheet resistance of ~35 mΩ/sq, which is better than most inkjet printed circuits with silver inks. Beyond 0.8 g/mL (~4.70 mΩ/sq), the decrease in sheet resistance slows down significantly, which is attributed to the limited loading of ascorbic

acid in the PVA film. The lowest sheet resistance of ~3.66 mΩ/sq is observed at 1.6 g/mL for the one-write group. Interestingly, the sheet resistance begins to increase slightly when the concentration of silver nitrate is higher than 1.6 g/mL. At this point, there is not enough ascorbic acid in the PVA film to reduce all the silver nitrate, and the non-reduced silver nitrate embeds in the PVA film, preventing the conductive silver plates/particles from contacting with each other and thus increasing the sheet resistance. A similar phenomenon is also observed in the double-stroke group. The double-stroke traces show its lowest sheet resistance of 3.62 mΩ/sq at a silver nitrate concentration of 1.0 g/mL, which is very close to what we achieved (3.66 mΩ/sq) with 1.6 g/mL ink by single stroke due to the limiting amount of ascorbic acid in PVA film. The sheet resistance then starts to increase at a faster rate than the single-stroke group. This was expected as more ink was written onto the substrate. The resistivity of one-stroke electrode was calculated according to the previously measured sheet resistance and film thickness; the result is shown in Figure 6-6(c). As a comparison, the bulk resistivity of four popular conductive materials used in printed electronics --- silver, copper, gold and nickel --- are also shown in the graph using dashed lines with different color. Similarly, the lowest resistivity is observed at 1.6 g/mL with a value of 2.74×10^{-8} Ω•m, which is about 1.7 times larger than that of the bulk silver (1.59×10^{-8} Ω•m) but several times smaller than that of nickel (6.99×10^{-8} Ω•m). To have a more in-depth understanding of the conductivity change, the morphology of the silver trace was investigated with field emission scanning electron microscopy (FE-SEM). The results are shown in Figure 6-7.

Figures 6-7(a-e) show the surface morphology of single-stroke traces written with 0.2 g/mL,0.6 g/mL,0.8 g/mL, 1.2 g/mL and 1.6 g/mL silver nitrate ink respectively. The reduced silver appears to be in the form of small plates with diameters ranging from 5 µm to 10 µm, with small silver particles generated through the secondary nucleation on the surface.[356] The size of the silver plates is much larger than that in commercially available silver ink, which are usually on the nanometer scale. The relatively large silver plates contribute to the good conductivity of the silver trace. At a concentration of 0.2 g/mL, the trace is not conductive (Figure 6-6(b)) since the silver plates are too spread out with minimal contact (Figure 6-7(a)). When the concentration reaches 0.6 g/mL, more silver plates of larger size (~10 µm) are generated, distributing in a random orientation and overlapping with one another, as shown in Figure 6-7(b). It can be clearly observed that some silver plates are half on the surface, half

inside the film (circles by red dot lines in Figure 6-7(b)), illustrating the formation of a three-dimensional silver-polymer structure.
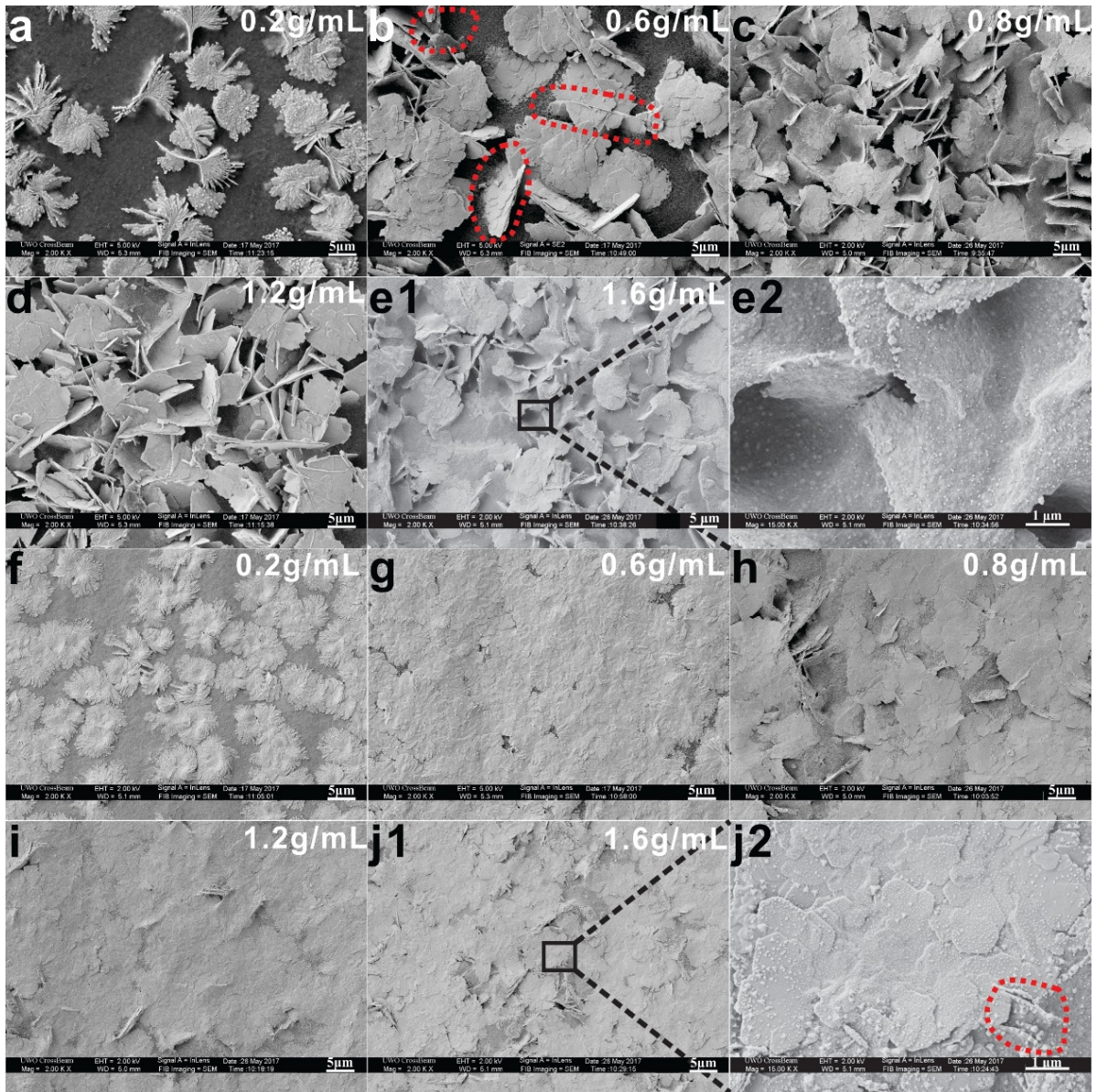
Figure 6-7. SEM images of the surface morphologies of single-stroke samples written with different silver nitrate concentration of a) 0.2 g/mL; b) 0.6 g/mL; c) 0.8 g/mL; d) 1.2 g/mL; e) 1.6 g/mL. SEM images of the surface morphologies of double-stroke samples written with different silver nitrate concentration of f) 0.2 g/mL; g) 0.6 g/mL; h) 0.8 g/mL; i) 1.2 g/mL; j) 1.6 g/mL.

The silver plates become denser and thicker with increasing concentration of silver nitrate in the inks, but the morphology remains essentially the same, as shown in Figures 6-7(c)-(e). At a concentration of 1.6 g/mL, the silver plates tend to "bond" with each other to form larger plates without gaps. The zoomed in SEM image (Figure 6-7(e2)) provides a close look at the boundary of different silver plates, from which we can see that the silver plates seem to "melt' into each other.Expectedly, the trace shows its lowest sheet resistivity of ~3.66 mΩ/sq at this concentration. Figures 6-7(f-j) show the surface morphology of double-stroke traces written with 0.2 g/mL,0.6 g/mL,0.8 g/mL, 1.2 g/mL and 1.6 g/mL sliver nitrate ink, respectively. The second stroke was repeated right after the first stroke after an interval of about 5 seconds. The shape of the silver plates is still visible, but the morphology appears to be pressed/flattened due to the writing of the second stroke. The growth of the silver plates starts immediately after the first layer of ink is written onto the substrate. Thus, when we begin writing the second layer, there are already some silver plates on the substrate. Those early generated nucleation centers are pressed when the tips pass by them, forcing them to lay horizontally on the surface. The newly orientated silver plates continue to grow and eventually forms a dense layer of silver metal, as shown in Figures 6-7(f-g). Due to the horizontally orientated silver plates and larger volume of ink, the sheet resistance is greatly reduced compared to the single-stroke group when the concentration is below 0.7 g/mL (Figure 6-6(b)). We observe the maximum difference in morphologies between single and double-stroke traces at the lowest concentration, 0.2 g/mL. Despite the increased number of overlapped silver plates in the double-stroke trace, many silver nanoparticles are generated and distributed evenly on the substrate, which is reflected by its much lower sheet resistance than that of the single-stroke group at the same concentration. We did not observe any significant changes in the surface morphology of the double-stroke traces after the concentration reached 0.6 g/mL. Though most of the silver plates lay horizontally on the surface, they are still randomly orientated inside the PVA film, as shown in Figure 6-7(j2) (encircled by red dotted lines).
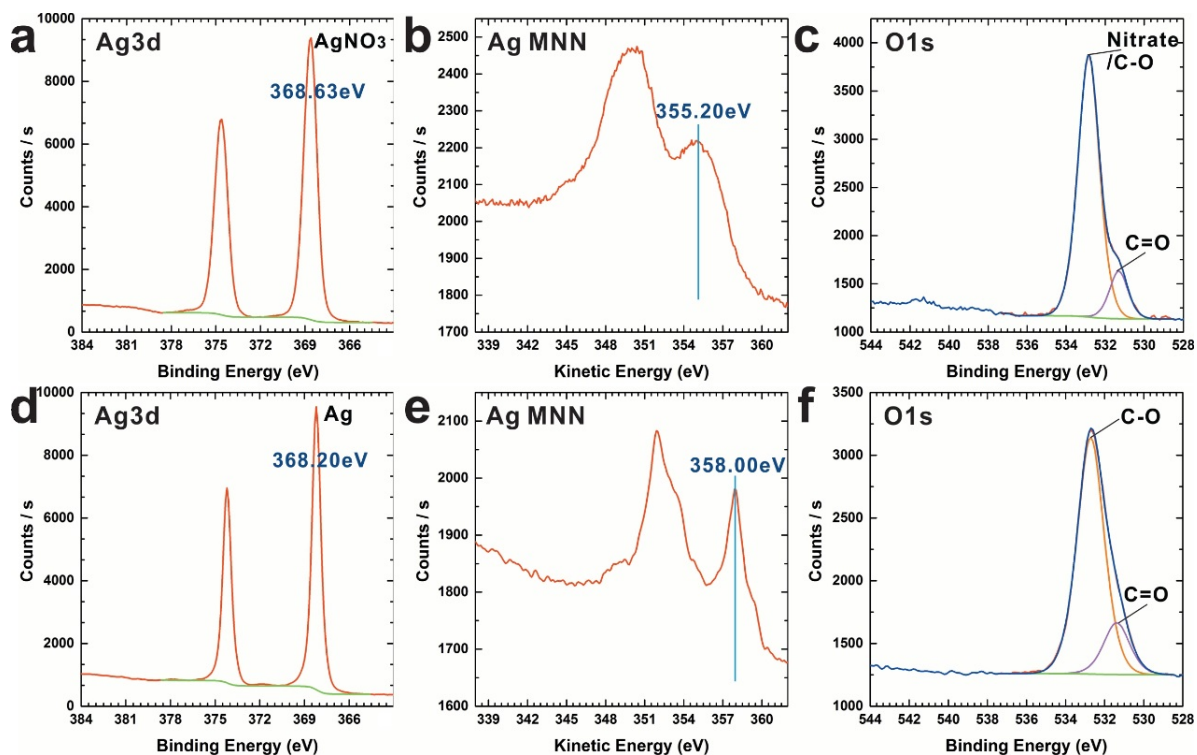
Figure 6-8. X-ray photoelectron spectroscopy (XPS) spectrums of a) Ag3d; b) Ag MNN; c) O1s from traces written with 1.2 g/mL silver nitrate ink on un-functionalized coatings. XPS spectrums of d) Ag3d; e) Ag MNN; f) O1s from traces written with 1.2g/mL silver nitrate ink on Vc functionalized coatings.

The chemical state of silver on the surface was investigated by X-ray photoelectron spectroscopy (XPS). The binding energy (B.E.) of Ag 3d was calibrated while considering the charge shift observed for the sp3 C-C and C-H bonds that are supposed to be centered at 285 eV. Figures 5(a)-(c) show the Ag 3d, Ag MNN and O 1s regions obtained from a single-stroke trace written with 1.6 g/mL silver nitrate ink on un-activated coating as a control group. Both the Ag 3d peak (368.63 eV, Figure 6-8(a)) and Ag MNN Auger peak (355.20 eV, Figure 6-8(b)) match the silver nitrate standard spectrum, indicating a single chemical state for silver. Combining this with the obtained Auger parameter (723.83 eV), we can confirm that only silver nitrate is presented on the surface. The O 1s region (Figure 6-8(c)) presents a strong peak at ~533 eV, which can be attributed to the nitrate groups and PVA film. Figures 6-8(d)-(f) show the same regions obtained from a single-stroke trace, written with the same concentration except on activated coating. Different from the control group, the Ag 3d peak appeared at 368.2 eV and the Ag MNN Auger peak appeared at 358 eV, which matches well with the silver metal

standard spectrum. With an Auger parameter of 726.2 eV, the surface can be confirmed to be covered in silver metal with no presence of other chemical states. Compared to the control group, a slightly larger area of C=O is observed in the O 1s region (Figure 6-8(f)), which can be explained by the newly loaded ascorbic acid. It also worth mentioning that we also conducted an XPS analysis on samples written with higher silver nitrate concentrations, up to 2.0 g/mL. However, the results looked almost identical to those shown in Figure 6-8-(d)-(f), with silver only present in the Ag^0 state.
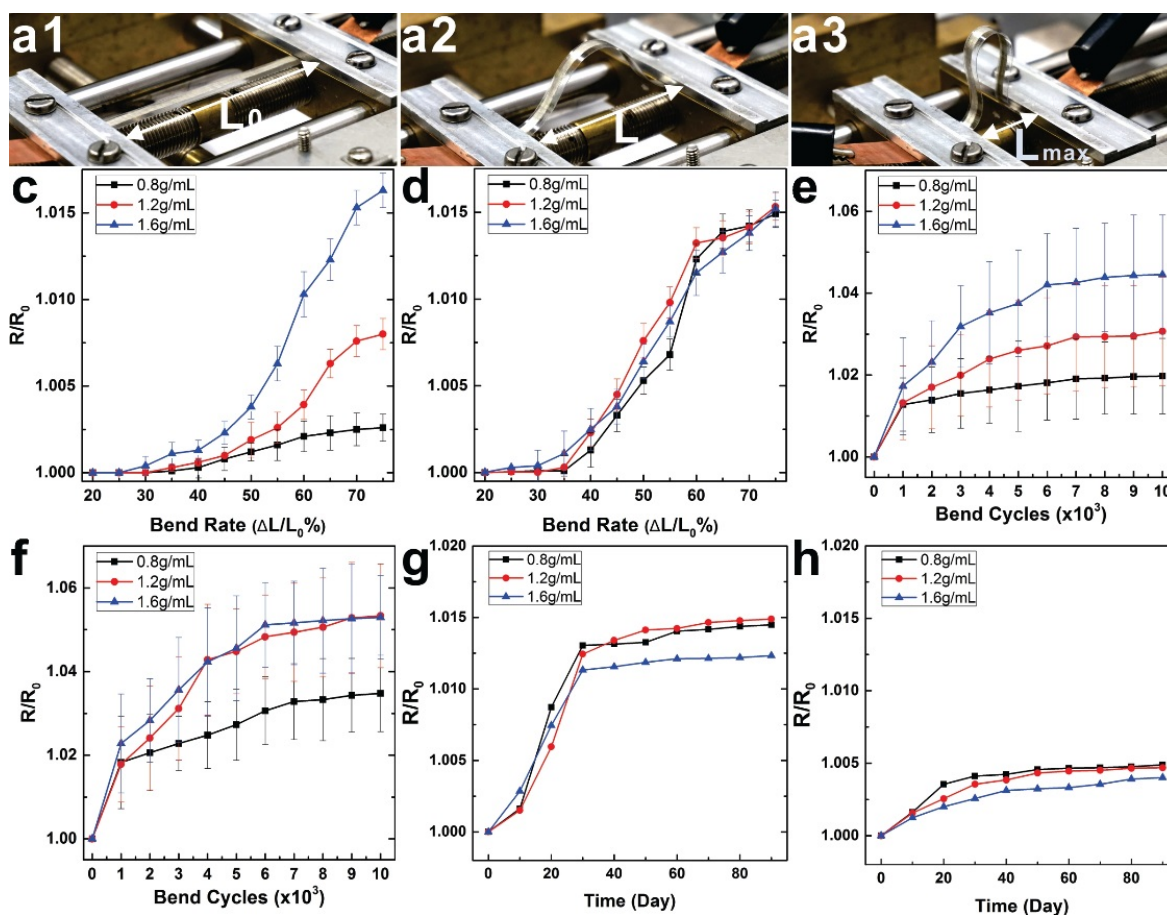
Figure 6-9. a) Optical images of a silver electrode in flat state with initial length of L0 (a1) and bent states with length of L (a2) and maximum bend radii with Lmin (a3). The change of electrical resistance in electrodes written with different silver nitrate concentration with c) single-stroke trace and d) double-stroke trace as a function of bend rate (ΔL/L0%); e) single-stroke trace and f) double-stroke trace as a function of bend cycles; g) single-stroke trace and h) double-stroke trace as a function of time.

To investigate the mechanical flexibility and stability of the metal-polymer structure, several resistance measurements were conducted. For the bending-resistance tests, traces with length of ~10 cm and width of ~3.5 mm was fabricated on PET substrate using the proposed RoD method. The electrode-patterned PET was actuated between flat and bent states at a rate of 2 cm/s using a custom-made stretching stage connected to a computer-controlled step motor. A Kethley multimeter was connected to the copper electrodes of the stretching stage in a four-probe sensing mode for accurate measurement of the resistance of the sample. Figure 6-9(a) shows the tested sample at different bent states. Figure 6-9(a1) shows the initial state of the sample with electrode distance of L_0. We use the initial distance L_0 and actual distance L (shown in Figure 6-9(a2)) to calculate the distance difference ΔL (L_0-L), and then divide this value by the initial distance L_0 to calculate the "bend rate" ($\Delta L/L_0\%$) of the sample. For instance, Figure 6-9(a3) displays a specimen with a bend rate of 75% (L_{min} = 2.5 cm, L_0 = 10 cm). Two groups of data showing the relationship between bend rate and resistance change are presented in Figures 6-9(c)-(d), corresponding to the single-stroke and double-stroke traces, respectively. We chose samples fabricated using inks of three different concentrations (0.8 g/mL, 1.2 g/mL and 1.6 g/mL) that gave us satisfactory conductivity. For the single-stroke group, as shown in Figure 6-9(c), the increasing rate of sheet resistance is positively correlated with the ink concentration, where the 0.8 g/mL trace exhibits the smallest resistance increasing rate of ~0.13% and the 1.6 g/mL trace shows the largest increasing rate of 0.8 % at the highest bend rate. The bending strain ε can be calculated by $\varepsilon = h_s/2R$, where h_s is the thickness of the sample and R is the bending curvature. [357, 358] The reducing distance between two terminals results in the increasing of the bending curvature R, and a thicker electrode has higher h_s value, both of which contribute to a larger strain value. Thus, the electrode written with 1.6 g/mL silver nitrate ink will bear the largest strain value during the bending test, which indeed presents the largest resistance increasing rate. In addition, the loss of conductivity is mainly attributed to the cracks and separation of silver plates on the PVA surface when bent outwards, and thus samples with a sparser silver layer (lower ink concentration) exhibited smaller increases in resistance. When the bend rate is less than 40%, the resistance is almost unaffected (<0.1%), and even when the bend rate reaches its maximum value (75%), the resistance increment is still smaller than 1%. As for the double-stroke group, as shown in Figure 6-9(d), the three types of traces show almost identical results, with a near-linear response to the bend rate. This can be explained by their similar surface morphology, as shown in Figures 6-7(h)-(j). Similarly, at

the maximum bend rate, all samples exhibit a similar resistance increasing rate of ~0.75%. Overall, the silver trances demonstrate excellent conductivity under bending thanks to its unique metal-polymer structure and the good flexibility of PVA film.

Flexible electronics are regularly subjected to bending, and its bending durability is an important consideration for its overall performance. Thus, we measured the electrical resistance change of traces written with different ink concentrations as a function of the number of bend cycles, and the average R/R_0 values obtained from five traces of each group are presented in Figures 6-9(e)-(f), corresponding to single-stroke and double-stroke samples, respectively. During the first 1000 cycles, the resistance initially undergoes a large increase, possibly due to newly formed cracks on the surface, but subsequently increases at a much slower steady speed for both groups. For the single-stroke trace, higher concentrations produce larger increases to the resistance as cycles increase. Similar results can be seen in the double-stroke group, with the only difference being that the 1.2 g/mL and 1.6 g/mL traces appear to be almost identical. After 10000 cycles, all samples exhibit a relatively small resistance change, with a maximum value of ~5% (double stroke, 1.2 g/mL) and minimum value of only ~2% (single stroke, 0.8 g/mL), reflecting superb bending durability. Compared to traditional surface-only conductive features, the bending durability is greatly enhanced by the metal-polymer conductive structure.

The three-dimensional metal-polymer structure greatly enhances its conductivity, adhesion and durability; however, due to the hydrophilic property of PVA, the silver may have higher risks of being oxidized in air and resultantly lose some conductivity. Hence, the relationship between resistance, ink concentration and storing time was investigated. All samples were left out in open air in a room without any temperature or humidity control. Figures 6-9(g) and (h) show the resistance change of single-stroke and double-stroke traces, respectively, at different concentrations over a period of 90 days. A steady increase in resistance is observed for the single-stroke group in the first 30 days, after which the resistance remains almost unchanged in the following 60 days after formation of an oxidizing balance. The double-stroke traces exhibit a much better stability over time than that of the single stroke, which may be largely attributed to its dense and pressed morphology. Overall, the single-stroke group shows an average resistance increase of ~1.4%, while the double-stroke group shows an average resistance increase of ~ 0.4% over a period of three months. An ASTM standard tape test was

conducted to evaluate adhesion of the conductive film in the previously prepared samples. During the test, the as-fabricated 3DMP structure conformally adhered to the surface during all iterations for electrodes written with different ink concentration except the first, when a small amount of surface particles was removed. The sheet resistance also remained unchanged throughout several iterations, demonstrating excellent adhesion according to the ASTM D3359 standard.
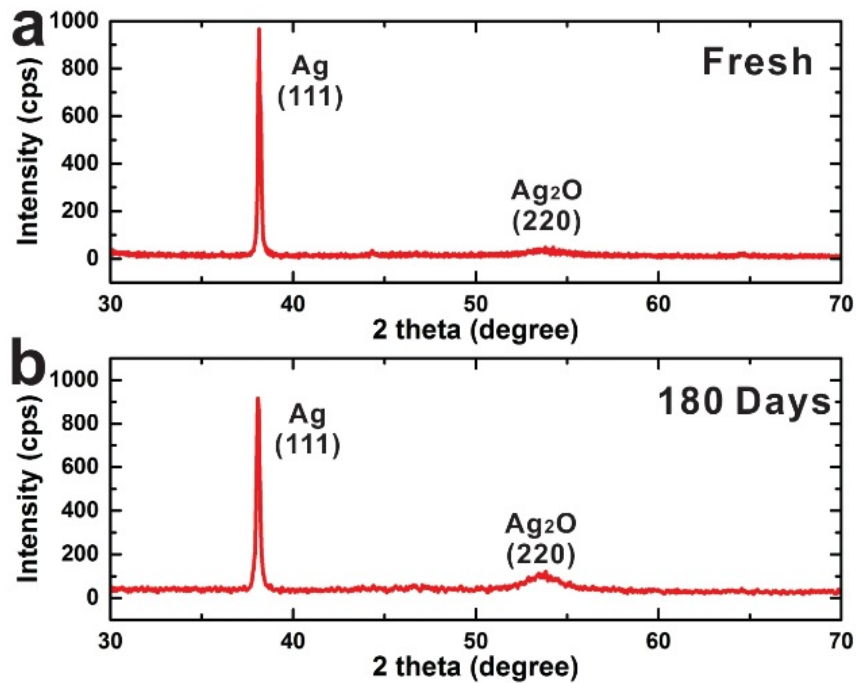
Figure 6-10. X-ray diffraction (XRD) spectra of a) freshly prepared single-stroke electrode written it 1.2 g/mL silver nitrate ink; b) after stored in air for 180 days.

X-ray diffraction (XRD) was conducted to study the crystalline structure of the resultant silver layer and surface metal composition of fresh samples compared to samples stored for 180 days. Figure 6-10 presents the XRD patterns of the freshly drawn silver and silver traces stored in air for 180 days. Both samples show peaks at 38.06° and 53.41°, which can be assigned to the silver crystal plane (111) and silver oxide crystal plane (220), respectively (JCPDS Data 04-0783, 41-1104). For the sample stored in air for 90 days, the peak for Ag_2O is slightly stronger than that of the freshly made sample, illustrating that a small amount of oxide is generated over

time. Both silver oxide peaks are very weak, and the peaks for (111) silver remain almost unchanged. Thus, we concluded that the samples are relatively stable in dry air over time.
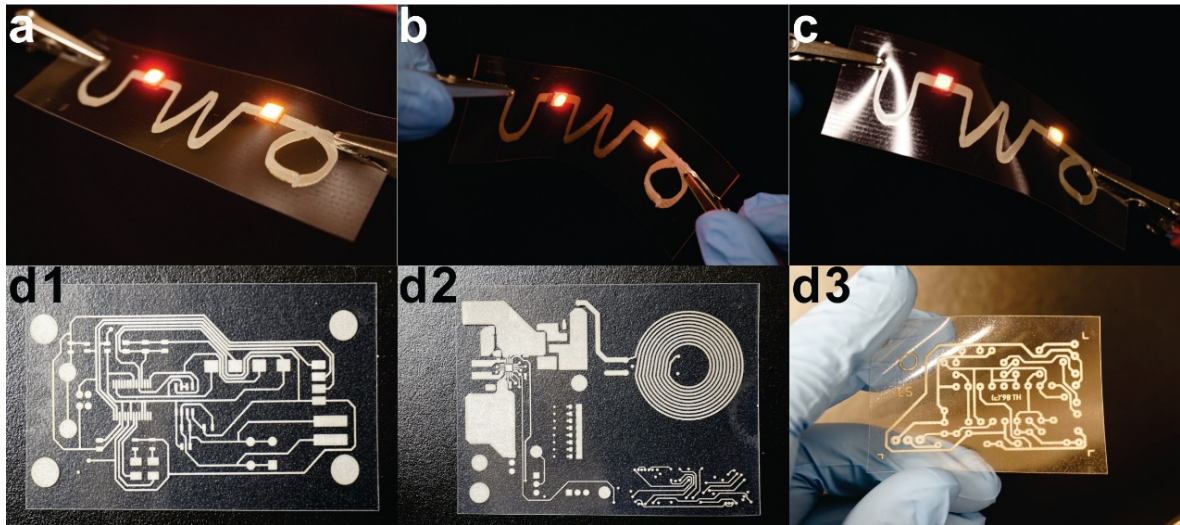
Figure 6-11. a) Optical images of LEDs powered by the hand-written metal-polymer conductive traces fabricated using the proposed RoD method operating as intended in normal flat state; b) when bent inward and c) when bent outward. d) Optical images of high resolution functional circuits fabricated by inkjet printing using the RoD method.

To demonstrate the versatility of the RoD technique in real world applications, we wrote conductive letters on PET and powered two LEDs through the conductive traces, as shown in Figure 6-11(a). The circuit maintains its function when subjected to inward bending (Figure 6-11(b)) and outward bending (Figure 6-11(c)). With the pen filled with silver nitrate ink, many types of functional circuits can be fabricated within in a few minutes. It is worth mentioning that the RoD method can also be used for manufacturing high performance and high resolution flexible circuit via inkjet printing at ultra-low cost. As a proof of concept, a silver nitrate solution was filled into a commercial available inkjet printer after tuning to the proper viscosity and surface tension. High quality functional circuits can be generated in a few seconds with a single click of "print". Figure 6-11(d) shows some of the functional circuits fabricated by RoD based inkjet printing. Since no post-treatment is required for the RoD method, the as-printed circuits can be used immediately for electronic component mounting or deposition of other materials. The RoD approach can also be used in other printing system, such as aerojet printing

and gravure printing, to achieve higher resolutions or higher speed of roll-to-roll (R2R) production of high performance flexible electronics.

6.4 Conclusion

In summary, we proposed a react-on-demand (RoD) approach for cost-effective fabrication of high performance flexible circuits with enhanced safety and durability. The RoD method brings the emerging handwritten electronics technology one step closer to end-users, who require performance and ease-of-use at the same time. By adopting a three-dimensional on-site synthesize of silver plates, a metal-polymer hybrid structure of ~ 7 µm thickness with ultralow sheet resistance of 4 mΩ/sq can be achieved within a few seconds. With little effort, the RoD approach can be extended to various printing systems, offering a particle-free, sintering-free solution for high resolution, high speed production of flexible functional circuits and devices.

Chapter 7

7. Conclusion and Future Work

7.1 Conclusion

Flexible electronics and devices represent an important direction of future electronics manufacturing and mechanical engineering. A lot of effort has been focused on the fabrication of printed electronics in recent years, however, many of these studies are still in infancy and mostly rely on sophisticated and expensive nano/microfabrication processes and facilities and involve high processing temperatures and toxic wastes. It is therefore highly desirable, yet extremely challenging, to develop low-cost and scalable facile methods that use inexpensive materials to make integratable and high-performance flexible electronics and devices. My PhD work focused on developing novel fabrication methods for printed flexible electronics, aimed to solve the above-mentioned challenges in the manufacturing of printed electronics (PE). By utilising recent developments in material and chemical sciences, several fabrication strategies have been demonstrated, accomplishing all the objectives proposed in Chapter 1.

Instead of using expensive nanomaterials, electroless deposition (ELD) technique was adopted and a particle-free, scalable and cost-effective method to for selective metallization of different substrates was developed. A special engineered coating composition which was used for fast surface modification of polyethylene terephthalate and cellulose paper was successfully developed. The coating can immobilize transition metal ions and form covalent bonding with the substrate and eliminate the diffusion of the deposited copper during ELD process, enhancing resolution and the adhesion between the metal and substrate in a great extent. With the proposed method, circuits with sheet resistance down to 5.4 mΩ/sq was achieved on highly porous cellulose paper, which was nearly 10 times better than regular PE product on the market (50 mΩ/sq). Furthermore, utilizing the unique properties of porous media, the proposed method enables the creation of highly conductive interconnects (VIAs) with ultra-low sheet resistance down to 2.6 mΩ/sq without the need for drilling or punching holes of in the substrate. Based on the proposed method, high performance double layer battery-free device with drill-less VIAs were successfully fabricated for the first time. It is worth mentioning that, with minimal additional development, the proposed fabrication strategy can be extended to other

fiber-based and porous substrates, expanding its usefulness to countless applications. To further explore the versatility of the proposed strategies, in Chapter 4, a scalable fabrication method for flexible, binder-free and all-solid-state supercapacitors was proposed based on the low-cost chemical engraving technique, to construct Cu_xO nanostructure *in-situ* on the three-dimensional metallized cellulose fiber structures. Benefitting from both the "2D Materials on 3D Structures" design and the binder-free nature of the fabricated electrodes, substantial improvements to electrical conductivity, aerial capacitance, and electrochemical performance of the resulting supercapacitors (SCs) are achieved, fulfilling the increasing demand of highly customized power systems in the IoT and wearable electronics industries.

All commercial available printers are using liquid ink for PE production and clogging of printers is unavoidable. To solve the problem, a digital solvent-free printing method based on the existing laser printing technique to produce PE was proposed in Chapter 5. The solvent-free toner is used as the "ink". Special functional groups, which can trigger the growth of copper, were grafted to the thermoplastic toner particles. The special modified toner was then printed out to form desired patterns and got metallized in the following ELD process. The whole printing process does not evolve any liquid ink, and thus, the clogging of the printer is completely eliminated. It is worth mentioning that this was the first demonstration of using electrostatic laser printing method to make PE. ELD technique was chosen for selective metallization of the substrate mainly because of its ability of generating highly conductive patterns and low cost. However, ELD process takes long time (hours). To solve this, a React-on-Demand (RoD) method for low-cost one-step fabrication of highly conductive electronics was proposed in Chapter 6. A special water-swellable functionalized coating with the ability of reducing metal salt was developed. When the silver precursor touches the coating, on-site synthesis of silver nano-plates was triggered in a three-dimensional manner, forming a highly conductive metal-polymer hybrid structure. Ultra-low sheet resistance down to 2.6 mΩ/sq was achieved by one-step RoD printing or writing in a few seconds.

7.2 Future Work

The main driving force of PE has been its promise of providing versatile electronics functionality with a price that will be eventually comparable to the price of producing regular printing products in a traditional printing press manufacturing plant. The printing processes

used today are extremely productive and cost-effective compared to the processes used to make silicon-based electronics. The fundamental of these benefits is low production unit costs and high production capacity. Printing production volumes per spent time can be very high with standard mass-printing equipment compared to the silicon wafer processing. The utilization of roll-to-roll (R2R) high speed printing process as a mean of manufacturing reduces the marginal cost of producing products, making it very close to the cost of raw-materials used to produce printing products. The ELD-based fabrication strategies proposed in this thesis greatly lower the cost of raw-materials and enhance the performance of the printed circuits, thanks to the nanomaterials-free process and thick deposited metal layer. However, traditional ELD process usually takes long deposition time to achieve that. This impose critical challenges for the implementation of the proposed fabrication strategies to a R2R system. High-speed electroless deposition formula which can deposit metal layer with a thickness of several microns in a few minutes has been developed in recent year. However, these formulas target at the rapid metallization of VIA holes and the thickening of the whole piece of copper layer on FR-4 or other substrates, in which selective metallization is not required. The deposited metal particles in these formulas will not only grow vertically, but also grow horizontally. When it comes to the printed electronics where only the metallization of selective area of the substrate is required, such high-speed formulas will cause significant loss of resolution, making them incompatible with the PE industry. Thus, it is recommended that one of the future projects focuses on the development of high-speed vertical-growth only electroless copper deposition formula to enable the low-cost R2R process for high resolution PE production.

Though porous substrates are not preferred by the fabrication process based on direct printing of functional materials due to all kinds of drawbacks as mentioned in Chapter 2, their unique micro structure of porous substrate can significantly speed up the electroless deposition rate of metal per unit area. The printed solvent-free catalyst ink will penetrate in to the substrate and create three-dimensional catalyst-loaded section which will trigger the following electroless deposition process in a three-dimensional manor. Meanwhile, the metallization depth can be controlled with the proposed method in Chapter 3, enabling the creation of multilayer functional features on the substrates without additional printing or physically drilling process. In addition, the porous structures are highly desired in energy storage and sensing systems. Such unique properties of porous substrates make them a promising candidate for a new

generation of PE. The investigation of PE fabrication on one of the nature-fiber based porous media — cellulose paper — is presented in this paper with promising results. It is therefore, recommended that future project focus on the fabrication of single/multilayer circuits and devices on other porous media such as cotton, wool fabric, porous polyimide, etc. The ink penetration behaviour on these porous substrates should be investigated thoroughly. The ink penetration depth is affected by the properties of inks (viscosity, surface tension, boiling point, etc.), the properties of substrate (surface energy, fiber diameters, porosity, etc.) and ambient environment (temperature, humidity, etc.). It is also recommended that research efforts focus on the development of a mathematical model to describe the ink penetration behaviour accounting most of the factors mentioned above.

Laser printing holds the advantages of solvent-free process, fast printing speed and reduced chemical waste. The proposed laser-printing fabrication approach in Chapter 5 still requires ELD process to complete the metallization of the printed pattern, which offset its advantage in printing speed. The main content of the toner is a type of thermoplastic materials, and for a conventional office-use laser printer, the printed toner usually has a thickness of more than 10 microns, much thicker than that achieved by inkjet printing (a few hundred nanometers). By proper modification of the toner composition to load sufficient amount of metal precursor as well as sufficient amount of thermoplastic-based reducing agent, the laser printed patterns hold the potential be directly converted to thin metal films with high conductivity. The newly developed intensive pulsed light (IPL) sintering system can provide enough energy in a short period of time (<1 second) to evaporate the polymer in the toner and, at the same time, trigger the metallization of the modified toner. Thus, it is recommended that future work focus on the development of metal precursor loaded laser printable toner composition and the development of IPL post treatment process to achieve the direct metallization of laser printed patterns.

The proposed RoD method in Chapter 6 also points a promising way for low-cost production of high performance PE. It holds the potential for R2R high-speed production of PE. The resultant 3DMP conductive structure also eliminate the safety concerns of PE products. The functionalized coating can be applied onto the substrate in one of the rolls prior to the printing of metal precursor ink. One of the challenges facing here is how to efficiently dry the coating in a short period of time (a few seconds) to fit the high speed R2R production line, while at the same keep the chemical activity of the coating. One of the promising solutions is to develop a

UV curable water-swellable polymer composition as the coating composition. Currently, UV curable PVA and other water-swellable polymer has been developed, however, after the cross-linking reaction during the UV curing process, the cured polymer film will no longer show water-swellable property. Thus, it is recommended that future work also focus on the implementation of the RoD method to the R2R printing system.

References

[1]   W. Gao, H. Y. Nyein, Z. Shahpar, H. M. Fahad, K. Chen, S. Emaminejad, *et al.*, "Wearable microsensor array for multiplexed heavy metal monitoring of body fluids," *Acs Sensors,* vol. 1, pp. 866-874, 2016.

[2]   M. Berggren, D. Nilsson, and N. D. Robinson, "Organic materials for printed electronics," *Nature materials,* vol. 6, p. 3, 2007.

[3]   W. Gao, S. Emaminejad, H. Y. Y. Nyein, S. Challa, K. Chen, A. Peck, *et al.*, "Fully integrated wearable sensor arrays for multiplexed in situ perspiration analysis," *Nature,* vol. 529, p. 509, 2016.

[4]   J. Noh, M. Jung, Y. Jung, C. Yeom, M. Pyo, and G. Cho, "Key issues with printed flexible thin film transistors and their application in disposable RF sensors," *Proceedings of the IEEE,* vol. 103, pp. 554-566, 2015.

[5]   M. Zirkl, A. Sawatdee, U. Helbig, M. Krause, G. Scheipl, E. Kraker, *et al.*, "An All-Printed Ferroelectric Active Matrix Sensor Network Based on Only Five Functional Materials Forming a Touchless Control Interface," *Advanced Materials,* vol. 23, pp. 2069-2074, 2011.

[6]   L. W. F. Chaves and C. Decker, "A survey on organic smart labels for the Internet-of-Things," in *Networked Sensing Systems (INSS), 2010 Seventh International Conference on*, 2010, pp. 161-164.

[7]   J. A. Rogers, Z. Bao, K. Baldwin, A. Dodabalapur, B. Crone, V. Raju, *et al.*, "like electronic displays: Large-area rubber-stamped plastic sheets of electronics and microencapsulated electrophoretic inks," *Proceedings of the National Academy of Sciences,* vol. 98, pp. 4835-4840, 2001.

[8]   M. K. Choi, J. Yang, K. Kang, D. C. Kim, C. Choi, C. Park, *et al.*, "Wearable red–green–blue quantum dot light-emitting diode array using high-resolution intaglio transfer printing," *Nature communications,* vol. 6, p. 7149, 2015.

[9]   R. Søndergaard, M. Hösel, D. Angmo, T. T. Larsen-Olsen, and F. C. Krebs, "Roll-to-roll fabrication of polymer solar cells," *Materials today,* vol. 15, pp. 36-49, 2012.

[10]   C. Yeom, K. Chen, D. Kiriya, Z. Yu, G. Cho, and A. Javey, "Large-Area Compliant Tactile Sensors Using Printed Carbon Nanotube Active-Matrix Backplanes," *Advanced Materials,* vol. 27, pp. 1561-1566, 2015.

[11]   T. Yokota, Y. Inoue, Y. Terakawa, J. Reeder, M. Kaltenbrunner, T. Ware*, et al.*, "Ultraflexible, large-area, physiological temperature sensors for multipoint measurements," *Proceedings of the National Academy of Sciences,* vol. 112, pp. 14533-14538, 2015.

[12]   K. Fukuda, T. Minamiki, T. Minami, M. Watanabe, T. Fukuda, D. Kumaki*, et al.*, "Printed organic transistors with uniform electrical performance and their application to amplifiers in biosensors," *Advanced Electronic Materials,* vol. 1, 2015.

[13]   H. Jinno, K. Kuribara, M. Kaltenbrunner, N. Matsuhisa, T. Someya, T. Yokota*, et al.*, "Printable elastic conductors with a high conductivity for electronic textile applications," *Nature communications,* vol. 6, p. 7461, 2015.

[14]   Y. S. Rim, S. H. Bae, H. Chen, N. De Marco, and Y. Yang, "Recent progress in materials and devices toward printable and flexible sensors," *Advanced Materials,* vol. 28, pp. 4415-4440, 2016.

[15]   Z. Bao, Y. Feng, A. Dodabalapur, V. Raju, and A. J. Lovinger, "High-performance plastic transistors fabricated by printing techniques," *Chemistry of Materials,* vol. 9, pp. 1299-1301, 1997.

[16]   J. Bharathan and Y. Yang, "Polymer electroluminescent devices processed by inkjet printing: I. Polymer light-emitting logo," *Applied Physics Letters,* vol. 72, pp. 2660-2662, 1998.

[17]   K. J. Lee, B. H. Jun, T. H. Kim, and J. Joung, "Direct synthesis and inkjetting of silver nanoparticles toward printed electronics," *Nanotechnology,* vol. 17, pp. 2424-2428, 2006.

[18]   M. A. M. Leenen, V. Arning, H. Thiem, J. Steiger, and R. Anselmann, "Printable electronics: flexibility for the future," *Physica Status Solidi A,* vol. 206, pp. 588-597, 2009.

[19]   W. Shen, X. Zhang, Q. Huang, Q. Xu, and W. Song, "Preparation of solid silver nanoparticles for inkjet printed flexible electronics with high conductivity," *Nanoscale,* vol. 6, pp. 1622-1628, 2014.

[20]   D. Deng, S. Feng, M. Shi, and C. Huang, "In situ preparation of silver nanoparticles decorated graphene conductive ink for inkjet printing," *Journal of Materials Science: Materials in Electronics,* vol. 28, pp. 15411-15417, 2017.

[21]   Z. S. Wu, Z. Liu, K. Parvez, X. Feng, and K. Müllen, "Ultrathin Printable Graphene Supercapacitors with AC Line-Filtering Performance," *Advanced Materials,* vol. 27, pp. 3669-3675, 2015.

[22]   B. Kim, M. L. Geier, M. C. Hersam, and A. Dodabalapur, "Inkjet printed circuits based on ambipolar and p-type carbon nanotube thin-film transistors," *Scientific Reports,* vol. 7, p. 39627, 2017.

[23]   C. Qiu, Z. Zhang, M. Xiao, Y. Yang, D. Zhong, and L.-M. Peng, "Scaling carbon nanotube complementary transistors to 5-nm gate lengths," *Science,* vol. 355, pp. 271-276, 2017.

[24]   Q. Wang, Y. Yu, J. Yang, and J. Liu, "Fast fabrication of flexible functional circuits based on liquid metal dual-trans printing," *Advanced Materials,* vol. 27, pp. 7109-7116, 2015.

[25]   H. Minemawari, T. Yamada, H. Matsui, J. y. Tsutsumi, S. Haas, R. Chiba*, et al.*, "Inkjet printing of single-crystal films," *Nature,* vol. 475, p. 364, 2011.

[26]   T. T. Baby, S. K. Garlapati, S. Dehm, M. Häming, R. Kruk, H. Hahn*, et al.*, "A general route toward complete room temperature processing of printed and high performance oxide electronics," *ACS nano,* vol. 9, pp. 3075-3083, 2015.

[27]   M. Jung, J. Kim, J. Noh, N. Lim, C. Lim, G. Lee*, et al.*, "All-printed and roll-to-roll-printable 13.56-MHz-operated 1-bit RF tag on plastic foils," *IEEE Transactions on Electron Devices,* vol. 57, pp. 571-580, 2010.

[28]   N. Matsuhisa, D. Inoue, P. Zalar, H. Jin, Y. Matsuba, A. Itoh*, et al.*, "Printable elastic conductors by in situ formation of silver nanoparticles from silver flakes," *Nature materials,* vol. 16, p. 834, 2017.

[29]   J. Li, Z. Sun, and F. Yan, "Solution Processable Low-Voltage Organic Thin Film Transistors with High-k Relaxor Ferroelectric Polymer as Gate Insulator," *Advanced Materials,* vol. 24, pp. 88-93, 2012.

[30]   W. J. Lee, W. T. Park, S. Park, S. Sung, Y. Y. Noh, and M. H. Yoon, "Large-Scale Precise Printing of Ultrathin Sol–Gel Oxide Dielectrics for Directly Patterned Solution-Processed Metal Oxide Transistor Arrays," *Advanced Materials,* vol. 27, pp. 5043-5048, 2015.

[31] K. Fukuda and T. Someya, "Recent Progress in the Development of Printed Thin-Film Transistors and Circuits With High-Resolution Printing Technology," *Advanced Materials,* vol. 29, 2017.

[32] H. P. Le, "Progress and trends in ink-jet printing technology," *Journal of Imaging Science and Technology,* vol. 42, pp. 49-62, 1998.

[33] M. Ikegawa, E. Ishii, N. Harada, and T. Takagishi, "Development of Ink-Particle Flight Simulation for Continuous Inkjet Printers," *Journal of Manufacturing Science and Engineering,* vol. 136, pp. 051021-051021-7, 2014.

[34] B. Derby, "Inkjet printing of functional and structural materials: fluid property requirements, feature stability, and resolution," *Annual Review of Materials Research,* vol. 40, pp. 395-414, 2010.

[35] Dax. (2017). *MIT is building a better 3d printer*. Available: https://hackaday.com/2017/12/09/mit-is-building-a-better-3d-printer/

[36] *On-demand type inkjet Printers*. Available: https://www.keyence.com/ss/products/marking/inkjet_central/inkjet/method/

[37] K. F. Teng and R. W. Vest, "Application of Ink Jet Technology on Photovoltaic Metallization," *IEEE Electron Device Letters,* vol. 9, pp. 591-593, 1988.

[38] K. Yamada, T. G. Henares, K. Suzuki, and D. Citterio, "Paper-based inkjet-printed microfluidic analytical devices," *Angewandte Chemie International Edition,* vol. 54, pp. 5294-5310, 2015.

[39] C. Dixon, A. H. Ng, R. Fobel, M. B. Miltenburg, and A. R. Wheeler, "An inkjet printed, roll-coated digital microfluidic device for inexpensive, miniaturized diagnostic assays," *Lab on a Chip,* vol. 16, pp. 4560-4568, 2016.

[40] D. McManus, S. Vranic, F. Withers, V. Sanchez-Romaguera, M. Macucci, H. Yang*, et al.*, "Water-based and biocompatible 2D crystal inks for all-inkjet-printed heterostructures," *Nature nanotechnology,* vol. 12, p. 343, 2017.

[41] M. Rizwan, A. A. Kutty, M. Kgwadi, T. D. Drysdale, L. Sydänheimo, L. Ukkonen*, et al.*, "Possibilities of Fabricating Copper-Based RFID Tags With Photonic-Sintered Inkjet Printing and Thermal Transfer Printing," *IEEE Antennas and Wireless Propagation Letters,* vol. 16, pp. 1828-1831, 2017.

[42]   H. He, J. Tajima, L. Sydänheimo, H. Nishikawa, L. Ukkonen, and J. Virkki, "Inkjet-printed antenna-electronics interconnections in passive UHF RFID tags," in *Microwave Symposium (IMS), 2017 IEEE MTT-S International*, 2017, pp. 598-601.

[43]   Y. Xu, I. Hennig, D. Freyberg, A. J. Strudwick, M. G. Schwab, T. Weitz*, et al.*, "Inkjet-printed energy storage device using graphene/polyaniline inks," *Journal of Power Sources,* vol. 248, pp. 483-488, 2014.

[44]   A. Chiolerio, S. Bocchini, and S. Porro, "Flexible Electronics: Inkjet Printed Negative Supercapacitors: Synthesis of Polyaniline-Based Inks, Doping Agent Effect, and Advanced Electronic Devices Applications (Adv. Funct. Mater. 22/2014)," *Advanced Functional Materials,* vol. 24, pp. 3472-3472, 2014.

[45]   T. Cheng, Y.-Z. Zhang, J.-P. Yi, L. Yang, J.-D. Zhang, W.-Y. Lai*, et al.*, "Inkjet-printed flexible, transparent and aesthetic energy storage devices based on PEDOT: PSS/Ag grid electrodes," *Journal of Materials Chemistry A,* vol. 4, pp. 13754-13763, 2016.

[46]   T.-Y. Chu, Z. Zhang, A. Dadvand, C. Py, S. Lang, and Y. Tao, "Direct writing of inkjet-printed short channel organic thin film transistors," *Organic Electronics,* vol. 51, pp. 485-489, 2017.

[47]   S. Conti, S. Lai, P. Cosseddu, and A. Bonfiglio, "An Inkjet-Printed, Ultralow Voltage, Flexible Organic Field Effect Transistor," *Advanced Materials Technologies,* vol. 2, 2017.

[48]   S.-P. Chen, H.-L. Chiu, P.-H. Wang, and Y.-C. Liao, "Inkjet printed conductive tracks for printed electronics," *ECS Journal of Solid State Science and Technology,* vol. 4, pp. P3026-P3033, 2015.

[49]   A. Kamyshny and S. Magdassi, "Conductive nanomaterials for printed electronics," *Small,* vol. 10, pp. 3515-3535, 2014.

[50]   J. Perelaer, P. J. Smith, D. Mager, D. Soltman, S. K. Volkman, V. Subramanian*, et al.*, "Printed electronics: the challenges involved in printing devices, interconnects, and contacts based on inorganic materials," *Journal of Materials Chemistry,* vol. 20, pp. 8446-8453, 2010.

[51]   M. Layani, I. Cooperstein, and S. Magdassi, "UV crosslinkable emulsions with silver nanoparticles for inkjet printing of conductive 3D structures," *Journal of Materials Chemistry C,* vol. 1, pp. 3244-3249, 2013.

[52] S. Wünscher, R. Abbel, J. Perelaer, and U. S. Schubert, "Progress of alternative sintering approaches of inkjet-printed metal inks and their application for manufacturing of flexible electronic devices," *Journal of Materials Chemistry C,* vol. 2, pp. 10232-10261, 2014.

[53] S. B. Walker and J. A. Lewis, "Reactive silver inks for patterning high-conductivity features at mild temperatures," *Journal of the American Chemical Society,* vol. 134, pp. 1419-1421, 2012.

[54] M. Vaseem, G. McKerricher, and A. Shamim, "Robust design of a particle-free silver-organo-complex ink with high conductivity and inkjet stability for flexible electronics," *ACS applied materials & interfaces,* vol. 8, pp. 177-186, 2015.

[55] G. Jabbour, M. Abulikamu, H. W. Choi, and H. Haverinen, "Reactive Inkjet Printing as a Tool for in situ Synthesis of Self-Assembled Nanoparticles," *Nanomaterials for 2D and 3D Printing,* 2017.

[56] K. R. Zope, D. Cormier, and S. Williams, "Reactive Silver Oxalate Ink Composition with Enhanced Curing Conditions for Flexible Substrates," *ACS applied materials & interfaces,* 2018.

[57] A. Samusjew, A. Lassnig, M. J. Cordill, K. K. Krawczyk, and T. Griesser, "Inkjet Printed Wiring Boards with Vertical Interconnect Access on Flexible, Fully Compostable Cellulose Substrates," *Advanced Materials Technologies,* 2017.

[58] S.-P. Chen, Z.-K. Kao, J.-L. Lin, and Y.-C. Liao, "Silver conductive features on flexible substrates from a thermally accelerated chain reaction at low sintering temperatures," *ACS applied materials & interfaces,* vol. 4, pp. 7064-7068, 2012.

[59] V. Bromberg, S. Ma, F. D. Egitto, and T. J. Singler, "Highly conductive lines by plasma-induced conversion of inkjet-printed silver nitrate traces," *Journal of Materials Chemistry C,* vol. 1, pp. 6842-6849, 2013.

[60] J. J. Valeton, K. Hermans, C. W. Bastiaansen, D. J. Broer, J. Perelaer, U. S. Schubert*, et al.*, "Room temperature preparation of conductive silver features using spin-coating and inkjet printing," *Journal of Materials Chemistry,* vol. 20, pp. 543-546, 2010.

[61] H.-S. Kim, S. R. Dhage, D.-E. Shim, and H. T. Hahn, "Intense pulsed light sintering of copper nanoink for printed electronics," *Applied Physics A,* vol. 97, p. 791, 2009.

[62]   B. Feleki, G. Bex, R. Andriessen, Y. Galagan, and F. Di Giacomo, "Rapid and low temperature processing of mesoporous TiO2 for perovskite solar cells on flexible and rigid substrates," *Materials Today Communications,* vol. 13, pp. 232-240, 2017.

[63]   D. Mitra and R. R. Baumann, "Conductivity and microstructure of inkjet printed nanoparticle silver layers processed with intense pulsed light (IPL) sintering on various polymeric substrates," in *NIP & Digital Fabrication Conference*, 2017, pp. 92-96.

[64]   T. Y. Zhang, X. L. Wang, T. J. Li, Q. Q. Guo, and J. Yang, "Fabrication of flexible copper-based electronics with high-resolution and high-conductivity on paper via inkjet printing," *Journal of Materials Chemistry C,* vol. 2, pp. 286-294, 2014.

[65]   S. Bidoki, D. Lewis, M. Clark, A. Vakorov, P. Millner, and D. McGorman, "Ink-jet fabrication of electronic components," *Journal of Micromechanics and Microengineering,* vol. 17, p. 967, 2007.

[66]   Z.-K. Kao, S.-P. Chen, J.-L. Lin, and Y.-C. Liao, "Low temperature synthesis of conductive silver tracks with polymer addition," *Journal of the Taiwan Institute of chemical engineers,* vol. 43, pp. 965-970, 2012.

[67]   Y. C. Liao and Z. K. Kao, "Direct Writing Patterns for Electroless Plated Copper Thin Film on Plastic Substrates," *Acs Applied Materials & Interfaces,* vol. 4, pp. 5109-5113, Oct 2012.

[68]   C. Y. Kao and K. S. Chou, "Electroless copper plating onto printed lines of nanosized silver seeds," *Electrochemical and Solid State Letters,* vol. 10, pp. D32-D34, 2007.

[69]   X. Liu, H. Chang, Y. Li, W. T. Huck, and Z. Zheng, "Polyelectrolyte-bridged metal/cotton hierarchical structures for highly durable conductive yarns," *ACS applied materials & interfaces,* vol. 2, pp. 529-535, 2010.

[70]   D. Zabetakis and W. J. Dressick, "Statistical Analysis of Plating Variable Effects on the Electrical Conductivity of Electroless Copper Patterns on Paper," *Acs Applied Materials & Interfaces,* vol. 4, pp. 2358-2368, May 2012.

[71]   Pirmin C. Hidber, W. Helbig, E. Kim, and G. M. Whitesides, "Microcontact Printing of Palladium Colloids: Micron-Scale Patterning by Electroless Deposition of Copper," *Langmuir,* vol. 12, pp. 1375-1380, 1996.

[72]   G. O. Mallory and J. B. Hajdu, *Electroless plating: fundamentals and applications*: William Andrew, 1990.

[73]   M. Hu, Q. Guo, T. Zhang, S. Zhou, and J. Yang, "SU-8-Induced Strong Bonding of Polymer Ligands to Flexible Substrates via in Situ Cross-Linked Reaction for Improved Surface Metallization and Fast Fabrication of High-Quality Flexible Circuits," *ACS applied materials & interfaces,* vol. 8, pp. 4280-4286, 2016.

[74]   T. Zhang, X. Cai, J. Liu, M. Hu, Q. Guo, and J. Yang, "Facile Fabrication of Hybrid Copper–Fiber Conductive Features with Enhanced Durability and Ultralow Sheet Resistance for Low-Cost High-Performance Paper-Based Electronics," *Advanced Sustainable Systems,* vol. 1, pp. 1700062-n/a, 2017.

[75]   J. H. Byeon and J. T. Roberts, "Silver deposition on a polymer substrate catalyzed by singly charged monodisperse copper nanoparticles," *ACS applied materials & interfaces,* vol. 4, pp. 2515-2520, 2012.

[76]   S. Ma, L. Liu, V. Bromberg, and T. J. Singler, "Electroless copper plating of inkjet-printed polydopamine nanoparticles: A facile method to fabricate highly conductive patterns at near room temperature," *ACS applied materials & interfaces,* vol. 6, pp. 19494-19498, 2014.

[77]   Y. Kobayashi, V. Salgueirino-Maceira, and L. M. Liz-Marzán, "Deposition of silver nanoparticles on silica spheres by pretreatment steps in electroless plating," *Chemistry of Materials,* vol. 13, pp. 1630-1633, 2001.

[78]   G. T. Carroll, J. R. Lancaster, N. J. Turro, J. T. Koberstein, and A. Mammana, "Electroless deposition of nickel on photografted polymeric microscale patterns," *Macromolecular rapid communications,* vol. 38, 2017.

[79]   F. Muench, S. Schaefer, L. Hagelüken, L. Molina-Luna, M. Duerrschnabel, H.-J. Kleebe*, et al.*, "Template-Free Electroless Plating of Gold Nanowires: Direct Surface Functionalization with Shape-Selective Nanostructures for Electrochemical Applications," *ACS applied materials & interfaces,* vol. 9, pp. 31142-31152, 2017.

[80]   D. P. de Jesus, L. Blanes, and C. L. do Lago, "Microchip free-flow electrophoresis on glass substrate using laser-printing toner as structural material," *Electrophoresis,* vol. 27, pp. 4935-4942, 2006.

[81]   K. Ellinas, M. Chatzipetrou, I. Zergioti, A. Tserepi, and E. Gogolides, "Superamphiphobic polymeric surfaces sustaining ultrahigh impact pressures of aqueous high-and low-surface-tension mixtures, tested with laser-induced forward transfer of drops," *Advanced Materials,* vol. 27, pp. 2231-2235, 2015.

[82]   P. Delaporte and A.-P. Alloncle, "Laser-induced forward transfer: a high resolution additive manufacturing technology," *Optics & Laser Technology,* vol. 78, pp. 33-41, 2016.

[83]   T. Araki, R. Mandamparambil, J. Jiu, T. Sekitani, and K. Suganuma, "Application of Printed Silver Nanowires Based on Laser-Induced Forward Transfer," *Nanomaterials for 2D and 3D Printing,* 2017.

[84]   J.-U. Park, M. Hardy, S. J. Kang, K. Barton, K. Adair, D. kishore Mukhopadhyay*, et al.*, "High-resolution electrohydrodynamic jet printing," *Nature materials,* vol. 6, p. 782, 2007.

[85]   H. Ding, C. Zhu, L. Tian, C. Liu, G. Fu, L. Shang*, et al.*, "Structural Color Patterns by Electrohydrodynamic Jet Printed Photonic Crystals," *ACS applied materials & interfaces,* vol. 9, pp. 11933-11941, 2017.

[86]   E. Sutanto, K. Shigeta, Y. Kim, P. Graf, D. Hoelzle, K. Barton*, et al.*, "A multimaterial electrohydrodynamic jet (E-jet) printing system," *Journal of Micromechanics and Microengineering,* vol. 22, p. 045008, 2012.

[87]   Y. Huang, N. Bu, Y. Duan, Y. Pan, H. Liu, Z. Yin*, et al.*, "Electrohydrodynamic direct-writing," *Nanoscale,* vol. 5, pp. 12007-12017, 2013.

[88]   A. Mette, P. Richter, M. Hörteis, and S. Glunz, "Metal aerosol jet printing for solar cell metallization," *Progress in Photovoltaics: Research and Applications,* vol. 15, pp. 621-627, 2007.

[89]   C. Cao, J. B. Andrews, and A. D. Franklin, "Completely Printed, Flexible, Stable, and Hysteresis-Free Carbon Nanotube Thin-Film Transistors via Aerosol Jet Printing," *Advanced Electronic Materials,* vol. 3, 2017.

[90]   J. A. Paulsen, M. Renn, K. Christenson, and R. Plourde, "Printing conformal electronics on 3D structures with Aerosol Jet technology," in *Future of Instrumentation International Workshop (FIIW), 2012*, 2012, pp. 1-4.

[91]   M. O'Reilly and J. Leal, "Jetting your way to fine-pitch 3D interconnects," *Chip Scale Review,* vol. 14, pp. 18-21, 2010.

[92]   W. Xie, X. Zhang, C. Leighton, and C. D. Frisbie, "2D Insulator–Metal Transition in Aerosol-Jet-Printed Electrolyte-Gated Indium Oxide Thin Film Transistors," *Advanced Electronic Materials,* vol. 3, 2017.

[93]   L. J. Deiner and T. L. Reitz, "Inkjet and aerosol jet printing of electrochemical devices for energy conversion and storage," *Advanced Engineering Materials,* 2017.

[94]   G. L. Goh, S. Agarwala, Y. J. Tan, and W. Y. Yeong, "A Low Cost and Flexible Carbon Nanotube pH Sensor fabricated using Aerosol Jet Technology for Live Cell Applications," *Sensors and Actuators B: Chemical,* 2017.

[95]   I. Grunwald, E. Groth, I. Wirth, J. Schumacher, M. Maiwald, V. Zoellmer*, et al.*, "Surface biofunctionalization and production of miniaturized sensor structures using aerosol printing technologies," *Biofabrication,* vol. 2, p. 014106, 2010.

[96]   H. R. Kang, "Water-Based Ink-Jet Ink. I. Formulation," *Journal of Imaging Science,* vol. 35, pp. 179-188, 1991.

[97]   H. R. Kang, "Water-Based Ink-Jet Ink. II. Characterization," *Journal of Imaging Science,* vol. 35, pp. 189-194, 1991.

[98]   H. R. Kang, "Water-Based Ink-Jet Ink. III. Performance Studies," *Journal of Imaging Science,* vol. 35, pp. 195-201, 1991.

[99]   P. Calvert, "Inkjet Printing ofr Materials and Devices," *Chemistry of Materials,* vol. 13, 2001.

[100]   K. X. Steirer, J. J. Berry, M. O. Reese, M. F. A. M. v. Hest, A. Miendaner, M. W. Liberatore*, et al.*, "Ultrasonically sprayed and inkjet printed thin film electrodes for organic solar cells," *Thin Sold Films,* vol. 517, pp. 2781-2786, 2009.

[101]   T. Zhang, X. Wang, T. Li, Q. Guo, and J. Yang, "Fabrication of flexible copper-based electronics with high-resolution and high-conductivity on paper *via* inkjet printing," *Jounal of Materials Chemistry C,* vol. 2, pp. 286-294, 2014.

[102]   L. Rapp, J. Ailuno, A. P. Alloncle, and P. Delaporte, "Pulsed-laser printing of silver nanoparticle ink: controlling morphological properties," *Optics Express,* vol. 19, pp. 21563-21574, 2011.

[103]   K. Arapov, E. Rubingh, R. Abbel, J. Laven, G. de With, and H. Friedrich, "Conductive screen printing inks by gelation of graphene dispersions," *Advanced Functional Materials,* vol. 26, pp. 586-593, 2016.

[104]   D. A. Pardo, G. E. Jabbour, and N. Peyghambarian, "Application of screen printing in the fabrication of organic light-emitting devices," *Advanced Materials,* vol. 12, pp. 1249-1252, 2000.

[105]   S. Bae, H. Kim, Y. Lee, X. Xu, J.-S. Park, Y. Zheng, *et al.*, "Roll-to-roll production of 30-inch graphene films for transparent electrodes," *Nature nanotechnology,* vol. 5, p. 574, 2010.

[106]   M. Singh, H. M. Haverinen, P. Dhagat, and G. E. Jabbour, "Inkjet printing—process and its applications," *Advanced materials,* vol. 22, pp. 673-685, 2010.

[107]   J. Jiang, B. Bao, M. Li, J. Sun, C. Zhang, Y. Li, *et al.*, "Fabrication of transparent multilayer circuits by inkjet printing," *Advanced Materials,* vol. 28, pp. 1420-1426, 2016.

[108]   X. Peng, J. Yuan, S. Shen, M. Gao, A. S. Chesman, H. Yin, *et al.*, "Perovskite and Organic Solar Cells Fabricated by Inkjet Printing: Progress and Prospects," *Advanced Functional Materials,* vol. 27, 2017.

[109]   M. M. Voigt, A. Guite, D. Y. Chung, R. U. Khan, A. J. Campbell, D. D. Bradley, *et al.*, "Polymer field-effect transistors fabricated by the sequential gravure printing of polythiophene, two insulator layers, and a metal ink gate," *Advanced Functional Materials,* vol. 20, pp. 239-246, 2010.

[110]   E. B. Secor, S. Lim, H. Zhang, C. D. Frisbie, L. F. Francis, and M. C. Hersam, "Gravure printing of graphene for large-area flexible electronics," *Advanced materials,* vol. 26, pp. 4533-4538, 2014.

[111]   Y. Takeda, Y. Yoshimura, R. Shiwaku, K. Hayasaka, T. Sekine, T. Okamoto, *et al.*, "Organic Complementary Inverter Circuits Fabricated with Reverse Offset Printing," *Advanced Electronic Materials,* 2017.

[112]   S. Raupp, D. Daume, S. Tekoglu, L. Merklein, U. Lemmer, G. Hernandez-Sosa, *et al.*, "Slot die coated and flexo printed highly efficient SMOLEDs," *Advanced Materials Technologies,* vol. 2, 2017.

[113]   F. C. Krebs, J. Fyenbo, and M. Jørgensen, "Product integration of compact roll-to-roll processed polymer solar cell modules: methods and manufacture using flexographic printing, slot-die coating and rotary screen printing," *Journal of Materials Chemistry,* vol. 20, pp. 8994-9001, 2010.

[114]   C. B. Arnold, P. Serra, and A. Piqué, "Laser direct-write techniques for printing of complex materials," *Mrs Bulletin,* vol. 32, pp. 23-31, 2007.

[115]   G.-W. Huang, Q.-P. Feng, H.-M. Xiao, N. Li, and S.-Y. Fu, "Rapid Laser Printing of Paper-Based Multilayer Circuits," *ACS nano,* vol. 10, pp. 8895-8903, 2016.

[116] T. Zhang, M. Hu, Y. Liu, Q. Guo, X. Wang, W. Zhang*, et al.*, "A laser printing based approach for printed electronics," *Applied Physics Letters,* vol. 108, p. 103501, 2016.

[117] J. A. Lewis and B. Y. Ahn, "Device fabrication: Three-dimensional printed electronics," *Nature,* vol. 518, p. 42, 2015.

[118] J. T. Muth, D. M. Vogt, R. L. Truby, Y. Mengüç, D. B. Kolesky, R. J. Wood*, et al.*, "Embedded 3D printing of strain sensors within highly stretchable elastomers," *Advanced Materials,* vol. 26, pp. 6307-6312, 2014.

[119] Y. L. Kong, I. A. Tamargo, H. Kim, B. N. Johnson, M. K. Gupta, T.-W. Koh*, et al.*, "3D printed quantum dot light-emitting diodes," *Nano letters,* vol. 14, pp. 7017-7023, 2014.

[120] A. Russo, B. Y. Ahn, J. J. Adams, E. B. Duoss, J. T. Bernhard, and J. A. Lewis, "Pen-on-paper flexible electronics," *Advanced materials,* vol. 23, pp. 3426-3430, 2011.

[121] M. Hu, X. Cai, Q. Guo, B. Bian, T. Zhang, and J. Yang, "Direct pen writing of adhesive particle-free ultrahigh silver salt-loaded composite ink for stretchable circuits," *ACS nano,* vol. 10, pp. 396-404, 2015.

[122] Y. L. Han, J. Hu, G. M. Genin, T. J. Lu, and F. Xu, "BioPen: direct writing of functional materials at the point of care," *Scientific reports,* vol. 4, p. 4872, 2014.

[123] V. Brus and P. Maryanchuk, "Graphite traces on water surface–A step toward low-cost pencil-on-semiconductor electronics and optoelectronics," *Carbon,* vol. 78, pp. 613-616, 2014.

[124] Y. Li, J. Wang, X. Li, D. Geng, R. Li, and X. Sun, "Superior energy capacity of graphene nanosheets for a nonaqueous lithium-oxygen battery," *Chemical Communications,* vol. 47, pp. 9438-9440, 2011.

[125] K. Jost, C. R. Perez, J. K. McDonough, V. Presser, M. Heon, G. Dion*, et al.*, "Carbon coated textiles for flexible energy storage," *Energy & Environmental Science,* vol. 4, pp. 5060-5067, 2011.

[126] T. Zhang, J. Li, J. Liu, and J. Yang, "React-on-Demand (RoD) Fabrication of Highly Conductive Metal–Polymer Hybrid Structure for Flexible Electronics via One-Step Direct Writing or Printing," *Advanced Functional Materials,* vol. 28, pp. 1704671-n/a, 2018.

[127] Q. Jiang, N. Kurra, and H. N. Alshareef, "Marker Pen Lithography for Flexible and Curvilinear On-Chip Energy Storage," *Advanced Functional Materials,* vol. 25, pp. 4976-4984, 2015.

[128] Y. Gao, H. Li, and J. Liu, "Direct writing of flexible electronics through room temperature liquid metal ink," *PLoS One,* vol. 7, p. e45485, 2012.

[129] S. S. Kim, S. I. Na, J. Jo, G. Tae, and D. Y. Kim, "Efficient polymer solar cells fabricated by simple brush painting," *Advanced Materials,* vol. 19, pp. 4410-4415, 2007.

[130] Y. Gao, H. Li, and J. Liu, "Directly writing resistor, inductor and capacitor to composite functional circuits: a super-simple way for alternative electronics," *PloS one,* vol. 8, p. e69761, 2013.

[131] H. Warren, R. D. Gately, P. O'Brien, and R. Gorkin, "Electrical conductivity, impedance, and percolation behavior of carbon nanofiber and carbon nanotube containing gellan gum hydrogels," *Journal of Polymer Science Part B: Polymer Physics,* vol. 52, pp. 864-871, 2014.

[132] L. Polavarapu, A. L. Porta, S. M. Novikov, M. Coronado-Puchau, and L. M. Liz-Marzán, "Pen-on-Paper Approach Toward the Design of Universal Surface Enhanced Raman Scattering Substrates," *Small,* vol. 10, pp. 3065-3071, 2014.

[133] X. Liao, Q. Liao, X. Yan, Q. Liang, H. Si, M. Li*, et al.*, "Flexible and highly sensitive strain sensors fabricated by pencil drawn for wearable monitor," *Advanced Functional Materials,* vol. 25, pp. 2395-2401, 2015.

[134] A. J. Bandodkar, W. Jia, J. Ramírez, and J. Wang, "Biocompatible Enzymatic Roller Pens for Direct Writing of Biocatalytic Materials:"Do-it-Yourself" Electrochemical Biosensors," *Advanced healthcare materials,* vol. 4, pp. 1215-1224, 2015.

[135] Y. Yu, J. Zhang, and J. Liu, "Biomedical implementation of liquid metal ink as drawable ECG electrode and skin circuit," *PLoS One,* vol. 8, p. e58771, 2013.

[136] G. Zheng, L. Hu, H. Wu, X. Xie, and Y. Cui, "Paper supercapacitors by a solvent-free drawing method," *Energy & Environmental Science,* vol. 4, pp. 3368-3373, 2011.

[137] Y. Wang and H. Zhou, "To draw an air electrode of a Li–air battery by pencil," *Energy & Environmental Science,* vol. 4, pp. 1704-1707, 2011.

[138] S. Ghosh, R. Yang, M. Kaumeyer, C. A. Zorman, S. J. Rowan, P. X.-L. Feng*, et al.*, "Fabrication of electrically conductive metal patterns at the surface of polymer films

by microplasma-based direct writing," *ACS applied materials & interfaces,* vol. 6, pp. 3099-3104, 2014.

[139] Y. Chiang, *Chinese calligraphy: An introduction to its aesthetic and technique* vol. 60: Harvard University Press, 1973.

[140] S.-B. Kang, Y.-J. Noh, S.-I. Na, and H.-K. Kim, "Brush-painted flexible organic solar cells using highly transparent and flexible Ag nanowire network electrodes," *Solar Energy Materials and Solar Cells,* vol. 122, pp. 152-157, 2014.

[141] D.-Y. Cho, K. Eun, S.-H. Choa, and H.-K. Kim, "Highly flexible and stretchable carbon nanotube network electrodes prepared by simple brush painting for cost-effective flexible organic solar cells," *Carbon,* vol. 66, pp. 530-538, 2014.

[142] J.-W. Lim, D.-Y. Cho, S.-I. Na, and H.-K. Kim, "Simple brush-painting of flexible and transparent Ag nanowire network electrodes as an alternative ITO anode for cost-efficient flexible organic solar cells," *Solar Energy Materials and Solar Cells,* vol. 107, pp. 348-354, 2012.

[143] J.-A. Jeong, Y.-J. Jeon, S.-S. Kim, B. K. Kim, K.-B. Chung, and H.-K. Kim, "Simple brush-painting of Ti-doped In2O3 transparent conducting electrodes from nano-particle solution for organic solar cells," *Solar Energy Materials and Solar Cells,* vol. 122, pp. 241-250, 2014.

[144] Z. Qi, F. Zhang, C.-a. Di, J. Wang, and D. Zhu, "All-brush-painted top-gate organic thin-film transistors," *Journal of Materials Chemistry C,* vol. 1, pp. 3072-3077, 2013.

[145] S.-P. Cho, J.-S. Yeo, D.-Y. Kim, S.-i. Na, and S.-S. Kim, "Brush painted V2O5 hole transport layer for efficient and air-stable polymer solar cells," *Solar Energy Materials and Solar Cells,* vol. 132, pp. 196-203, 2015.

[146] S.-S. Kim, S.-I. Na, S.-J. Kang, and D.-Y. Kim, "Annealing-free fabrication of P3HT: PCBM solar cells via simple brush painting," *Solar Energy Materials and Solar Cells,* vol. 94, pp. 171-175, 2010.

[147] C. Guo, Y. Yu, and J. Liu, "Rapidly patterning conductive components on skin substrates as physiological testing devices via liquid metal spraying and pre-designed mask," *Journal of Materials Chemistry B,* vol. 2, pp. 5739-5745, 2014.

[148] Y. Zheng, Q. Zhang, and J. Liu, "Pervasive liquid metal based direct writing electronics with roller-ball pen," *Aip Advances,* vol. 3, p. 112117, 2013.

[149] Y.-L. Tai and Z.-G. Yang, "Fabrication of paper-based conductive patterns for flexible electronics by direct-writing," *Journal of Materials Chemistry,* vol. 21, pp. 5938-5943, 2011.

[150] Z. Li, F. Li, J. Hu, W. H. Wee, Y. L. Han, B. Pingguan-Murphy*, et al.*, "Direct writing electrodes using a ball pen for paper-based point-of-care testing," *Analyst,* vol. 140, pp. 5526-5535, 2015.

[151] L. Xu, G. Yang, H. Jing, J. Wei, and Y. Han, "Pressure-assisted low-temperature sintering for paper-based writing electronics," *Nanotechnology,* vol. 24, p. 355204, 2013.

[152] W. Li, W. Li, J. Wei, J. Tan, and M. Chen, "Preparation of conductive Cu patterns by directly writing using nano-Cu ink," *Materials Chemistry and Physics,* vol. 146, pp. 82-87, 2014.

[153] W. Li and M. Chen, "Synthesis of stable ultra-small Cu nanoparticles for direct writing flexible electronics," *Applied surface science,* vol. 290, pp. 240-245, 2014.

[154] W. Yang, C. Liu, Z. Zhang, Y. Liu, and S. Nie, "based nanosilver conductive ink," *Journal of Materials Science: Materials in Electronics,* vol. 24, pp. 628-634, 2013.

[155] Y. Wang, L. Chen, Q. Wang, H. Sun, X. Wang, Z. Hu*, et al.*, "Solution-processed organic crystals written directly with a rollerball pen for field-effect transistors," *Organic Electronics,* vol. 15, pp. 2234-2239, 2014/10/01/ 2014.

[156] J.-W. Han, B. Kim, J. Li, and M. Meyyappan, "Carbon nanotube ink for writing on cellulose paper," *Materials Research Bulletin,* vol. 50, pp. 249-253, 2014.

[157] H. Jia, J. Wang, X. Zhang, and Y. Wang, "Pen-writing polypyrrole arrays on paper for versatile cheap sensors," *ACS Macro Letters,* vol. 3, pp. 86-90, 2013.

[158] Z. Li, H. Liu, C. Ouyang, W. Hong Wee, X. Cui, T. Jian Lu*, et al.*, "Recent Advances in Pen-Based Writing Electronics and their Emerging Applications," *Advanced Functional Materials,* vol. 26, pp. 165-180, 2016.

[159] L. D. Woolf and H. H. Streckert, "Graphite pencil line for exploring resistance," *The Physics Teacher,* vol. 34, pp. 440-441, 1996.

[160] C.-W. Lin, Z. Zhao, J. Kim, and J. Huang, "Pencil drawn strain gauges and chemiresistors on paper," *Scientific reports,* vol. 4, p. 3812, 2014.

[161] N. Kurra, D. Dutta, and G. U. Kulkarni, "Field effect transistors and RC filters from pencil-trace on paper," *Physical Chemistry Chemical Physics,* vol. 15, pp. 8367-8372, 2013.

[162] B. Yao, L. Yuan, X. Xiao, J. Zhang, Y. Qi, J. Zhou*, et al.*, "based solid-state supercapacitors with pencil-drawing graphite/polyaniline networks hybrid electrodes," *Nano Energy,* vol. 2, pp. 1071-1078, 2013.

[163] T.-K. Kang, "Tunable piezoresistive sensors based on pencil-on-paper," *Applied Physics Letters,* vol. 104, p. 073117, 2014.

[164] T.-L. Ren, H. Tian, D. Xie, and Y. Yang, "Flexible graphite-on-paper piezoresistive sensors," *Sensors,* vol. 12, pp. 6685-6694, 2012.

[165] A. J. Gimenez, J. Yanez-Limon, and J. M. Seminario, "ZnO− paper based photoconductive UV sensor," *The Journal of Physical Chemistry C,* vol. 115, pp. 282-287, 2010.

[166] K. ul Hasan, O. Nur, and M. Willander, "Screen printed ZnO ultraviolet photoconductive sensor on pencil drawn circuitry over paper," *Applied Physics Letters,* vol. 100, p. 211104, 2012.

[167] N. Dossi, R. Toniolo, A. Pizzariello, F. Impellizzieri, E. Piccin, and G. Bontempelli, "Pencil-drawn paper supported electrodes as simple electrochemical detectors for paper-based fluidic devices," *Electrophoresis,* vol. 34, pp. 2085-2091, 2013.

[168] N. Dossi, R. Toniolo, E. Piccin, S. Susmel, A. Pizzariello, and G. Bontempelli, "Pencil-Drawn Dual Electrode Detectors to Discriminate Between Analytes Comigrating on Paper-Based Fluidic Devices but Undergoing Electrochemical Processes with Different Reversibility," *Electroanalysis,* vol. 25, pp. 2515-2522, 2013.

[169] V. Brus and P. Maryanchuk, "Photosensitive Schottky-type heterojunctions prepared by the drawing of graphite films," *Applied Physics Letters,* vol. 104, p. 173501, 2014.

[170] V. V. Singh, G. Gupta, A. Batra, A. K. Nigam, M. Boopathi, P. K. Gutch*, et al.*, "Greener electrochemical synthesis of high quality graphene nanosheets directly from pencil and its SPR sensing application," *Advanced Functional Materials,* vol. 22, pp. 2352-2362, 2012.

[171] K. M. Frazier, K. A. Mirica, J. J. Walish, and T. M. Swager, "Fully-drawn carbon-based chemical sensors on organic and inorganic surfaces," *Lab on a Chip,* vol. 14, pp. 4059-4066, 2014.

[172] N. Dossi, R. Toniolo, F. Terzi, F. Impellizzieri, and G. Bontempelli, "Pencil leads doped with electrochemically deposited Ag and AgCl for drawing reference electrodes on paper-based electrochemical devices," *Electrochimica Acta,* vol. 146, pp. 518-524, 2014.

[173] N. Dossi, R. Toniolo, F. Impellizzieri, and G. Bontempelli, "Doped pencil leads for drawing modified electrodes on paper-based electrochemical devices," *Journal of Electroanalytical Chemistry,* vol. 722, pp. 90-94, 2014.

[174] S. Magdassi, M. Grouchko, O. Berezin, and A. Kamyshny, "Triggering the Sintering of Silver Nanoparticles at Room Temperature," *ACS Nano,* vol. 4, pp. 1943-1948, 2010/04/27 2010.

[175] M. Layani and S. Magdassi, "Flexible transparent conductive coatings by combining self-assembly with sintering of silver nanoparticles performed at room temperature," *Journal of Materials Chemistry,* vol. 21, pp. 15378-15382, 2011.

[176] M. Grouchko, A. Kamyshny, C. F. Mihailescu, D. F. Anghel, and S. Magdassi, "Conductive Inks with a "Built-In" Mechanism That Enables Sintering at Room Temperature," *ACS Nano,* vol. 5, pp. 3354-3359, 2011/04/26 2011.

[177] F. Larese Filon, M. Mauro, G. Adami, M. Bovenzi, and M. Crosera, "Nanoparticles skin absorption: New aspects for a safety profile evaluation," *Regulatory Toxicology and Pharmacology,* vol. 72, pp. 310-322, 2015/07/01/ 2015.

[178] B. Baroli, "Penetration of nanoparticles and nanomaterials in the skin: Fiction or reality?," *Journal of Pharmaceutical Sciences,* vol. 99, pp. 21-50, 2010.

[179] P. V. AshaRani, G. Low Kah Mun, M. P. Hande, and S. Valiyaveettil, "Cytotoxicity and Genotoxicity of Silver Nanoparticles in Human Cells," *ACS Nano,* vol. 3, pp. 279-290, 2009/02/24 2009.

[180] M. Ahamed, M. S. AlSalhi, and M. K. J. Siddiqui, "Silver nanoparticle applications and human health," *Clinica Chimica Acta,* vol. 411, pp. 1841-1848, 2010/12/14/ 2010.

[181] I. V. Vrček, I. Žuntar, R. Petlevski, I. Pavičić, M. Dutour Sikirić, M. Ćurlin*, et al.*, "Comparison of in vitro toxicity of silver ions and silver nanoparticles on human hepatoma cells," *Environmental Toxicology,* vol. 31, pp. 679-692, 2016.

[182] K. Fukuda and T. Someya, "Recent Progress in the Development of Printed Thin-Film Transistors and Circuits with High-Resolution Printing Technology," *Advanced Materials,* pp. n/a-n/a, 2016.

[183] S. Park, M. Vosguerichian, and Z. Bao, "A review of fabrication and applications of carbon nanotube film-based flexible electronics," *Nanoscale,* vol. 5, pp. 1727-1752, 2013.

[184] J. Liang, K. Tong, and Q. Pei, "A Water-Based Silver-Nanowire Screen-Print Ink for the Fabrication of Stretchable Conductors and Wearable Thin-Film Transistors," *Advanced Materials,* vol. 28, pp. 5986-5996, 2016.

[185] S. Conti, S. Lai, P. Cosseddu, and A. Bonfiglio, "An Inkjet-Printed, Ultralow Voltage, Flexible Organic Field Effect Transistor," *Advanced Materials Technologies,* vol. 2, pp. n/a-n/a, 2017.

[186] K. Fukuda, Y. Takeda, Y. Yoshimura, R. Shiwaku, L. T. Tran, T. Sekine*, et al.*, "Fully-printed high-performance organic thin-film transistors and circuitry on one-micron-thick polymer films," *Nature communications,* vol. 5, 2014.

[187] M. G. Mohammed and R. Kramer, "All-Printed Flexible and Stretchable Electronics," *Advanced Materials,* pp. n/a-n/a, 2017.

[188] X. Huang, Y. Liu, S.-W. Hwang, S.-K. Kang, D. Patnaik, J. F. Cortes*, et al.*, "Biodegradable Materials for Multilayer Transient Printed Circuit Boards," *Advanced Materials,* vol. 26, pp. 7371-7377, 2014.

[189] J. R. Corea, A. M. Flynn, B. Lechêne, G. Scott, G. D. Reed, P. J. Shin*, et al.*, "Screen-printed flexible MRI receive coils," *Nature communications,* vol. 7, 2016.

[190] L. Hu, H. Wu, and Y. Cui, "Printed energy storage devices by integration of electrodes and separators into single sheets of paper," *Applied Physics Letters,* vol. 96, p. 183502, 2010.

[191] K. Jost, D. Stenger, C. R. Perez, J. K. McDonough, K. Lian, Y. Gogotsi*, et al.*, "Knitted and screen printed carbon-fiber supercapacitors for applications in wearable electronics," *Energy & Environmental Science,* vol. 6, pp. 2698-2705, 2013.

[192]   J. Gao, J. Sidén, H.-E. Nilsson, and M. Gulliksson, "Printed humidity sensor with memory functionality for passive RFID tags," *IEEE Sensors Journal,* vol. 13, pp. 1824-1834, 2013.

[193]   D.-H. Lien, Z.-K. Kao, T.-H. Huang, Y.-C. Liao, S.-C. Lee, and J.-H. He, "All-Printed Paper Memory," *ACS Nano,* vol. 8, pp. 7613-7619, 2014/08/26 2014.

[194]   F. R. Fan, W. Tang, and Z. L. Wang, "Flexible Nanogenerators for Energy Harvesting and Self-Powered Electronics," *Advanced Materials,* 2016.

[195]   B. C. Kjellander, W. T. Smaal, K. Myny, J. Genoe, W. Dehaene, P. Heremans*, et al.*, "Optimized circuit design for flexible 8-bit RFID transponders with active layer of ink-jet printed small molecule semiconductors," *Organic Electronics,* vol. 14, pp. 768-774, 2013.

[196]   Y. Lin, D. Gritsenko, Q. Liu, X. Lu, and J. Xu, "Recent Advancements in Functionalized Paper-Based Electronics," *ACS Applied Materials & Interfaces,* vol. 8, pp. 20501-20515, 2016/08/17 2016.

[197]   D. Tobjörk and R. Österbacka, "Paper Electronics," *Advanced Materials,* vol. 23, pp. 1935-1961, 2011.

[198]   L. Yang, A. Rida, R. Vyas, and M. M. Tentzeris, "RFID tag and RF structures on a paper substrate using inkjet-printing technology," *IEEE Transactions on Microwave Theory and Techniques,* vol. 55, pp. 2894-2901, 2007.

[199]   A. A. Abrikosov and A. Beknazarov, *Fundamentals of the Theory of Metals* vol. 1: North-Holland Amsterdam, 1988.

[200]   H. A. Wheeler, "Formulas for the skin effect," *Proceedings of the IRE,* vol. 30, pp. 412-424, 1942.

[201]   K. Li, H. Zhen, L. Niu, X. Fang, Y. Zhang, R. Guo*, et al.*, "Full-Solution Processed Flexible Organic Solar Cells Using Low-Cost Printable Copper Electrodes," *Advanced Materials,* vol. 26, pp. 7271-7278, 2014.

[202]   L. Liu, Y. Yu, C. Yan, K. Li, and Z. Zheng, "Wearable energy-dense and power-dense supercapacitor yarns enabled by scalable graphene-metallic textile composite electrodes," *Nature communications,* vol. 6, 2015.

[203]   Y.-C. Liao and Z.-K. Kao, "Direct writing patterns for electroless plated copper thin film on plastic substrates," *ACS applied materials & interfaces,* vol. 4, pp. 5109-5113, 2012.

[204]   M. Charbonnier and M. Romand, "Polymer pretreatments for enhanced adhesion of metals deposited by the electroless process," *International journal of adhesion and adhesives,* vol. 23, pp. 277-285, 2003.

[205]   A. C. Siegel, D. A. Bruzewicz, D. B. Weibel, and G. M. Whitesides, "Microsolidics: fabrication of three-dimensional metallic microstructures in poly (dimethylsiloxane)," *Advanced Materials,* vol. 19, pp. 727-733, 2007.

[206]   Y. Chang, C. Yang, X.-Y. Zheng, D.-Y. Wang, and Z.-G. Yang, "Fabrication of copper patterns on flexible substrate by patterning–adsorption–plating process," *ACS applied materials & interfaces,* vol. 6, pp. 768-772, 2014.

[207]   K. Cheng, M. H. Yang, W. W. Chiu, C. Y. Huang, J. Chang, T. F. Ying*, et al.*, "Ink-Jet Printing, Self-Assembled Polyelectrolytes, and Electroless Plating: Low Cost Fabrication of Circuits on a Flexible Substrate at Room Temperature," *Macromolecular Rapid Communications,* vol. 26, pp. 247-264, 2005.

[208]   T. Wang, B. Chen, M. Rubner, and R. Cohen, "Selective electroless nickel plating on polyelectrolyte multilayer platforms," *Langmuir,* vol. 17, pp. 6610-6615, 2001.

[209]   A. Garcia, T. Berthelot, P. Viel, A. Mesnage, P. Jégou, F. Nekelson*, et al.*, "ABS Polymer Electroless Plating through a One-Step Poly(acrylic acid) Covalent Grafting," *ACS Applied Materials & Interfaces,* vol. 2, pp. 1177-1183, 2010/04/28 2010.

[210]   W. Wang, E. Kang, and K. Neoh, "Electroless plating of copper on polyimide films modified by plasma graft copolymerization with 4-vinylpyridine," *Applied Surface Science,* vol. 199, pp. 52-66, 2002.

[211]   J. B. You, S. Y. Kim, Y. J. Park, Y. G. Ko, and S. G. Im, "A Vapor-Phase Deposited Polymer Film to Improve the Adhesion of Electroless-Deposited Copper Layer onto Various Kinds of Substrates," *Langmuir,* vol. 30, pp. 916-921, 2014/01/28 2014.

[212]   S. Malynych, I. Luzinov, and G. Chumanov, "Poly (vinyl pyridine) as a universal surface modifier for immobilization of nanoparticles," *The Journal of Physical Chemistry B,* vol. 106, pp. 1280-1285, 2002.

[213]   F. Meng, W. Zhang, and S. Zheng, "Epoxy resin cured with poly (4-vinyl pyridine)," *Journal of materials science,* vol. 40, pp. 6367-6373, 2005.

[214] G. Xue, H. Ishida, and J. Koenig, "Chemical reactions of poly (vinyl pyridine) s with epoxy compounds," *Macromolecular Materials and Engineering,* vol. 142, pp. 17-27, 1986.

[215] Y. Qiao, W. Li, G. Wang, X. Zhang, and N. Cao, "Application of ordered mesoporous silica nanocontainers in an anticorrosive epoxy coating on a magnesium alloy surface," *RSC Advances,* vol. 5, pp. 47778-47787, 2015.

[216] K. Anasuya, M. Veeraiah, and P. Hemalatha, "Synthesis and Characterisation of Poly (Vinylpyrrolidone)-Copper (II) Complexes," *Research Journal of Chemical Sciences,* vol. 5, pp. 64-69, 2015.

[217] X. Wang, T. Zhang, B. Kobe, W. M. Lau, and J. Yang, "Grafting of polyelectrolytes onto hydrocarbon surfaces by high-energy hydrogen induced cross-linking for making metallized polymer films," *Chemical Communications,* vol. 49, pp. 4658-4660, 2013.

[218] B. ASTM, "D3359-Standard Test Method for Measuring Adhesion by Tape Test," *Tool and Tape,* 2002.

[219] F. Ferrero and L. Lizzi, "Feasability of an Ultra narrow band antenna for the internet of things," in *Antennas and Propagation & USNC/URSI National Radio Science Meeting, 2015 IEEE International Symposium on*, 2015, pp. 776-777.

[220] P. Hall, P. Gardner, J. Kelly, E. Ebrahimi, M. Hamid, and F. Ghanem, "Antenna challenges in cognitive radio," in *Proc. ISAP*, 2008.

[221] D. M. Pozar and B. Kaufman, "Comparison of three methods for the measurement of printed antenna efficiency," *IEEE Transactions on Antennas and Propagation,* vol. 36, pp. 136-139, 1988.

[222] D.-Y. Khang, H. Jiang, Y. Huang, and J. A. Rogers, "A Stretchable Form of Single-Crystal Silicon for High-Performance Electronics on Rubber Substrates," *Science,* vol. 311, pp. 208-212, 2006.

[223] M. Berggren, D. Nilsson, and N. D. Robinson, "Organic materials for printed electronics," *Nat Mater,* vol. 6, pp. 3-5, 01//print 2007.

[224] K. Fukuda and T. Someya, "Recent Progress in the Development of Printed Thin-Film Transistors and Circuits with High-Resolution Printing Technology," *Advanced Materials,* vol. 29, pp. 1602736-n/a, 2017.

[225] J. A. Rogers, "Electronics: A diverse printed future," *Nature,* vol. 468, pp. 177-178, 11/11/print 2010.

[226] M. G. Mohammed and R. Kramer, "All-Printed Flexible and Stretchable Electronics," *Advanced Materials,* vol. 29, pp. 1604965-n/a, 2017.

[227] S. Ji, B. G. Hyun, K. Kim, S. Y. Lee, S.-H. Kim, J.-Y. Kim*, et al.*, "Photo-patternable and transparent films using cellulose nanofibers for stretchable origami electronics," *NPG Asia Materials,* vol. 8, p. e299, 2016.

[228] K. Fukuda, Y. Takeda, Y. Yoshimura, R. Shiwaku, L. T. Tran, T. Sekine*, et al.*, "Fully-printed high-performance organic thin-film transistors and circuitry on one-micron-thick polymer films," vol. 5, p. 4147, 06/20/online 2014.

[229] M. U. Ahmed, M. Hossain, M. Safavieh, Y. Lu Wong, I. Abd Rahman, M. Zourob*, et al.*, "Toward the development of smart and low cost point of care biosensors using screen printed electrodes," *Crit Rev Biotechnol.,* vol. 36, pp. 495-505, 2014.

[230] R. A. Street, T. N. Ng, D. E. Schwartz, G. L. Whiting, J. P. Lu, R. D. Bringans*, et al.*, "From Printed Transistors to Printed Smart Systems," *Proceedings of the IEEE,* vol. 103, pp. 607-618, 2015.

[231] F. R. Fan, W. Tang, and Z. L. Wang, "Flexible Nanogenerators for Energy Harvesting and Self-Powered Electronics," *Advanced Materials,* vol. 28, pp. 4283-4305, 2016.

[232] M. Kang, K.-J. Baeg, D. Khim, Y.-Y. Noh, and D.-Y. Kim, "Printed, Flexible, Organic Nano-Floating-Gate Memory: Effects of Metal Nanoparticles and Blocking Dielectrics on Memory Characteristics," *Advanced Functional Materials,* vol. 23, pp. 3503-3512, 2013.

[233] B. W. An, J. H. Shin, S.-Y. Kim, J. Kim, S. Ji, J. Park*, et al.*, "Smart Sensor Systems for Wearable Electronic Devices," *Polymers,* vol. 9, p. 303, 2017.

[234] J. R. Corea, A. M. Flynn, B. Lechêne, G. Scott, G. D. Reed, P. J. Shin*, et al.*, "Screen-printed flexible MRI receive coils," *Nature communications,* vol. 7, p. 10839, 03/10/online 2016.

[235] S. Genovesi, F. Costa, F. Fanciulli, and A. Monorchio, "Wearable Inkjet-Printed Wideband Antenna by Using Miniaturized AMC for Sub-GHz Applications," *IEEE Antennas and Wireless Propagation Letters,* vol. 15, pp. 1927-1930, 2016.

[236] C. Kappel, U. Hirn, M. Donoser, and W. Bauer, "Measurement of printing ink penetration in uncoated papers and its influence on print quality," in *94th Annual meeting pulp and paper technology association of canada*, 2008, pp. 540-542.

[237] S. Müller, F. Happ, X. Duan, R. Rimolo-Donadio, H. D. Brüns, and C. Schuster, "Complete Modeling of Large Via Constellations in Multilayer Printed Circuit Boards," *IEEE Transactions on Components, Packaging and Manufacturing Technology,* vol. 3, pp. 489-499, 2013.

[238] J. Park, J. Lee, S. Park, K.-H. Shin, and D. Lee, "Development of hybrid process for double-side flexible printed circuit boards using roll-to-roll gravure printing, via-hole printing, and electroless plating," *The International Journal of Advanced Manufacturing Technology,* vol. 82, pp. 1921-1931, February 01 2016.

[239] J. A. Lewis and B. Y. Ahn, "Device fabrication: Three-dimensional printed electronics," *Nature,* vol. 518, pp. 42-43, 02/05/print 2015.

[240] A. C. Siegel, S. T. Phillips, M. D. Dickey, N. Lu, Z. Suo, and G. M. Whitesides, "Foldable Printed Circuit Boards on Paper Substrates," *Advanced Functional Materials,* vol. 20, pp. 28-35, 2010.

[241] Z. Li, R. Zhang, K.-S. Moon, Y. Liu, K. Hansen, T. Le*, et al.*, "Highly Conductive, Flexible, Polyurethane-Based Adhesives for Flexible and Printed Electronics," *Advanced Functional Materials,* vol. 23, pp. 1459-1465, 2013.

[242] J. Byun, E. Oh, B. Lee, S. Kim, S. Lee, and Y. Hong, "A Single Droplet-Printed Double-Side Universal Soft Electronic Platform for Highly Integrated Stretchable Hybrid Electronics," *Advanced Functional Materials,* vol. 27, p. 1701912, 2017.

[243] B. Tehrani, J. Bito, B. Cook, and M. Tentzeris, "Fully inkjet-printed multilayer microstrip and T-resonator structures for the RF characterization of printable materials and interconnects," in *Microwave Symposium (IMS), 2014 IEEE MTT-S International*, 2014, pp. 1-4.

[244] S. H. Ko, J. Chung, H. Pan, C. P. Grigoropoulos, and D. Poulikakos, "Fabrication of multilayer passive and active electric components on polymer using inkjet printing and low temperature laser processing," *Sensors and Actuators A: Physical,* vol. 134, pp. 161-168, 2007/02/28/ 2007.

[245] J. Liu, C. Yang, H. Wu, Z. Lin, Z. Zhang, R. Wang*, et al.*, "Future paper based printed circuit boards for green electronics: fabrication and life cycle assessment," *Energy & Environmental Science,* vol. 7, pp. 3674-3682, 2014.

[246] M. Irimia-Vladu, ""Green" electronics: biodegradable and biocompatible materials and devices for sustainable future," *Chemical Society Reviews,* vol. 43, pp. 588-610, 2014.

[247] J. Sun, B. Bao, J. Jiang, M. He, X. Zhang, and Y. Song, "Facile fabrication of a superhydrophilic-superhydrophobic patterned surface by inkjet printing a sacrificial layer on a superhydrophilic surface," *RSC Advances,* vol. 6, pp. 31470-31475, 2016.

[248] W. C. Wang, E. T. Kang, and K. G. Neoh, "Electroless plating of copper on polyimide films modified by plasma graft copolymerization with 4-vinylpyridine," *Applied Surface Science,* vol. 199, pp. 52-66, 2002/10/30/ 2002.

[249] S. Malynych, I. Luzinov, and G. Chumanov, "Poly(Vinyl Pyridine) as a Universal Surface Modifier for Immobilization of Nanoparticles," *The Journal of Physical Chemistry B,* vol. 106, pp. 1280-1285, 2002/02/01 2002.

[250] F. Meng, W. Zhang, and S. Zheng, "Epoxy resin cured with poly(4-vinyl pyridine)," *Journal of Materials Science,* vol. 40, pp. 6367-6373, December 01 2005.

[251] G. Xue, H. Ishida, and J. L. Koenig, "CHEMICAL-REACTIONS OF POLYVINYL PYRIDINE)S WITH EPOXY COMPOUNDS," *Angewandte Makromolekulare Chemie,* vol. 142, pp. 17-27, Jul 1986.

[252] Z. Bitar, D. E.-S. Bakeer, and R. Awad, "The effect of PVP on morphology, optical properties and electron paramagnetic resonance of Zn 0.5 Co 0.5 Fe 2-x Pr x O 4 nanoparticles," *Journal of Physics: Conference Series,* vol. 869, p. 012045, 2017.

[253] J. Gubbi, R. Buyya, S. Marusic, and M. Palaniswami, "Internet of Things (IoT): A vision, architectural elements, and future directions," *Future generation computer systems,* vol. 29, pp. 1645-1660, 2013.

[254] J. S. Heo, J. Eom, Y. H. Kim, and S. K. Park, "Recent Progress of Textile-Based Wearable Electronics: A Comprehensive Review of Materials, Devices, and Applications," *Small,* 2017.

[255] M. Sugathan and M. D. Hendry, "Market Forecasts and Personal Adoption of Smart Textiles in Fitness Sector," *International Journal of Technology Diffusion (IJTD),* vol. 8, pp. 57-75, 2017.

[256] M. Moussa, M. F. El-Kady, Z. Zhao, P. Majewski, and J. Ma, "Recent progress and performance evaluation for polyaniline/graphene nanocomposites as supercapacitor electrodes," *Nanotechnology,* vol. 27, p. 442001, 2016.

[257] H. Chen, T. N. Cong, W. Yang, C. Tan, Y. Li, and Y. Ding, "Progress in electrical energy storage system: A critical review," *Progress in Natural Science,* vol. 19, pp. 291-312, 2009.

[258] Y. Ko, M. Kwon, W. K. Bae, B. Lee, S. W. Lee, and J. Cho, "Flexible supercapacitor electrodes based on real metal-like cellulose papers," *Nature communications,* vol. 8, p. 536, 2017.

[259] P. Simon, Y. Gogotsi, and B. Dunn, "Where do batteries end and supercapacitors begin?," *Science,* vol. 343, pp. 1210-1211, 2014.

[260] P. Simon and Y. Gogotsi, "Materials for electrochemical capacitors," *Nature materials,* vol. 7, p. 845, 2008.

[261] P. Yang and W. Mai, "Flexible solid-state electrochemical supercapacitors," *Nano Energy,* vol. 8, pp. 274-290, 2014.

[262] Z. Yu, B. Duong, D. Abbitt, and J. Thomas, "Highly ordered MnO2 nanopillars for enhanced supercapacitor performance," *Advanced materials,* vol. 25, pp. 3302-3306, 2013.

[263] T. M. Dinh, A. Achour, S. Vizireanu, G. Dinescu, L. Nistor, K. Armstrong, *et al.*, "Hydrous RuO 2/carbon nanowalls hierarchical structures for all-solid-state ultrahigh-energy-density micro-supercapacitors," *Nano Energy,* vol. 10, pp. 288-294, 2014.

[264] W. Wei, X. Cui, W. Chen, and D. G. Ivey, "Manganese oxide-based materials as electrochemical supercapacitor electrodes," *Chemical society reviews,* vol. 40, pp. 1697-1721, 2011.

[265] X. Lu, D. Zheng, T. Zhai, Z. Liu, Y. Huang, S. Xie, *et al.*, "Facile synthesis of large-area manganese oxide nanorod arrays as a high-performance electrochemical supercapacitor," *Energy & Environmental Science,* vol. 4, pp. 2915-2921, 2011.

[266] T. Y. Wei, C. H. Chen, H. C. Chien, S. Y. Lu, and C. C. Hu, "A cost-effective supercapacitor material of ultrahigh specific capacitances: spinel nickel cobaltite aerogels from an epoxide-driven sol–gel process," *Advanced materials,* vol. 22, pp. 347-351, 2010.

[267]   X. Wang, C. Yan, A. Sumboja, and P. S. Lee, "High performance porous nickel cobalt oxide nanowires for asymmetric supercapacitor," *Nano Energy,* vol. 3, pp. 119-126, 2014.

[268]   R. Rakhi, W. Chen, D. Cha, and H. N. Alshareef, "Substrate dependent self-organization of mesoporous cobalt oxide nanowires with remarkable pseudocapacitance," *Nano letters,* vol. 12, pp. 2559-2567, 2012.

[269]   D. Choi, G. E. Blomgren, and P. N. Kumta, "Fast and reversible surface redox reaction in nanocrystalline vanadium nitride supercapacitors," *Advanced Materials,* vol. 18, pp. 1178-1182, 2006.

[270]   K. Chen and D. Xue, "High energy density hybrid supercapacitor: in-situ functionalization of vanadium-based colloidal cathode," *ACS applied materials & interfaces,* vol. 8, pp. 29522-29528, 2016.

[271]   M. Momeni, Z. Nazari, A. Kazempour, M. Hakimiyan, and S. Mirhoseini, "Preparation of CuO nanostructures coating on copper as supercapacitor materials," *Surface Engineering,* vol. 30, pp. 775-778, 2014.

[272]   G. Wang, L. Zhang, and J. Zhang, "A review of electrode materials for electrochemical supercapacitors," *Chemical Society Reviews,* vol. 41, pp. 797-828, 2012.

[273]   S. Shinde, D. Dubal, G. Ghodake, and V. Fulari, "Hierarchical 3D-flower-like CuO nanostructure on copper foil for supercapacitors," *RSC Advances,* vol. 5, pp. 4443-4447, 2015.

[274]   A. Lamberti, M. Fontana, S. Bianco, and E. Tresso, "Flexible solid-state CuxO-based pseudo-supercapacitor by thermal oxidation of copper foils," *International Journal of Hydrogen Energy,* vol. 41, pp. 11700-11708, 2016.

[275]   Y. He, W. Chen, X. Li, Z. Zhang, J. Fu, C. Zhao*, et al.*, "Freestanding three-dimensional graphene/MnO2 composite networks as ultralight and flexible supercapacitor electrodes," *ACS nano,* vol. 7, pp. 174-182, 2012.

[276]   X. Wang, X. Lu, B. Liu, D. Chen, Y. Tong, and G. Shen, "Flexible Energy-Storage Devices: Design Consideration and Recent Progress," *Advanced materials,* vol. 26, pp. 4763-4782, 2014.

[277] B. C. Kim, J. Y. Hong, G. G. Wallace, and H. S. Park, "Recent progress in flexible electrochemical capacitors: electrode materials, device configuration, and functions," *Advanced Energy Materials,* vol. 5, 2015.

[278] Z. Liu, Z. S. Wu, S. Yang, R. Dong, X. Feng, and K. Müllen, "Ultraflexible in-plane micro-supercapacitors by direct printing of solution-processable electrochemically exfoliated graphene," *Advanced Materials,* vol. 28, pp. 2217-2222, 2016.

[279] H. Zhang, Y. Qiao, and Z. Lu, "Fully printed ultraflexible supercapacitor supported by a single-textile substrate," *ACS applied materials & interfaces,* vol. 8, pp. 32317-32323, 2016.

[280] K.-H. Choi, J. Yoo, C. K. Lee, and S.-Y. Lee, "All-inkjet-printed, solid-state flexible supercapacitors on paper," *Energy & Environmental Science,* vol. 9, pp. 2812-2821, 2016.

[281] Z. Yu, L. Tetard, L. Zhai, and J. Thomas, "Supercapacitor electrode materials: nanostructures from 0 to 3 dimensions," *Energy & Environmental Science,* vol. 8, pp. 702-730, 2015.

[282] C. Zhou, Y. Zhang, Y. Li, and J. Liu, "Construction of high-capacitance 3D CoO@ polypyrrole nanowire array electrode for aqueous asymmetric supercapacitor," *Nano letters,* vol. 13, pp. 2078-2085, 2013.

[283] C. K. Chan, H. Peng, G. Liu, K. McIlwrath, X. F. Zhang, R. A. Huggins*, et al.*, "High-performance lithium battery anodes using silicon nanowires," *Nature nanotechnology,* vol. 3, p. 31, 2008.

[284] H. Zhang, X. Yu, and P. V. Braun, "Three-dimensional bicontinuous ultrafast-charge and-discharge bulk battery electrodes," *Nature nanotechnology,* vol. 6, p. 277, 2011.

[285] R. R. Salunkhe, K. Jang, H. Yu, S. Yu, T. Ganesh, S.-H. Han*, et al.*, "Chemical synthesis and electrochemical analysis of nickel cobaltite nanostructures for supercapacitor applications," *Journal of Alloys and Compounds,* vol. 509, pp. 6677-6682, 2011.

[286] Z. Tang, C. h. Tang, and H. Gong, "A High Energy Density Asymmetric Supercapacitor from Nano-architectured Ni (OH) 2/Carbon Nanotube Electrodes," *Advanced Functional Materials,* vol. 22, pp. 1272-1278, 2012.

[287] S. Yuan, X. l. Huang, D. l. Ma, H. g. Wang, F. z. Meng, and X. b. Zhang, "Engraving Copper Foil to Give Large-Scale Binder-Free Porous CuO Arrays for a High-

Performance Sodium-Ion Battery Anode," *Advanced Materials,* vol. 26, pp. 2273-2279, 2014.

[288] D. Dubal, D. Dhawale, R. Salunkhe, V. Jamdade, and C. Lokhande, "Fabrication of copper oxide multilayer nanosheets for supercapacitor application," *Journal of Alloys and Compounds,* vol. 492, pp. 26-30, 2010.

[289] Z. Endut, M. Hamdi, and W. Basirun, "Pseudocapacitive performance of vertical copper oxide nanoflakes," *Thin Solid Films,* vol. 528, pp. 213-216, 2013.

[290] W. Wang, E. Kang, and K. Neoh, "Electroless plating of copper on polyimide films modified by plasma graft copolymerization with 4-vinylpyridine," *Applied Surface Science,* vol. 199, pp. 52-66, 2002.

[291] J. A. Rogers, "ELECTRONICS A diverse printed future," *Nature,* vol. 468, pp. 177-178, Nov 11 2010.

[292] D. Tobjork and R. Osterbacka, "Paper Electronics," *Advanced Materials,* vol. 23, pp. 1935-1961, May 3 2011.

[293] S. H. Kim, K. Hong, W. Xie, K. H. Lee, S. Zhang, T. P. Lodge*, et al.*, "Electrolyte-gated transistors for organic and printed electronics," *Adv Mater,* vol. 25, pp. 1822-46, Apr 4 2013.

[294] S. E. Habas, H. A. S. Platt, M. F. A. M. van Hest, and D. S. Ginley, "Low-Cost Inorganic Solar Cells: From Ink To Printed Device," *Chemical Reviews,* vol. 110, pp. 6571-6594, Nov 2010.

[295] J. Perelaer, B. J. de Gans, and U. S. Schubert, "Ink-jet printing and microwave sintering of conductive silver tracks," *Advanced Materials,* vol. 18, pp. 2101-+, Aug 18 2006.

[296] J. Lessing, A. C. Glavan, S. B. Walker, C. Keplinger, J. A. Lewis, and G. M. Whitesides, "Inkjet Printing of Conductive Inks with High Lateral Resolution on Omniphobic "R Paper" for Paper-Based Electronics and MEMS," *Adv Mater,* May 30 2014.

[297] E. B. Secor, S. Lim, H. Zhang, C. D. Frisbie, L. F. Francis, and M. C. Hersam, "Gravure Printing of Graphene for Large-area Flexible Electronics," *Adv Mater,* Apr 29 2014.

[298] W. Wu, S. Yang, S. Zhang, H. Zhang, and C. Jiang, "Fabrication, characterization and screen printing of conductive ink based on carbon@Ag core–shell nanoparticles," *Journal of Colloid and Interface Science,* vol. 427, pp. 15-19, 8/1/ 2014.

[299] K. Yang, C. Freeman, R. Torah, S. Beeby, and J. Tudor, "Screen printed fabric electrode array for wearable functional electrical stimulation," *Sensors and Actuators A: Physical,* vol. 213, pp. 108-115, 7/1/ 2014.

[300] K. Hong, Y. H. Kim, S. H. Kim, W. Xie, W. D. Xu, C. H. Kim*, et al.*, "Aerosol Jet Printed, Sub-2 V Complementary Circuits Constructed from P- and N-Type Electrolyte Gated Transistors," *Adv Mater,* Jun 27 2014.

[301] M. Makrygianni, I. Kalpyris, C. Boutopoulos, and I. Zergioti, "Laser induced forward transfer of Ag nanoparticles ink deposition and characterization," *Applied Surface Science,* vol. 297, pp. 40-44, Apr 1 2014.

[302] C. Boutopoulos, I. Kalpyris, E. Serpetzoglou, and I. Zergioti, "Laser-induced forward transfer of silver nanoparticle ink: time-resolved imaging of the jetting dynamics and correlation with the printing quality," *Microfluidics and Nanofluidics,* vol. 16, pp. 493-500, Mar 2014.

[303] H. Kim, T. E. Sutto, J. Proell, R. Kohler, W. Pfleging, and A. Pique, "Laser-printed/structured thick-film electrodes for Li-ion microbatteries," *Laser-Based Micro- and Nanoprocessing Viii,* vol. 8968, 2014.

[304] S. Gamerith, A. Klug, H. Scheiber, U. Scherf, E. Moderegger, and E. J. W. List, "Direct Ink-Jet Printing of Ag–Cu Nanoparticle and Ag-Precursor Based Electrodes for OFET Applications," *Advanced Functional Materials,* vol. 17, pp. 3111-3118, 2007.

[305] J. Liu, Y. Gao, D. Cao, L. Zhang, and Z. Guo, "Nanoparticle Dispersion and Aggregation in Polymer Nanocomposites: Insights from Molecular Dynamics Simulation," *Langmuir,* vol. 27, pp. 7926-7933, 2011/06/21 2011.

[306] M. E. Mackay, A. Tuteja, P. M. Duxbury, C. J. Hawker, B. Van Horn, Z. Guan*, et al.*, "General Strategies for Nanoparticle Dispersion," *Science,* vol. 311, pp. 1740-1743, March 24, 2006 2006.

[307] S. Hong, J. Yeo, G. Kim, D. Kim, H. Lee, J. Kwon*, et al.*, "Nonvacuum, Maskless Fabrication of a Flexible Metal Grid Transparent Conductor by Low-Temperature

Selective Laser Sintering of Nanoparticle Ink," *Acs Nano,* vol. 7, pp. 5024-5031, Jun 2013.

[308] H. Kang, E. Sowade, and R. R. Baumann, "Direct Intense Pulsed Light Sintering of Inkjet-Printed Copper Oxide Layers within Six Milliseconds," *Acs Applied Materials & Interfaces,* vol. 6, pp. 1682-1687, Feb 12 2014.

[309] J. Perelaer, R. Abbel, S. Wunscher, R. Jani, T. van Lammeren, and U. S. Schubert, "Roll-to-Roll Compatible Sintering of Inkjet Printed Features by Photonic and Microwave Exposure: From Non-Conductive Ink to 40% Bulk Silver Conductivity in Less Than 15 Seconds," *Advanced Materials,* vol. 24, pp. 2620-2625, May 15 2012.

[310] J. Perelaer, R. Jani, M. Grouchko, A. Kamyshny, S. Magdassi, and U. S. Schubert, "Plasma and Microwave Flash Sintering of a Tailored Silver Nanoparticle Ink, Yielding 60% Bulk Conductivity on Cost-Effective Polymer Foils," *Advanced Materials,* vol. 24, pp. 3993-3998, 2012.

[311] B. Y. Ahn, E. B. Duoss, M. J. Motala, X. Y. Guo, S. I. Park, Y. J. Xiong*, et al.*, "Omnidirectional Printing of Flexible, Stretchable, and Spanning Silver Microelectrodes," *Science,* vol. 323, pp. 1590-1593, Mar 20 2009.

[312] Y. G. Sun and Y. N. Xia, "Shape-controlled synthesis of gold and silver nanoparticles," *Science,* vol. 298, pp. 2176-2179, Dec 13 2002.

[313] R. Guo, Y. Yu, Z. Xie, X. Liu, X. Zhou, Y. Gao*, et al.*, "Matrix-Assisted Catalytic Printing for the Fabrication of Multiscale, Flexible, Foldable, and Stretchable Metal Conductors," *Advanced Materials,* vol. 25, pp. 3343-3350, 2013.

[314] X. L. Wang, H. Hu, Y. D. Shen, X. C. Zhou, and Z. J. Zheng, "Stretchable Conductors with Ultrahigh Tensile Strain and Stable Metallic Conductance Enabled by Prestrained Polyelectrolyte Nanoplatforms," *Advanced Materials,* vol. 23, pp. 3090-+, Jul 19 2011.

[315] K. Cheng, M. H. Yang, W. W. W. Chiu, C. Y. Huang, J. Chang, T. F. Ying*, et al.*, "Ink-jet printing, self-assembled polyelectrolytes, and electroless plating: Low cost fabrication of circuits on a flexible substrate at room temperature," *Macromolecular Rapid Communications,* vol. 26, pp. 247-264, Feb 21 2005.

[316] T. Zhang, X. Wang, T. Li, Q. Guo, and J. Yang, "Fabrication of flexible copper-based electronics with high-resolution and high-conductivity on paper via inkjet printing," *Journal of Materials Chemistry C,* 2013.

[317] U. Zywietz, A. B. Evlyukhin, C. Reinhardt, and B. N. Chichkov, "Laser printing of silicon nanoparticles with resonant optical electric and magnetic responses," *Nature Communications,* vol. 5, Mar 2014.

[318] W. K. T. Coltro, D. P. de Jesus, J. A. F. da Silva, C. L. do Lago, and E. Carrilho, "Toner and paper-based fabrication techniques for microfluidic applications," *ELECTROPHORESIS,* vol. 31, pp. 2487-2498, 2010.

[319] E. S. Polsen, A. G. Stevens, and A. J. Hart, "Laser Printing of Nanoparticle Toner Enables Digital Control of Micropatterned Carbon Nanotube Growth," *Acs Applied Materials & Interfaces,* vol. 5, pp. 3656-3662, May 8 2013.

[320] W. K. T. Coltro, E. Piccin, J. A. F. da Silva, C. L. do Lago, and E. Carrilho, "A toner-mediated lithographic technology for rapid prototyping of glass microchannels," *Lab on a Chip,* vol. 7, pp. 931-934, 2007.

[321] S. R. Forrest, "The path to ubiquitous and low-cost organic electronic appliances on plastic," *Nature,* vol. 428, pp. 911-918, 04/29/print 2004.

[322] W. Zeng, L. Shu, Q. Li, S. Chen, F. Wang, and X.-M. Tao, "Fiber-Based Wearable Electronics: A Review of Materials, Fabrication, Devices, and Applications," *Advanced Materials,* vol. 26, pp. 5310-5336, 2014.

[323] S. K. Sarkar, H. Gupta, and D. Gupta, "Flash Light Sintering of Silver Nanoink for Inkjet-Printed Thin-Film Transistor on Flexible Substrate," *IEEE Transactions on Nanotechnology,* vol. 16, pp. 375-382, 2017.

[324] F. Torricelli, L. Colalongo, D. Raiteri, Z. M. Kovács-Vajna, and E. Cantatore, "Ultra-high gain diffusion-driven organic transistor," vol. 7, p. 10550, 02/01/online 2016.

[325] X. Cao, C. Lau, Y. Liu, F. Wu, H. Gui, Q. Liu*, et al.*, "Fully Screen-Printed, Large-Area, and Flexible Active-Matrix Electrochromic Displays Using Carbon Nanotube Thin-Film Transistors," *ACS Nano,* vol. 10, pp. 9816-9822, 2016/11/22 2016.

[326] G. Zhou, F. Li, and H.-M. Cheng, "Progress in flexible lithium batteries and future prospects," *Energy & Environmental Science,* vol. 7, pp. 1307-1338, 2014.

[327] X. Wang, X. Lu, B. Liu, D. Chen, Y. Tong, and G. Shen, "Flexible Energy-Storage Devices: Design Consideration and Recent Progress," *Advanced Materials,* vol. 26, pp. 4763-4782, 2014.

[328] J. C. Ruiz-Morales, A. Tarancon, J. Canales-Vazquez, J. Mendez-Ramos, L. Hernandez-Afonso, P. Acosta-Mora*, et al.*, "Three dimensional printing of

components and functional devices for energy and environmental applications," *Energy & Environmental Science,* vol. 10, pp. 846-859, 2017.

[329] Y. Feng, L. Xie, Q. Chen, and L. R. Zheng, "Low-Cost Printed Chipless RFID Humidity Sensor Tag for Intelligent Packaging," *IEEE Sensors Journal,* vol. 15, pp. 3201-3208, 2015.

[330] R. J. Morrison, S. J. Hollister, M. F. Niedner, M. G. Mahani, A. H. Park, D. K. Mehta*, et al.*, "Mitigation of tracheobronchomalacia with 3D-printed personalized medical devices in pediatric patients," *Science Translational Medicine,* vol. 7, pp. 285ra64-285ra64, 2015.

[331] J. R. Corea, A. M. Flynn, B. Lechêne, G. Scott, G. D. Reed, P. J. Shin*, et al.*, "Screen-printed flexible MRI receive coils," vol. 7, p. 10839, 03/10/online 2016.

[332] Y. Khan, F. J. Pavinatto, M. C. Lin, A. Liao, S. L. Swisher, K. Mann*, et al.*, "Inkjet-Printed Flexible Gold Electrode Arrays for Bioelectronic Interfaces," *Advanced Functional Materials,* vol. 26, pp. 1004-1013, 2016.

[333] E. B. Secor, S. Lim, H. Zhang, C. D. Frisbie, L. F. Francis, and M. C. Hersam, "Gravure Printing of Graphene for Large-area Flexible Electronics," *Advanced Materials,* vol. 26, pp. 4533-4538, 2014.

[334] W. J. Hyun, E. B. Secor, M. C. Hersam, C. D. Frisbie, and L. F. Francis, "High-Resolution Patterning of Graphene by Screen Printing with a Silicon Stencil for Highly Flexible Printed Electronics," *Advanced Materials,* vol. 27, pp. 109-115, 2015.

[335] A. A. Bessonov, M. N. Kirikova, D. I. Petukhov, M. Allen, T. Ryhänen, and M. J. A. Bailey, "Layered memristive and memcapacitive switches for printable electronics," *Nat Mater,* vol. 14, pp. 199-204, 02//print 2015.

[336] B. Jeong, I. Hwang, S. H. Cho, E. H. Kim, S. Cha, J. Lee*, et al.*, "Solvent-Assisted Gel Printing for Micropatterning Thin Organic–Inorganic Hybrid Perovskite Films," *ACS Nano,* vol. 10, pp. 9026-9035, 2016/09/27 2016.

[337] C. Yang, X. Cui, Z. Zhang, S. W. Chiang, W. Lin, H. Duan*, et al.*, "Fractal dendrite-based electrically conductive composites for laser-scribed flexible circuits," vol. 6, p. 8150, 09/03/online 2015.

[338] G. D. Spyropoulos, C. O. Ramirez Quiroz, M. Salvador, Y. Hou, N. Gasparini, P. Schweizer*, et al.*, "Organic and perovskite solar modules innovated by adhesive top

electrode and depth-resolved laser patterning," *Energy & Environmental Science,* vol. 9, pp. 2302-2313, 2016.

[339] F. Zare Bidoky and C. D. Frisbie, "Parasitic Capacitance Effect on Dynamic Performance of Aerosol-Jet-Printed Sub 2 V Poly(3-hexylthiophene) Electrolyte-Gated Transistors," *ACS Applied Materials & Interfaces,* vol. 8, pp. 27012-27017, 2016/10/12 2016.

[340] W.-H. Yeo, Y.-S. Kim, J. Lee, A. Ameen, L. Shi, M. Li*, et al.*, "Multifunctional Epidermal Electronics Printed Directly Onto the Skin," *Advanced Materials,* vol. 25, pp. 2773-2778, 2013.

[341] Z. Li, H. Liu, C. Ouyang, W. Hong Wee, X. Cui, T. Jian Lu*, et al.*, "Recent Advances in Pen-Based Writing Electronics and their Emerging Applications," *Advanced Functional Materials,* vol. 26, pp. 165-180, 2016.

[342] M. Hu, X. Cai, Q. Guo, B. Bian, T. Zhang, and J. Yang, "Direct Pen Writing of Adhesive Particle-Free Ultrahigh Silver Salt-Loaded Composite Ink for Stretchable Circuits," *ACS Nano,* vol. 10, pp. 396-404, 2016/01/26 2016.

[343] A. Russo, B. Y. Ahn, J. J. Adams, E. B. Duoss, J. T. Bernhard, and J. A. Lewis, "Pen-on-Paper Flexible Electronics," *Advanced Materials,* vol. 23, pp. 3426-3430, 2011.

[344] A. J. Bandodkar, W. Jia, J. Ramírez, and J. Wang, "Biocompatible Enzymatic Roller Pens for Direct Writing of Biocatalytic Materials: "Do-it-Yourself" Electrochemical Biosensors," *Advanced Healthcare Materials,* vol. 4, pp. 1215-1224, 2015.

[345] V. V. Singh, G. Gupta, A. Batra, A. K. Nigam, M. Boopathi, P. K. Gutch*, et al.*, "Greener Electrochemical Synthesis of High Quality Graphene Nanosheets Directly from Pencil and its SPR Sensing Application," *Advanced Functional Materials,* vol. 22, pp. 2352-2362, 2012.

[346] H. Jia, J. Wang, X. Zhang, and Y. Wang, "Pen-Writing Polypyrrole Arrays on Paper for Versatile Cheap Sensors," *ACS Macro Letters,* vol. 3, pp. 86-90, 2014/01/21 2014.

[347] L. Polavarapu, A. L. Porta, S. M. Novikov, M. Coronado-Puchau, and L. M. Liz-Marzán, "Pen-on-Paper Approach Toward the Design of Universal Surface Enhanced Raman Scattering Substrates," *Small,* vol. 10, pp. 3065-3071, 2014.

[348] K. G. Nair, D. Jayaseelan, and P. Biji, "Direct-writing of circuit interconnects on cellulose paper using ultra-long, silver nanowires based conducting ink," *RSC Advances,* vol. 5, pp. 76092-76100, 2015.

[349] L. Y. Xu, G. Y. Yang, H. Y. Jing, J. Wei, and Y. D. Han, "Pressure-assisted low-temperature sintering for paper-based writing electronics," *Nanotechnology,* vol. 24, p. 355204, 2013.

[350] T. Zhang, X. Cai, J. Liu, M. Hu, Q. Guo, and J. Yang, "Facile Fabrication of Hybrid Copper–Fiber Conductive Features with Enhanced Durability and Ultralow Sheet Resistance for Low-Cost High-Performance Paper-Based Electronics," *Advanced Sustainable Systems,* pp. n/a-n/a.

[351] V. K. Sharma, R. A. Yngard, and Y. Lin, "Silver nanoparticles: Green synthesis and their antimicrobial activities," *Advances in Colloid and Interface Science,* vol. 145, pp. 83-96, 2009/01/30/ 2009.

[352] N. R. Jana, L. Gearheart, and C. J. Murphy, "Wet chemical synthesis of silver nanorods and nanowires of controllable aspect ratio," *Chemical Communications,* pp. 617-618, 2001.

[353] H. K. Lee, M. K. Joyce, P. D. Fleming, and J. E. Cawthorne, "Influence of silica and alumina oxide on coating structure and print quality of ink-jet papers," *Tappi Journal,* vol. 4, pp. 11-16, 2005.

[354] R. W. Korsmeyer, R. Gurny, E. Doelker, P. Buri, and N. A. Peppas, "Mechanisms of solute release from porous hydrophilic polymers," *International Journal of Pharmaceutics,* vol. 15, pp. 25-35, 1983/05/01/ 1983.

[355] C. S. Brazel and N. A. Peppas, "Mechanisms of solute and drug transport in relaxing, swellable, hydrophilic glassy polymers," *Polymer,* vol. 40, pp. 3383-3398, 1999/06/01/ 1999.

[356] G. D. Botsaris, "Secondary Nucleation — A Review," in *Industrial Crystallization*, J. W. Mullin, Ed., ed Boston, MA: Springer US, 1976, pp. 3-22.

[357] A. P. Boresi, R. J. Schmidt, and O. M. Sidebottom, *Advanced mechanics of materials* vol. 6: Wiley New York, 1993.

[358] H. K. Lin, S. M. Chiu, T. P. Cho, and J. C. Huang, "Improved bending fatigue behavior of flexible PET/ITO film with thin metallic glass interlayer," *Materials Letters,* vol. 113, pp. 182-185, 2013/12/15/ 2013.

Curriculum Vitae

Name:	Tengyuan Zhang
Post-secondary Education and Degrees:	Beijing Institute of Technology Beijing, China 2008-2012 B.A.
	The University of Western Ontario London, Ontario, Canada 2012-2014 M.E.Sc.
	The University of Western Ontario London, Ontario, Canada 2014-2018 Ph.D.
Honours and Awards:	Vanier Canada Graduate Scholarship 2015-2018
	Doctoral Excellence Research Award 2016-2017
Related Work Experience	Teaching Assistant The University of Western Ontario 2012-2018
	Co-founder & CEO Nectro Inc. 2015-
	Research Assistant Delft University of Technology 2012-2012

Publications:

T. Zhang, E. Asher and J. Yang, A New Printed Electronics Approach Eliminating Redundant Fabrication Process of Vertical Interconnect Accesses: Building Multilayered Circuits in Porous Materials, Advanced Materials Technologies, 2018, 1700346, DOI: 10.1002/admt.201700346

T. Zhang, J. Li and J. Yang, React-on-Demand (RoD) Fabrication of Highly Conductive Metal-Polymer Hybrid Structure for Flexible Electronics via One-Step Direct Writing or Printing, Advanced Functional Materials, 2018, 28(4): 1704671

W. Zhang*, T. Zhang*, Q. Guo et al., A 3D High-Efficiency Wireless Power Transfer System for Volume, Unstationary Free-Positioning and Multi-Object Charging, IET Electric Power Applications, 2018, DOI: 10.1049/iet-epa.2017.0581

T. Zhang, X. Cai et al., Hybrid Copper–Fiber Conductive Features with Enhanced Durability and Ultralow Sheet Resistance for Low-Cost High-Performance Paper-Based Electronics, Advanced Sustainable Systems, 2017, 1(9): 1700062

T. Zhang, E. Asher et al., Thinking about Science: Understanding the Science, Technology, Society and Environment Education of Canada, International Journal of Education and Social Science, 2017, 4(2): 15-20

T. Zhang, M. Hu et al., A Laser Printing Based Approach for Printed Electronics, Applied Physics Letters, 2016, 108(10): 103501

T. Zhang, X. Wang et al., Fabrication of Flexible Copper-Based Electronics with High-Resolution and High-Conductivity on Paper via Inkjet Printing, Journal of Materials Chemistry C, 2014, 2(2): 286-294

T. Zhang, W. Zhang et al., A 3D High-Efficiency Wireless Power Transfer System for Volume, Un-stationary Free-Positioning and Multi-Object Charging, IET Electric Power Applications, 2018 (Under Revision)

T. Zhang and Y. Mei, Research on Mechanics Problems in Frame Construction Design, Guide of Sci-tech, 2011, 2011(29): 46-47.